UNIVERSITÉ DE STRASBOURG

ÉCOLE DOCTORALE DES SCIENCES CHIMIQUES

UMR 7199 CNRS – Laboratoire de Conception et Application de Molécules Bioactives

THÈSE

présentée par :

Justine WALLYN

soutenue en : **11 Décembre 2017**

pour obtenir le grade de : **Docteur de l'Université de Strasbourg**

Discipline/ Spécialité : Chimie

Nanoparticules furtives pour l'imagerie préclinique à rayons X et multimodale rayons X/IRM (imagerie à résonance magnétique)

THÈSE dirigée par :

M VANDAMME Thierry	Professeur, Université de Strasbourg

RAPPORTEURS :

Mme ANDRY Marie-Christine	Professeur, Université de Reims Champagne-Ardennes
Mme LESIEUR Sylvianne	Directeur de recherche CNRS, Université de Paris-Sud

---

AUTRES MEMBRES DU JURY ET INVITE :

Mme BRIANÇON Stéphanie	Professeur, Université Claude Bernard Lyon I
M ANTON Nicolas	Maître de conférences, Université de Strasbourg

This thesis is dedicated to my sisters,

Marion and Camille,

who unfailingly stand by me.

Acknowledgements & Remerciements

Acknowledgements

This PhD work represents for me my final achievement as a student, my final challenge for myself… before the next one I assume. I sincerely think that I own my accomplishments from some people I met because they brung me support and made me feel more confident in what I was able to accomplish.

First, I would like to sincerely thank and express my deepest gratitude to my supervisor Prof. Thierry Vandamme and co-supervisor Dr. Nicolas Anton for their guidance and advice, our stimulating discussions to enrich research ideas. I am also really glad that they offer me the possibility to work independently on novel nanotechnologies for our group; I also thank them for their thrust in my capacities to carry out such task. Furthermore, their motivations, encouragements and supports to see me pursue in research and to join them as PhD student were one the most crucial things that I needed to feel truly justified in applying and capable of doing a PhD.

Second, I express my sincere gratitude to the committee members, Prof. Marie-Christine Andry from the University of Reims, Dr. Sylvianne Lesieur from University of Paris-Sud and Prof. Stéphanie Briançon from University Claude Bernard Lyon I, for their time and approval to be part of my committee for my final defense.

Third, I wish express my gratitude to all collaborators for providing me their expertise, knowledge and time. Their professional work and wise advice helped me to go further in work thanks to relevant comments and smart pointers. I would like in this way to thank Prof. Christophe Serra and Michel Bouquey (Institut Charles Chadron, Strasbourg) for their precious advice in polymer science; Prof. Sylvie Bégin-Colin and Damien Mertz (Institut de Physique et Chimie des Matériaux de Strasbourg, Strasbourg) for letting me the liberty to work with their advanced equipment; Florence Franconi (Plateforme d'Ingénierie et d'Analyse Moléculaire, Angers), Laurent Lemaire (Ingénierie de la Vectorisation Particulaire, Angers) and Hélène Libouban (UFR de santé, Angers) for MRI and X-rays experiments on mice, the very stimulating discussions and welcoming in their lab; Nadia Messaddeq and Jean-Luc Weickert (Institut de Génétique et de Biologie Moléculaire et Cellulaire, Illkirch) for electron microscopy investigations; Caroline Bouillot for *in vivo* experiment and X-ray imaging (CERMEP-Imagerie du vivant, Bron); Mayeul Collot (Laboratoire de Biophotonique et Pharmacologie, Illkirch) for its contributions in my work.

Then, my sincere thanks and appreciation go to my past and present colleagues who all bring enthusiasm and support, they all contribute to make these three years of PhD interesting not only regarding a scientific point of view but also as human experience owing to our difference of origins. It was a really great experience to be in such group where people were all open-minded and full of wisdom for each other. I wish the very best for their career and personal life to past colleagues Mohamed Attia, a very smart person, always putting other's interest before his own, Thi Trinh Lan Nguyen, an example of kindness and always full of noble sentiments for others and Shukaï Ding, such a hard worker and friendly fellow. To my current colleagues, I would to thank Aïdar, Ali, Asad, Bilal, Germain, Mady, Salman and Sidy and wish them the best of luck to achieve their PhD and reach their goals. I do admire them for their determination, their courage and the sacrifices that they are capable of to build their future.

Finally, I would like to thank people who contributed into my PhD on other professional axes. I deeply thank Saïd, Martin and Ludivine for helping me and training me in teaching and also persons involved into Doctoriales® d'Alsace for the great experience.

Remerciements

Les remerciements qui suivent sont adressés aux personnes touchant davantage à la sphère personnelle. Ils sont dirigés à des personnes qui ont personnellement comptés ces dernières années et qui selon moi m'ont permis d'arriver là où j'en suis aujourd'hui.

Tout d'abord, je tiens à remercier les personnes que j'ai pu rencontrer au sein de la faculté de pharmacie et qui sont devenues pour moi plus que simples relations de travail. Je tiens ainsi à faire part à Christophe, Diane, Ludivine et Sonia du réel plaisir que cela a été pour moi de vous rencontrer et d'avoir pu partager de nombreux bons moments. A ces derniers s'ajoutent ceux qui ont quitté la faculté, Randa et Manuela. Pour poursuivre, je ne pourrais manquer de remercier mes amis et ce, tout autant ceux de longue date que ceux rencontrés à Strasbourg : Perrine, Anthony, Mehdi, Cédric, Romain, Angel, Zélie, Manal, Charline, Hélène, Karima, Johan, Loïc et Magali.

Finalement, mes derniers et plus profonds remerciements vont bien évidemment à mes parents et mes sœurs. Il n'y a pas de propos suffisamment adéquats selon moi pour décrire ce que je leur dois et ce pourquoi je les remercie. Je pense cependant ne pas me tromper en

disant qu'il doit s'agir des personnes qui ont toujours été là pour moi et qui le seront toujours, indéfectiblement.

Table of contents

Table of contents

Abbreviations

Abbreviations

API	Active pharmaceutical ingredient
CA	Contrast agent
CNS	Central nervous system
CT	Computed tomography
DDS	Drug delivery system
DE	Dendrimer
DLS	Dynamic light scattering
DSC	Differential scanning calorimetry
HU	Hounsfield unit
LP	Liposome
LPP	Lipoprotein
Micro-CT	Microcomputed tomography
MPS	Mononuclear phagocyte system
MRI	Magnetic resonance imaging
NC	Nanocarrier
NE	Nano-emulsion
NMR	Nuclear magnetic resonance
NP	Nanoparticle
PDI	Polydispersity index
PEG	Poly(ethylene glycol)
PET	Positron emission tomography
PNP	Polymeric nanoparticle
RES	Reticuloendothelial system
ROI	Region of interest
SEM	Scanning electron microscopy
SOR	Surfactant/(Surfactant + oil) weight ratio
SPECT	Single positron emission computed tomography
SPION	Superparamagnetic iron oxide nanoparticle
SPM	Superparamagnetic
SPR	Surfactant/(Surfactant + polymer) weigh ratio
SOWR	(Surfactant + oil)/(Surfactant + oil + water) weight ratio
TEM	Transmission electron microscopy

Résumé de thèse

Résumé de thèse

Objectif de la thèse

Cette thèse a pour objectif de réaliser la préparation de systèmes nanoparticulaires en tant que produit de contraste dispersé injectable destiné à l'imagerie médicale pour le diagnostic médical non-invasif. Deux modalités majeures, à savoir le scanner à rayons X connu comme le tomodensitomètre à rayons X et l'imagerie par résonance magnétique communément nommé IRM, ont été les instruments sur lesquels nous nous sommes focalisés et pour lesquels nous avons élaboré des sondes nanoparticulaires. Il va sans dire que chaque modalité d'imagerie repose sur son propre principe de fonctionnement et qu'à chaque instrument est associé un type de produit de contraste dont la composition permet de générer un contraste significatif sur les images. Par conséquent, différents systèmes dispersés, sous forme de suspension colloïdale, ont été formulés avec des composés chargés en élément(s) nécessaire(s) à l'amélioration du contraste respectivement pour scanner à rayons X et IRM et étudiés jusqu'à l'application sur un modèle animal. Cette dissertation doctorale a pour but d'étudier le profil pharmacocinétique *in vivo* ainsi que les paramètres de formulation menant à l'élaboration de produits de contraste injectables et concentrés en élément servant de source de contraste. Les paramètres physico-chimiques tels que la taille des colloïdes, les rapports massiques des constituants, la stabilité en milieu physiologique et le profil de biodistribution et d'accumulation ont été les paramètres principalement évalués.

L'imagerie médicale et ses modalités : atouts et champ de possibilité

Depuis des décennies, l'imagerie médicale est devenue un outil incontournable en clinique afin de visualiser de manière non-invasive l'intérieur d'un corps humain. Les méthodes d'imagerie actuelles permettent de juger de l'état de santé d'un patient en établissant un diagnostic suite à l'observation des tissus et fluides biologiques, l'évaluation des fonctions des organes, de leurs anatomies, de leurs morphologies et de leurs potentiels dysfonctionnements et pathologies telles que des tumeurs, bénignes ou malines. Cela va même au-delà de cela puisque les outils d'imagerie sont à présent davantage exploités car ils ne servent plus uniquement en amont de la procédure de gestion de la maladie d'un patient mais aussi en cours de traitement afin d'en observer les effets sur les tissus. Les images 2D et/ou 3D reconstruites servent ainsi de support afin d'établir un diagnostic, évaluer la progression d'une pathologie ou lésion, évaluer l'efficacité d'un traitement et faciliter la prise

de décision afin d'établir une stratégie thérapeutique pour un patient. Tout ceci est rendu possible grâce à la combinaison de produits de contraste et d'une technique d'imagerie qui facilite la visualisation de certaines structures internes du corps humain dont le contraste est similaire *i.e.* les tissus mous. Les agents de contraste employés peuvent en effet être localement accumulés dans une région d'intérêt ciblée selon la formulation des composés. Chaque méthode nécessite une certaine dose de substance contrastante, principalement due aux caractéristiques de la modalité (sensibilité, résolution, source, type de sonde nécessaire). Le Tableau 1 regroupe brièvement les principales caractéristiques des cinq principales modalités d'imagerie préclinique et clinique, à savoir le scanner à rayons X, l'IRM, le scanner à imagerie nucléaire tomographique (tomographe par émission de photons (TEP) et tomographe à émission monophtonique (TEMP)), l'imageur à ultrasons et l'imagerie optique (fluorescence (Fluo) et bioluminescence (Biolum)):

Tableau 1: Comparaison des techniques d'imagerie courantes en recherche préclinique et clinique.

	Scanner à rayons X	**IRM**	**Imagerie nucléaire**	**Imagerie à ultrason**	**Imagerie optique**
Source	Rayons X	Champ magnétique et radiofréquence	Rayons γ	Son	Lumière visible, proche infrarouge
Résolution spatiale	50–200 µm	25–100 µm	2-10 mm	50–500 µm	1–5 mm
Sondes	Elément lourds *i.e.* I, Ba, Au…	Matériaux magnétiques : Fe_3O_4, chélates de Gd	Radioisotopes : ^{18}F, ^{11}C, ^{13}N, ^{15}O, ^{64}Cu, ^{124}I ^{11}In, ^{99}mTc	Microbulle, émulsion, micelle	Sonde fluorescente et du domaine des infrarouges proches, quantum dots
Dose de sonde (mol/L)	10^{-3}	10^{-3}–10^{-5}	10^{-10}–10^{-12}	Non définie	Biolum: 10^{-15}–10^{-17} Fluo: 10^{-9}–10^{-12}
*Information**	A et P	A, P et F	A, P et F	A et P	P et M
Avantages	Haute résolution, pas de limite de pénétration	Haute résolution, pas de radiation, pas de limite de pénétration	Haute sensibilité à la dose de sonde	Facile, rapide, peu chère, pas de radiation	Imagerie sur plusieurs canaux, pas de radiation, sensible à la dose de sonde
Limitations	Radiation, faible différenciation des tissus mous, faible sensibilité à la dose de sonde	Faible sensibilité à la dose de sonde	Besoin de sonde, radiation, coûteux, faible résolution	Faible pénétration des tissus, faible contraste, inadaptée aux organes contenant de l'air	Besoin de sonde, inadaptée à l'échelle clinique, faible pénétration des tissus, faible résolution

* Information: A: anatomique, P: physiologique, F: fonctionnelle et M: moléculaire.

Chaque méthode possède ses propres atouts et limitations, ce qui les rend au final complémentaires. Le choix d'une modalité à défaut d'une autre se base principalement sur l'information qui est recherchée et bien évidemment sur l'état de santé du patient. Par

exemple, une personne portant des pièces métalliques telles que des broches ne peut être candidate à l'IRM, de même qu'une femme enceinte ne peut être sujette à l'imagerie à rayons X. De plus, la résolution et la profondeur de pénétration du faisceau envoyé par la source de chaque instrument sont différentes, ce qui permet d'obtenir des informations plus ou moins précises et à différentes échelles. Chaque imageur donne des images dont les informations pourront être corrélées, complétées, confirmées avec celles d'une ou de plusieurs modalités afin d'aboutir à un bilan complet sur l'état de la région d'intérêt étudiée.

Le scanner à rayons X et l'IRM

La technique la plus employée à l'heure actuelle est le scanner à rayons X à l'échelle clinique ; son équivalent à l'échelle préclinique est le micro-tomodensitomètre à rayons X. Son invention remonte aux années 60, son développement n'a cessé de se poursuivre depuis son implantation en clinique en 1972. Ces années de progrès en ont fait un outil de faible coût et ce, pour une bonne résolution spatiale, une rapidité d'acquisition et une absence de limite de profondeur de pénétration des tissus. Typiquement, des substances iodées à base de petites molécules hydrosolubles et de faibles masses moléculaires sont administrées comme produit de contraste. Elles sont très généralement basées sur une structure moléculaire incluant un ou deux cycles benzoïques triiodés afin qu'un rapport massique en élément lourd, ici l'iode, soit conséquent pour assurer la génération d'un important contraste. Le scanner à rayons X repose sur l'atténuation des rayons X par les matériaux denses du corps humain comme par exemple les os du squelette, qui apparaissent sur les images reconstruites par blanchissement (hypersignal par contraste positif). Les tissus mous et les fluides ne sont que très peu contrastés, car très pauvres en éléments lourds tels que les minéraux trouvés dans les os, pour pouvoir en effectuer une observation précise. Les agents de contraste iodés sont donc essentiels pour les visualiser correctement. Une accumulation préférentielle des produits de contraste dits radio-opaques dans ces tissus est alors nécessaire.

Bien que l'iode soit un des éléments les plus utilisés pour formuler des produits de contraste radio-opaques, de nombreux autres éléments tels que le thorium, le tantale, ou encore le plomb ont été employés mais leur utilisation a rapidement été interdite en raison de leur toxicité et de leurs effets secondaires sur l'Homme. Actuellement, les produits iodés sont les plus utilisés en tant que produits de contraste injectables par voie intraveineuse pour l'imagerie de l'abdomen et de ses organes ou tissus mous. La radiographie est évidemment beaucoup employée pour l'imagerie des os puisque ces derniers sont très facilement visibles

sans qu'un agent de contraste soit administré. Pour le tube digestif, des suspensions orales de sulfate de baryum sont généralement utilisées. Toutefois, le problème majeur des produits iodés réside dans leur profil pharmacocinétique indiquant une très faible rétention dans la zone où ils se sont accumulés et une rapide élimination. Cette rapide excrétion est due à leur caractère hydrosoluble qui les rend très solubles dans la circulation sanguine et donc facilement filtrés par les reins, soit excrétés par clairance rénale. La rapide élimination du produit de contraste requiert alors l'injection de doses importantes qui peuvent générer une toxicité rénale et des néphropathies. D'autres effets secondaires sont également notables : allergies à l'iode, nausées, rougeurs et plaques cutanées, maux de tête, dysfonctionnements de la thyroïde, problèmes cardiovasculaires, etc. Le second problème récurrent est l'osmolalité et la viscosité, souvent élevées, qui rendent l'injection inconfortable. De nouvelles solutions émergent pour surmonter les problèmes actuels des produits iodés. Ces derniers concernent notamment le domaine des nanotechnologies et de la nanomédecine.

L'IRM est aussi une modalité d'imagerie très prisée car elle est plus précise et offre la possibilité de travailler selon deux contrastes : par blanchissement (IRM en pondération T1) ou par assombrissement (IRM en pondération T2) des zones d'intérêts. De plus, elle permet bien souvent de compléter les données obtenues par imagerie à rayons X. Son coût plus important la place après le scanner à rayons X en termes de choix d'utilisation. Son développement est également plus récent mais son fonctionnement et principe sont bien plus complexes que le scanner à rayons X. Très semblable à la résonance magnétique nucléaire des protons, l'IRM repose sur les phénomènes de relaxations des protons des molécules d'eau présentes dans le tissus du corps humain pour permettre la distinction d'un tissu par rapport à un autre. Chaque tissu a sa propre densité due à sa nature (cellules, fluides, composition, densité, etc.) qui lui est propre. Ainsi, pour un tissu donné, tous les protons se trouveront dans un environnement spécifique au tissu en question. Par conséquent, deux tissus différents mais adjacents auront un contraste par IRM qui leur est propre. Les produits de contraste utilisés en combinaison avec l'IRM sont à séparer en deux catégories du fait de la possibilité de réaliser des images IRM en pondération dite T1 ou T2.

L'IRM en pondération T1 qui produit un contraste positif en hypersignal (blanchissement de la zone d'intérêt) se base sur la mesure du temps de relaxation de protons selon l'axe z tandis qu'en pondération T2, qui génère un contraste négatif en hyposignal (noircissement de la zone d'intérêt), l'estimation du temps de relaxation se fait selon le plan xy. On parlera, respectivement, de relaxation longitudinale et transverse pour l'IRM en pondération T1 et T2.

Les substances utilisées pour l'IRM en pondération T1 sont principalement des complexes paramagnétiques tels que les chélates de gadolinium (Gd^{3+}) et vont favoriser l'amélioration du contraste des fluides interstitiels, la barrière sang-cerveau et dans certains cas celui du foie et de quelques organes du tube digestif. La chélation du gadolinium est nécessaire afin de contenir la toxicité de l'élément par une efficace stabilisation sous forme de complexe. Toutefois, ces substances sont très peu recommandées pour les patients atteints de défaillance rénale car une complication chronique, la fibrose nephrogénique systémique, pourrait se développer. Quelque autres effets secondaires sont également ressentis tels qu'une sensation de nausées, des maux de tête, une sensation de froid, de l'inconfort à l'injection, ou encore des vertiges.

L'IRM en pondération T2 requiert l'administration de produits superparamagnétiques comme des nanoparticules d'oxyde de fer. Ces nanoparticules s'accumulent de manière prédominante dans certains tissus selon leur taille. De façon concise, cela permet de cibler bon nombre d'organes et glandes d'un organisme tels que le foie, la rate, les ganglions lymphatiques, et la moëlle épinière par exemple. De par leur très faible dimension, les nanoparticules d'oxyde de fer permettent d'imager les organes du système réticuloendothélial car elles subissent une rapide séquestration par les cellules hépatiques, les cellules de Kupffer, et les macrophages. Bien que ceci semble être un atout, cette séquestration n'est en réalité que la première étape menant à l'excrétion des oxydes de fer par opsonisation. Actuellement un sujet est encore source de débats et concerne le devenir *in vivo* des nanoparticules d'oxyde de fer. Bien que ces nano-objets soient très efficaces et déjà introduits dans des formulations commercialisées de produits de contraste, l'impact des nanoparticules avant dégradation reste un sujet soulevant des interrogations. Les quelques effets secondaires relevés suite à l'utilisation de tels produits commercialisés sont de l'hypotension, des douleurs lombaires et des jambes, de la vasodilatation et, dans de rares cas, de la paresthésie.

Besoins actuels : comment y répondre et que faut-il prendre en compte pour cela ?

Afin de faire évoluer les produits de contraste pour surmonter les actuelles limites de ceux disponibles en clinique, de nombreux progrès ont rapidement été faits dans le domaine de la nanomédecine impliquant l'application de nanoparticules dans le domaine médical. Plusieurs facteurs ont conduit peu à peu au concept d'utilisation de nanotechnologies dans domaine de la santé comme le résume le Tableau 2 :

Tableau 2 : Résumé des problèmes et des considérations à prendre en compte pour l'évolution des produits de contraste vers les nanotechnologies applicables à l'Homme.

Problèmes et considérations	Solutions apportées par les nanotechnologies
Les produits de contraste à l'échelle clinique	
1) Les substances iodées sont trop rapidement éliminées du torrent sanguin, des importantes doses doivent alors être administrées ce qui provoque de sévères effets indésirables sur la santé ; 2) L'IRM et ses produits semblent une bonne alternative mais elle reste la seconde modalité utilisée vis-à-vis du scanner à rayons X car il est moins coûteux et plus rapide à l'acquisition ; 3) Les progrès à envisager concernent l'optimisation des produits de contraste pour la radiographie.	Les nanoparticules peuvent transporter et protéger des substances biologiques actives, comme des traitements ou des agents de contraste, et rester accumulées de manière prolongées ; De nombreux matériaux biocompatibles sont disponibles pour formuler des nanoparticules non-toxiques et tolérables pour un organisme vivant.
L'optimisation à l'échelle préclinique	
1) Faire évoluer la recherche à l'échelle clinique requiert la réalisation de travaux en amont c'est-à-dire au niveau préclinique sur de petits animaux de laboratoire ; 2) Le travail sur des animaux de laboratoire exige, évidemment, que les animaux soient bien traités (conditions de vie et de santé, traitements et manipulations réalisés en veillant à assurer et à respecter le bien-être de l'animal) et l'adaptation des outils à leur échelle ; 3) Adapter les outils à la souris induit l'usage de scanners précliniques et de sondes adaptées capables de générer un contraste suffisant, soit des sondes avec un temps de rétention long, une accumulation locale et une concentration suffisante en élément de contraste permettant d'administrer un volume compatible (10% de la volémie maximum) avec le volume du compartiment sanguin d'une souris.	Les nanoparticules peuvent concentrer une quantité relativement importante en substance active compte tenu de leur dimension ; La taille des objets leur permet de circuler dans les vaisseaux sans produire d'embolisation ou d'être trop rapidement éliminés ; Elles peuvent être fonctionnalisées en surface pour cibler un tissu et y rester.

Bien que les nanoparticules semblent être une alternative prometteuse à l'échelle clinique et très utile pour progresser à l'échelle préclinique, l'extrapolation vers l'Homme reste sujette à débat puisque le devenir des nanoparticules *in vivo* est encore incertain aujourd'hui, notamment celui des nanoparticules inorganiques ou « rigides ». Certains produits de contraste mais aussi certains agents thérapeutiques du marché sont déjà formulés sous forme de systèmes nanoparticulaires comme par exemple le Doxil®, à base de liposomes encapsulant la doxorubicine, ou encore les produits de contraste iodé Fenestra® sous forme d'émulsion, qui ont reçu l'autorisation de la FDA, l'organisation américaine « Food and Drug Administration » en charge de la protection de la santé publique par la régulation des produits alimentaires, vétérinaires, médicaux, cosmétiques et du tabac. En outre, les nanoparticules

employées à des fins biomédicales peuvent être multifonctionnelles et transporter plusieurs types de substances actives comme un, deux voire trois agents de contraste (multimodalité) et un agent thérapeutique. Cette multifonctionnalité constitue un des plus importants atouts des nanoparticules puisqu'elles offrent de par leur versatilité un très large panel d'applications qui s'étend de l'imagerie médicale unimodale ou multimodale à la discipline dite de théranostique (contraction de thérapie et de diagnostic) par l'incorporation de sondes et d'agents thérapeutiques.

Les nanoparticules en tant que sondes idéales pour l'imagerie

Pour obtenir des agents de contraste nanoparticulaires, plusieurs conditions, regroupées dans le Tableau 3, sont à réunir afin de générer une sonde sûre et efficace.

Tableau 3: Conditions à remplir quant aux paramètres influençant le comportement *in vivo*, la pharmacocinétique et la biodistribution de sondes nanoparticulaires.

Paramètres	**Conditions**
Composition	Biocompatible, non-toxique, biodégradable/excrétable, sous-produit(s) non toxique(s), inerte vis-à-vis des tissus
Taille (∅)	- Nanoparticules rapidement excrétées par clairance rénale : ∅ < 20 nm - Nanoparticules accumulées et retenues dans les tissus : 50 nm < ∅ < 200 nm (gamme optimale) - Nanoparticules sujettes à une rapide opsonisation : 150 nm < ∅ < 300 nm - Nanoparticules générant des embolisations : 200-300 nm < ∅ - Nanoparticules sujettes à l'extravasion (tissus tumoraux*) : 200 nm < ∅ < 600 nm
Forme	Pas de restriction particulière, paramètre peu documenté, potentiel impact sur la biodistribution dû à des différences dans les interactions avec les entités biologiques
Surface	Neutre, hydrophile et conjuguée par des ligands/macromolécules de type poly(éthylène glycol) pour générer des propriétés de furtivité (ciblage passif) pour éviter l'absorption de protéines du plasma menant à l'opsonisation, et, au besoin, des agents de ciblages (anticorps, protéines, vitamines, peptides, aptamères) (ciblage actif) pour cibler spécifiquement un tissu
Contraste	Concentration élevée en éléments à l'origine du signal, rapport massique en éléments contrastant important par rapport à la structure sur laquelle il est lié
Stabilité	Stabilité colloïdale, chimiquement stable en milieu physiologique, encapsulation efficace des substances actives incorporées à l'assemblage nanométrique

*Les tissus tumoraux sont des tissus à la structure complexe (zone nécrotique, hémorragique, vascularisation anarchique) et présente un réseau vasculaire défectueux très perméable menant à l'extravasation (« fuite ») des nanoparticules lorsqu'elles sont en circulation dans le sang vers le tissu tumoral et à leur rétention. Ceci est décrit par l'effet de perméation et de rétention augmentées (de l'anglais « enhanced permeation and retention effect » souvent mentionné « EPR effect » dans la littérature).

Les différents types de nanoparticules

La littérature recense un grand nombre d'objets nanoparticulaires pouvant servir de véhicules à des substances actives telles que des agents de contraste et/ou des agents thérapeutiques. Ces nano-véhicules ont la possibilité, comme indiqué dans le Tableau 3 précédent, d'être le résultat d'une conception polyvalente et versatile adaptable à l'application visée. Quelques restrictions sont bien évidemment à respecter notamment au niveau de la composition et de la taille afin de ne pas générer d'effets indésirables sur la santé de l'être vivant recevant une injection de suspension colloïdale.

Les systèmes nanoparticulaires les plus courants peuvent être regroupés selon deux familles : les nanoparticules lipidiques et polymériques (souples ou rigides) et les systèmes hybrides tels que les nanocomposites (organiques et inorganiques). Il est à noter que toutes particules impliquées dans des applications *in vivo* devront être dotées de propriétés de furtivité, qui sont générées par des polymères. Par conséquent, mêmes les nanoparticules principalement inorganiques (cœur) seront recouvertes ou fonctionnalisées par un composé organique hydrophile. Chaque assemblage possède ses propres atouts et limites pour l'application biomédicale telle que l'imagerie médicale. Ainsi, on recense les nano-systèmes suivants :

. Nanoparticules lipidiques et polymériques: liposomes, nano-émulsions, dendrimères, lipoprotéines, nanoparticules de polymères, nanocapsules, micelles polymériques ;

. Systèmes hybrides ou nanocomposites : complexes ou chélates, encapsulation de nanoparticules inorganiques dans un milieu lipidique, systèmes cœur organique/couronne inorganique.

L'ensemble des informations présentées ci-dessus représente un résumé du chapitre I (« **Chapter I – Introduction** ») de ce manuscrit. Dans le cadre de cette thèse, deux types de nanoparticules ont été étudiés, le premier dédié à l'imagerie à rayons X et le second à l'imagerie multimodale rayons X/IRM.

Élaboration de nanoparticules de polymères iodés pour l'imagerie à rayons X

Pour le scanner à rayons X, des nanoparticules solides de polymères hautement chargées en iode ont été élaborées en tant que produit de contraste injectable et radio-opaque. Nous nous sommes ainsi intéressés à la polymérisation radicalaire par activation thermique du peroxyde de benzoyle d'un monomère, le 2,3,5-triiodobenzoate de 2-méthacryloyloxyethyle (MAOTIB), issu de la modification par estérification entre le méthacrylate de 2-hydroxyléthyle et le chlorure de 2,3,5-triiodobenzoyle (lui-même issu d'une réaction d'acylation). Le polymère poly(MAOTIB) (Tg=65°C, Mn=2.761 10^5 g/mol (Mw/Mn = 1.968)) ainsi synthétisé a déjà été étudié dans la littérature mais a principalement été produit par polymérisation en dispersion et sous forme de copolymère.

Dans le cadre de cette étude, nous proposons de synthétiser le poly(MAOTIB) en masse puis de le nanoprécipiter en présence du Kolliphor ELP® Castor Oil PEG-35 afin de pouvoir contrôler la taille des particules de polymères en fonction des paramètres de formulation. Le principal compromis était de trouver la quantité optimale de polymère, c'est-à-dire la quantité en élément iodé servant de source de contraste sous rayons X, et la gamme de taille de nanoparticules compatible avec l'administration par voie intraveineuse et l'application sur le modèle de la souris. Il est à noter que plus la concentration en polymère et donc en iode est élevée dans un échantillon, plus la distribution de tailles des nanoparticules est large. Par conséquent, il était nécessaire de contrôler cet effet par l'usage d'un agent tensio-actif. Notre choix s'est porté sur un agent de surface PEGylé afin que les nanoparticules bénéficient de propriété de furtivité et aient une surface hydrophile favorisant leur dispersion en milieux aqueux telle que dans la circulation sanguine. Différents rapports massiques polymère-agent tensio-actif ont alors été testés de sorte que trois familles de concentration en iode fixe (six échantillons par famille pour lesquels étaient associés une quantité d'agent tensio-actif) ont été préparées. Les suspensions colloïdales finales de polymère iodé avaient une concentration finale théorique en iode allant de 15,5 mgI/mL (PNPs-1), 31,0 mgI/mL (PNPs-2) à 62,0 mgI/mL (PNPs-3). Les quantités d'agent tensio-actif s'élevaient à 30, 40, 50, 60, 70 et 80 %m (pourcentage massique) par rapport au polymère.

Dans la mesure où la radio-opacité est directement reliée à la quantité en élément lourd absorbant les rayons X, ici l'iode, il était à prévoir que l'efficacité des familles d'échantillons serait croissante de PNPs-1 à PNPs-3. Cependant, il a été possible de produire des suspensions dont les tailles varient respectivement pour PNPs-1, PNPs-2 et PNPs-3 de 178±3,5 à 137±3,5 nm, 183±2,9 à 142±2,1 nm et 184±5,6 à 153±3,9 nm (par diffusion dynamique de la lumière). Sachant que nous visions de formuler des suspensions hautement

chargées en iode, les formulations de PNPs-3 étaient déjà les plus prometteuses. Qui plus est, l'administration de nanoparticules *in vivo* requiert de ne pas excéder 200 nm afin de ne pas générer d'embolisation. Aux vues des tailles, nous avons pu conclure que PNPs-3 fournissaient des échantillons dont les distributions des tailles étaient en-dessous de cette limite. Nous avons donc sélectionné parmi les échantillons de PNPs-3 l'échantillon formulé avec 60 %m d'agent tensio-actif (163,7±2.1 nm, PDI 0,09) car au-delà de cette quantité, l'effet de l'agent tensio-actif sur le profil de taille n'était plus significatif par rapport à la quantité d'agent tensio-actif utilisée. Cette suspension a fait l'objet de différentes analyses :

. de la microscopie électronique à balayage pour évaluer la morphologie qui a révélé la présence de nanoparticules sphériques et homogènes ;

. un dosage de l'iode (59 mgI/mL) par détermination de l'atténuation des rayons X générée par la suspension et par comparaison à celle d'un produit de contraste commercial utilisé comme calibration ;

. des tests de stabilité plasmatique dans le sérum afin de vérifier l'absence de formation d'agrégats ou de dégradation des particules une fois mises en contact avec les conditions simulant le sang (dilution, température, agitation, pH, présence de protéines du plasma) ;

. des tests *in vitro* sur cellule pour estimer les interactions des nanoparticules pour des cellules de type KB : aucune internalisation ne s'est produite, les nanoparticules avaient un potentiel zêta de -30 mV ce qui ne favorisait pas leur absorption sur la membrane également chargée négativement des cellules, les interactions ont donc été non-spécifiques ;

. des tests *in vivo* sur 3 souris Swiss qui ont reçu une dose correspondant à 10% de leur volémie : aucun signe négatif sur la santé des souris n'a été détecté suite à l'administration de l'agent de contraste, un suivi sur 4 jours a montré que le produit s'accumulait dans le foie et majoritairement dans la rate de par l'atténuation des rayons X plus importante pour cet organe, les tissus étaient parfaitement distingués des autres tissus mous et ce, 1h après injection jusqu'à la fin du suivi des animaux.

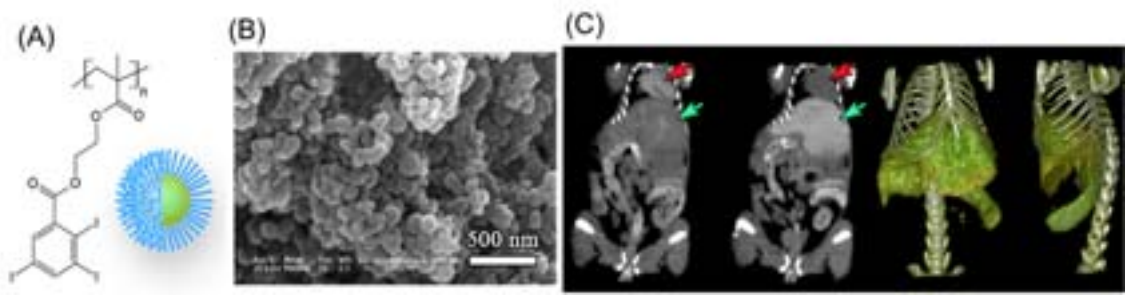

Figure 1: (A) Représentations schématiques du polymère synthétisé et du type de nanoparticule formulée, (B) visualisation par microscopie électronique à transmission des nanoparticules de polymère iodé et (C) essais *in vivo* par imagerie à rayons X.

Actuellement, l'ensemble des données collectées ont été regroupées afin de constituer un premier article qui a été soumis au journal Acta Biomaterialia (facteur d'impact 6,3). Nous attendons actuellement le retour de l'éditeur. L'article est présenté au chapitre II (« **Chapter II - Radiopaque polymeric nanoparticles for preclinical X-ray imaging** ») de ce manuscrit.

Élaboration de nanoparticules bimodales pour l'imagerie à rayons X et l'IRM

Pour introduire cette étude traitant de l'utilisation de nanoparticules magnétiques en tant que produit de contraste pour l'IRM en pondération T2 (« **Chapter III.2 - Magnetite and iodine-containing nano-emulsion as contrast agent for X-Ray/MR imaging** »), une revue bibliographique sur les nanoparticules d'oxyde de fer de type magnétite est présentée en amont de cette étude. Cette revue bibliographique constitue le chapitre III.1 (« **Chapter III.1 - Initiation to magnetite nanoparticles for *in vivo* uses** ») de ce manuscrit. Les travaux effectués sur le projet qui suit sont donc ainsi repris en détail dans le chapitre III.2 de ce manuscrit et ce, sous la forme d'un article à la suite de la revue bibliographique introduite ci-dessus.

Des nano-émulsions bimodales ont été formulées en synthétisant des nanoparticules d'oxyde de fer superparamagnétiques (SPIONs) de type magnétite Fe_3O_4 par décomposition thermique et en modifiant la vitamine E (α-tocophérol) par greffage d'un groupement aromatique triiodé par estérification.

Les nanoparticules de magnétite ont été produites en adaptant une procédure à haute température. L'impact du temps de réaction (2h, 4h ou 6h) sur leurs morphologies a été étudié. En effet, les propriétés magnétiques découlent non seulement de la composition des nanoparticules mais aussi de leur taille et de leur forme. Ainsi, afin de générer le meilleur contraste en IRM en pondération T2, nous avons choisi de synthétiser des SPIONs de morphologies différentes à partir d'une composition identique du milieu réactionnel. La présence de ligands lipophiles (oléylamine et acide oléique) ont permis de contrôler la croissance des SPIONs et de former des nanoparticules dotées d'une surface lipophile, parfaitement adaptées à leur dispersion dans une huile telle que la vitamine E iodée utilisée

comme phase interne des nano-émulsions bimodales. Les différents lots de SPIONs synthétisés pendant 2h (SPIONs 2h), 4h (SPIONs 4h) et 6h (SPIONs 6h) ont fait l'objet de caractérisations physico-chimiques :

. une observation par microscopie électronique en transmission pour identifier le type de morphologie et la gamme de tailles de chaque lot : les SPIONs 2h et SPIONs 6h étaient sphériques et d'une taille allant respectivement de 5 à 7 nm et de 7-10 nm tandis que les SPIONs 4h constituaient un lot intermédiaire et possédaient des SPIONs de taille de 4 nm à 10 nm et de forme anisotrope ;

. un dosage du fer par relaxométrie afin de connaître avec précision la composition des SPIONs : les SPIONs 2h, 4h et 6h possédaient respectivement 55,44 %m Fe (soit 44,56 %m de ligands), 56,86 %m Fe (soit 43,14 %m de ligands) et 46,28 %m Fe (soit 53, 72 %m de ligands) ce qui indiquait que l'accumulation de ligands était également liée au temps de réaction et que les SPIONs 4h présentaient la meilleure teneur en élément magnétique (les propriétés magnétiques devraient être supérieures pour ce lot);

. de la diffraction des rayons X pour confirmer le type magnétite Fe_3O_4 des SPIONs : du fait de la très petite taille des SPIONs, une très grande surface spécifique est disponible et en raison de la grande sensibilité de la magnétite à l'oxydation par l'air une fine couche de maghémite (γ-Fe_2O_3, forme oxyde de la Fe_3O_4) a été détectée ;

. de la spectroscopie infrarouge à transformée de Fourier qui a permis de corroborer ce qui a été vu par diffraction des rayons X sur la composition des SPIONs mais aussi sur la présence des ligands lipophiles en C18 adsorbés en surface des SPIONs.

La vitamine E iodée a été synthétisée par une procédure d'estérification en milieu organique. Cette huile s'est avérée particulièrement intéressante puisqu'elle était hautement chargée en iode (41,7 %m d'iode) et facilement émulsifiable par émulsification spontanée. De plus, elle favorisait la dispersion des SPIONs et fournissait des nano-émulsions bimodales très stables et à la distribution de tailles adaptée à l'administration par voie intraveineuse. De nouveau, le Kolliphor ELP® Castor Oil PEG-35 a été utilisé pour conférer des propriétés de furtivité, d'hydrophilie et de stabilité pour le milieu physiologique aux nano-gouttelettes.

Les nano-émulsions ont donc été comparées quant à différents critères afin de déterminer la plus optimale pour des essais *in vivo*. Il est à noter que chaque nano-émulsion radio-opaque et magnétique a été formulée en respectant les mêmes proportions soient : 0,28 %m de SPIONs, 23,72 %m de vitamine E iodée, 16 %m d'agent tensio-actif et 60 %m de phase continue (pH

7,4) afin de les discriminer uniquement sur leurs propriétés de contraste. Les 3 suspensions ont donc été étudiées comme suit :

. par diffusion dynamique de la lumière pour définir la taille des nano-gouttelettes : les valeurs de diamètres moyens suivants 60,65±0,18 nm, 57,86±0,35 nm et 62,16±0,64 nm (respectivement pour les nano-émulsions encapsulant les SPIONs 2h (NE-SPIONs 2h), 4h (NE-SPIONs 4h) et 6h (NE-SPIONs 6h)) ont été obtenus et indiquent que les nano-émulsions étaient similaires en termes de taille;

. par microscopie électronique à transmission pour observer l'organisation des SPIONs et de l'huile iodée qui a réussi à confiner les SPIONs dans le cœur des nano-gouttelettes ;

. des tests de stabilité dans le sérum sanguin afin de vérifier l'absence de formation d'agrégats ou de dégradations des particules une fois mises en contact avec les conditions simulant le milieu sanguin (dilution, température, agitation, pH, présence de protéines du plasma) ;

. par relaxométrie (1,41T) pour définir les paramètres de relaxivités (r2 et r1) qui permettent d'évaluer les propriétés des substances à être de bons produits de contraste pour l'IRM *via* le rapport r2/r1. En raison d'une morphologie différente, les SPIONs 4h ont permis de formuler une nano-émulsion avec le rapport r2/r1 le plus intéressant (r2/r1(NE-SPIONs 4h)=16,00 contre r2/r1(NE-SPIONs 2h)=12,51 et r2/r1(NE-SPIONs 6h)=14,27) faisant de la nano-émulsion le meilleur candidat pour l'IRM.

Suite à ces observations, la formulation NE-SPIONs 4h a fait l'objet de tests *in vivo* sur 5 souris Swiss pour des tests d'imagerie par IRM et par scanner rayons à X. Les résultats ont indiqué que les souris supportaient très bien le produit (administré à 10% de leur volémie). Par ailleurs, une accumulation massive dans le foie a été constatée 5h après injection de par un fort contraste de ce tissu visualisé par IRM. Les reins ont aussi été très clairement observés indiquant que des nano-gouttelettes se sont aussi distribuées dans ce compartiment. Les essais sur scanner à rayons X des mêmes animaux à 24h après injection ont aussi permis de mettre en évidence le foie et la rate dont le contraste en IRM ne pouvait pas être considéré comme significatif compte tenu de l'hétérogénéité du tissu par observation par IRM. Cependant, les reins n'ont pu être observés par cette modalité d'imagerie laissant comprendre que les nano-gouttelettes ont dû être altérées dans la partie filtrante des reins conduisant à l'élimination de l'huile iodée et à l'emprisonnement des SPIONs 4h dans les tissus des reins. Ceci nous a permis de conclure que le produit injecté peut être distribué dans le foie sans générer d'effet néfaste sur la santé des modèles vivants étudiés, que son accumulation produit un contraste

très important pour les deux modalités dans ce tissu et qu'il peut être éliminé partiellement par l'organisme par voie rénale.

La Figure 2 ci-après représente schématiquement les objets nanométriques développés et formulés durant ce projet de recherche, les effets *in vivo* en termes de contraste générer suite à l'administration de la NE-SPIONs 4h sont également fournis.

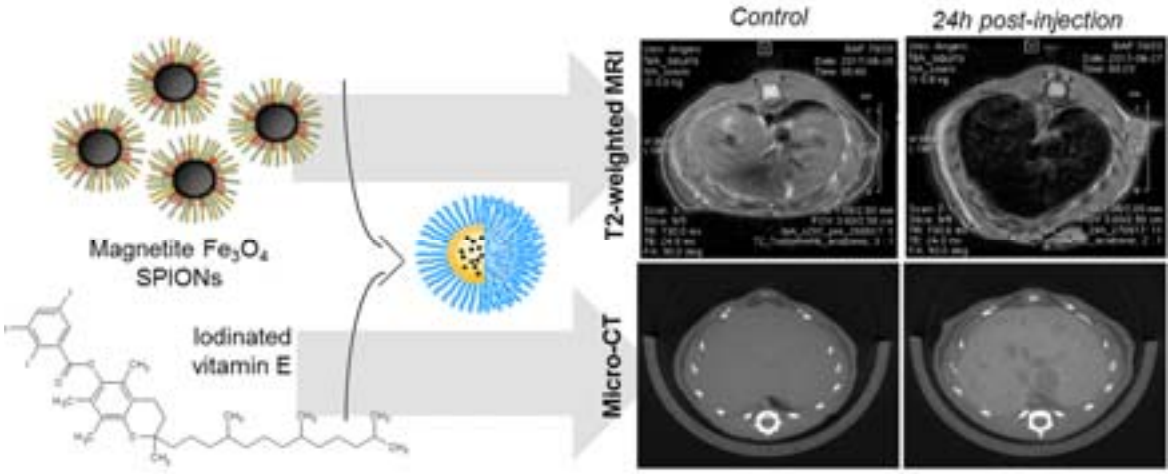

Figure 2 : (Gauche) Description du système nanoparticulaire développé (NE-SPIONs 4h) incluant de la vitamine E iodée et des SPIONs 4h. (Droite) Visualisation par IRM en pondération T2 et par imagerie à rayons X (Micro-CT) du contraste produit à différent temps après l'administration de NE-SPIONs 4h.

A ce jour, il est envisagé de compléter les résultats par des tests *in vitro* afin d'évaluer l'interaction des NEs-SPIONs 4h avec des cellules comme celles du foie et de la rate. En outre, les tissus dont le contraste a été significatif ont été prélevés et feront l'objet d'un dosage d'iode et de fer pour évaluer la dose présente dans les tissus.

Travaux parallèles

Une troisième étude de formulation a été réalisée et consiste à préparer des nanoparticules magnétiques et de polymères par une technique de microfluidique permettant de faire *in situ* et en simultanée l'encapsulation de SPIONs durant la polymérisation d'un polymère. Ces travaux de recherche ont été soumis au journal Langmuir.

Deux revues bibliographiques ont aussi été rédigées. La première a pour but de présenter les différents nano-véhicules (de l'anglais « nanocarriers ») comme plate-forme nanoparticulaire pour le relargage de substances actives telles que des agents thérapeutiques. Ce travail a été soumis à Expert Opinion on Drug Delivery. La seconde revue bibliographique

a été consacrée à la présentation des différentes nanoparticules inorganiques dédiées à l'imagerie à rayons X. Cet écrit a été soumis à Critical Review. Bien que ces deux revues bibliographiques ne soient pas fournies dans ce manuscrit, ces écrits ont permis de réaliser des recherches bibliographiques très approfondies sur le domaine des nanoparticules appliquées au domaine biomédical.

Les résumés de ces travaux de rédaction et de recherches introduits ci-dessus sont regroupés en annexe (« **Appendices - Additional research works and scientific contributions** ») de ce manuscrit.

En annexes sont également fournies la liste des présentations sous forme de communication orale et/ou poster en congrès des projets de recherches et la liste des publications scientifiques réalisées durant ce travail doctoral.

General introduction

General introduction

The present manuscript aims at providing scientific achievements made during this PhD in chemistry. The first chapter **(Chapter I – Introduction)**, is outlining a general bibliographical background required to begin studies about elaborations of nanoparticles as contrast agent for X-ray imaging and bimodal imaging (X-ray imaging/magnetic resonance imaging). Main points presented in this chapter are introduced below to introduce to the field of study and to provide keys to understand research directions chosen in next chapters.

Since several decades, biomedical imaging became an essential tool in clinics to get a visualization of the inside of human body without surgery for non-invasive diagnostic ends. Current imaging techniques allow to evaluate the general state of health of a patient by establishing a diagnostic by means of observation of tissues and biological fluids, evaluation of organs function(s), their anatomy, their morphologies and their potential dysfunctions and pathologies such as benign or malignant tumors. Imaging is even more exploded because it is not anymore a tool only dedicated to diagnosis but also to perform treatment efficacy follow-up to help to manage disease treatment strategy. Two-dimensions and/or three-dimension reconstructed images are consequently an important support to set up diagnostics, estimate disease progression, treatment efficacy and plan treatment strategy.

Combination of imaging instrument with contrast enhancer pharmaceutics is a key to obtain accurate images of a desired tissue. By accumulation of a contrast agent into a specific target allows to see its internal structure compared to surrounding tissues. Soft tissues have generally similar contrast; a clear delineation of each is as a result difficult depending on the imaging modality used. To date, there are five prime imaging modalities with their own assets and limitations: i) X-ray scanner or X-ray computed tomography scanner (X-ray CT), related to the radiography, ii) magnetic resonance imaging (MRI), iii) optical imagers corresponding to fluorescence and bioluminescence preclinical imaging, iv) positron emission tomography (PET) and single photon emission computed tomography (SPECT) imagers for the nuclear imaging field and v) ultrasound imaging instrument. This range of modalities is in fact really useful because it represents a range of options among which a modality can be picked depending on what we are seeking for by imaging (target, scale, accuracy need) and the patient health. Besides, owing to their inherent differences, they are quite complementary and their data can be correlated, interlaced and/or confirmed by each other information. This

complementary is at the origin of multimodal imaging consisting in using two or three modalities to image a target in order to obtain a complete insight of human body.

The two main imagers among all abovementioned instruments are the X-ray scanner and the MRI. X-ray CT is the oldest method: it is cost-effective, fast to acquire high resolution images (spatial resolution 50-200 µm) and available in clinics. MRI is however more accurate because it can provide anatomical and physiological *in vivo* information like the X-ray scanner does but also functional information and its spatial resolution is higher (25-100 µm). Furthermore, it does not induce patient radiation unlike the X-ray CT. It should be noticed that imaging procedure is not usually performed on a given patient several times over a short period in order to avoid radiation exposure. However, since MRI is also more expensive, X-ray CT is the predominant instrument applied to image a patient in clinic.

Typically, low-molecular weight hydrosoluble iodinated molecules are used as injectable contrasting material for radiography of vasculature, organs (brain, liver, spleen, kidney and gallbladder) spinal canal (spine, lumbar, thoracic and columnar zones and disks), urinary track, uterine track and their related pathological tissues. Gastrointestinal track is mostly imaged by means of oral administration of barium sulfate suspension. Contrast enhancement by X-ray CT relies on ability of dense materials in human body to attenuate by scattering, diffracting or reflecting the X-ray beam emitted from the instrument towards the specimen. Basically bones which are mineralized materials are dense in electron and appear by brightening on images whereas biological fluids and air seem dark. Soft tissues exhibit similar capacity to attenuate X-ray and appear by gray scale on engineered images. For these tissues, contrast agent, defined as radiopaque contrasting probe, is necessary. The main drawback of formulation containing iodinated molecules is their physico-chemical properties, like their high viscosity and their high osmolality, and the hydrosoluble character of iodinated molecules. Water-soluble molecules are quickly eliminated by renal clearance; high dose of contrast agent is consequently administrated to patient causing in some cases renal failure, nephropathy and cardiovascular issues.

The MRI is based on nuclear magnetic resonance principle and aims at measuring signal of protons from water molecules located in human body tissues. By applying large magnetic field B_0 and radiofrequence sequence pulses, protons from tissues are subjected to spin flipping from z-axis to xy-plan. Once radiofrequence sequence pulses are ended, magnetic moments relax and process to get back aligned along z-axis (*i.e.* along B_0). Relaxation signals

from protons can be divided up into two phenomena: the longitudinal relaxation and the transverse relaxation. MRI can consequently be related to one single relaxation phenomenon which means that it can be performed T1-weighted MRI based on the measurement of longitudinal relaxation time (T1) or T2-weighted MRI based on the measurement of the transverse relaxation time (T2). Respectively, T1-weighted MRI and T2-weighted MRI yield brightening or positive contrast (hyperintense signal) and darkening or negative contrast (hypointense signal) on their respective reconstructed images.

Two families of contrast agents are dedicated to T1-weighted MRI and T2-weighted MRI. T1-weigthed MRI involves paramagnetic gadolinium chelates to promote mainly contrast enhancement of biological fluids and interstitial spaces. Disruption of blood-brain barrier is one the most common lesion imaged *via* T1-weighted MRI. For safety concerns, lanthanide such as gadolinium must be chelated in order to cut down inherent toxicity. Complexes are basically a stable assembling made with ligands or chelates as outer corona surrounding the contrasting paramagnetic core. T2-weigthed MRI needs superparamagnetic formulations, generally made of iron oxide nanoparticles with polymeric coating to render them hydrophilic and compatible with the physiological conditions. Their bioaccumulation is size-dependent and aim at imaging various organs by their specific biodistribution. Most of organs and tissues from the reticuloendothelial system like liver, spleen and lymph nodes are easily contrasted because of premature opsonization of iron oxide nanoparticles.

Compared to X-ray CT contrast agents, MRI contrast agents are much less suffering from important issues, few side effects can still be pointed out as for most of pharmaceutics. Consequently, there is a current need to improve radiopaque contrast agents since X-ray scanners are the main devices used in clinics as abovementioned. More and more, nanotechnologies are taking part in medicine, more precisely in a new field named nanomedicine. Thereby, nanoparticulate systems are nowadays widely present in literature for a lot of biomedical applications and are described as multifunctional owing to their versatile and tunable characteristics. So, not only nanotechnologies seem to be an outstanding platform for medical purpose but also because they match perfectly for preclinical research on small laboratory animals due to their nano-sized dimension. The Table 1 sums up main needs to enhance preclinical and clinical probes and how nanotechnologies are able to fulfill those needs.

Table 1: Needs and solutions provided by nanotechnologies for the preclinical and clinical research.

	Current considerations and needs	Solutions provided by nanotechnologies
Clinical contrast agents	1) Iodinated substances are quickly excreted from bloodstream, high doses have to be administrated and may cause severe side effects on health; 2) MRI and its associated contrast agents seem an interesting alternative but the instrument and its use are expensive compared to X-ray CT; 3) Innovations are thus focused on radiography contrast agents.	Nanoparticles can carry, protect a cargo of active ingredients, such as therapeutics and imaging probes, and remain within a target for certain amount of time; Various biocompatible materials are available to formulate non-toxic and innocute nanoparticles for organism.
Preclinical optimization	1) Preclinical research means working on small laboratory animal; 2) Using small laboratory animals require to ensure the welfare of animals and to adapt tools to animal scale; 3) Suitable tools correspond to preclinical imager, like X-ray micro-computed tomography scanner (micro-CT) and probes with a long-time retention, a local accumulation into a target area and high concentration of contrasting material in order to inject small volume (compatible with the blood compartment volume of the animal).	Nanoparticles can be loaded with high dose of active substances in respect to their nano-scale dimension; Their size leads nanoparticles to have extended circulation time in the bloodstream without causing embolization issues or being subjected to fast excretion; Nanoparticles surface can be functionalized to target a specific tissue (active targeting strategy) and to remain accumulated in it.

To introduce nanoparticles into biomedical applications, few items must be followed to produce innocute and efficient nanoparticles. Most of these items rely on the design and the composition of nanoparticulate systems as described in Table 2:

Table 2: Requirements to fulfill in order to produce ideal nanoparticulate probe for *in vivo* uses.

Parameters	Requirements on nanoparticles
Composition	Biocompatible, biodegradable if possible, non-toxic (nanoparticles and break-down products)
Size (∅)	50 nm < ∅ < 200 nm for optimal retention and located accumulation (no embolization issue, excretion postponed)
Shape	May impact interaction with biological entities due to differences of surface-to-volume ratio depends on the shape (spherical, rod, cylinder, cube, anisotrope)
Surface	Neutral (not positively or negatively charged), hydrophilic, conjugated by ligands/macromolecules such as poly(ethylene glycol) for stealth property (passive targeting) and to delay plasma proteins absorption leading to premature opsonization and targeting moieties (antibodies, proteins, vitamins, aptamers, peptides) to promote specific bioaccumulation
Contrast	High content of contrasting element to provide enough signal for contrast enhancement, weight ratio of contrasting element high in respect to the structure bearing it
Stability	Colloidal stability (steric barrier thanks to ligands), stable in physiological conditions, efficient encapsulation of active ingredient(s) within or onto the nano-scale assembly

Numerous kinds of nanoparticles can be formulated as contrast agent for imaging. Most of the time, nanoparticles can be described as nanocarriers since a double structure is involved: a

core as signal enhancer and a shell working as hindrance shield for the inner core. To date, we can identify the following nanoparticles and/or nanocarriers used as injectable convective transport of probe(s): liposomes, nano-emulsions, dendrimers, polymeric micelles, polymeric nanospheres, polymeric nanocapsules, lipoproteins and hybrids (nanocomposites, polymer-coated inorganic nanoparticles, chelates). It should be noted that lipid-based nanoparticles and/or nanocarriers (Figure 1) became very popular in literature owing to their versatility and the facility to make them suitable for *in vivo* application. It means that such probes can gather most of the abovementioned criteria from Table 2.

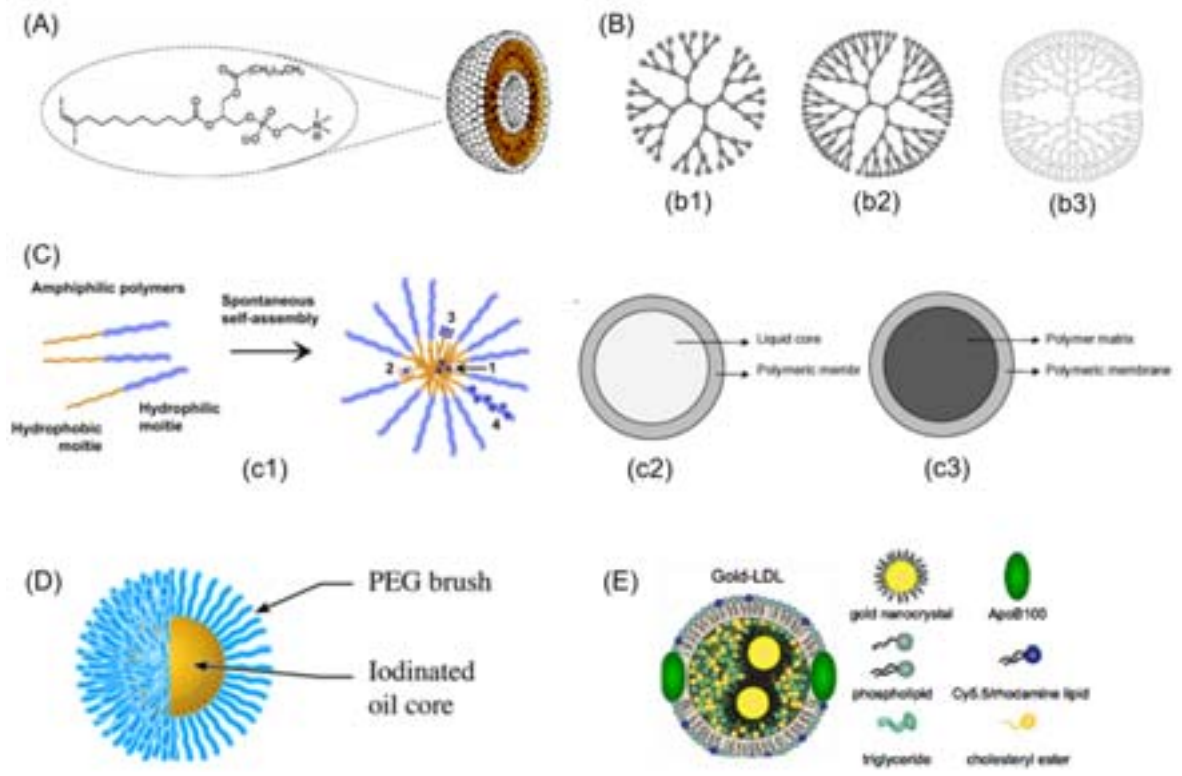

Figure 1: Summary of schematic chemical structures of nanocarriers used to formulation various probes for imaging purposes: (A) Iodine-grafted liposome (Iodoliposome); (B) dendrimers with (b1) 3, (b2) 4 and (b3) 5 generations of poly(amidoamine) polymer (PANAM) units; (C) three types of polymeric nanoparticles: (c1) polymeric micelles, (c2) polymeric nanocapsule and (c3) polymeric nanosphere; (D) iodine-containing nano-emulsion and (E) lipoprotein with gold nanoparticles loading and fluorescent dyes (Cys 5.5) attached onto the surface.

All of these nanoparticulate systems possess their own inherent advantages and limitations; this is why we chose in our studies to focus on two types of nanocarriers and nanoparticles. Furthermore, we were looking for producing alternative formulations to cope with current drawback of contrast agents on the market, like for those dedicated to X-ray imaging and also to provide innovating formulations for multimodal imaging.

The chapter II (**Chapter II - Radiopaque polymeric nanoparticles for preclinical X-ray imaging**) emphasizes the study of novel contrast agent for X-ray imaging based on stealth iodinated polymer-based nanoparticles. We selected here to involve rigid nanostructures with enhanced pharmacokinetic and biodistribution, in order to prevent iodine leakage from assembling and consequently ensure the iodine content carried *in vivo* and good contrast property. Colloidal polymeric nanoparticles (PNPs) have been reported as very suitable to fulfill those needs. Iodinated PNPs have been mentioned as highly stable construct capable of being delivered to site of interest and, consequently, as efficient CA kind. Here, we developed a new PNPs system from synthesis to characterization and *in vivo* imaging.

Iodinated homopolymer was formed by radical polymerization of 2-methacryloyloxyethyle 2,3,5-triiodobenzoate monomer. The as-prepared polymer was subjected to nanoprecipitation in presence of PEGylated surfactant to yield intravenously injectable radiopaque suspension based on hydrophilic PNPs. Impacts of polymer and surfactant weight ratio were studied to find the best compromise between suitable size for *in vivo* and iodine content for radio-opacity property. After discrimination of formulations, best PNPs formulation was characterized first by dynamic light scattering and scanning electron microscopy for size distribution and morphology investigations. The optimum radiopaque PNPs suspension chosen was based on spherical nanoparticles which had 163.7 nm narrow size distributions (PDI 0.09), stability properties over time and in plasma serum were both satisfying. *In vivo* micro-CT imaging on mice was run to follow biodistribution after intravenous administration. PNPs were spontaneously bioaccumulated in liver and spleen for which significant enhanced contrast was visible over a week, indicating very good retention of the contrast agent. The passive targeting strategy applied lead as a result to image *via* micro-CT soft tissues belonging to macrophage system. No side effects were observed on mice.

This work has been submitted to Acta Biomaterialia journal, we are looking forward to answering from them.

The chapter III (**Chapter III – Study and use of magnetite nanoparticles for biomedical applications**) is divided into two subcategories.

The chapter III.1 (**Chapter III.1 - Initiation to magnetite nanoparticles for *in vivo* uses**) is a bibliographical review presenting a state of the art of magnetite Fe_3O_4 iron oxide nanoparticles dedicated to biomedical applications. It outlines all aspects from the basic of

nanoparticles magnetism, so-called superparamagnetism, the synthesis and characterization of magnetite to its range of applications in nanomedicine.

Following this overview about magnetite iron oxide nanoparticles, we proposed a novel study on the use of magnetite-loaded radiopaque nano-emulsion as bimodal contrast agent for X-rays/MRI modalities in the chapter III.2 (**Chapter III.2 – Magnetite and iodine-containing nano-emulsion as contrast agent for X-Ray/MR imaging**). This project was carried out in order to propose a dual modal contrast agent in case of multimodality needs. As introduced before, conjecture of several imagers' information may furnish useful and complementary data about a target. In this study, we selected to produce contrast agents exhibiting radiopaque and magnetic properties to promote contrast enhancement for X-ray imaging and MRI.

Oil-in-water nano-emulsion (NE) is a lipid-based nanocarrier capable of being loaded with lipophilic ingredients in its oily inner core. We chose to use a radiopaque oil from the modification of vitamin E (α-tocopherol) by grafting of triiodo-benzoic aromatic compound as oily phase. Magnetite Fe_3O_4 iron oxide nanoparticles were also incorporated into this oily phase to generate contrast enhancement for T2-weighted MRI. It should be mentioned that we selected this iron oxide phase owing to its high magnetism (called superparamagnetism for nanoparticles).They were synthetized by high temperature process, named thermal decomposition, with lipophilic ligands for *in situ* functionalization of their surface. Three times of reaction (2h, 4h and 6h) were performed to estimate the impact on morphology and magnetic properties of the iron oxide nanoparticles. This radiopaque and magnetic oil was subjected to spontaneous emulsification process to yield bimodal NE with PEGylated surfactant for stealth properties.

Owing to their differences of sensitivity, MRI and X-ray scanners need a specific concentration of contrasting material in a target to offer a clear delineation of the tissue on their reconstructed images. We chose to formulate NE for each batch of magnetite (2h, 4h and 6h) as follows: 0.28 wt.% of magnetite nanoparticles, 23.72 wt.% of iodinated vitamin E, 16 wt.% of surfactant and 60 wt.% of aqueous phase. A wide range of characterization analyses were performed not only on the NE but also on magnetite nanoparticles. Infrared spectroscopy and X-ray diffraction proved that iron oxide nanoparticles were all Fe_3O_4 with a thin outer shell of maghemite, the oxidized from of magnetite. Iron titration also indicated that magnetite nanoparticles had an iron content close to 50 wt.%, the remaining weight ratio

corresponded to lipophilic ligands. Transmission electron microscopy investigations showed slight differences of morphology, magnetite nanoparticles (4h) were the most anisorope and had a size distribution comprising nanoparticles with both range of sizes of nanoparticles (2h) (5-7 nm) and nanoparticles (6h) (7-10 nm).

Once formulated into NE, magnetic properties were assessed and r2/r1 ratios were determined. Results demonstrated that magnetite nanoparticles (4h) were the best candidates as contrast agents for T2-weighted MRI because of the highest value of ratio (r2/r1 = 16). Size distribution of each NE was quite similar and around 60 nm (by dynamic light scattering) with good monodispersity. NE with magnetite nanoparticles (4h) was selected as optimum formulation regarding magnetism, since all NEs were loaded with same amount of radiopaque oil, magnetic property was used as discrimination parameter. *In vivo* bimodal imaging study was run on 5 Swiss mice. MRI showed a high accumulation after 5h post-injection of contrast agent in liver and kidneys (contrast in spleen is debatable owing to the heterogeneity aspect of this tissue by MRI). Same observations were done at 24h post-injection. X-rays imaging was executed at 24h post-injection and allowed to visualize the liver and the spleen. Kidneys were not detected indicating that NE assembly was damaged once it passed through kidneys filters: the iodinated part was excreted whereas magnetite nanoparticles remained in the tissues to provide MRI contrast. No adverse effects on animals were observed. This study was initially carried out to propose a novel bimodal contrast agent based on nanocarriers, and as the results confirmed, this novel probe was quite efficient for liver investigations. However, it provided also an insight of biodistribution and elimination route of NEs, thanks to such probe it seems that understanding pharmacokinetic profile of nanoparticles would be possible and easier thanks to bimodal imaging. Currently, this work could be complete by *in vitro* test on cells to investigate internalization of NE but also by iodine and iron titration in tissues in which NE accumulated.

In **appendices section**, summary of additional research works will be provided: two bibliographical revues, respectively on targeted nanocarriers for drug release and on inorganic nanoparticles for X-ray imaging, and an article about microfluidics process to form magnetic nanocomposites based on iron oxide nanoparticles embedded in a polymeric matrix.

Chapter I:

Introduction

Chapter I - Introduction

This first chapter presents a state of the art of the major imaging modalities supplying relevant information of patient health by real time monitoring to set up accurate diagnostic and potential treatment plan. Aspects highlighted below will be about comparing features of imagers to end focusing on two main scanners, the X-ray CT scanner and the MRI. Imaging probes will be described for both imaging techniques. Afterward, we will describe current needs for the development of diagnostic contrast agents (CA) for imaging and how nanoparticles (NPs) may be promising alternatives and how they are already paving new routes in nanomedicine field.

1. Non-invasive imaging modalities: from principle to prevalent techniques

1.1. Diagnostic by imaging techniques

Non-invasive diagnostic field has seen outstanding progresses due to advanced imagers' development. Owing to computing power growth, current imaging techniques aim at providing complete visualizations from molecular scale to cellular and organs, tissues, lesions to whole organism scales. An arsenal of tools dedicated to imaging has emerged over several decades and allows nowadays to understand and to examine health troubles of patient by acquiring reconstructed 2D or 3D images without invasive gesture to patient. Thanks to difference of contrast from one region to another one, images show clear delineation of internal structure (anatomy), morphology, and physiological functions at the different abovementioned scales. Consequently, engineered images form consistent support for detection of early-stage pathology, evaluating progression of diseases, cancer staging, treatment efficacy follow-up, etc. and assist in clinical decision making for patient disease management. Improved and fast screening by imaging became the most essential and efficient non-invasion method to reduce mortality of patients caused by a lack of reliable information about *in vivo* systems. To increase the visibility of internal body structure by changing the contrast between healthy to unhealthy area, exogenous pharmaceutical contrast enhancers, so-called contrast agents (CA) or traceable probes, can be administrated to patients to increase sensitivity and/or specificity of modality to a targeted region of interest (ROI).[1-5]

In this way, all imaging techniques provide precious information at their own scale and limits. Finding the appropriate modality is dictated by what we are looking for, the data that clinicians and physicians are trying to obtain (such as *in vivo* phenomena *i.e.* functional

processes or biochemical mechanisms or biological entities and tissues *i.e.* cells, stem cells, pathological tissues) by means of unimodal or multimodal imaging use. A step-by-step approach to guide the choice toward one modality (and, if necessary, a complementary one) seems most appropriate way to render the diagnostic process efficient and relevant.[6] The Figure 1 displays basic and schematic methodology to end to this goal.

Figure 1: Step-by-step guide to perform diagnostic procedure by non-invasive imaging (Adapted from Ref. [6]).

To sum-up, diagnostic methodology relies on some key steps: 1) patricians should first define the scale level that must be precisely observed in order to then 2) find suitable probes, if needed, to administrate to the patient to provide enough contrast enhancement to the ROI. Obviously, selection probe is modality-dependent. Consequently, figuring out how to detect an *in vivo* target is related 3) to find imaging instrumentation(s) performant enough to image the target. In addition, signaling component-based probe must be well-tolerated to the person regarding its own health statement. The next step might be skip if the case of study is already well-documented in clinics, otherwise iv) study at small-scale in preclinical research should be run not only to optimize the acquisition process but also the CA composition and formulation. After all, meaningful information can be recorded by v) performing imaging after CA administration once translation to human scale is developed and reliable.

1.2. Overview and comparison of imaging instruments

There are five prime imaging techniques dedicated for preclinical and clinical biomedical applications. The most used imaging modalities are X-ray computed tomography (X-ray CT), magnetic resonance imaging (MRI), optical imaging by fluorescence and bioluminescence, nuclear imaging including positron emission tomography (PET) and single photon emission computed tomography (SPECT) and ultrasound imaging. The existence of such wide range of imaging techniques is mainly due to their respective ability to reveal structural and/or functional information at different scale and accuracy levels. All modalities rely on their own principle and possess therefore their own strengths and disadvantages regarding their resolution, sensibility, depth of tissues penetration and contrast quantification. In reason to their inherent principle, each imager requires its own kind of probe to yield more efficient monitoring and to highlight some poorly contrasted tissues.[1-5] Most features of imagers are gathered in Table 1.

Table 1: Comparison of most common imaging techniques (Adapted from Ref. [1,2,4,5,7]).

	X-ray CT	**MRI**	**PET/SPECT**	**Ultrasound**	**Optical***
Source	X-ray	Magnetic field and radiofrequency	γ-rays	Sound	Near infrared, visible light
Spatial resolution	50–200 µm	25–100 µm	2-10 mm	50–500 µm	1–5 mm
Probes	Heavy elements *i.e.* I, Ba, Au…	Magnetizable materials: Fe_3O_4, Gd chelates	Radionuclides: ^{18}F, ^{11}C, ^{13}N, ^{15}O, ^{64}Cu, ^{124}I ^{11}In, ^{99}mTc	Microbubble, emulsion, micelle	Fluorescent dye, quantum dots, near-infrared dyes
Probe dose (mol/L)	10^{-3}	10^{-3}–10^{-5}	10^{-10}–10^{-12}	Not characterized	Biolum: 10^{-15}–10^{-17} Fluo: 10^{-9}–10^{-12}
*Information***	A and P	A, P and F	A, P and F	A and P	P and M
Advantages	High resolution, no depth limit	High spatial resolution, no radiation, no depth limit	High sensitivity to probes	Easy, fast, no radiation, cost-effective	Multichannel imaging, no radiation, sensitive to probe dose
Drawbacks	Radiation, poor soft tissue delineation, low sensitivity to probes	Poor sensitivity to probes, expensive	Need of probes, radiation, expensive, low resolution	Depth limit (cm), poor contrast, not suitable for air-containing organ	Need of probes, not yet available in clinics, low depth penetration, low resolution

* Optical imaging gathers bioluminescence (biolum) and fluorescence (fluo) modalities.

** Information: A: anatomical, P: physiological, F: functional and M: molecular.

In order to take best benefits from imaging modalities, instrumental limitations and interaction between the source, the body tissues and fluids and the probes must also be considered and well-though to find out most suitable technique for tracking a specific *in vivo* target as mentioned before.[1,5,7] Accuracy of diagnostic through non-invasive imaging tools relies on the quality of images, amount of details which can be extracted from engineered pictures. It means that high resolution is requested even if CAs are used. Taking in account data from Table 1, it clearly appears that imagers based on ultrasound technology, PET and SPECT show a lack to this regard. Furthermore, PET and SPECT involve radioactive materials, provide only physiological information and are not reliable for *in vivo* location rendering those two techniques uncomplete.[8] Usually, physicians prefer what it is commonly called cold modality for which no radiative probes are administrated or they combine nuclear imaging with complementary imaging technique. As to ultrasound imaging, it has recently seen tremendous evolution thanks to the progress of computed 3D reconstruction and palliation of motion artefact. Typically applied in clinical research in obstetric, cardiology, surgery guidance and urology, ultrasound techniques remain also not convenient when come needs to observe subtle details of anatomy of deep tissue. However, promising outcomes in molecular imaging render ultrasound imaging more and more interesting.[9,10] Concerning optical imaging, such method is basically employed in combination with fluorophore such as organic dye and inorganic nanoprobes like quantum dots for molecular and cellular imaging, sensing, drug delivery, and targeting.[11-13] So far, this technique is not yet adapted for clinical use. The two last methods are the X-ray CT scanner and the MRI. X-ray CT scanner is the oldest imager and involves ionizing beam but remains one the most used techniques in clinics due to its cost-effectiveness, the quantitative information depicted on scans, and fast image acquisition processing. However, compared to non-radiative-based MRI technique, X-ray CT is not as efficient as MRI to contrast soft tissues but still constitute an alternative to patient bearing magnetizable device.[14,15]

Using features from Table 1, classification of imagers based on their cost, the dose of CA required to get contrast enhancement, the impact of the source and the toxicity of probe, the spatial resolution to have accurate reconstruction of ROI and the *in vivo* information is introduced in Figure 2. Criteria were also classified from the less (bottom) to the most (top) important point to focus on to set up diagnostic. By comparing each modality along with each criterion, it is clearly demonstrated that MRI and X-ray CT level up compared to clinical modalities typically due to the collection of meaningful data from their high resolution scans.

It also appears that they are not as sensitive to probe as PET and SPECT but at least radiopaque CA and magnetic formulation are safer. Furthermore, they both have no limit of depth penetration meaning that organism may be completely scoped.

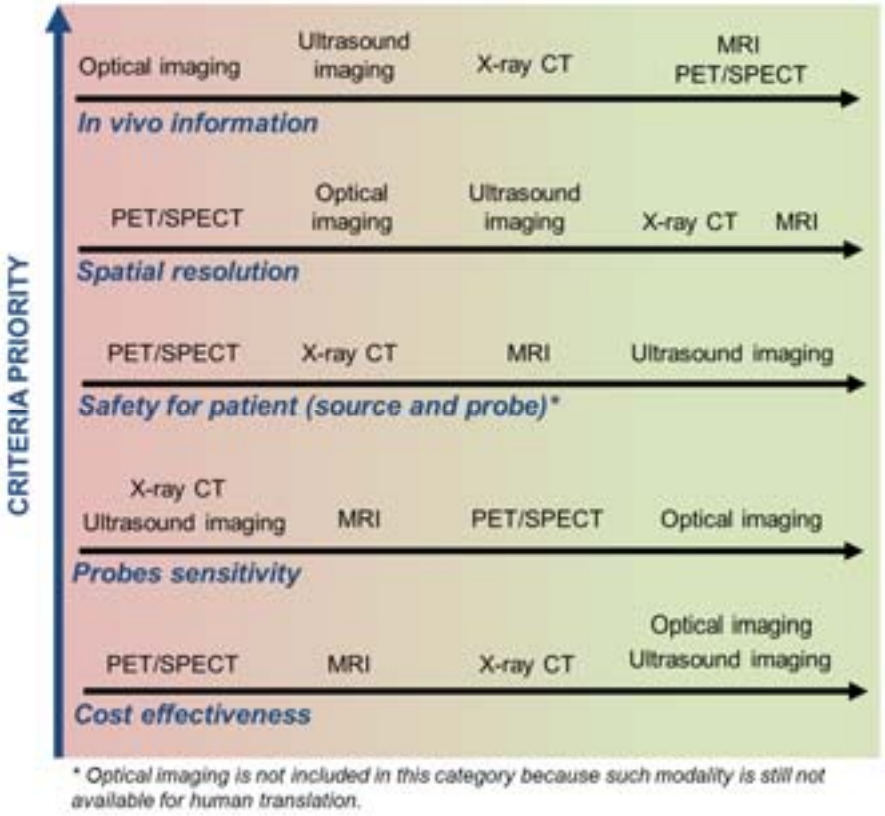

Figure 2: Classification of clinical imaging modalities based on Table 1.

According to this, MRI and X-ray scanner are nowadays most performant imaging instruments. This occurred also because of their easy access in clinics which has been promoted by the huge progress done in preclinical research on small laboratory animal thanks to advanced preclinical version of such technologies. However, as mentioned by Oliva *et al.*[16] no consensus has finally been defined to attribute to each disease or health issue an imaging technique. But in many studies, MRI and X-ray scanners were selected as instruments or complementary devices for each other with the highest efficacy to set diagnostic free of equivocal information like, for instance, abdominal imaging (soft tissues)[17], hepatic lesions[16,18], real masses[19] and pancreatic cancer[20,21] investigations.

The next part will aim to summarize basic principles of X-ray CT and MRI. Their main characteristics and corresponding CAs will be introduced as well as their advances and issues

will be outlined to furnish a complete overview. We will emphasize why these two clinical scanners became outstanding technology for the development of diagnostic by imaging investigation.

2. X-ray scanner

2.1. From X-ray discovery to X-ray imagers

Application of X-rays for biomedical imaging was recognized soon after discovery of X-rays by W.C. Röntgen, a German physicist, in 1895. The amazement and fascination of Röntgen for this unknown kind of ray led him to write "On a new kind of rays"[22] in which he had described in 17 points his observations on what he finally named "X-ray" since no one had been reported such kind of ray at this time. Although, understanding X-ray phenomenon was laborious, it appeared as substantial breakthrough in physics and many fast advances emerged since. Several decades later, during the 60s, development of X-rays use for insight visualization of living being became very promising and drove A.M. Cormack and G.N. Hounsfield to create the first X-ray imager for biomedical imaging purpose. The first computer-assisted X-ray tomography prototype was so set up in clinics in 1972. A.M. Cormack and G.N. Hounsfield shared along Nobel Prize in Physiology or Medicine 1979 for this tremendous innovation for preclinical research and medicine.[23-28]

2.2. Radiography: principle and instruments

X-ray imager furnishes images on which tissues can be identified by exhibiting differences of opacification thanks to their ability to attenuate X-rays by absorption of a part of its energy. Scanner and contrasting process work as illustrated in Figure 3 and as followed: i) X-rays have to be generated and ii) to pass through the specimen. Production of X-ray photons is carried out by an electron beam generated by high voltage, accelerated within vacuum chamber and guided towards a heavy metal anode. iii) The as-resulting electromagnetic radiations penetrate then into specimen. Depends on the nature of molecules from *in vivo* matter, iv) interaction with X-ray photons may occur and may lead to absorption, reflection, or scattering of the incident X-ray photon. X-ray attenuation follows Beer-Lambert exponential attenuation law and is multifactorial-dependent because it can be promoted by the electron-density and the absorption coefficient of element present within the *in vivo* media, the energy of X-ray photon, the thickness of the subject, etc.. Then, v) the total attenuation produced by the body is measured by detection of the emergent X-ray beam. Opacification of

tissues can then be visualized on tomographic 2D images *i.e.* sectional images reconstructed by algorithm, volumetric 3D reconstruction can be performed by stacking transverse sections. Contrast is notified by means of a gray scale. Dense materials absorb significant part of X-ray energy and lead to a whitening on image (from white to light gray). Water, on the contrary is not able to attenuate such photon; this is why fluids appear dark (from dark gray to black). Other tissues, like soft tissues are mostly contrasted by gray shades.

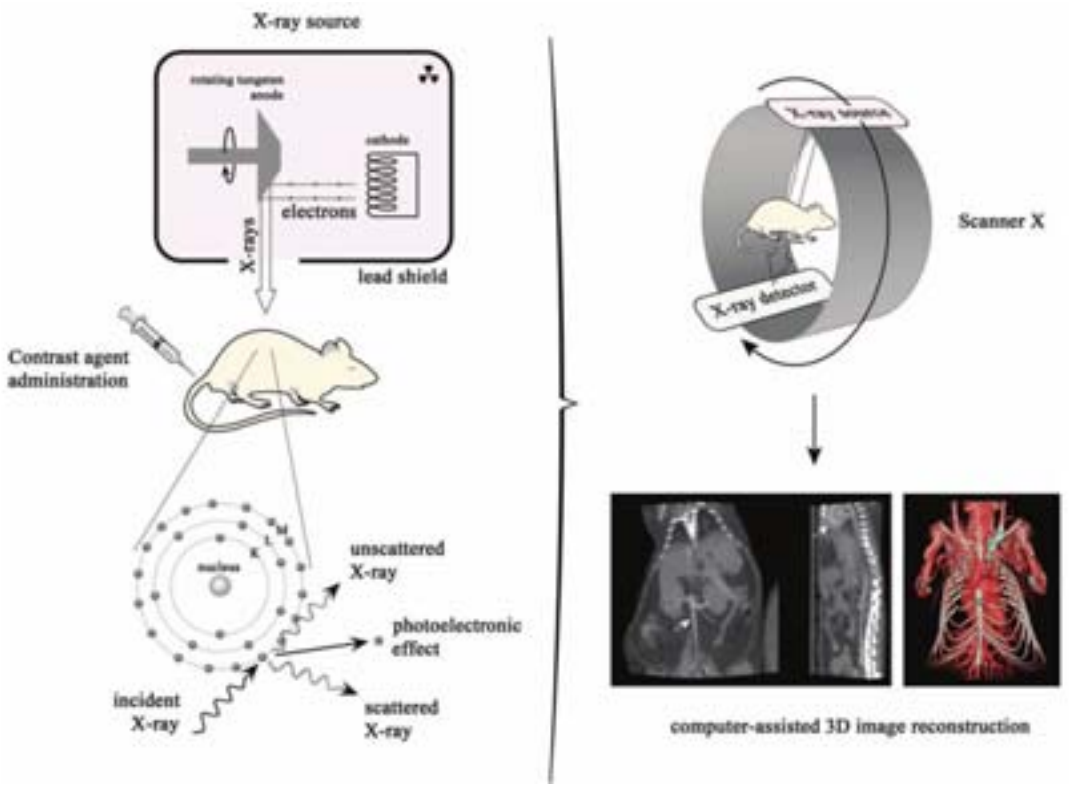

Figure 3: Schematic representation of X-ray scanner principle and typical 3D reconstructed images obtained by X-ray imaging protocol.[26]

Quantification of opacification is done using the Hounsfield unit calibrated with water. Using Hounsfield scale, water and air are respectively attributed to values 0 HU and -1000 HU. Soft tissues are generally around -100 HU to +100 HU. Mineralized materials, like skeleton, vary from +400 to +1000 HU (-1000 HU for air-containing organs like lungs) as attenuation value. Based on this scale, attenuation value for a target of interest is determined following eqution:

$$HU=1000\times\left(\frac{\mu-\mu_{water}}{\mu_{water}}\right)$$

Where (μ_{water}) is the linear X-ray attenuation coefficient of water.[1,2,14,24,25,27,29]

Radiography corresponds to the general term to name the family gathering all types of X-ray scanners. The clinical device is known as X-ray computed tomography (*i.e.* X-ray CT) whereas the preclinical prototype instrument, dedicated to small animal study for research laboratory, is the microcomputed tomography (*i.e.* micro-CT). Those two scanners differ from their resolution. Indeed investigation on small laboratory subject requires tools allowing to examine at scale equivalence and so with higher spatial and time resolution. Nevertheless, micro-CT is simply inaccurately used as a broad term to refer to a group of three X-ray microscopic scanners with specific spatial resolution: mini-CT (50-200 µm), micro-CT (1-50 µm) and nano-CT (0.1-1 µm) (Figure 4). Commonly, preclinical imaging uses micro-CT to study small laboratory animal like mice to small-scale investigation.[29-33]

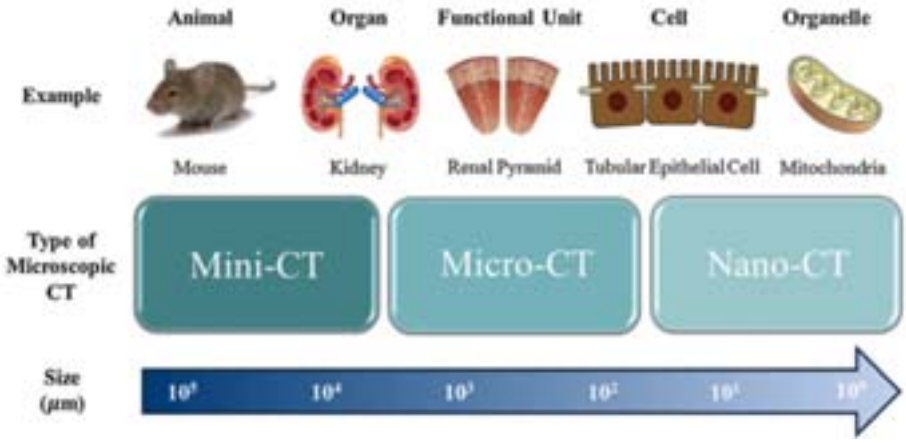

Figure 4: Types of microscopic computed tomography with their typical *in vivo* scale at which investigation can be performed. [29]

It has to be note that all X-ray scanners face up with dilemma between the impact of X-ray exposure to patients and all advantages to use such scanner for diagnostic purpose and treatment respond follow-up. Indeed, the main limitation of such device is the delivery of high radiation dose, evaluating with gray scale (Gy), causing long-term genetic damage. Even though radiation dose is adjusted to the desired *in vivo* target, radiation may induce cancer and/or extent a cancer lifetime. A study showed that radiation impact was multi-factorial and might be more or less important depens on numbers of scans, photon energy, number of X-ray sources, closeness of specimen to source(s), scan speed applied which are all adjusted to the area to image and the type of specimen. Nevertheless, it could be slightly offset if physicians would agree compromising quality of image to prevent from acute tissue damage and patient health. Such debate might therefore be lowered taking in account that in case of cumulative

exposure to ionizing radiation by means of repeated X-ray imaging procedures, imaging parameters are adjusted.[2,33-35]

Despite the radiation issue, X-ray scanners remains still an important tool for clinics since it is a cost-effective, fast, high resolution and no depth limit imaging technique. However, early diagnostic of soft tissues pathology can be challenging due to a lack of clear delineation between soft tissues. Indeed, very subtle changes in their X-ray attenuation are observed on CT scans rendering difficult identification of soft tissue among other and interface between two adjacent soft tissues in contact with blood or other physiological fluids. Radiopaque CAs, which are by the way cold marker, are so generally involved. Sensitivity of X-ray scanners to traceable radiopaque probes remains so far a little bit low. Typically, a difference of 50−100 HU leads to differentiate easily adjacent compartment and can be obtained by administration of significant dose of CA.[14,28,29,36-38]

2.3. Radiopaque contrast agents for X-ray scanner imaging

Typically, X-ray scanners finds key role for various tissues imaging by means of administration of clinically approved (by "Food and Drugs Administration" (FDA), an American organization in charge of the public health protection) radiopaque substances as reported in Table 2.

Table 2: Summary of body systems and their diagnostic procedures by X-ray imaging with contrast enhancer.[3,14,24,39]

Body system	Organs or tissues (Procedure)
Vasculature	Vessels (angiography), arteries (arteriography), veins (venography), chambers of the heart (ventriculography)
Organs	Brain (brain CT), liver and spleen (abdominal CT), kidney (pyelography), gallbladder (cholescystography)
Spinal canal	Spine, lumbar, thoracic, cervical, total columnar (myelography), brain (cysternography)
Urinary track	Bladder (urethrography)
Gastrointestinal track (GI)	Upper GI including buccal cavity, pharynx, esophagus, stomach, and duodenum and lower GI corresponding to small and large intestines
Joints	Joint (arthrography), disks (diskography)
Uterine cavity	Uterus and fallopian tubes (hysterosalpingography)

To ensure significant local contrast, radiopaque CAs, or radiographic CAs or roentgenographic agents, are associated in the diagnostic procedure by X-ray imaging and aim at accumulating and concentrating into a desired target to this end. History of radiopaque CA

has seen significant evolution over decades from the 1920s to 1970s. As briefly described before in Table 1, contrasting media for X-ray attenuation can be formulated with heavy elements, capable of attenuate X-rays, like cesium Ce, gadolinium Gd, terbium Tb, dysprosium Dy, ytterbium Yb and lutetium Lu (lanthanide) iodine I (halogen), barium Ba (alkaline earth metal), thorium Th (actinide), lead Pb, bismuth Bi (post-transition metal), gold Au, tungsten W, tantalum Ta and rhenium Re (transition metal).[24,28] Many elements like thorium[40], a radiative element, and formulations were so tried before being withdraw from *in vivo* radiography application or replaced by safer compounds for toxicity and immediate and delayed adverse side reactions concerns (like skin rashes, nausea, headache, allergy, painful injection, thyroid dysfunction, nephropathy, renal toxicity, cardiovascular issue) due to their compositions and/or their formulations with high osmolality and viscosity. It has to be mentioned there are some patients for whom X-ray CT is counter-indicated because of high dose of CA, for example renal failure, severe diabetic, iodine-sensitive people.[41-43] Currently, oral barium sulfate suspension for GI investigation and injectable small water-soluble iodinated molecules for intravenous administration are mostly used. More and more, iodine turned into an appealing element, even for GI visualization, to cope with harmful *in vivo* effect and because of its low cost. Salts, like sodium iodine or lithium iodine, were first tried as radiopaque tracers but turned out no convenient due to charge separation once exposed to *in vivo* fluids. Several attempts of formulation were also performed with iodine element from ionic to high osmolality to nonionic with low osmolality. Finally low molecular weight (< 2000 Da) and hydrosoluble iodinated molecules with tri-iodobenzene group(s) appear as best compromise between contrast enhancement and side effect.[3,14,24,26,28,37] Typical iodinated molecules from commercially available CAs are displays in Figure 5.

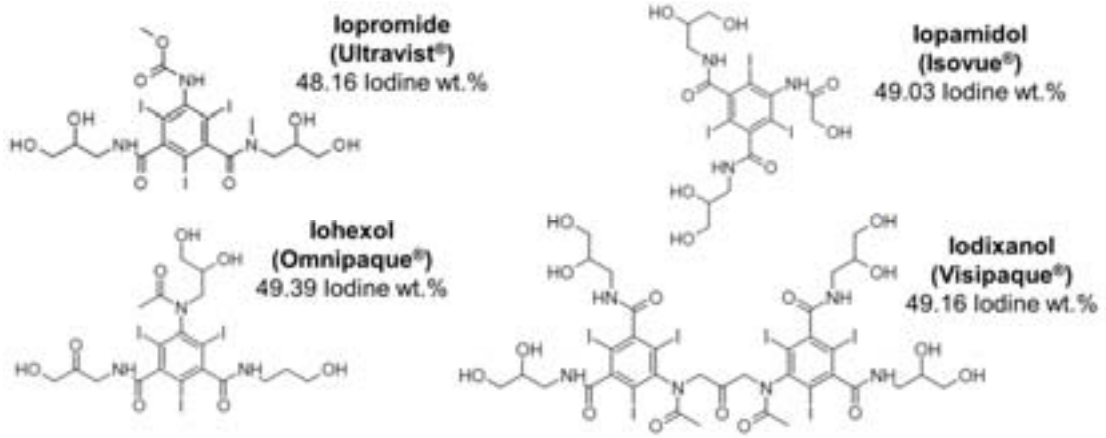

Figure 5: Chemical structures of representative commercial nonionic iodinated CAs with their commercial names and iodine contents (Adapted from Ref. [14,24,37,44]).

Aromatic molecules are so far more stable than aliphatic ones and similar observations are done with nonionic organic molecules. When ionic organic molecules were employed as contrast media, most molecules were positively charged to promote electrostatic interaction with *in vivo* entities (cells, proteins…), mostly negatively charged. At first sight, it looked like an asset to get easily closer to *in vivo* materials, but it turned out those compounds were subjected to severe inconvenient on patient health such as neurotoxicity and hemodynamic issues. As a result, focus on injectable nonionic and aromatic iodinated molecules occurred and so improvements of biotolerance and toxicity as well.[3,14,24,26,28,37]

Nevertheless, those probes exhibit still some drawbacks directly correlated to their physico-chemical properties. Blood-pool contrast media requires being soluble in aqueous environment to be intravenous injected and distributed to tissues. Because of their hydrophilic characteristics, molecules suffer from fast renal excretion. Not only, high dose has to be administrated for this reason (and may cause acute renal toxicity) but also because of the poor sensitivity of X-ray scanners to detect probes signal. Nephropathy is one of the first issues, but cardiovascular events are also another issue. Furthermore, some patients are allergic to iodine and are not allowed to be subjected to injection of iodinated CA before X-ray scanner procedure, most of them will instead be subjected to MRI scanner. Next concerns are related to the high osmolality and viscosity of some radiopaque CAs rendering injection complicated to handle. Parallel to water-soluble iodinated molecules, an emerging class of CA is more and more reported in literature. This class is basically relying on lipid-based radiopaque active material for *in vivo* target. Some products are already supplied in market like Lipiodol®[36] and Fenestra® formulation[45]. Another class is based on nanotechnology and constitutes a new kind of substances used the nanomedicine field. [1,3,14,25,29,37,46,47]

In so far as scanners have already been well-developed, all efforts finally led to a quasi-systematic association with CAs to ensure efficient observation of tissues. To go further in the improvements of the current radiopaque contrasting formulations, a few requirements should be followed to prepare optimum iodine-based injectable preparation:

. The content of radiopaque element such as iodine should be high to promote good X-ray attenuation (high iodine-to-particle or iodine-to-molecule weight ratio) and material used should be biocompatible, inert with respect to tissues and chemically stable in physiological media;

.The formulation should avoid as much as possible to cause potential side effect on patient health;

.The administration should be pain-free and viscosity, osmolality and pH should be compatible with intravenous injection, blood pool environment and *in vivo* fluids;

.The radiopaque substance should, once administrated, have specific biodistribution to yield to local contrast enhancement within the zone of accumulation;

.The time of retention within the ROI should be long enough to prevent from injecting repeated dose, but, compound should be finally excreted after a significant amount of time without producing harmful metabolites.

The following part will aim to introduce the second diagnostic tool, the MRI. As for the X-ray scanner, principles, main characteristics and CAs will be present.

3. MRI imager

3.1. History of MRI scanner

Since now many decades, it is well-known that magnetic fields can cross human tissues without causing any harmful adverse effects for living beings bearing no magnetizable materials.[48,49] Since and ever, the use of magnetic field has so been extended to biomedical applications like diagnostic and therapeutic domains (drug and gene delivery, hyperthermia cancer therapy, magnetic separation, etc.).[48-51] Initially inspired by nuclear magnetic resonance, MRI is nowadays one of the most developed magnetism-based technique for human insight visualization. MRI development began with tremendous and fast progresses.[52] Firstly, MRI was commonly called nuclear magnetic resonance tomography. In 1971, R.V. Damadian opened a new route to improve cancer diagnosis using NMR technology.[53] Following this new way, works of P.C. Lauterbur and P. Mansfield, who shared Nobel Prize in Physiology or Medicine in 2003 for their discoveries, and then A.N. Garroway study led to develop creation of 2D images by NMR in the 1970s.[54,55] The first small laboratory animal was then imaged and the first abdominal investigation of human body[56] occurred quite soon after that. Later on, the first clinical MRI was set in 1980 and produced its first images of whole body with W.A Edelstein study.[57,58] Real time imaging technique emerged finally by the end of the 1980s.[59]

3.2. Principe of MRI

MR imaging is actually a non-invasive and non-ionizing imaging technique providing 3D images of deep and soft tissues with high resolution mostly used for the detection of tumors and their metastases, for observing the brain and its nervous system or for the evaluation of cardiovascular functions. MRI aims to provide images by evaluating relaxation times (longitudinal T1 and transverse T2) of protons, mainly of water molecules exposed to magnetic field and radiofrequency pulse. Due to their location in different tissues, each compartment would have water molecules with their own relaxation speed.[1,48,49,52,60]

The Figure 6 gets together general physic phenomena at the origin of NMR signal from water molecules during a MRI procedure.

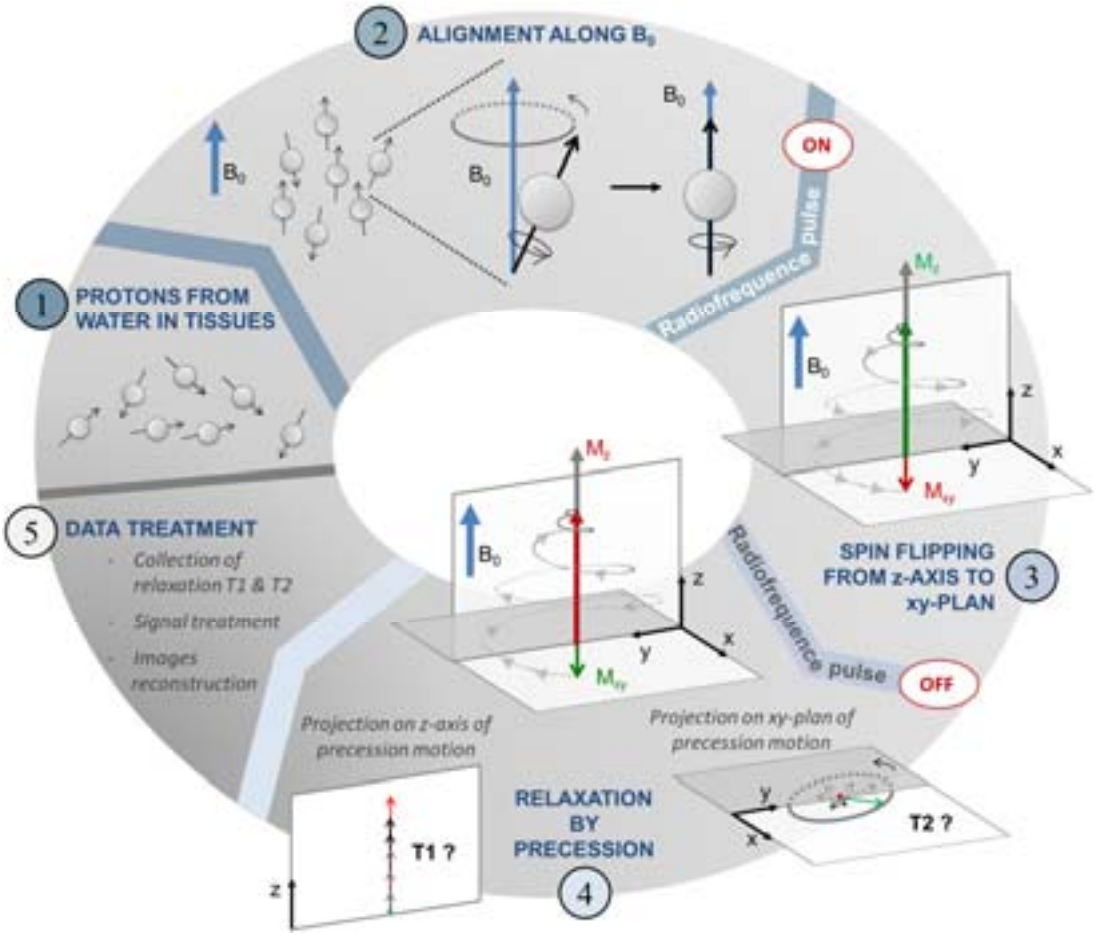

Figure 6: Schematic illustration of MRI effect on magnetic moment of hydrogen nuclei from water molecules containing in tissues to yield to reconstructed images.

As illustrated in Figure 6, MRI relies on the property of protons from water in human body tissues to respond to strong magnetic field (B_0 > 2T) and a transverse radiofrequency pulse

sequence (5-100 MHz). Although magnetic moment of water molecule is small, their large number within biological medium lead to a measurable effect due to collection of all signal of hydrogen nuclei once exposed to B_0. Like in proton NMR principle, applying a magnetic field B_0 leads magnetic moments or spins of hydrogen to align along Bo axis (z-axis), spins are not static but spin about B_0 at precession frequency (Larmor frequency ω_0). Then rf-pulses are introduced to proton nuclei which absorb the energy and make the net magnetization (M_z) of each spin switch from z-axis to xy-plane (M_{xy}). When transmission of radiofrequency pulse ceases, magnetic moments relax in coherent respond and process at Larmor frequency to get back align along Bo. Relaxation times are so measured, then precession signals are treated by Fourier transform and provide signals to build 3D images. [48,49,51,60]

3.3. Origin of MRI contrasts

Relaxation is actually based on two phenomena: i) the longitudinal relaxation, commonly called T1 relaxation or T1-recovery or "spin-lattice" relaxation due to the dissipation of the absorbed energy from radiofrequence pulses to the surrounding tissues; and ii) the transversal relaxation, generally named T2 relaxation or T2-decay or "spin-spin" relaxation because of the loss of phase coherence by spin-spin interactions during spins precession. As it is implied, longitudinal and transverse relaxations are characterized by times of relaxations, respectively T1 and T2.[2,48,49,51,60] Whereas T1 corresponds to the time to recover 63% of longitudinal magnetization from spin to the surrounding media, generally as energy like heat, T2 is the time that transverse magnetization needs to decrease of 37%.[49] The following Figure 7 shows example of curves of Mz and Mxy net magnetizations as a function of time measurement allowing to estimate T1 and T2.

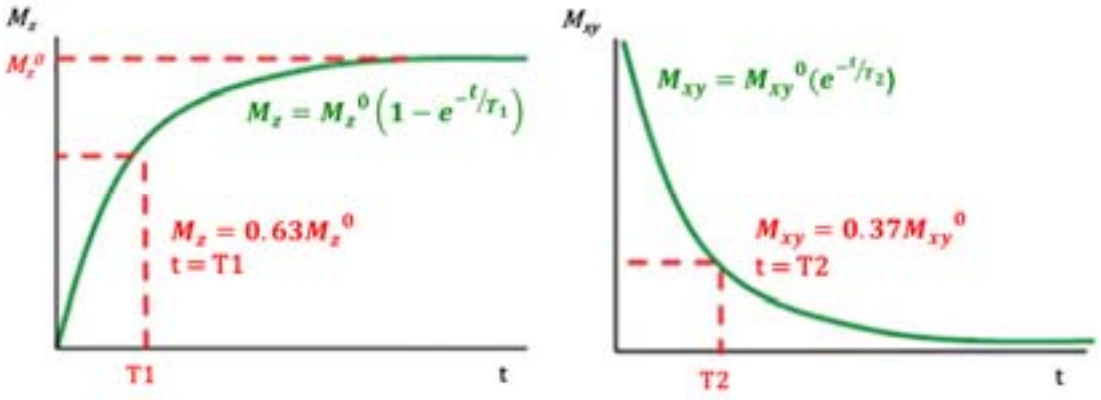

Figure 7: Curves of relaxation process. Determination of (left) T1 longitudinal relaxation time and (right) T2 transverse relaxation time (Adapted from Ref. [60]).

Furthermore and as abovementioned, longitudinal and transverse relaxations are two parallel magnetic phenomena, they so provide their own type of contrast: T1-recovery and T2-decay have respectively brightening (positive contrast, hyperintense signal) and darkening (negative contrast, hypointense signal) effects[1]. Regardless differences in contrasting effects from T1-recovery and T2-decay, it has to be noted that the MRI contrast is only related to the magnetic behavior of one type of element, the protons. However, some variations of T1 and T2 within organs and surrounding organs are noticeable which means that protons do not act in a same fashion. Because of differences from one tissue to another one such as the composition and the density, the spins will not relax in a same time since they will not be subjected to similar interactions within their respective tissues.[48,60] Last phenomenon to highlight about MRI relaxation process is dephasing mechanism occurring during spin-spin relaxation because of magnetic field inhomogeneity within tissue, notably detected during T2-weighted MRI imaging of *in vivo* entities with high payload of paramagnetic components. This new relaxation decay is describes by T2* transverse relaxation time and provide subsequent information for functional MRI and perfusion imaging. T2* is consequently even more sensitive to detect macroscopic magnetization.[61,62]

However, like for all imagers, contrast enhancement for MRI needs to be improved by means of introducing magnetic materials as CAs. Owing the possibility to obtain images with on the hand brightening and on the other hand darkening depends on the measurement of respectively T1 and T2, two families of MRI contrast medium exist.

3.4. Magnetic probe for MRI contrast enhancement

Although MRI is an advanced technology and provides much more accurate images than other modalities, contrasting materials can be associated to improve contrast of some specific *in vivo* compartment by being near or within it. MRI relies on the magnetization of protons to provide signal which can be converted into accurate image of the insight of a living organism. Obviously, MRI CAs are consequently magnetic compounds for both contrast, for the so-called T1-weighted MRI and the T2- and T2*-weigthed MRI.[63,64] Two categories of CAs are prevalent: gadolinium-based CAs for T1-weighted MRI and iron oxide-based CAs T2- and T2*-weighted MRI. Both kind of MRI probes are nanoparticles (NPs), more precisely coated NPs, and belong so to nanotechnology and nanomedicine fields.

The first category is nowadays widely used in clinics. Many substances are already FDA approved. Some are described in Table 3. There are two subcategories for gadolinium-based

CAs: i) extracellular fluid agents for perfusion imaging (lymphatic system and vessels), interstitial and intravascular space imaging and ii) blood-pool CAs, mostly for intravascular space and angiography investigations. In any case, as shown in Table 3, gadolinium-based CAs aim mainly for fluid compartment and extracellular spaces imaging, some more versatile ones target specific tissues like liver, spleen, lymph nodes, etc.. Regarding oral and gases CAs, GI and lungs can also be visualized.

Table 3: Examples of Gd^{3+} chelates T1-weighted MRI CAs commercially available and their *in vivo* target (Adapted from Ref. [37,63-66]).

Commercial Gadolinium-based CAs	Organs or tissues
Gadopentetate dimeglumine (Magnevist®)	Central nervous system (CNS) (for blood-brain barrier, tumors, spine imaging), whole body
Gadoterate meglumine, (Dotarem®)	
Gadoteridol (ProHance®)	
Gadodiamide (Omniscan®)	CNS, abdominal cavities
Gadobutrol (Gadovist®)	CNS
Gadobenate dimeglumine (MultiHance®)	CNS and liver
Gadoversetamide (OptiMark®)	
Gadoxetic acid (Primovist® or Eovist®)	Liver
Gadofosveset (Vasovist®)	Abdominal cavities, limb vessels, vascularization

Gadolinium is involved into CAs formulation under its ionic form Gd^{3+}. As a free paramagnetic metal ion, Gd^{3+} has undesirable biodistribution and relatively high toxicity issue (exchanged with *in vivo* cations, dysfunction of enzymes and reticuloendothelial system (RES), deposits in tissues and bones). However, owing to the ability to reduce T1, complexation with various ligands was used to overcome Gd^{3+} inherent and unfortunate issues for *in vivo* applications. Gd^{3+} chelates have better kinetic and thermodynamic stabilities and yield to image different interstitial spaces upon administration as contrasting media for MRI depend on the nature of ligands. It has to be noted that Gd^{3+} chelates are hydrophilic species and do not pass through the blood-brain barrier and aim mostly to enhance contrast of brain vessels and tumors. Their physico-chemical nature allows then to be filtered by kidneys and to be consequently excreted by renal clearance before any potential gadolinium leakage. Other elements than lanthanide may form good candidates, those are for instance transition metal elements (Mn^{2+}, Fe^{3+}, Cu^{2+}…) or metal alloy due to their large number of unpaired electrons providing paramagnetic ions suitable for T1-weighted MRI. So far, gadolinium-

based compounds remain most common CAs for positive contrast imaging. Nevertheless, stability should be mastered to prevent from Gd^{3+} leakage. Great attention has been devoted on ligands selection, linear or macrocyclic and ionic or nonionic, and Gd^{3+} core to ligands ratio to ensure efficient Gd^{3+} trapping. Patient suffering from kidney dysfunction or failure may not receive such kind of probes. At least, special cautions must be taken in this particular case in order to avoid nephrogenic systemic fibrosis, a chronic complication. Acute side effects may happen quite soon after administration but all remain controllable and soft (nausea, dizziness, itching intravenous injection, feeling cold, headache).[49,60,63,65-67]

The second class, the T2- and T2*-weigthed CAs, is also present on the CAs market but less products are supplied. Iron oxides are generally magnetite and/or maghemite phase, respectively Fe_3O_4 and γ-Fe_2O_3. Actually, iron oxide NPs (IONPs) has been studied and developed as MRI tracers for only 30 years whereas gadolinium has been know much earlier.[60] Indeed, some concerns are still mentioned in literature about IONPs due to the lack of knowledge on their *in vivo* fate.[68] Like for T1-weighted CAs, all T2- and T2*-weighted MRI CAs approved by FDA are coated IONPs as shown in Table 4. Depends on physico-chemical properties of coating, also named outer shell, the biodistribution is different for the as-introduced IONPs-based CAs. In addition, the overall size is also a key parameter to play on in order to promote accumulation within desired or at least local ROI.

Table 4: Examples of IONPs T2-weighted MRI CAs commercially available, their *in vivo* target and the IONPs size involved within each CAs formulation (Adapted from Ref. [49,50,69-72]).

Commercial iron-oxide-based CAs	**Target**	**IONPs size (∅)**
Ferumoxsil (Lumirem® or GastroMark®) - *Silicon coating*	Bowel, lumen organs	300 nm > ∅ > 3.5 µm
Ferristene (Abdoscan®) - *Sulphonated styrene-divinylbenzene copolymer citrate coating*		
Feruxomide (Endorem®) - *Dextran coated-Fe_3O_4*	Liver, spleen	80 nm < ∅ < 180 nm
Ferucarbotran (Resovist®) - *Carboxyldextran coating*		∅ = 60 nm
Ferumoxtran-10 (Sinerem® or Combinex®) - *Dextran coating*	Lymph node	20 nm < ∅ < 40 nm
Feruglose (Clariscan®) - *PEG starch coating*	Bone marrow, perfusion, vessel	∅ = 20 nm

To clarify, IONPs is a general term to refer to families of IONPs with different size range: micro-sized paramagnetic IONPs (few micrometers), superparamagnetic (SPM) IONPs (SPIONs) (~100 nm), ultra-small IONPs (USPIOs) (<50 nm) and monocrystalline IONPs (10-30 nm).[49,64,67,73] As it can be understood with CAs description in Table 4, the smaller

IONPs get the narrower area they can reach. Indeed depending on their size, those nanoprobes are basically used to provide negative contrast for liver and spleen (50-100 nm SPIONs) or lymph node and bone marrow (<50 nm UPSIOs). Smallest IONPs are capable of extravasion through capillary system and are not subjected to opsonization. Consequently the *in vivo* biodistribution and bioaccumulation of decorated-IONPs are not only lying on surface chemistry but are also size-dependent.[1,48,49,51,60,67,74]

IONPs CAs are consequently more suitable for perfusion imaging because of their very small dimension and for soft tissue imaging rather than T1-weighted CAs. For instance, owing to ability of SPIONs to be opsonized by RES cells like Kupffer cells located in liver parenchyma, pathological tissue in hepatic area is easily diagnosed. Although phagocytose consequence is excretion after metabolization (opsonization mechanism) of the contrasting materials, such sequestration of SPIONs allows to perform efficient liver mapping to detect unhealthy cells, devoid of RES cells, among healthy ones.[1,51,60,69,71] As a result, SPIONs CAs are eliminated by hepatic route, but also through splenic route, on contrary to gadolinium compounds cleaned from body by urinary pathway. Although clearance mechanism is still debated for SPIONs, metabolization of iron oxide may promote formation of a non-SPM ion form which may then become part of normal iron pool and incorporated in red cells or involved in another *in vivo* process and entities (hemoglobin, ferritin). Few side effects of CAs on the market are also mentioned in literature like hypotension, lumbar pain, leg pain, and vasodilatation and in very rare cases paraesthasia. Toxicity issues, usually based on potential interaction with nano-scale *in vivo* entities and SPIONs, are also still debated.[1,69,71,72]

Regarding now the evaluation of the contrast and the efficiency of paramagnetic and SPM CAs, impact of their presence surrounding tissues by means of lowering relaxation times is evaluated. For this purpose, the contrast enhancing efficiency of MRI CA is expressed through longitudinal and transversal relaxivity, respectively r1 and r2, expressed in $(mmol/L)^{-1}.s^{-1}$ or $mM^{-1}.s^{-1}$. Such parameters are defined as the increment of relaxation rate (1/T1 or 1/T2) of water protons induced by 1 mmol/L or mM of active iron. To determine if a contrasting product is more suitable for T1- or T2-weighted imaging (and so for T2*-weighted MRI), r2/r1 ratio has to be evaluated: the higher r2/r1 is, the more suitable the product contrasts for T2-weighted-imaging ($r2/r1 > 10$). Experimentally, r2 and r1 are obtained from a plot 1/T1 and 1/T2 versus the iron concentration, the following equation correlates relaxation rate and concentration and provides r1 and r2 as slope:

$$1/T_i = 1/T_i^0 + r_i C \qquad i=1,2$$

Where T1, T2 are the longitudinal and transverse relaxation times, $T1^0$, $T2^0$ are the relaxations in pure water, r1, r2 are the relaxivities and C is the concentration of active element within CA formulation.[50,60,67] Example of such plot is depicted in Figure 8.

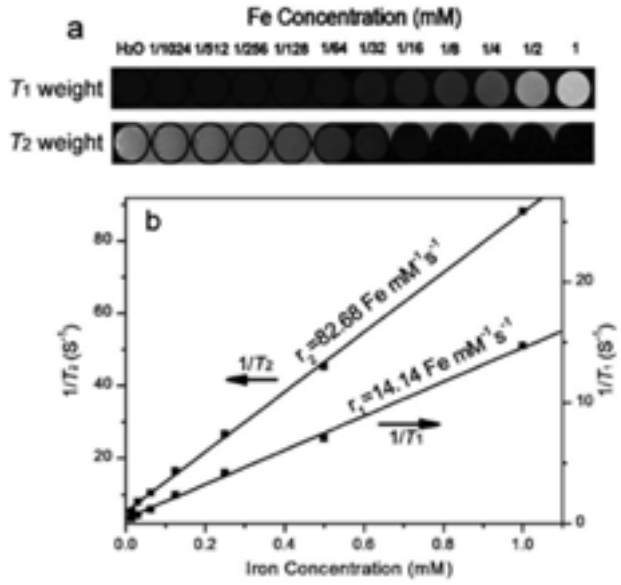

Figure 8: Example of r1 and r2 measurement. a) T1-weighted and T2-weighted *in vitro* MRI images of aqueous solutions at different Fe concentrations and b) 1/T1 and 1/T2 plotted versus Fe concentration.[75]

To go further, some improvements of the current paramagnetic and SPM contrasting formulations, a few requirements should be followed to prepare optimum injectable preparation:

. The content of paramagnetic and SPM element such as Gd^{3+} and SPIONs should be high enough to promote good contrast enhancement and material used to coat or chelate should be biocompatible, inert with respect to tissues and confer stability to Gd^{3+} complexes and SPIONs in physiological media;

. Formulations should have limited adverse effect(s) on patient health;

. The formulation should be well-designed to prevent from Gd^{3+} leakage by trapping with suitable ligands or from large SPIONs use to avoid embolism of small vessel;

. The administration should be pain-free and viscosity, osmolality and pH should be compatible with intravenous injection or oral administration, blood pool environment and *in vivo* fluids;

.The radiopaque substance should, once administrated, have specific biodistribution to yield local contrast enhancement within the ROI;

.The time of retention within the ROI should be long enough to administrate bearable dose, but, compound should be finally excreted after a significant amount of time without producing harmful metabolites;

.Special care should be taken concerning ROI (fluids space, organs, and lesions) to investigate in order to inquire which image weighting is more suitable, then finding appropriate CA compatible to the patient health statement.

To conclude on MRI, X-ray scanners and their associated probes, it has to be precise that both modalities remain important and efficient tools for non-invasive and early-stage diagnostic practice. On one hand, the first-lin used modality, the as-X-ray scanner, and radiopaque have some inherent drawbacks like radiation exposure and iodine allergy risk prohibiting some patients from being subjected to X-ray scanning with contrast enhancer administration. On the other hand, MRI may constitute a more expensive but more accurate alternative for such patients, however it is counter-indicated for person with magnetizable devices. Regarding to the types of MRI CAs, they are based on NPs or complexes for which stability and *in vivo* fate should be deeply studied. As a result, both techniques are required and may be used in conjuncture to get complete and non-equivocal diagnostic. Their actual lacks need thus to be overcome and development of new unimodal or bimodal CAs would be a very interesting first step to render diagnostic procedure by imaging easier for patient.

The next section will focus on present-day needs for clinical imaging and the CAs associated in case of MRI and X-ray scanners. The following part aims actually to highlight the importance to move forward in research on non-invasive diagnostic field and how it can be carried out by pursuing advances at preclinical stage. Promising and emerging preclinical probes based on nanoparticulate systems will be introduced for both modalities.

4. Current limitations and challenges: an increasing need for a new generation of contrast agent for preclinical and clinical imaging

4.1. Multimodal imaging: combination of independent imaging results

As pointed out in the last section, one modality can be replaced by another one in the case of incompatibility with patients' health. Other circumstances may lead to switch from technique to another one; the most common reason is the need of complementary information. More and more, literature shows studies of applications of one, two or three imaging instruments to combine their independent data as shown in Figure 9.

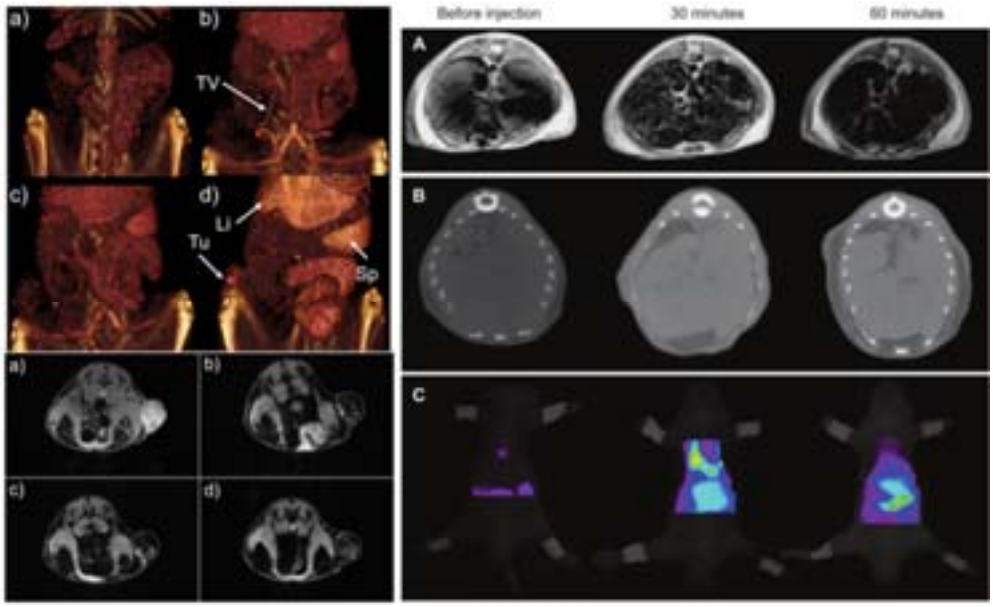

Figure 9: (Left) *In vivo* images of rat bearing tumors by (top) X-ray micro-CT and (bottom) T2-weighted MRI a) before injection, b) 1h, c) 2h and d) 24h post-injection of bimodal CA based on SPIONs core coated with tantalum oxide shell (TV, Li, Tu, and Sp indicate respectively the tumor vessel, liver, tumor and spleen) (Adapted from Ref. [76]). (Right) *In vivo* imaging by A) T2-weighted MRI, B) X-ray micro-CT and C) fluorescence of trimodal probes biodistribution in liver before, 30 min and 60 min post-injection (Adapted from Ref. [77]).

Much more details about disease, treatment efficacy and understanding of biochemical processes can be obtained by involving several imaging strategies for the exploration of ROI. This will aim at improving the diagnosis process; findings from each imaging modality will be validated, interlaced and correlated to this end. In addition, this multimodal approach lies on exploiting strengths and compensating weaknesses of current imaging techniques.[5,6,47,78] For instance, conjuncture of near-infrared fluorescence and MRI was performed for breast cancer detection using multivalent traceable probes. High sensitivity to probe of optical imaging allowed to get quick overview of probes accumulation within tumor, T2-weighted MRI provided excellent delineation of tumor structure including margin and

necrotic zones.[79] Same combination of optical imaging along with MRI were chosen to detect epithelial cancer cells.[80] Other studies used also bimodal imaging approach with MRI/X-ray scanners to image complete tumor vasculature[76] as illustrated in Figure 9 (Left), or for embolization follow-up[81]. Trimodal imaging is also more and more common, for example optical/MRI/X-rays scanners were used for *in vivo* liver imaging and detection of probe internalization by liver cells (Figure 9 (Right)). [77]

4.2. Towards novel preclinical probes with additional features and tunable design

All these promising conjunctures of modalities might become potential breakthrough for preclinical diagnostic field and later on, for clinical translation. Indeed, not only diagnostic process would be even more efficient and accurate but also novel treatment strategy could be imagined. By improving time retention and accumulation of probes, real inherent disadvantage of iodinated CAs from the market, visualizations of ROI might be possible over a longer period. Consequently, tissue and lesions could be monitored as long as the CA remains accumulated. In case of treatment respond monitoring, longevity and extended retention within the investigated ROI is an important asset to avoid repeated administration of CAs. Thereby novel field, like theranostic field, based on drug release, treatment efficacy follow-up and imaging is now more and more developed and is nowadays well-documented in literature. The so-called theranostic platform aims at designing delivery system gathering therapeutics and imaging compounds. It involves a system with an architecture allowing to carry a cargo of pharmaceutics or active pharmaceutical ingredients (API) like CA(s) and drug(s), that is to say a system with a multifunctional payload which can be transported within blood pool, distributed to ROI and then accumulated and/or released within the surrounding tissue.[82] Twinning CAs with therapeutics or treatment strategy were adapted by many authors to apply different treatment strategy on specific diseases along with the suitable imaging tool. For example, Barsanti *et al.*[83] explained how promising it could be to join imaging CAs, mostly MRI probes and PET/SPECT radionuclides, with API for diabete management to observe pancreas, pancreas cells or β-cells function and respond to anti-diabete treatment. Study on the detection of atherosclerotic ruptured plaque and antiangiogenic plaque therapy was also carried out, drug release study with MRI follow-up was performed by encapsulating SPIONs within phospholipids cross-linked shell with controlled dissolution properties.[84] Some other cases in literature report also theranostic strategy but without incorporating API other than CA. Recently, an overview described assets

of dye-conjugated polymers for theranostic application. These near-infrared absorbing conjugated polymers were used to apply local photothermal cancer treatment. They were also pointed out as interesting nano-constructs for doxorubicin drug release with synergic effect along with the photothermal treatment on tumor.[85] Another group used manganese ferrite NPs with dye-doped silica coating as MRI CA to locate ROI, to visualize its anatomy and to apply hyperthermia treatment; fluorescent dye was implied to evaluate efficacy of treatment on cells.[86] Thereby, all multivalent probes just abovementioned dedicated to both imaging and therapy were actually designed into nanoparticulate systems as illustrated in Figure 10, as nano-assembling co-encapsulating APIs and transporting them to local ROI. Nanocarriers (NCs) and NPs offer efficient design to cope with common disadvantages of API like low bioavailability (poor cell penetration, interaction with ROI, selectivity to the ROI), poor solubility in blood-pool and lack of chemical stability once exposed to biosystem by trapping them within their core. It should be noted that the term multifunctionality covers a wide range of functions (imaging, therapy, targeting, penetration within biological entities, stealth property and others) which can all be displayed in one versatile NC.[87]

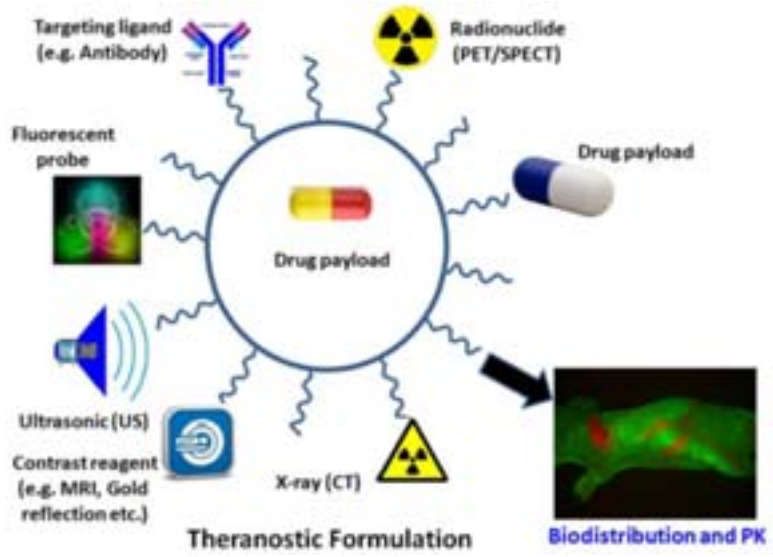

Figure 10: Range of possibilities of preclinical multifunctional NPs as delivery system dedicated to theranostic purpose. Targeting moieties might be incorporated on NPs surface for vectorization purpose to promote specific biodistribution of NPs and interaction with selected ROI. Imaging moieties aim at monitoring NPs accumulation to the targeted ROI and provide also information about the pharmacokinetics (PK) and clearance mechanism.[82]

Although they are promising, all abovementioned multifunctional probes were also designed as NPs because of their uses for preclinical trials on small laboratory animals, which actually make researchers to pass through difficulties owing the animal model scale.

4.3. Dilemma on nanoparticulate systems-based contrast agents to scale-up from preclinical to clinical application

All multifunctional structures presented in previous examples were built-up with nanoparticulate designs. But it has to be highlighted that, even though it is quite obvious, preclinical studies are mostly done on small laboratory animals to ensure safety of innovating pharmaceutics like CAs and to extend use of current imaging modalities towards more efficient diagnostic strategies for further human application.[30] There are considerations to undertake regarding the welfare of animals (duration of anesthesia, temperature control, breath and heart monitoring, side effect, symptoms of pain or intolerance) but there are also technical hurdles to overcome like the difficult vascular access and the small blood pool volume.[7,33] Because of the animal model scale, substances under preclinical study must consequently only be administrated in limited volume, be capable of avoiding or at least postponing clearance mechanism (faster for animal than human) and have a high loading of contrasting material, and potential additional API, to offer good contrast enhancement property once exposed to *in vivo* environment.[25,46] To fulfill these needs, NPs are perfectly adequate for such animal model and seem also promising for scale-up due to their versatility as multifunctional probes. The optimum ending of preclinical studies should be translation to clinical trial if they answer to current needs and requirements (Figure 11). However, even though NPs appear nowadays as future generation of versatile probes for clinical uses, translating such nanodevices to human needs to consider their behavior and *in vivo* fate once introduced into human body environment. Clinical scale-up and translation to human is indeed only performed once CA or theranostic probe got FDA approval after having being tested during clinical trials.[88,89]

Figure 11: Translation from preclinical to clinical stage of NPs-based CA (Adapted from Ref. [6]).

Consequently, NPs can be pointed out as next generation of CAs, with some additional features to yield supplementary functions like for theranostic cases, to overcome the

limitations of probes currently applied in clinics. In spite of concerns about NPs *in vivo* fate once administrated into human body, some NPs-based CAs have notwithstanding already been introduced to humans like for MRI imaging with SPIONs as contrast enhancer. As a result, it turned out that NPs were first of all suitable to carry out study on animals but are nowadays more and more demanded for human model application due to their huge potential as ideal probes thanks to their versatility.

To pursue in this new trend, the following part will introduce in depth NPs, especially those dedicated to imaging *via* for X-rays scanner and MRI.

5. Nanoparticles and nanocarriers as future multifunctional traceable probes platform for imaging

5.1. Introduction to nanoparticles

"Nano" derives from the Greek and refers to tiny dimension beyond the limit of visibility for naked eye. It makes all object described with "nano" as nanometric-sized entity (1 nm = 10^{-9} m). The term NP was used for the first time during the 1980s, before it was mentioned as "small particle".[90,91] "Small particles" were under the scope for more than a century at that time because of manifold size-dependent physical and chemical properties appealing researchers (like M. Faraday whom work contributed to explain how size of gold NPs and color were linked[92]). Soon, after the 1980s, great interests arose from the scientific community and, thus, until now with the development of nanotechnology devoted to nanoscience and nanomedicine application.[93]

NP appellation includes all kind of material such as organic, inorganic, hybrid, alloy, composite etc. Furthermore, usually produced with spherical shape, others morphologies can be found in NPs family like rods, cylinders, stars, cages and other geometries more or less complex (inhomogeneous NPs). General definition of NP is a tiny particle with one of its dimension between 1 nm and 100 nm.[93] As shown in Figure 12, the nanoscale of NPs render them comparable to several biological entities, like cells (10–100 μm), viruses (20-450 nm), genes (2 nm wide and 10-100 nm length) or proteins (5–50 nm), and allows them to get close to these entities (depends on features exhibited on their surface to promote specific interaction).[51,93-96]

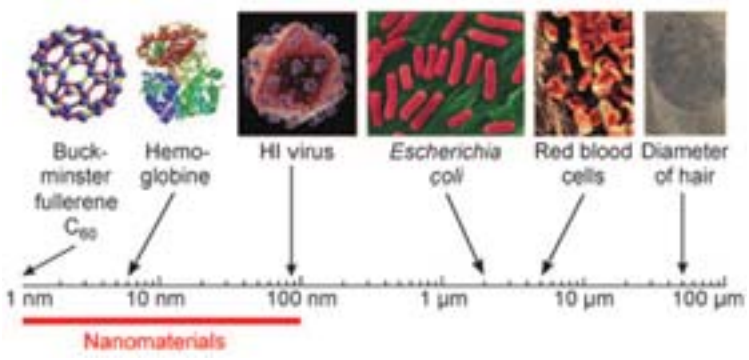

Figure 12: Length scale to compare NP dimension to biological materials size (Adapted from Ref. [93,97]).

NPs are also referred in literature as colloids when they are in dispersion or in suspension. Depending on the size of NPs, colloidal suspension allows to observe light scattering. Few conditions have to be gathered for that: i) colloid matter with radius ranging the wavelength of light (λ), that is to say nanometer scale, and with ii) good dispersion property within the medium of dispersion which has to be iii) a light-transmitting medium (liquid, gas). Light scattering by NPs was also studied a while ago. It began with J. Tyndall during the XIX^{e} century who was the first to get interested in turbidy, a so-called "Tyndall effect", an optical phenomenon visible when big particles scatter sunlight.[98] Then, in 1908 G. Mie and L. Lorenz produced the Lorenz-Mie theory to describe light scattering by nanosphere (radius ranging λ).[99] Finally, the last important law was from J.W. Strutt, 3rd baron Rayleigh; Rayleigh scattering was actually a particular case of Lorenz-Mie theory applicable for NPs with radius smaller to wavelength of light (λ /10).[93,100] Example of light scattering by NPs is depicted in Figure 13. It has to be highlighted that such bluish aspect is a common qualitative characteristic allowing nanoscientists to quickly detect presence of nanoscale particle in dispersion.

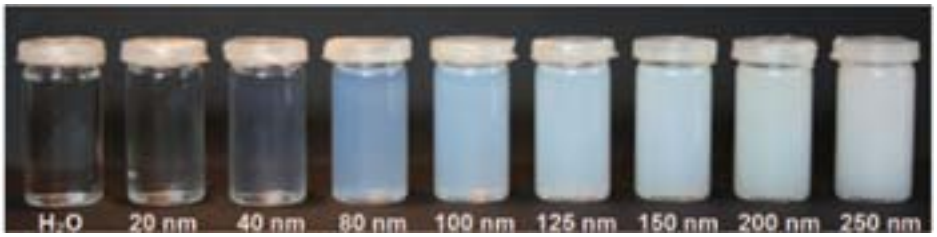

Figure 13: Light scattering optical phenomenon occurring in SiO_2 NPs suspension with various size distribution (Adapted from Ref. [93,97]).

Another interesting fact about NPs is the high surface-to-volume ratio that convey large surface available for anchoring or electrostatic attachment of ligands or specific moieties.

Surface and size of NPs offer many opportunities to tune chemical, physical and optical properties and, consequently to design NPs with specific features for a desired application.[29,101,102] The Figure 14 supports how surface area increases along with the size decreases. It depicts as well that the number of atoms at the NP surfaces follows the same trend, providing as abovementioned a large amount of atoms for potential chemical reaction and physical adsorption by electrostatic forces for surface tailoring purpose.

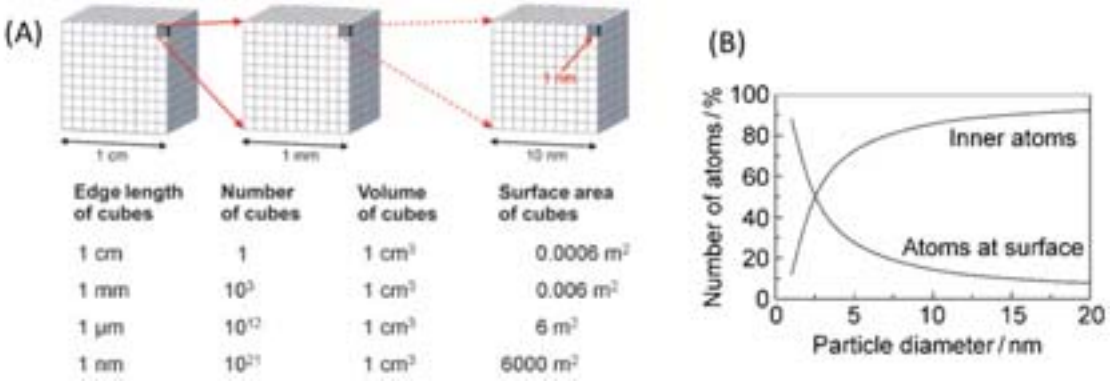

Figure 14: (A) Variation of the surface-to-volume ratio and (B) repartition of atoms *vs* the NP size (Adapted from Ref. [93]).

To keep introducing how the size is meaningful for NPs, it has to be mentioned that several properties are dictated by such parameter. For instance, the colloidal stability require Brownian NPs with efficient surface property to aim good dispersion. The surface of NPs is also size-dependent because: the smaller NPs are, the higher surface area is, the more ligands can be attached. Besides, colloidal stability is also related to surface charge and is a well-documented topic due to the old theory from B. Derjaguin, L. Landau, E. Verwey and T. Overbeek, known as DLVO theory.[103,104] Although all information collected here were for both types of organic and inorganic NPs, it has to be specified that in case of inorganic NPs, many properties like magnetism, but also fluorescence in case of quantum dots, are drastically impacted due to quantum effect and surface area changes from bulk material to NPs scale. The case of magnetism is particularly interesting since it deals with inherent properties that are related to MRI and CAs.[93,94,96,105]

The next section will outline NPs prepared for *in vivo* uses, especially for the field diagnostic by imaging. Requirements and specifications related to biomedical concerns will be detailed in order to figure out characteristics of ideal nanoprobes.

5.2. Nanoparticles dedicated to biomedical imaging: requirements and in vivo concerns

NPs endow willingly assets as introduced before to form drug delivery system (DDS) of API due to their controllable and tunable design. They can indeed be easily adjusted to fit with *in vivo* environment and contribute to move forward the nanomedicine field including imaging and therapy strategies. Not only NPs offer controlled release of API(s) but also confirmation of the site-specific delivery of the substance(s) by incorporation of imaging agent. In fact, NP involved into biomedical applications is generally a double structure construct including a core and a shell and are also known as nanocarriers (NCs). Thereby, NPs are able to be loaded with API(s) onto or into their core-shell assembling *via* encapsulation, embedment, surface attachment or entrapment. In order to carry their payload, which can be therapeutics, imaging agents or both, to a selected target, tailored NPs and/or NCs must bypass several biological barriers.

Human body has a very performant defense system to clean out foreign xenobiotics and preserve it from these ones. Immune system is one obstacle for NPs; indeed upon administration NPs encounter change of pH, osmolality and ionic force which can alter NPs construct (agglomeration, physical degradation, modification of their property). Their introduction in the bloodstream may also induce negative host response imparting potential premature clearance by opsonization or renal filtration from the organism. The *in vivo* fate of NPs once exposed to biological media is governed by physicochemical properties. Typical biodistribution few minutes after NPs blood clearance is 90 % in the liver, 2 % in the spleen and 8 % in the bone marrow, but that remains highly dependent to NPs characteristics. Likewise, biodistribution and pharmacokinetics can *ipso facto* be anticipated by playing on design (size, shape, surface, targeting, composition).[47,49,106-109]

· *Size:*

Mean diameter of NPs is a key parameter governing the NPs concentration in blood pool, affecting the clearance process and the biodistribution (extravasation through tumor vascular system, permeability out of regular vasculature). Small NPs may be able to penetrate physiological barrier due their similar dimension, to gain access to many areas and to avoid embolization outcome. Typical NPs administrated are smaller than 200 nm whereas the smallest capillary pore diameter is around 2.3 nm. Using NPs for imaging has been endeavored not only for preclinical testing on animal model but as introduced to overcome fast elimination of hydrophilic iodinated CA. Size is effectively the most impacting parameter

to regulate NPs-based CA elimination and accumulation. Basically, large NPs (150-300 nm) will mostly be excreted by hepatic and splenic routes once opsonization mechanism occurred. Opsonization process is conducted by the RES or mononuclear phagocyte system (MPS) implying plasma proteins (opsonins) absorption as biochemical signaling of foreign entity intrusion. Sequestration and excretion of NPs is then carried out by phagocytic cells located in RES organs like liver with Kupffer cells and spleen with macrophages. To postpone MPS uptake and subsequent clearance process, NPs must have high curvature which means a very small hydrodynamic diameter. Nevertheless, NPs smaller than 20 nm will be subjected to renal clearance whereas medium NPs (50-150 nm) will be generally accumulated in bone marrow, heart, kidney and stomach.[106,108-112]

· *Surface chemistry:*

Another prerequisite for longevity and RES bypass of NPs within the blood-pool is the surface property. Surface decoration relies here on surface charge, hydrophilic or hydrophobic properties, passive targeting ligands or active targeting moieties conjugation. The simplest design of NPs is based on stealth and neutral NPs. Stealth property implies uses of biocompatible and water-soluble polymer as flexible hairy shell such as poly(ethylene glycol) (PEG). PEGylated amphiphilic macromolecules and dextran were both used on SPIONs and UPIOs; excellent stabilization against opsonin absorption and low cytotoxicity compared to bare NPs were noticed.[113,114] Polyesters were also widely used, especially lactide and glycolide polymers and copolymers like poly(lactic acid) (PLA), poly(lactic-co-glycolic acid) (PLGA), poly(ε-caprolactone) (PCL) for DDS because of their biocompatibility, low degradation rate and controlled drug release.[115,116] Some other polymers are already on the market and used as coating for long-time retention like poloxamer (Pluronic®), a triblock polymer (poly(propylene oxide) (PO) flanked with two hydrophilic PEG chains) and poloxamine (Tetronic®), a tetra-functional block copolymer of PO and PEG.[117,118]

A lot of modified polymers were applied, notably for liposome NCs for passive targeting strategy. It should be mentioned that liposome NC was one the first PEGylated NC type marketed during the mid-1990s, known as Doxil® or Caelyx® as passive tumor targeted DDS of doxorubicin. All those polymers act as hindrance shield, attracting water molecule as cloud fooling the immune system. Such “chameleon effect” avoids premature opsonization and provides as well steric stabilization preventing NPs from aggregation. Most often time, PEGylated shell is used to prolong circulation time of NPs and reduce cytotoxicity. The case

of active targeting, detailed in a following part, is much more developed and involves a wide range of ligands (aptamers, peptides, vitamins, antibodies, small molecules). Playing on surface charge and hydrophilic property may lead to a non-specific interaction with biological entities, generally negatively charged. Positively charged NPs will have random binding with non-targeted cells, hydrophobic ones will encounter aggregation issues in physiological medium and will be clean out by RES. It appears that optimum surface decoration would be neutral and hydrophilic.[87,102,106,108-112,119-122]

The Figure 15 summarizes how surface property and size ranging affect biodistribution of NPs. It clearly appears that these two parameters are interlaced and require to be well-controlled to guarantee accumulation in ROI and bypassing *in vivo* obstacles.

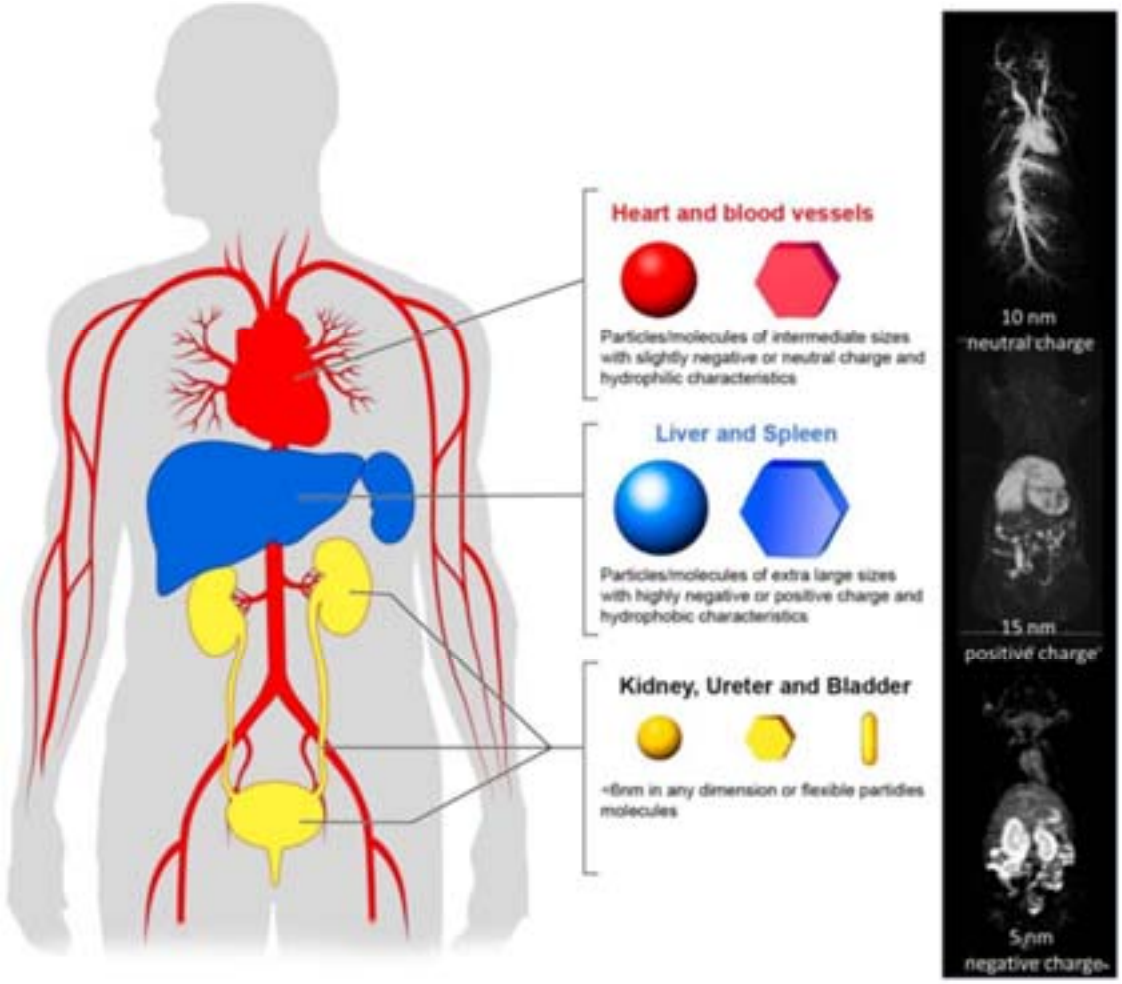

Figure 15: Classical pharmacokinetic profile of NPs depends on their size and their surface. [111]

·*Shape:*

The effect of NPs shape has not been yet well-documented: few studies proved that biodistribution, *in vivo* interaction and toxicity were shape-dependent.[123,124] However, a

limited number of comparative studies is available to discuss about impact of nanorods, nanospheres, nanocubes, nanotubes, etc. on the pharmacokinetics of NPs. Hypothetically, the flexibility and the hardness of the nanoconstruct might influence filtration and consequently the clearance mechanism.[106,111]

· *Targeting*

Vectorization of NPs is particularly appealing for DDS in order to cut down injected dose of drugs and to overcome the lack of specificity and selectivity to ROI. It prevents as well healthy cells form the cytotoxicity of the therapeutic agent(s). Active targeting is a key to optimize the intracellular uptake of the API by the desired target. Applying local treatment is a strategy mainly developed to enhance the bioavailability of API by reaching not only targeted cells but rather the nucleus of cells to carry out an intracellular delivery. To predetermine the biodistribution and guarantee the internalization of API, NPs must so be functionalized with targeting moieties capable of interacting with specific receptors overexpressed by the ROI to help cells penetration. Classical targeting moieties, FDA approved and used to promote localized accumulation of NPs serving as DDS, are summarized in Table 5:

Table 5: Classical targeting moieties conjugated onto NPs surface.

Class	Ligand (marketed formulation)	Target	Ref.
Antibody	Anti-HER2 (Herceptin®)	Human epidermal growth factor receptor 2 (HER2) from breast, ovarian, gastric, prostate cancer cells	[125]
	Rutiximab, anti-CD20 (Rituxan®)	CD20 antigen on malignant B-cell from lymphoma	[126,127]
Aptamers	Anti-VEGF (Pegaptanib®), DNA, RNA	Vascular endothelial growth factor (VEGF), antigens on cancer cells	[128-131]
Protein	Transferrin	Brain parenchyma (blood-brain barrier crossing), various of cancer cells	[132-135]
Peptide	Cecropin A (Anti-microbial peptides), Antennapedia (cell penetrating peptides), RGD, NGR	Cell membrane (pore forming for apoptosis ending), intracellular matrix, $\alpha_v\beta_3$ integrin receptor on tumor cell	[136,137]
Vitamin	Folic acid	Folate receptor to reach intracellular matrix	[138,139]

Stealth property is obviously still required, even in case of active targeting, because of the gradual accumulation to a given biological site can only be done by letting time to NPs to circulate, reach their target and interact by specific affinities. Binding with a target may be achieved by attaching targeting agents such as ligands conjugated by covalent or electrostatic

bond at the NPs surface. Programming API release is also possible by involving stimuli responsive ligands like pH-sensitive, thermos-sensitive macromolecules or sensitive to the ROI microenvironment.[102,106,109,112,122]

A lot of those ligands are used to target cancer cells. Tumors are quite interesting tissues with complex structures with heterogeneous compartments such as necrotic zones, densely vascularized regions, vessels with tortuosity, hemorrhages issues, non-transformed and malignant cells.[140,141] For a long time, tumor targeting was based on their defective vascular architecture causing NPs permeation inside the tumor microenvironment. The endothelial lining is indeed much more permeable than healthy tissue due to endothelium pore size of 200-600 nm, NPs are thus easily engulfed by extravasation. This high permeability is described as enhanced permeation and retention (EPR) effect. EPR effect promotes effectively meeting between NPs and cellular target but it does not improve cellular uptake or specific interaction. The “leaky” blood vessels are in fact an advantageous defect to deliver NPs into the tumor microenvironment; in addition the dysfunctional and impaired lymphatic drainage guarantees their retention in interstitial space upon fenestration through endothelial lining. However, to yield internalization, NPs must have targeting moieties to improve the bioavailability of API towards cells and if necessary towards the inside of cells. Because of lack of diffusion of API-loaded NPs, targeting is required. Furthermore, some drugs are very difficult to drive into cells and may induce the so-called phenomenon of multiple-drug resistance making fail some treatments on patients. Development of NPs may consequently overcome such problem by trapping API in their core and releasing if once tumor microenvironment is reached.[106,108,142] The Figure 16 described how NPs improve the permeation of API for cancer therapy.

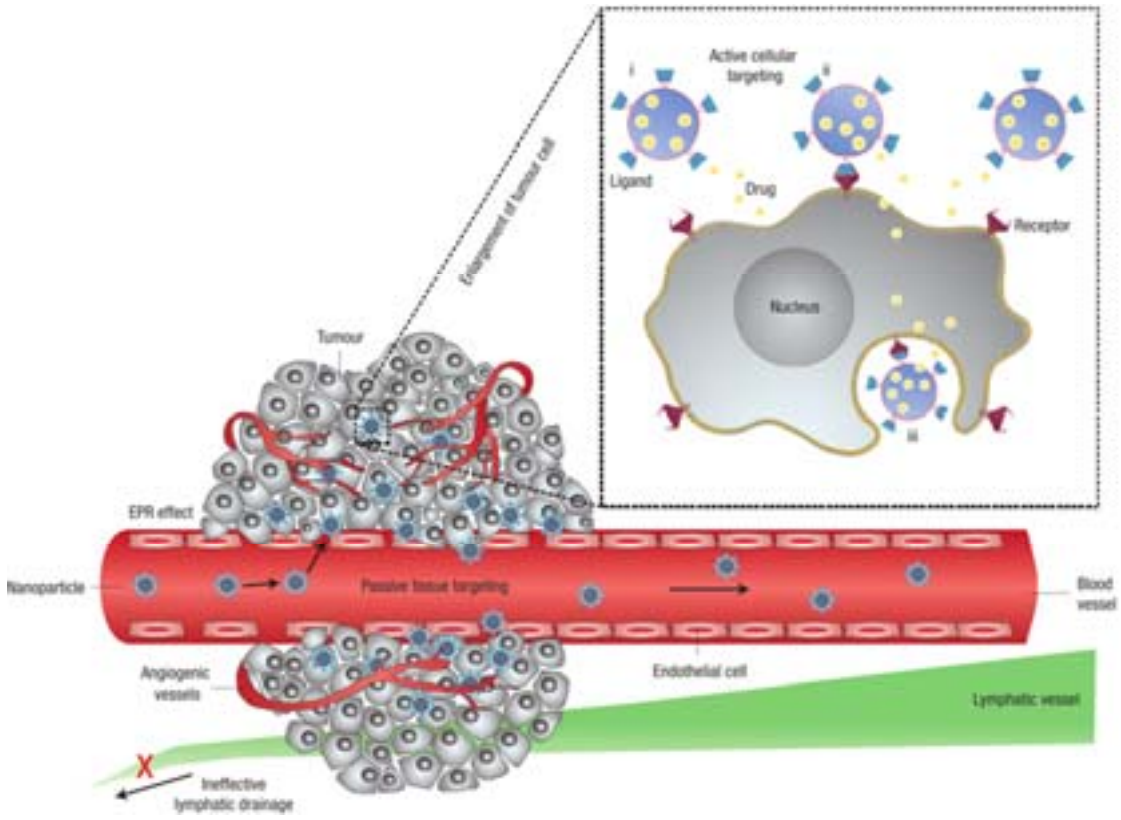

Figure 16: Schematic representation of passive and active targeting mechanisms to deliver API-loaded NPs to tumor. Passive tissue targeting is achieved by extravasation of NPs through EPR effect. Active cellular targeting is achieved by functionalization of NPs surface to promote cell-specific recognition and binding. Three delivery pathways of NPs payload are depicted: i) near the target cells, ii) at extracellular level after attachment onto cell membrane and iii) upon cellular uptake of NPs.[112]

. *Toxicity:*

The *in vivo* fate of NPs includes considerations about the toxicity of NPs (composition, metabolites, interaction with physiological media, impairment of biological entities and/or functions), their composition and break-down products once metabolization occurred. Nanotoxicity is an emerging field but since nanomedicine is more and more extended, there is a real need to understand how long-term retention of NPs and/or their degradation might impair functionality of human body.[68,106]

To conclude it seems that NPs dedicated to biomedical uses should exhibit stringent properties to prevent from adverse effect on health once in contact with biological tissues, fluids and entities. To be used as imaging CA, NPs should also be loaded with contrasting element and prone to be as safe and efficient as possible. Their versatility is a valuable asset

and makes them quite appealing nano-vehicle as much as imaging CA rather than for treatment real-time monitoring.

Optimum nanoparticulate CA should as a result fulfill following specifications: first of all regarding their physicochemical characteristics and their composition, they must be i) made of biocompatible components easily formulated into non-toxic nanoparticulate systems. Colloids should be constituted of ii-1) a core-shell assembling based on ii-2) a protective shield with PEGylated hairy shell to provide stealth properties, steric barrier against aggregation and preventing inner part of the assembling from leaking by efficient encapsulation or trapping of the inner materials and ii-3) a cargo with API(s) as core. For imaging purpose, the core must exhibit very high contrast enhancement ability by means of high payload of contrasting materials to reduce the dose to administrate and avoid as possible side effects. The design should include iii) neutral and hydrophilic surface thanks to PEG and a narrow size distribution (between 50 nm and 200 nm as mean diameter) to avoid embolism, premature clearance by fooling immune system and to promote colloidal stability, prolonged circulation time in blood-pool and homogenous biodistribution and accumulation. The surface may also be functionalized for iv) vectorization needs towards targeted ROI and the associated cells and/or intracellular matrix with active targeting moieties able to bind with overexpressed receptors onto target surface. v-1) The pharmacokinetics and biodistribution should so be programmed in order to v-2) ensure localized accumulation to concentrate the probe and to v-3) avoid administration of NPs-based CA with unpredictable degradation leading to harmful break-down product(s).

Now, concerning the properties required to be considered as an upgraded kind of multifunctional CA, NPs should have intrinsic advantages to be then translated to clinical scale: they have got to offer vi) good solubilization of drugs within their core, vii) protection of API against degradation while encapsulation as an hermetic assembly, viii) controlled release of therapeutic-based API to reduce cytotoxicity on non-targeted tissue and ix) if necessary, improve the intracellular uptake for bioavailability enhancement. The Figure 17 gathers main features of a multifunctional probe based on nanoparticulate system for tumor imaging and therapy.

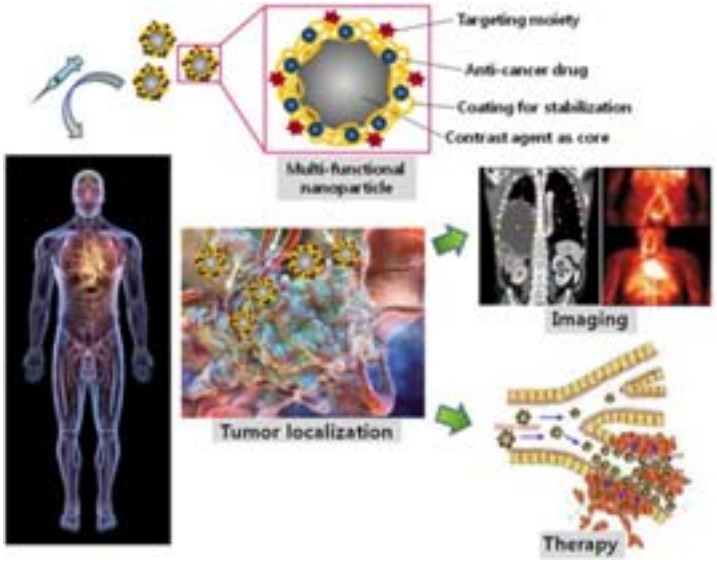

Figure 17: Schematic representation of optimum NPs used for biomedical application.[110]

5.3. Overview of types of NPs and NCs for biomedical applications

A wide range of NPs are nowadays described in literature. They can be constituted of organic, inorganic, hybrid, rigid or flexible materials. As mentioned before for MRI CAs, Gd^{3+} chelates and SPIONs are already applied in clinics and are based on a nanoscale structure, which means that some inorganic NPs and/or nano-assembling involving inorganic core and organic shell are marketed. It should be mentioned that core-shell structure can also be inorganic-inorganic assembling with metallic coating[143,144] or nanocomposite such silica shell[86,145] and carbon coating[146].

More and more NPs investigated are based on NC systems with inner and outer parts. These NCs are generally based on a lipid-based structure and are appealing owing to their high biocompatibility (non-toxic and chemically stable components, stable in physiological media, inert to tissue), high loading capacity of API(s), easy formulation, tailorable surface to apply any kind of targeting strategy, an improved biodistribution and pharmacokinetic profile. Considering all previous advantages abovementioned, they offer a great alternative to iodine-based molecules used as CAs for X-ray imaging but also excellent potential nano-vehicles stabilizing inorganic compounds used for MRI contrast enhancement.[1,47,87,102] General inventory of NCs allows to cite as colloidal CAs for MRI and X-ray imaging the following carriers: liposomes (LPs), dendrimers (DEs), nano-emulsions (NEs), polymeric macromolecules-based carriers or polymeric NPs (PNPs) (micelles, nanospheres and

nanocapsules), and lipoproteins (LPP).[1,14,25,28,44,46,47,87,147] Descriptions and a couple of examples of each NC used to drive CAs *in vivo* are presented hereinafter.

Liposomes: Long-time circulating LPs are based on spherical vesicular self-assembling PEGylated phospholipids enclosing an aqueous core within a lipid bilayer shell. Hydrophilic and lipophilic API(s) can respectively be encapsulated either within the inner core and the outer lipid membrane. A common technique to produce them is ultrasonication method. They constitute one of the oldest NCs used as DDS. Tremendous progresses were done to extent their circulating time by surface functionalization with stealth polymers such as PEG. As shown in Figure 18, they were used as much as stabilizing carriers of inorganic CAs like SPIONs (magnetoliposomes) and gadolinium-based compounds rather than convective transporters of iodinated compounds (iodoliposomes, iodine-containing LPs) for imaging purpose. Their extreme versatility make them be promising multifunctional NCs.[110,122,148]

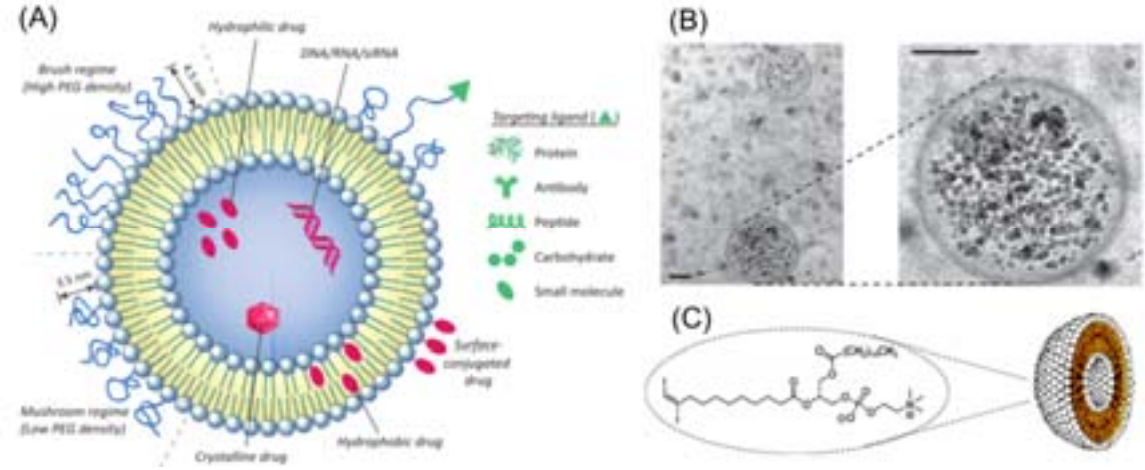

Figure 18: (A) Various features to form multifunctional LP as targeted DDS (Adapted from Ref. [122]). (B) TEM micrograph of magnetoliposomes based on SPIONs-loaded LPs for T2-weighted MRI (black bars represent 100 nm) (Adapted from Ref. [149]). (C) Chemical structure of iodinated phospholipid involved into lipids bilayer of iodoliposome for X-ray imaging (Adapted from Ref. [44]).

Dendrimers: DEs are perfect structured assembling relying on branched molecules with a globular shape. DEs have a three-part topology: i) an inner core which trap or anchor a single element or a group, ii) a multilayer made of repeating units, called generations, and iii) an outer surface with peripheral functions directed outward available for functionalization. Three main pathways of preparation are provided in the literature: convergent, divergent and “click” chemistry methods. DEs were very often time employed to carry SPIONs, T1-weighted CAs

based on gadolinium derivatives product (magnetodendrimers) but also for inorganic NPs like gold NPs for X-rays imaging.[139,150] DEs, like poly(amidoamine) (PAMAM) DEs, were extensively investigated as DDS for GI track by oral administration (Figure 19).[26,64,109,151,152]

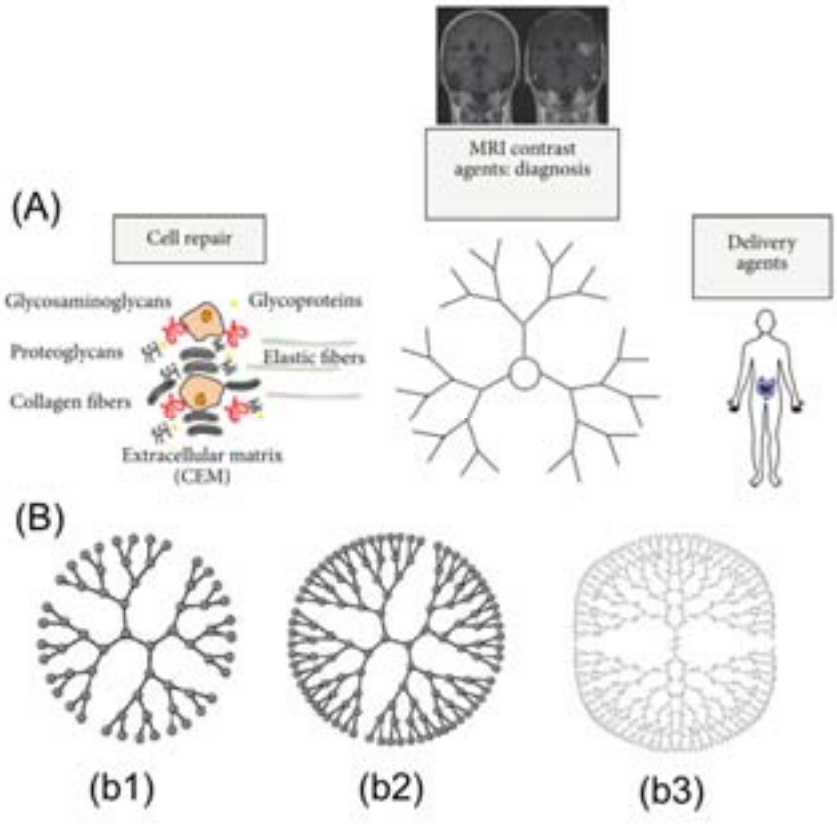

Figure 19: (A) Fields of biomedical applications of DEs. (B) PANAM DEs with (b1) 3, (b2) 4 and (b3) 5 generations (Adapted from Ref. [192]).

Nano-emulsions: NEs are submicron emulsified droplets, commonly oil-in-water suspensions, with sizes between 20-200 nm. Actually, these are thermodynamically stable isotropic system made of a mixture of immiscible liquids forming a single phase by means of surfactant macromolecules. Two main processes are applied to obtain NEs: low energy (spontaneous emulsification) and high energy (ultrasonication, microfluidic) processes [153-157] They offer excellent NCs properties for multiple APIs loading as much as for imaging purpose than for therapy. For instance, and as depicted in Figure 20, iodinated NEs were produced for liver and spleen X-rays imaging[158-160], bimodal NEs as MRI/optical CAs were also described for xenograft cancer targeting showing efficient accumulation of probes by EPR effect *via* all imaging modalities.[161]

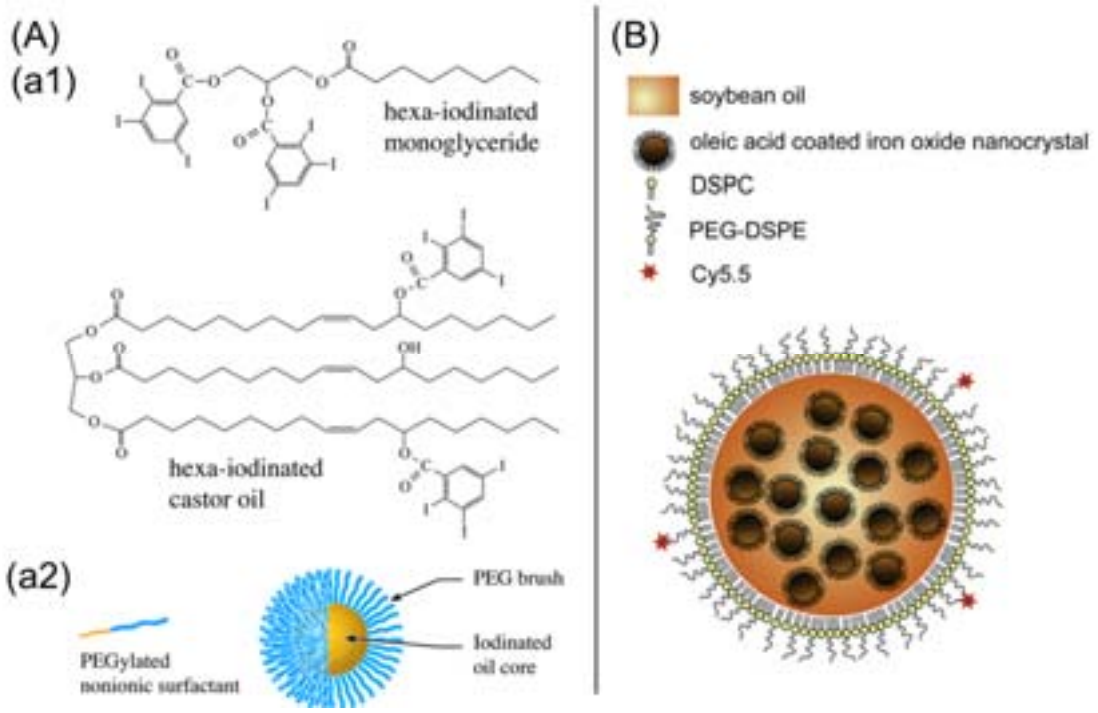

Figure 20: (A) Examples of (a1) iodinated oils respectively formulated into NE and (a2) schematic representation of iodinated nano-droplet (Adapted from Ref. [160]). (B) Dual modal NE drolplet including iron oxide in its core and cysteine 5.5 (Cys5.5) as a fluorescent dye and decorating moieties respectively as T2-weighted MRI and optical imaging contrast enhancer probes (Adapted from Ref. [161]).

Polymeric NCs: This family of NCs comprises a broad group gathering several types of PNPs with their own designs based on polymeric macromolecules (Figure 21(A,B)) with amphiphilic properties. It includes polymeric micelles, nanocapsules and nanospheres.

Micelles are surfactant macromolecule assembling; block copolymers are mostly used and need to be introduced above the so-called critical micellar concentration (CMC) to yield micelles. With an hydrophobic core, they can only be loaded with lipophilic API(s). Targeted PEGylated polymeric micelles were thus applied as a theranostic platform with SPIONs and doxorubicine co-loading for drug delivery to cancer cells and MRI monitoring.[162] PEGylated micelles were also investigated as vehicles of different CAs for X-ray, MRI and γ-rays imaging, like for instance for blood-pool and liver imaging.[120,163] However, their outer part, corresponding to the hydrophilic parts of surfactant, can be stimuli-responsive block in order to promote drug controlled release upon specific conditions (pH, temperature, redox, external conditions).[164-166]

Polymer-based NCs can be formulated as nanospheres and nanocapsules. The first design is a rigid construct with an insoluble polymeric matrix as a core; corona shell is mostly polymer

proving stealth properties. API(s) can be directly grafted onto the polymer backbone, attached onto the surface or embedded within the matrix. In the case of nanocapsules, the inner core is a liquid phase surrounding by a rigid crosslinked polymeric membrane formed by cross-linking (like Pluronic®/PEG nanocapsules[167]). Such NCs are usually involved for drug encapsulation.[168–175] A lot of iodinated polymers were investigated for X-ray imaging[176,177]. Nanospheres were also used to embedded SPIONs for MRI[178] (Figure 21C) but also for bimodal imaging with X-ray/MRI[81,179]. Hybrids with polymer, SPIONs and gold NPs were also reported, in such case SPIONs and gold NPs were not embedded in polymeric matrix but were coated to yield nanocomposite design with very good magnetic properties for MRI and radiopaque properties.[180-181]

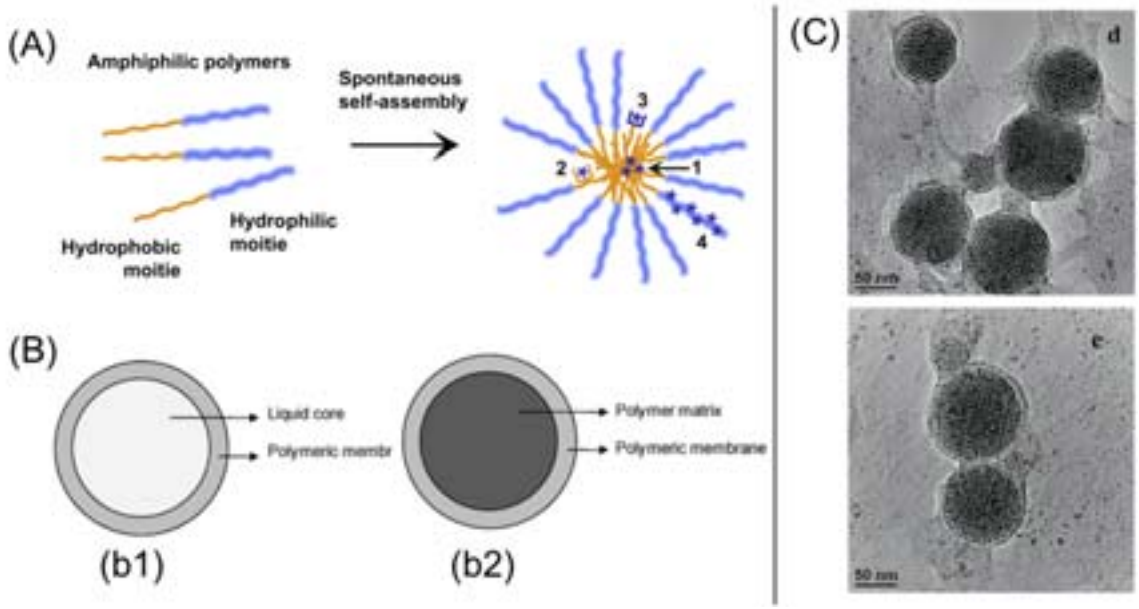

Figure 21: (A) Polymeric micelles self –assembling to yield micelle with (blue star) API (1) solubilized inside the core, (2) linked to lipophilic moieties, (3) covalently conjugated to lipophilic moieties and (4) linked to the hydrophilic moieties (Adapted from Ref. [25]). (B) PNPs designed as (b1) nanocapsule and (b2) nanosphere (Adapted from Ref. [175]). (C) Fe_3O_4/PMMA nanocomposites TEM micrographs (Adapted from Ref. [182]).

Lipoproteins: LPPs are natural-inspired NPs based on a lipid-protein system made of a phospholipid inner part for hydrophobic payload and proteins as outer corona layer. Natural endogenous LPPs can be low-density (LDL) (18-25 nm) or high-density (HDL) (5-12 nm) types of LPs and transport poorly water-soluble compounds like lipids and cholesterol through the bloodstream. Chylomicrons and very low density LPs (VLDL) are also biological LPs involved in lipids transportation. Chylomicrons are biggest LPs with a mean size around 1000 nm. VLDLs are produced by liver and may be turned into LDL. Study of LPs was a

huge breakthrough for the understanding of cholesterol metabolism. Their differences of mean diameter and composition (Figure 22A) make LDL and HDL have specific pharmacokinetic profiles: LDLs suit for cancer targeting whereas HDLs are more suitable to across limited access area like endothelial lining and underlying tissue. HDLs have been pointed out as promising for cancer cell uptake.[183,184]Both LPs were already used for CAs encapsulation like, for example, for X-rays and fluorescence imaging *via* gold NPs-loaded LDLs with dye-labelled surface and for T2-weighted MRI for magnetically driven anti-cancer drug-loaded HDLs-based DDS as illustrated in Figure 22(B,C).[185,186] Cormode *et al.* also showed that HDLs were outstanding nano-scale imaging platform for improved visualization of atherosclerosis and cancer related processes.[187]

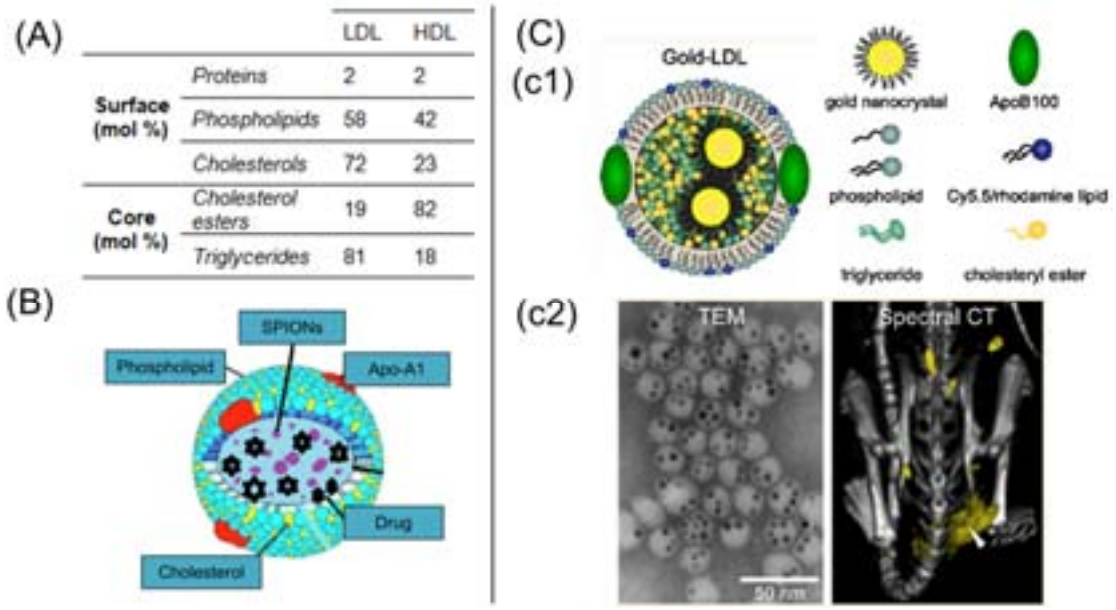

Figure 22: (A) Composition of LDL and HDL (Adapted from Ref. [184]). (B) Schematic representation of multifunctional HDL theranostic probe containing SPIONs for MRI T2-weight contrast enhancement and valrubicin as anti-cancer drug (Adapted from Ref. [185]). (C) (c1) Schematic structure of radiopaque gold NPs-labelled LDL with fluorescent dyes on surface, (c2) (Left) their TEM micrograph and (right) an *in vivo* X-ray investigation of tumor mouse model after administration of these bimodal LDL probes (Adapted from Ref. [186]).

Since all NCs previously described have already been employed to drive either contrasting and therapeutics agents, figuring out best NCs for a specific applications need to go over their inherent advantages and limitations. These are provided in Table 6:

Table 6: Assets and drawbacks of typical lipid-based NCs dedicated for DDS and CAs carriers.

NCs	Advantages	Limitations
LPs	Biocompatible, biodegradable, very versatile (multifunctionality, tailorable)	API leakage from aqueous core, low stability, difficult purification
DEs	Well-structured, high anchoring ability, biocompatible, stable	Low yield for large DEs production, expensive to produce, elimination routes still unclear
NEs	Stable over several months, improved pharmacokinetic of poorly water-soluble compound, biodegradable, high payload capacity	Ostwald ripening destabilization, high amount of surfactant, expensive to produce
Micelles	High loading capacity, stimuli-responsive, Spontaneous formation upon CMC, cost-effective production	Disassembly upon dilution, fast drug release
Nanospheres, Nanocapsules	Inert to biological tissues, easy to prepare, loading of various compounds, no leakage	Not always biodegradable polymer, aggregation, lack of knowledge about their *in vivo* fate,
LPPs	Biocompatibility, mimicking natural biological entity, co-loading, low toxicity	Loading of hydrophobic compounds, limited number of formulation technique, difficult purification process

6. Conclusion

An overview of main imaging techniques was presented. Taking into account their own characteristics, it appeared that X-ray scanner and MRI were the two most popular instruments for non-invasive diagnosis purposes. Huge developments led them to be nowadays to the top of their capacities to yield high resolution images with complementary data. Thereby, organs, lesions, interstitial fluids and skeleton imaging are feasible without any limit of depth penetration. Additionally, contrast enhancement substances are more and more developed and are moving forward to nanotechnology to cope with adverse effects and limitations of current blood-pool probes. Novel and appealing contrast enhancer formulations are consequently introduced to clinics thanks to extensive research in preclinical stages. NPs and NCs represent thus a wide family of nano-vehicles of APIs. These smart and multifunctional colloids are becoming the next generation of probes for all imaging instruments. Their versatile designs are a key to go beyond currents limits and further in the field of theranostic and nanomedicine.

7. References

[1] M.A. Hahn, A.K. Singh, P. Sharma, S.C. Brown, B.M. Moudgil, Nanoparticles as contrast agents for in-vivo bioimaging: Current status and future perspectives, Anal. Bioanal. Chem. 399 (2011) 3–27. doi:10.1007/s00216-010-4207-5.

[2] J. Key, J.F. Leary, Nanoparticles for multimodal *in vivo* imaging in nanomedicine, Int. J. Nanomedicine. 9 (2014) 711–726. doi:10.2147/IJN.S53717.

[3] X. Li, N. Anton, G. Zuber, T. Vandamme, Contrast agents for preclinical targeted X-ray imaging, Adv. Drug Deliv. Rev. 76 (2014) 116–133. doi:10.1016/j.addr.2014.07.013.

[4] M. Elsabahy, G.S. Heo, S.-M. Lim, G. Sun, K.L. Wooley, Polymeric Nanostructures for Imaging and Therapy, Chem. Rev. 115 (2015) 10967–11011. doi:10.1021/acs.chemrev.5b00135.

[5] L. Fass, Imaging and cancer: A review, Mol. Oncol. 2 (2008) 115–152. doi:10.1016/j.molonc.2008.04.001.

[6] M.L. James, S.S. Gambhir, A Molecular Imaging Primer: Modalities, Imaging Agents, and Applications, Physiol. Rev. 92 (2012) 897–965. doi:10.1152/physrev.00049.2010.

[7] V. Koo, P.W. Hamilton, K. Williamson, Non-invasive *in vivo* imaging in small animal research, Cell. Oncol. 28 (2006) 127–139. doi:10.1155/2006/245619.

[8] M.G. Van Der Vaart, R. Meerwaldt, R.H.J.A. Slart, G.M. Van Dam, R.A. Tio, C.J. Zeebregts, Application of PET / SPECT Imaging in Vascular Disease, Eur J Vasc Endovasc Surg. 51335 (2008) 507–513. doi:10.1016/j.ejvs.2007.11.016.

[9] Q. Huang, Z. Zeng, A Review on Real-Time 3D Ultrasound Imaging Technology, BioMed Res. Int. Res. Int. 2017 (2017) 1–20.

[10]N. Deshpande, A. Needles, J.K. Willmann, Molecular ultrasound imaging : current status and future directions, Clin. Radiol. 65 (2010) 567–581. doi:10.1016/j.crad.2010.02.013.

[11]X. Michalet, F.F. Pinaud, L.A. Bentolila, J.M. Tsay, S. Doose, J.J. Li, G. Sundaresan, A.M. Wu, S.S. Gambhir, S. Weiss, Quantum Dots for Live Cells, *In Vivo* Imaging, and Diagnostics, Science (80-.). 307 (2005) 538–544. doi:10.1016/j.biotechadv.2011.08.021.Secreted.

[12]Y. Volkov, Quantum dots in naomedecine: recent trends, advances and unresolved issues, Biochem. Biophys. Res. Commun. (2015) 1–9. doi:10.1016/j.bbrc.2015.07.039.

[13]X. He, N. Ma, An overview of recent advance of quantum dots for biomedical applications, Colloids Surfaces B Biointerfaces. 124 (2014) 118–131. doi:10.1016/j.colsurfb.2014.06.002.

[14]H. Lusic, M.W. Grinstaff, X-ray Computed Tomography Contrast Agents, Chem. Rev. 113 (2013) 1641–1666. doi:doi.org/10.1021/cr200358s.

[15]V. Koo, P.W. Hamilton, K. Williamson, Non-invasive *in vivo* imaging in small animal research., Cell. Oncol. 28 (2006) 127–139. doi:10.1155/2006/245619.

[16]M.R. Oliva, S. Saini, M.G. Hospital, M.G. Hospital, Liver cancer imaging: role of CT, MRI, US and PET, Cancer Imaging. 4 (2004) 42–46. doi:10.1102/1470-7330.2004.0011.

[17]T.C. Noone, R.C. Semelka, D.M. Chaney, C. Reinhold, Abdominal imaging studies : comparison of diagnostic accuracies resulting from ultrasound, computed tomography, and magnetic resonance imaging in the same individual, Magn. Reson. Imaging. 22 (2004) 19–24. doi:10.1016/j.mri.2003.01.001.

[18]R.C. Semelka, D.R. Martin, C. Balci, T. Lance, Focal Liver Lesions : Comparison of Dual-Phase CT and Multisequence Multiplanar MR Imaging Including Dynamic Gadolinium Enhancement, J. Magn. Reson. Imaging. 13 (2001) 397–401.

[19]A. Elstob, M. Gonsalves, U. Patel, Diagnostic modalities, Int. J. Surg. 36 (2016) 504–512. doi:10.1016/j.ijsu.2016.06.005.

[20]J. Elias, R.C. Semelka, E. Altun, M. Tsurusaki, E. Pamuklar, M. Zapparoli, V. Voultsinos, D.M. Armao, T. Rubinas, Pancreatic Cancer : Correlation of MR Findings, Clinical Features, and Tumor Grade, J. M. 26 (2007) 1556–1563. doi:10.1002/jmri.21210.

[21]E.S. Lee, J.M. Lee, Imaging diagnosis of pancreatic cancer : A state-of-the-art review, 20 (2014) 7864–7877. doi:10.3748/wjg.v20.i24.7864.

[22]W.C. Röntgen, On a new kind of rays, Science (80). 3 (1896) 227–231. doi:DOI: 10.1126/science.3.59.227.

[23]G.N. Hounsfield, Computerized transverse axial scanning(tomography): Part I description of system, Br. J. Radiol. 46 (1973) 1016–1022. doi:10.1259/0007-1285-46-552-1016.

[24]S.-B. Yu, A.D. Watson, Metal-Based X-ray Contrast Media, Chem. Rev. 99 (1999) 2353–2378. doi:10.1021/cr980441p.

[25]F. Hallouard, N. Anton, P. Choquet, A. Constantinesco, T. Vandamme, Iodinated blood pool contrast media for preclinical X-ray imaging applications - A review, Biomaterials. 31 (2010) 6249–6268. doi:10.1016/j.biomaterials.2010.04.066.

[26]A. Jakhmola, N. Anton, T.F. Vandamme, Inorganic nanoparticles based contrast agents for X-ray computed tomography, Adv. Healthc. Mater. 1 (2012) 413–431. doi:10.1002/adhm.201200032.

[27]D.P. Cormode, P.C. Naha, Z.A. Fayad, Nanoparticle contrast agents for computed tomography: A focus on micelles, Contrast Media Mol. Imaging. 9 (2014) 37–52. doi:10.1002/cmmi.1551.

[28]N. Lee, S.H. Choi, T. Hyeon, Nano-sized CT contrast agents, Adv. Mater. 25 (2013) 2641–2660. doi:10.1002/adma.201300081.

[29]J.C. De La Vega, U.O. Häfeli, Utilization of nanoparticles as X-ray contrast agents for diagnostic imaging applications, Contrast Media Mol. Imaging. 10 (2014) 81–95. doi:10.1002/cmmi.1613.

[30]C.T. Badea, M. Drangova, D.W. Holdsworth, G.A. Johnson, *In vivo* small-animal imaging using micro-CT and digital subtraction angiography., Phys. Med. Biol. 53 (2008) R319–R350. doi:10.1088/0031-9155/53/19/R01.

[31]D.W. Holdsworth, M.M. Thornton, Micro-CT in small animal and specimen imaging, Trends Biotechnol. 20 (2002) 34–39. doi:10.1016/S0167-7799(02)02004-8.

[32]S.J. Schambach, S. Bag, L. Schilling, C. Groden, M.A. Brockmann, Application of micro-CT in small animal imaging, Methods. 50 (2010) 2–13. doi:10.1016/j.ymeth.2009.08.007.

[33]E.L. Ritman, Small-animal CT: Its difference from, and impact on, clinical CT, Nucl. Instruments Methods Phys. Res. Sect. A. 580 (2007) 968–970. doi:10.1016/j.nima.2007.06.040.

[34]J. Jones, C. Mills, M. Mogensen, C. Lee, Radiation Dose From Medical Imaging: A Primer for Emergency Physicians, West. J. Emerg. Med. 13 (2012) 202–210. doi:10.5811/westjem.2011.11.6804.

[35]D.J. Brenner, E.J. Hall, Computed tomography--an increasing source of radiation exposure, N. Engl. J. Med. 357 (2007) 2277–2284. doi:10.1056/NEJMra072149.

[36]J.-M. Idée, B. Guiu, Use of Lipiodol as a drug-delivery system for transcatheter arterial chemoembolization of hepatocellular carcinoma: A review, Crit. Rev. Oncol. Hematol. 88 (2013) 530–549. doi:10.1016/j.critrevonc.2013.07.003.

[37]J.M. Widmark, Imaging-related medications: a class overview, Proc. (Baylor Univ. Med. Center). 20 (2007) 408–417.

[38]H. Suzuki, H. Oshima, N. Shiraki, C. Ikeya, Y. Shibamoto, Comparison of two contrast materials with different iodine concentrations in enhancing the density of the the aorta, portal vein and liver at multi-detector row CT: A randomized study, Eur. Radiol. 14 (2004) 2099–2104. doi:10.1007/s00330-004-2439-5.

[39]L. Zagorchev, P. Oses, Z. Zhuang, K. Moodie, M. Simons, T. Couffinhal, L. Zagorchev, P. Oses, Z. Zhuang, K. Moodie, M. Mulligan-kehoe, L. Zagorchev, P. Oses, Z.W. Zhuang, K. Moodie, M.J. Mulligan-kehoe, Micro computed tomography for vascular exploration, Journal of Angiogenesis Research. 2:7 (2010). doi:10.1186/2040-2384-2-7.

[40]M.S. Kandanapitiye, M. Gao, J. Molter, C.A. Flask, S.D. Huang, Synthesis, characterization, and X-ray attenuation properties of ultrasmall BiOI nanoparticles: Toward renal clearable particulate CT contrast agents, Inorg. Chem. 53 (2014) 10189–10194. doi:10.1021/ic5011709.

[41]C. Briguori, D. Tavano, A. Colombo, Contrast agent-associated nephrotoxicity, Prog. Cardiovasc. Dis. 45 (2003) 493–503. doi:10.1053/pcad.2003.YPCAD16.

[42]S.Y. Lee, C.M. Rhee, A.M. Leung, L.E. Braverman, G.A. Brent, E.N. Pearce, A review: Radiographic iodinated contrast media-induced thyroid dysfunction, J. Clin. Endocrinol. Metab. 100 (2015) 376–383. doi:10.1210/jc.2014-3292.

[43]W. Bottinor, P. Polkampally, I. Jovin, Adverse reactions to iodinated contrast media, Int. J. Angiol. 22 (2013) 149–154. doi:10.1007/s003300000729.

[44]W. He, K. Ai, L. Lu, Nanoparticulate X-ray CT contrast agents, Sci. China Chem. 58 (2015) 753–760. doi:10.1007/s11426-015-5351-8.

[45]C.E. Suckow, D.B. Stout, MicroCT liver contrast agent enhancement over time, dose, and mouse strain, Mol. Imaging Biol. 10 (2008) 114–120. doi:10.1007/s11307-007-0128-x.

[46]N. Anton, T.F. Vandamme, Nanotechnology for computed tomography: A real potential recently disclosed, Pharm. Res. 31 (2014) 20–34. doi:10.1007/s11095-013-1131-3.

[47]D.P. Cormode, T. Skajaa, Z.A. Fayad, W.J.M. Mulder, Nanotechnology in medical imaging: probe design and applications, Arter. Thromb Vasc Biol. 29 (2010) 992–1000. doi:10.1161/ATVBAHA.108.165506.

[48]C. Sun, J.S.H. Lee, M. Zhang, Magnetic nanoparticles in MR imaging and drug delivery, Adv. Drug Deliv. Rev. 60 (2008) 1252–1265. doi:10.1016/j.addr.2008.03.018.

[49]S. Mornet, S. Vasseur, F. Grasset, E. Duguet, Magnetic nanoparticle design for medical diagnosis and therapy, J. Mater. Chem. 14 (2004) 2161–2175.

[50]S. Laurent, D. Forge, M. Port, A. Roch, C. Robic, L. Vander Elst, R.N. Muller, Magnetic iron oxide nanoparticles: Synthesis, stabilization, vectorization, physicochemical characterizations and biological applications, Chem. Rev. 108 (2008) 2064–2110. doi:10.1021/cr068445e.

[51]Q.A. Pankhurst, J. Connolly, S.K. Jones, J. Dobson, Applications of magnetic nanoparticles in biomedicine, J. Phys. D. Appl. Phys. 36 (2003) R167–R181. doi:10.1088/0022-3727/36/13/201.

[52]V.P.B. Grover, J.M. Tognarelli, M.M.E. Crossey, I.J. Cox, S.D. Taylor-Robinson, M.J.W. McPhail, Magnetic Resonance Imaging: Principles and Techniques: Lessons for Clinicians, J. Clin. Exp. Hepatol. 5 (2015) 246–255. doi:10.1016/j.jceh.2015.08.001.

[53]R. Damadian, Tumor Detection by Nuclear Magnetic Resonance, Science (80-.). 171 (1971) 1151–1153. doi:10.1126/science.171.3976.1151.

[54]P.C. Lauterbur, Image Formation by Induced Local Interactions: Examples Employing Nuclear Magnetic Resonance, Nature. 242 (1973) 190–191. doi:10.1038/242190a0.

[55]A.N. Garroway, P.K. Grannell, P. Mansfield, Image formation in NMR by a selective irradiative process, J. Phys. C Solid State Phys. 7 (1974) L457–L462. doi:10.1088/0022-3719/7/24/006.

[56]P. Mansfield, A.A. Maudsley, Medical imaging by NMR, J. Magn. Reson. 27 (1977) 101–119. doi:10.1259/0007-1285-50-591-188.

[57]W.A. Edelstein, J.M.S. Hutchison, G. Johnson, T. Redpath, Spin warp NMR imaging and applications to human whole-body imaging, Phys. Med. Biol. 25 (1980) 751–756. doi:10.1088/0031-9155/25/4/017.

[58]J.M.S. Hutchinson, W.A. Edelstein, G. Johnson, A whole-body NMR imaging machine, J. Phys. E. 13 (1980) 947–955. doi:10.1088/0022-3735/13/9/013.

[59]I.L. Pykett, R.R. Rzedzian, Instant images of the body by magnetic resonance, Magn. Reson. Med. 5 (1987) 563–571. doi:10.1002/mrm.1910050607.

[60]H. Bin Na, I.C. Song, T. Hyeon, Inorganic nanoparticles for MRI contrast agents, Adv. Mater. 21 (2009) 2133–2148. doi:10.1002/adma.200802366.

[61]W.R. Nitz, P. Reimer, Contrast mechanisms in MR imaging, Eur. Radiol. 9 (1999) 1032–1046. doi:10.1007/s003300050789.

[62]G.B. Chavhan, P.S. Babyn, B. Thomas, M.M. Shroff, E.M. Haacke, Principles, techniques, and applications of T2*-based MR imaging and its special applications., RadioGraphics. 29 (2009) 1433–1449. doi:10.1148/rg.295095034.

[63]G. Strijkers, W. M. Mulder, G. F. van Tilborg, K. Nicolay, MRI Contrast Agents: Current Status and Future Perspectives, Anticancer. Agents Med. Chem. 7 (2007) 291–305. doi:10.2174/187152007780618135.

[64]C.F.G.C. Geraldes, S. Laurent, Classification and basic properties of contrast agents for magnetic resonance imaging, Contrast Media Mol Imaging. 4 (2009) 1–23. doi:10.1002/cmmi.265.

[65]D. Hao, T. Ai, F. Goerner, X. Hu, V.M. Runge, M. Tweedle, MRI contrast agents: Basic chemistry and safety, J. Magn. Reson. Imaging. 36 (2012) 1060–1071. doi:10.1002/jmri.23725.

[66]Z. Sahraei, M. Mirabzadeh, D. Fadaei-Fouladi, N. Eslami, A. Eshraghi, Magnetic Resonance Imaging Contrast Agents: A Review of Literature, J. Pharm. Care. 2 (2014) 177–182.

[67]W. Chen, D.P. Cormode, Z.A. Fayad, W.J.M. Mulder, Nanoparticles as magnetic resonance imaging contrast agents for vascular and cardiac diseases, Nanomedicine and Nanobiotechnology. (2012) 1-25.

[68]N. Singh, G.J.S. Jenkins, R. Asadi, S.H. Doak, Potential toxicity of superparamagnetic iron oxide nanoparticles (SPION), Nano Rev. (2010) 1:5358 . doi:10.3402/nano.v1i0.5358.

[69]Y.J. Wang, Superparamagnetic iron oxide based MRI contrast agents : Current status of clinical application, 1 (2011) 35–40. doi:10.3978/j.issn.2223-4292.2011.08.03.

[70]Y.-X.J. Wang, Current status of superparamagnetic iron oxide contrast agents for liver magnetic resonance imaging, World J. Gastroenterol. 21 (2015) 13400–13402. doi:DOI: 10.3748/wjg.v21.i47.13400.

[71]Y.X.J. Wang, S.M. Hussain, G.P. Krestin, Superparamagnetic iron oxide contrast agents: Physicochemical characteristics and applications in MR imaging, Eur. Radiol. 11 (2001) 2319–2331. doi:10.1007/s003300100908.

[72]C. Corot, P. Robert, J.M. Idée, M. Port, Recent advances in iron oxide nanocrystal technology for medical imaging, Adv. Drug Deliv. Rev. 58 (2006) 1471–1504. doi:10.1016/j.addr.2006.09.013.

[73]R. Lawaczeck, M. Menzel, H. Pietsch, Superparamagnetic iron oxide particles: Contrast media for magnetic resonance imaging, Appl. Organometal. Chem. 18 (2004) 506–513. doi:10.1002/aoc.753.

[74]J. Lodhia, G. Mandarano, N.J. Ferris, P. Eu, S.F. Cowell, Development and use of iron oxide nanoparticles (Part 1): Synthesis of iron oxide nanoparticles for MRI, Biomed. Imaging Interv. J. 6 (2010) e12. doi:10.2349/biij.6.2.e12.

[75]J. Wan, W. Cai, X. Meng, E. Liu, Monodisperse water-soluble magnetite nanoparticles prepared by polyol process for high-performance magnetic resonance imaging., Chem. Commun. 4 (2007) 5004–5006. doi:10.1039/b712795b.

[76]N. Lee, H.R. Cho, M.H. Oh, S.H. Lee, K. Kim, B.H. Kim, K. Shin, T. Ahn, J.W. Choi, Y. Kim, S.H. Choi, T. Hyeon, Multifunctional Fe_3O_4/TaO_x Core/Shell Nanoparticles for Simultaneous Magnetic Resonance Imaging and X-Ray Computer Tomography, J Am Chem Soc. 134 (2012) 10309–10312. doi:10.1021/ja3016582.

[77]S. Xue, Y. Wang, M. Wang, L. Zhang, X. Du, H. Gu, C. Zhang, Iodinated oil-loaded, fluorescent mesoporous silica-coated iron oxide nanoparticles for magnetic resonance imaging/computed tomography/fluorescence trimodal imaging, Int. J. Nanomedicine. 9 (2014) 2527–2538. doi:10.2147/IJN.S59754.

[78]P.A. Jarzyna, A. Gianella, T. Skajaa, G. Knudsen, L.H. Deddens, D.P. Cormode, Z. a. Fayad, W.J.M. Mulder, Multifunctional imaging nanoprobes, Wiley Interdiscip. Rev. Nanomedicine Nanobiotechnology. 2 (2010) 138–150. doi:10.1002/wnan.72.

[79]R. Bardhan, W. Chen, M. Bartels, C. Perez-Torres, M.F. Botero, R.W. McAninch, A. Contreras, R. Schiff, R.G. Pautler, N.J. Halas, A. Joshi, Tracking of multimodal therapeutic nanocomplexes targeting breast cancer *in vivo*, Nano Lett. 10 (2010) 4920–4928. doi:10.1021/nl102889y.

[80]J. Yang, E.-K. Lim, H.J. Lee, J. Park, S.C. Lee, K. Lee, H.-G. Yoon, J.-S. Suh, Y.-M. Huh, S. Haam, Fluorescent magnetic nanohybrids as multimodal imaging agents for human epithelial cancer detection., Biomaterials. 29 (2008) 2548–2555. doi:10.1016/j.biomaterials.2007.12.036.

[81]H. Aviv, S. Bartling, J. Budjan, S. Margel, Synthesis and characterization of dual modality (CT/MRI) core-shell microparticles for embolization purposes, Biomacromolecules. 11 (2010) 1600–1607. doi:10.1021/bm100251s.

[82]H. Ding, F. Wu, Image guided biodistribution and pharmacokinetic studies of theranostics, Theranostics. 2 (2012) 1040–1053. doi:10.7150/thno.4652.

[83]C. Barsanti, F. Lenzarini, C. Kusmic, Diagnostic and prognostic utility of non-invasive imaging in diabetes management, World J Diabetes. 6 (2015) 792–806. doi:10.4239/wjd.v6.i6.792.

[84]A. Senpan, S.D. Caruthers, I. Rhee, N.A. Mauro, D. Pan, G. Hu, M.J. Scott, R.W. Fuhrhop, P.J. Gaffney, S.A. Wickline, G.M. Lanza, Conquering the dark side: Colloidal iron oxide nanoparticles, ACS Nano. 3 (2009) 3917–3926. doi:10.1021/nn900819y.

[85]L. Xu, L. Cheng, C. Wang, R. Peng, Z. Liu, Conjugated polymers for photothermal therapy of cancer, Polym. Chem. 5 (2014) 1573–1580. doi:10.1039/C3PY01196H.

[86]S. Kumar, A. Daverey, V. Khalilzad-Sharghi, N.K. Sahu, S. Kidambi, S.F. Othman, D. Bahadur, Theranostic fluorescent silica encapsulated magnetic nanoassemblies for *in vitro* MRI imaging and hyperthermia, RSC Adv. 5 (2015) 53180–53188. doi:10.1039/C5RA07632C.

[87]V.P. Torchilin, Multifunctional nanocarriers, Adv. Drug Deliv. Rev. 64 (2012) 302–315. doi:10.1016/j.addr.2012.09.031.

[88]L.K. Bogart, G. Pourroy, C.J. Murphy, V. Puntes, T. Pellegrino, D. Rosenblum, D. Peer, R. Lévy, Nanoparticles for imaging, sensing, and therapeutic intervention, ACS Nano. 8 (2014) 3107–3122. doi:10.1021/nn500962q.

[89]M.F. Kircher, J.K. Willmann, Molecular Body Imaging : MR Imaging, CT, and US. Part II. Applications, Radiology. 264 (2012) 349–368.

[90]M.D. Morse, Clusters of Transition-Metal Atoms, Chem. Rev. 86 (1986) 1049–1109. doi:10.1021/cr00076a005.

[91]A. Henglein, Small-particle research: physicochemical properties of extremely small colloidal metal and semiconductor particles, Chem. Rev. 89 (1989) 1861–1873. doi:10.1021/cr00098a010.

[92]M. Faraday, The Bakerian lecture: experimental relations of gold (and other metals) to light, Phil. Trans. R. Soc. Lond.147 (1857) 145–181. doi:10.1098/rstl.1857.0011.

[93]H. Goesmann, C. Feldmann, Nanoparticulate functional materials, Angew. Chemie - Int. Ed. 49 (2010) 1362–1395. doi:10.1002/anie.200903053.

[94]B. Issa, I.M. Obaidat, B. a. Albiss, Y. Haik, Magnetic nanoparticles: Surface effects and properties related to biomedicine applications, Int. J. Mol. Sci. 14 (2013) 21266–21305. doi:10.3390/ijms141121266.

[95]T. Indira, P.K. Lakshmi Magnetic Nanoparticles - A Review, Int. J. Pharm. Sc. Nano. 3 (2010) 1035–1042. http://ijpsnonline.com/Issues/1035_full.pdf.

[96] V.N. Nikiforov, E.Y. Filinova, Biomedical Applications of Magnetic Nanoparticles, (2010) 393-455 doi:10.1142/S1793292010002165.

[97]S. Becht, S. Ernst, R. Bappert, C. Feldmann, Do-it-yourself! Nanomaterialien zum anfassen, Chemie Unserer Zeit. 44 (2010) 14–23. doi:10.1002/ciuz.200900508.

[98]J.L.D.. Tyndall, On the Blue Color of the Sky , the Polarization of Sky-Light, and Polarization of Light By Cloudy Matter Generally, Mech. Phys. Chem. 88 (1869) 34–40.

[99] von G. Mie, Beiträge zur Optik trüber Medien, speziell kolloidaler Metallösungen, Ann. Phys. 25 (1908) 377–445. doi:10.1002/andp.19083300302.

[100] A.T. Young, Rayleigh scattering, Appl. Opt. 20 (1981) 533–535.

[101] J. Gao, H. Gu, B Xu, Multifunctional magnetic nanoparticles: design, synthesis, and biomedical applications, Acc. Chem. Res. 42 (2009) 1097–1107. doi:10.1021/ar9000026.

[102] V.P. Torchilin, Targeted pharmaceutical nanocarriers for cancer therapy and imaging., AAPS J. 9 (2007) E128–E147. doi:10.1208/aapsj0902015.

[103] Y. Liang, N. Hilal, P. Langston, V. Starov, Interaction forces between colloidal particles in liquid: Theory and experiment, Adv. Colloid Interface Sci. 134–135 (2007) 151–166. doi:10.1016/j.cis.2007.04.003.

[104] E.J.W. Verwey, Theory of the stability of lyophobic colloids, J. Phys. Colloid Chem. 51 (1947) 631–636. doi:10.1038/162315b0.

[105] A.G. Kolhatkar, A.C. Jamison, D. Litvinov, R.C. Willson, T.R. Lee, Tuning the magnetic properties of nanoparticles, Int. J. Mol. Sci. 14 (2013) 15977–16009. doi:10.3390/ijms140815977.

[106] O. Veiseh, J.W. Gunn, M. Zhang, Design and fabrication of magnetic nanoparticles for targeted drug delivery and imaging, Adv. Drug Deliv. Rev. 62 (2010) 284–304. doi:10.1016/j.addr.2009.11.002.

[107] P. Aggarwal, J.B. Hall, C.B. McLeland, M.A. Dobrovolskaia, S.E. McNeil, Nanoparticle interaction with plasma proteins as it relates to particle biodistribution, biocompatibility and therapeutic efficacy, Adv. Drug Deliv. Rev. 61 (2009) 428–437. doi:10.1016/j.addr.2009.03.009.

[108] I. Brigger, C. Dubernet, P. Couvreur, Nanoparticles in cancer therapy and diagnosis, Adv. Drug Deliv. Rev. 54 (2002) 631–651. doi:10.1016/S0169-409X(02)00044-3.

[109] S. Parveen, R. Misra, S.K. Sahoo, Nanoparticles: a boon to drug delivery, therapeutics, diagnostics and imaging, Nanomedicine: Nanotechnology, Biol. Med. 8 (2012) 147–166. doi:10.1016/j.nano.2011.05.016.

[110] K.H. Bae, H.J. Chung, T.G. Park, Nanomaterials for cancer therapy and imaging, Mol. Cells. 31 (2011) 295–302. doi:10.1007/s10059-011-0051-5.

[111] H. Kobayashi, R. Watanabe, P.L. Choyke, Improving conventional enhanced permeability and retention (EPR) effects; What is the appropriate target?, Theranostics. 4 (2014) 81–89. doi:10.7150/thno.7193.

[112] D. Peer, J.M. Karp, S. Hong, O.C. Farokhzad, R. Margalit, R. Langer, Nanocarriers as an emerging platform for cancer therapy., Nat. Nanotechnol. 2 (2007) 751–760. doi:10.1038/nnano.2007.387.

[113] M. Yu, S. Huang, K.J. Yu, A.M. Clyne, Dextran and polymer polyethylene glycol (PEG) coating reduce both 5 and 30 nm iron oxide nanoparticle cytotoxicity in 2D and 3D cell culture, Int. J. Mol. Sci. 13 (2012) 5554–5570. doi:10.3390/ijms13055554.

[114] Z. Shaterabadi, G. Nabiyouni, M. Soleymani, High impact of *in situ* dextran coating on biocompatibility, stability and magnetic properties of iron oxide nanoparticles, Mater. Sci. Eng. C. 75 (2017) 947–956. doi:10.1016/j.msec.2017.02.143.

[115] R. Kenley, M. Lee, T. Mahoney, L. Sanders, Poly (lactide-co-glycolide) decomposition kinetics *in vivo* and *in vitro*, Macromolecules. 20 (1987) 2398–2403. doi:10.1021/ma00176a012.

[116] Y.Y. Yang, T.S. Chung, N. Ping Ng, Morphology, drug distribution, and *in vitro* release profiles of biodegradable polymeric microspheres containing protein fabricated by double-emulsion solvent extraction/evaporation method, Biomaterials. 22 (2001) 231–241. doi:10.1016/S0142-9612(00)00178-2.

[117] H.M. Redhead, S.S. Davis, L. Illum, Drug delivery in poly(lactide-co-glycolide) nanoparticles surface modified with poloxamer 407 and poloxamine 908: *In vitro* characterisation and *in vivo* evaluation, J. Control. Release. 70 (2001) 353–363. doi:10.1016/S0168-3659(00)00367-9.

[118] C. Alvarez-Lorenzo, A. Rey-Rico, A. Sosnik, P. Taboada, A. Concheiro, Poloxamine-based nanomaterials for drug delivery., Front. Biosci. Elit. Ed. (2010) 1-17. doi:10.1126/science.1219657.

[119] V.P. Torchilin, V.S. Trubetskoy, Which polymers can make nanoparticulate drug carriers long-circulating?, Adv. Drug Deliv. Rev. 16 (1995) 141–155. doi:10.1016/0169-409X(95)00022-Y.

[120] V.P. Torchilin, PEG-based micelles as carriers of contrast agents for different imaging modalities, Adv. Drug Deliv. Rev. 54 (2002) 235–252. doi:10.1016/S0169-409X(02)00019-4.

[121] G. Storm, S.O. Belliot, T. Daemen, D.D. Lasic, Surface modification of nanoparticles to oppose uptake by the mononuclear phagocyte system, Adv. Drug Deliv. Rev. 17 (1995) 31–48. doi:10.1016/0169-409X(95)00039-A.

[122] G.T. Noble, J.F. Stefanick, J.D. Ashley, T. Kiziltepe, B. Bilgicer, Ligand-targeted liposome design: Challenges and fundamental considerations, Trends Biotechnol. 32 (2014) 32–45. doi:10.1016/j.tibtech.2013.09.007.

[123] X. Huang, X. Teng, D. Chen, F. Tang, J. He, The effect of the shape of mesoporous silica nanoparticles on cellular uptake and cell function, Biomaterials. 31 (2010) 438–448. doi:10.1016/j.biomaterials.2009.09.060.

[124] X. Huang, L. Li, T. Liu, N. Hao, H. Liu, D. Chen, F. Tang, The shape effect of mesoporous silica nanoparticles on biodistribution, clearance, and biocompatibility *in vivo*, ACS Nano. 5 (2011) 5390–5399. doi:10.1021/nn200365a.

[125] W. Tai, R. Mahato, K. Cheng, The role of HER2 in cancer therapy and targeted drug delivery, J. Control. Release. 146 (2010) 264–275. doi:10.1016/j.jconrel.2010.04.009.

[126] D.R. Anderson, A. Grillo-López, C. Varns, K.S. Chambers, N. Hanna, Targeted anti-cancer therapy using rituximab, a chimaeric anti-CD20 antibody (IDEC-C2B8) in the treatment of non-Hodgkin's B-cell lymphoma., Biochem. Soc. Trans. 25 (1997) 705–708.

[127] S.H. Lim, S.A. Beers, R.R. French, P.W.M. Johnson, M.J. Glennie, M.S. Cragg, Anti-CD20 monoclonal antibodies: historical and future perspectives., Haematologica. 95 (2010) 135–143. doi:10.3324/haematol.2008.001628.

[128] E.W.M. Ng, D.T. Shima, P. Calias, E.T. Cunningham, D.R. Guyer, A.P. Adamis, Pegaptanib, a targeted anti-VEGF aptamer for ocular vascular disease., Nat. Rev. Drug Discov. 5 (2006) 123–132. doi:10.1038/nrd1955.

[129] S.E. Baek, K.H. Lee, Y.S. Park, D.-K. Oh, S. Oh, K.-S. Kim, D.-E. Kim, RNA aptamer-conjugated liposome as an efficient anticancer drug delivery vehicle targeting cancer cells *in vivo*, J. Control. Release. 196 (2014) 234–242. doi:10.1016/j.jconrel.2014.10.018.

[130] X. Li, Q. Zhao, L. Qiu, Smart ligand: Aptamer-mediated targeted delivery of chemotherapeutic drugs and siRNA for cancer therapy, J. Control. Release. 171 (2013) 152–162. doi:10.1016/j.jconrel.2013.06.006.

[131] L. Yang, X. Zhang, M. Ye, J. Jiang, R. Yang, T. Fu, Y. Chen, K. Wang, C. Liu, W. Tan, Aptamer-conjugated nanomaterials and their applications, Adv. Drug Deliv. Rev. 63 (2011) 1361–1370. doi:10.1016/j.addr.2011.10.002.

[132] A.J. Clark, M.E. Davis, Increased brain uptake of targeted nanoparticles by adding an acid-cleavable linkage between transferrin and the nanoparticle core., Proc. Natl. Acad. Sci. U. S. A. 112 (2015) 12486–12491. doi:10.1073/pnas.1517048112.

[133] Y. Yuan, L. Zhang, H. Cao, Y. Yang, Y. Zheng, X.J. Yang, A Polyethylenimine-Containing and Transferrin-Conjugated Lipid Nanoparticle System for Antisense Oligonucleotide Delivery to AML, Biomed Res. Int. 2016 (2016) 1-8. doi:10.1155/2016/1287128.

[134] D.T. Wiley, P. Webster, A. Gale, M.E. Davis, Transcytosis and brain uptake of transferrin-containing nanoparticles by tuning avidity to transferrin receptor., Proc. Natl. Acad. Sci. U. S. A. 110 (2013) 8662–8667. doi:10.1073/pnas.1307152110.

[135] K. Liu, L. Dai, C. Li, J. Liu, L. Wang, J. Lei, Self-assembled targeted nanoparticles based on transferrin-modified eight-arm-polyethylene glycol–dihydroartemisinin conjugate, Sci. Rep. 6 (2016) 29461. doi:10.1038/srep29461.

[136] R.J. Boohaker, M.W. Lee, P. Vishnubhotla, J.M. Perez, and A.R. Khaled, The Use of Therapeutic Peptides to Target and to Kill Cancer Cells, Curr Med Chem. 19 (2012) 3794-3804.

[137] I. Dijkgraaf, J.A.W. Kruijtzer, C. Frielink, F.H.M. Corstens, W.J.G. Oyen, R.M.J. Liskamp, O.C. Boerman, αvβ3 integrin-targeting of intraperitoneally growing tumors with a radiolabeled RGD peptide, Int. J. Cancer. 120 (2007) 605–610. doi:10.1002/ijc.22297.

[138] R.K. Jain, Transport of molecules, particles, and cells in solid tumors, Annu. Rev. Biomed. Eng. 1 (1999) 241–263. doi:10.1146/annurev.bioeng.1.1.241.

[139] C. Peng, J. Qin, B. Zhou, Q. Chen, M. Shen, M. Zhu, X. Lu, X. Shi, Targeted tumor CT imaging using folic acid-modified PEGylated dendrimer-entrapped gold nanoparticles, Polym. Chem. 4 (2013) 4412-4424 doi:10.1039/c3py00521f.

[140] F.R. Balkwill, M. Capasso, T. Hagemann, The tumor microenvironment at a glance, J. Cell Sci. 125 (2012) 5591–5596. doi:10.1242/jcs.116392.

[141] H. Li, X. Fan, J. Houghton, Tumor microenvironment: The role of the tumor stroma in cancer, J. Cell. Biochem. 101 (2007) 805–815. doi:10.1002/jcb.21159.

[142] H. Maeda, The enhanced permeability and retention (EPR) effect in tumor vasculature: the key role of tumor-selective macromolecular drug targeting, Adv Enzym. Regul. 41 (2001) 189–207. doi:http://dx.doi.org/10.1016/S0065-2571(00)00013-3.

[143] J. Gallo, I. García, D. Padro, B. Arnáiz, S. Penadés, Water-soluble magnetic glyconanoparticles based on metal-doped ferrites coated with gold: Synthesis and characterization, J. Mater. Chem. 20 (2010) 10010-10020 doi:10.1039/c0jm01756f.

[144] M. Mandal, S. Kundu, S.K. Ghosh, S. Panigrahi, T.K. Sau, S.M. Yusuf, T. Pal, Magnetite nanoparticles with tunable gold or silver shell, J. Colloid Interface Sci. 286 (2005) 187–194. doi:10.1016/j.jcis.2005.01.013.

[145] B. Sahoo, K.S.P. Devi, S. Dutta, T.K. Maiti, P. Pramanik, D. Dhara, Biocompatible mesoporous silica-coated superparamagnetic manganese ferrite nanoparticles for targeted drug delivery and MR imaging applications, J. Colloid Interface Sci. 431 (2014) 31–41. doi:10.1016/j.jcis.2014.06.003.

[146] H. Bae, T. Ahmad, I. Rhee, Y. Chang, S.-U. Jin, S. Hong, Carbon-coated iron oxide nanoparticles as contrast agents in magnetic resonance imaging, Nanoscale Res. Lett. (2012) 7:44. doi:10.1186/1556-276X-7-44.

[147] S. Nazir, T. Hussain, A. Ayub, U. Rashid, A.J. MacRobert, Nanomaterials in combating cancer: Therapeutic applications and developments, Nanomedicine Nanotechnology, Biol. Med. 10 (2014) 19–34. doi:10.1016/j.nano.2013.07.001.

[148] S.E. Jin, H.E. Jin, S.S. Hong, Targeted delivery system of nanobiomaterials in anticancer therapy: From cells to clinics, Biomed Res. Int. 2014 (2014) 1-24. doi:10.1155/2014/814208.

[149] H. Marie, L. Lemaire, F. Franconi, S. Lajnef, Y.M. Frapart, V. Nicolas, G. Frébourg, M. Trichet, C. Ménager, S. Lesieur, Superparamagnetic liposomes for MRI monitoring and external magnetic field-induced selective targeting of malignant brain tumors, Adv. Funct. Mater. 25 (2015) 1258–1269. doi:10.1002/adfm.201402289.

[150] S.H. Wang, X. Shi, M. Van Antwerp, Z. Cao, S.D. Swanson, X. Bi, J.R.B. Jr., Dendrimer-Functionalized Iron Oxide Nanoparticles for Specific Targeting and Imaging of Cancer Cells, Adv. Funct. Mater. 17 (2007) 3043–3050. doi:10.1002/adfm.200601139.

[151] P. Tartaj, M. a del P. Morales, S. Veintemillas-Verdaguer, T. Gonz lez-Carre o, C.J. Serna, The preparation of magnetic nanoparticles for applications in biomedicine, J. Phys. D. Appl. Phys. 36 (2003) R182–R197.

[152] B. Noriega-Luna, L.A. Godínez, F.J. Rodríguez, A. Rodríguez, G. Zaldívar-Lelo De Larrea, C.F. Sosa-Ferreyra, R.F. Mercado-Curiel, J. Manríquez, E. Bustos, Applications of dendrimers in drug delivery agents, diagnosis, therapy, and detection, J. Nanomater. 2014 (2014) 1-20. doi:10.1155/2014/507273.

[153] Y. Sangwan, T. Hooda, H. Kumar, Nanoemulsions : A Pharmaceutical Review, Inter. J. Pharm. Pro. Res. 5 (2014) 1031–1038.

[154] R.K. Mishra, G.C. Soni, R.P. Mishra, A Review Article : on Nanoemulsion, WJPPS. 3 (2014) 258–274.

[155] N. Anton, T.F. Vandamme, Nano-emulsions and micro-emulsions: Clarifications of the critical differences, Pharm. Res. 28 (2011) 978–985. doi:10.1007/s11095-010-0309-1.

[156] T.F. Vandamme, N. Anton, Low-energy nanoemulsification to design veterinary controlled drug delivery devices, Int. J. Nanomedicine. 5 (2010) 867–873. doi:10.2147/IJN.S13273.

[157] M. Jaiswal, R. Dudhe, P.K. Sharma, Nanoemulsion: an advanced mode of drug delivery system, 3 Biotech. 5 (2015) 123–127. doi:10.1007/s13205-014-0214-0.

[158] X. Li, N. Anton, G. Zuber, M. Zhao, N. Messaddeq, F. Hallouard, H. Fessi, T.F. Vandamme, Iodinated α-tocopherol nano-emulsions as non-toxic contrast agents for preclinical X-ray imaging, Biomaterials. 34 (2013) 481–491. doi:10.1016/j.biomaterials.2012.09.026.

[159] M.F. Attia, N. Anton, R. Akasov, M. Chiper, E. Markvicheva, T.F. Vandamme, Biodistribution and Toxicity of X-Ray Iodinated Contrast Agent in Nano-emulsions in Function of Their Size., Pharm. Res. 33 (2016) 603–614. doi:10.1007/s11095-015-1813-0.

[160] M.F. Attia, N. Anton, M. Chiper, R. Akasov, H. Anton, N. Messaddeq, S. Fournel, A.S. Klymchenko, Y. Mély, T.F. Vandamme, Biodistribution of X-ray iodinated contrast agent in nano-emulsions is controlled by the chemical nature of the oily core., ACS Nano. 8 (2014) 10537–50. doi:10.1021/nn503973z.

[161] P.A. Jarzyna, T. Skajaa, A. Gianella, D.P. Cormode, D.D. Samber, S.D. Dickson, W. Chen, A.W. Griffioen, Z. a. Fayad, W.J.M. Mulder, Iron oxide core oil-in-water emulsions as a multifunctional nanoparticle platform for tumor targeting and imaging, Biomaterials. 30 (2009) 6947–6954. doi:10.1016/j.biomaterials.2009.09.004.

[162] A.M. Jhaveri, V.P. Torchilin, Multifunctional polymeric micelles for delivery of drugs and siRNA, Front. Pharmacol. 5 (2014) 1–26. doi:10.3389/fphar.2014.00077.

[163] V.S. Trubetskoy, Polymeric micelles as carriers of diagnostic agents, Adv. Drug Deliv. Rev. 37 (1999) 81–88. doi:10.1016/S0169-409X(98)00100-8.

[164] S. Ganta, H. Devalapally, A. Shahiwala, M. Amiji, A review of stimuli-responsive nanocarriers for drug and gene delivery, J. Control. Release. 126 (2008) 187–204. doi:10.1016/j.jconrel.2007.12.017.

[165] M.A. Ward, T.K. Georgiou, Thermoresponsive polymers for biomedical applications, Polymers. 3 (2011) 1215–1242. doi:10.3390/polym3031215.

[166] R. Cheng, F. Meng, C. Deng, H.A. Klok, Z. Zhong, Dual and multi-stimuli responsive polymeric nanoparticles for programmed site-specific drug delivery, Biomaterials. 34 (2013) 3647–3657. doi:10.1016/j.biomaterials.2013.01.084.

[167] W.H. Kong, W.J. Lee, Z.Y. Cui, K.H. Bae, T.G. Park, J.H. Kim, K. Park, S.W. Seo, Nanoparticulate carrier containing water-insoluble iodinated oil as a multifunctional contrast agent for computed tomography imaging, Biomaterials. 28 (2007) 5555–5561. doi:10.1016/j.biomaterials.2007.08.044.

[168] K.S. Soppimath, T.M. Aminabhavi, A.R. Kulkarni, W.E. Rudzinski, Biodegradable polymeric nanoparticles as drug delivery devices, J. Control. Release. 70 (2001) 1–20. doi:10.1016/S0168-3659(00)00339-4.

[169] R. Duncan, The dawning era of polymer therapeutics., Nat. Rev. Drug Discov. 2 (2003) 347–360. doi:10.1038/nrd1088.

[170] A. V Fuchs, A.C. Gemmell, K.J. Thurecht, Utilising polymers to understand diseases: advanced molecular imaging agents, Polym. Chem. 6 (2015) 868–880. doi:10.1039/c4py01311e.

[171] A. Mahapatro, D.K. Singh, Biodegradable nanoparticles are excellent vehicle for site directed *in-vivo* delivery of drugs and vaccines., J. Nanobiotechnology. (2011) 9:55. doi:10.1186/1477-3155-9-55.

[172] C. Pinto Reis, R.J. Neufeld, A.J. Ribeiro, F. Veiga, Nanoencapsulation I. Methods for preparation of drug-loaded polymeric nanoparticles, Nanomedicine Nanotechnology, Biol. Med. 2 (2006) 8–21. doi:10.1016/j.nano.2005.12.003.

[173] P. Pereira dos Santos, S.H. Flôres, A. de Oliveira Rios, R.C. Chisté, Biodegradable polymers as wall materials to the synthesis of bioactive compound nanocapsules, Trends Food Sci. Technol. 53 (2016) 23–33. doi:10.1016/j.tifs.2016.05.005.

[174] A. Kumari, S.K. Yadav, S.C. Yadav, Biodegradable polymeric nanoparticles based drug delivery systems, Colloids Surfaces B Biointerfaces. 75 (2010) 1–18. doi:10.1016/j.colsurfb.2009.09.001.

[175] C.E. Mora-Huertas, H. Fessi, A. Elaissari, Polymer-based nanocapsules for drug delivery, Int. J. Pharm. 385 (2010) 113–142. doi:10.1016/j.ijpharm.2009.10.018.

[176] A. Benzina, M.A.B. Kruft, F. Bar, F.H. Van der Veen, C.W. Bastiaansen, V. Heijnen, C. Reutelingsperger, L.H. Koole, Studies on a new radiopaque polymeric biomaterial, Biomaterials. 15 (1994) 1122–1128. doi:10.1016/0142-9612(94)90232-1.

[177] D. Mawad, H. Mouaziz, A. Penciu, H. Méhier, B. Fenet, H. Fessi, Y. Chevalier, Elaboration of radiopaque iodinated nanoparticles for *in situ* control of local drug delivery., Biomaterials. 30 (2009) 5667–5674. doi:10.1016/j.biomaterials.2009.06.027.

[178] N. Pimpha, S. Chaleawlert-Umpon, P. Sunintaboon, Core/shell polymethyl methacrylate/polyethyleneimine particles incorporating large amounts of iron oxide nanoparticles prepared by emulsifier-free emulsion polymerization, Polymer. 53 (2012) 2015–2022. doi:10.1016/j.polymer.2012.03.019.

[179] A. Galperin, S. Margel, Synthesis and characterization of radiopaque magnetic core-shell nanoparticles for X-ray imaging applications, J. Biomed. Mater. Res. - Part B Appl. Biomater. 83 (2007) 490–498. doi:10.1002/jbm.b.30821.

[180] D. Kim, M.K. Yu, T.S. Lee, J.J. Park, Y.Y. Jeong, S. Jon, Amphiphilic polymer-coated hybrid nanoparticles as CT/MRI dual contrast agents., Nanotechnology. 22 (2011) 155101(7pp). doi:10.1088/0957-4484/22/15/155101.

[181] D. Kim, J.W. Kim, Y.Y. Jeong, S. Jon, Antibiofouling Polymer Coated Gold@Iron Oxide Nanoparticle (GION) as a Dual Contrast Agent for CT and MRI, Bull. Korean Chem. Soc. 30 (2009) 1855–1857. doi:10.5012/bkcs.2009.30.8.1855.

[182] F. Lan, K.-X. Liu, W. Jiang, X.-B. Zeng, Y. Wu, Z.-W. Gu, Facile synthesis of monodisperse superparamagnetic Fe_3O_4/PMMA composite nanospheres with high magnetization., Nanotechnology. 22 (2011) 225604 (7pp). doi:10.1088/0957-4484/22/22/225604.

[183] M.C. Wick, I.E. Chemelli-Steingruber, C. Kremser, High density lipoprotein-based contrast agents for multimodal imaging of atherosclerosis, Arterioscler Thromb Vasc Biol. 30 (2014) 169-176. doi:10.1007/978-3-7091-0338-8_29.

[184] K.K. Ng, J.F. Lovell, G. Zheng, Lipoprotein-inspired nanoparticles for cancer theranostics, Acc. Chem. Res. 44 (2011) 1105–1113. doi:10.1021/ar200017e.

[185] I.E. Allijn, W. Leong, J. Tang, A. Gianella, A.J. Mieszawska, F. Fay, G. Ma, S. Russell, C.B. Callo, R.E. Gordon, E. Korkmaz, J.A. Post, Y. Zhao, H.C. Gerritsen, A. Thran, R. Proksa, H. Daerr, G. Storm, V. Fuster, E.A. Fisher, Z.A. Fayad, W.J.M. Mulder, D.P. Cormode, Gold nanocrystal labeling allows low-density lipoprotein imaging from the subcellular to macroscopic level, ACS Nano. 7 (2013) 9761–9770. doi:10.1021/nn403258w.

[186] S. Sabnis, N.A. Sabnis, S. Raut, A.G. Lacko, Superparamagnetic reconstituted high-density lipoprotein nanocarriers for magnetically guided drug delivery, Int. J. Nanomedicine. 12 (2017) 1453–1464. doi:10.2147/IJN.S122036.

[187] D.P. Cormode, T. Skajaa, M.M. Van Schooneveld, R. Koole, M.E. Lobatto, C. Calcagno, A. Barazza, E. Ronald, P. Zanzonico, E. a Fisher, Z. a Fayad, W.J.M. Mulder, Nanocrystal core high-density lipoproteins: A multimodality contrast agent platform, Nano Lett. 8 (2009) 3715–3723. doi:10.1021/nl801958b.Nanocrystal.

Chapter II:

Radiopaque polymeric nanoparticles for preclinical X-ray imaging

Chapitre II - Radiopaque polymeric nanoparticles for preclinical X-ray imaging

Contrast agents (CAs) for X-ray imaging are nowadays unavoidable in clinics to provide contrast enhancement in tissues by attenuating X-ray upon accumulation. However, CAs suffer from a lack of long-time retention and fast excretion issues leading to use high doses for a poor efficiency and causing toxic side effects. Colloidal iodinated polymeric nanoparticles (PNPs), like radiopaque nanospheres, have been reported as very suitable to fulfill those needs. They have been mentioned as i) stable nanocarriers, based on double part nanostructure including a rigid polymeric core and stealth shell, capable of being iii) loaded with high iodine content within the inner core imparting iv) good radiopaque property. Furthermore, PNPs have been pointed out to have v) a controllable size distribution and surface properties. Owing to such tunable design, radiopaque PNPs can be vi) delivered to site of interest and show vii) enhanced pharmacokinetics profile compared to current clinical CAs. Nano-sized biocompatible assembly made of colloidal iodine-loaded nanospheres appear though as an efficient and innovating kind of CA for non-invasive diagnostic purpose by X-ray imaging. However, there is still a challenge of that is to find a compromise between iodine content for strong X-ray attenuation ability and size distribution for a safe *in vivo* administration. To answer to current radiopaque CAs and to this challenge, we carried out the following study as described below:

We reported in the hereinafter **chapter II** a straightforward approach to produce biocompatible and controllable size distribution iodine-grafted polymer-based CAs. We applied nanoprecipitation dripping technique to obtain PEGylated PNPs from a preformed iodinated homopolymer, poly(MAOTIB), synthetized by radical polymerization of a modified monomer (the 2-methacryloyloxyethyl(2,3,5-triiodobenzoate) monomer named MAOTIB). The strategy applied here was to encapsulate a high amount of iodine by grafting it onto a polymer backbone (62 wt.% of iodine). Nanoprecipitation is a very efficient technique to formulate monodisperse and colloids by playing on key parameters such as the polymer and the surfactant weight ratio. In our case, it appears as the most suitable method to cope with trouble of balancing size distribution and iodine content. In this way, the strength of such PNPs formulation lies not only on its X-ray attenuation properties but also on the control over the design of PNPs to impart suitable physicochemical features for *in vivo* use. The roles of polymer loaded as a core of nanoconstructs and the surfactant-to-polymer weight ratio during

nanoprecipitation process were both elucidated to identify the best compromise between size distribution, colloidal stability and high iodine content. The selected PNPs suspension was based on spherical PNPs with a mean diameter of 163.7 nm (PDI 0.09) and formulated with 60 wt.% of surfactant and with an iodine content of 59 mg I/mL which was assumed quite significant and adequate to yield satisfying contrast enhancement. The *in vivo* assays were all performed with micro-CT for follow-up after intravenous injection in the tail vein of Swiss mice. It is off noted that a passive strategy was applied here since stealth and non-functionalized surface radiopaque PNPs were prepared. Reconstructed 2D and 3D images clearly demonstrated that PNPs were spontaneously and quickly accumulated in liver and spleen 1h after injection. Contrast enhancement was quantified using Hounsfield scale and was respectively 191 HU for spleen and 141 HU for liver. Contrasts remained similar over the whole follow-up period indicating that retention was much better than for regular marketed radiopaque CAs. According to these results, it was assumed that blood clearance might have been done by hepatic and splenic routes. No side effects were observed, toxicity test might be interesting to perform to define limit of tolerance of our CA.

The schematic representation describes the proposed study:

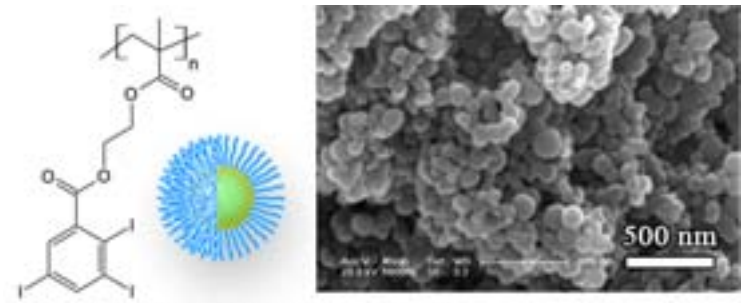

Poly(MOATIB) PEGylated NPs by nanoprecipitation

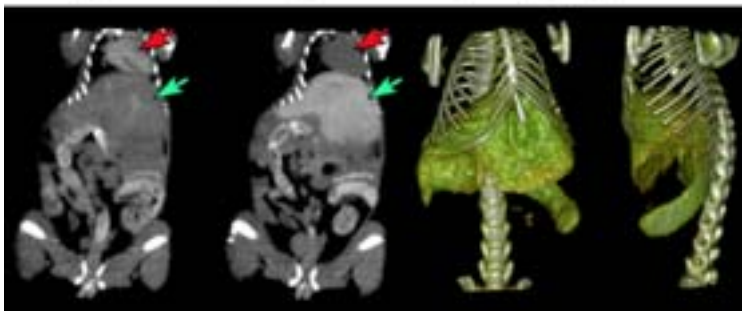

This work has been submitted to Acta Biomaterialia journal, we are looking forward to hearing from them at present time. The following part provides the submission version of this as-described work.

Application of poly(MAOTIB) homopolymer as an injectable iodinated nanoparticulate contrast agent from nanoprecipitation technique for *in vivo* preclinical XR imaging

Justine Wallyn,[a] Nicolas Anton,[a,*] Christophe Serra,[b] Michel Bouquey,[b] Mayeul Collot,[c] Jean-Luc Weickert,[e] Nadia Messaddeq,[e] Thierry F. Vandamme[a]

[a] Université de Strasbourg, CNRS, CAMB UMR 7199, F-67000 Strasbourg, France

[b] Université de Strasbourg, CNRS, ICS UPR 22, F-67000 Strasbourg, France

[d] Université de Strasbourg, CNRS, LBP UMR 7213, F-67000 Strasbourg, France

[e] Université de Strasbourg CNRS, INSERM, Collège de France, IGBMC UMR 7104/UMR_S 964, F-67000 Strasbourg, France

*Corresponding author: nanton@unistra.fr (N. Anton)

Abstract

Polymeric nanoparticles (PNPs) are gaining more and more importance as nanocarriers or contrasting material for preclinical diagnostic *via* X-ray (XR) micro-CT scanner. Here, we investigated a straightforward approach to produce biocompatible, radiopaque and stable polymer-based nanoparticle contrast agent, that was evaluated on mice. To this end, we applied a nanoprecipitation dropping technique to obtain PEGylated PNPs from a preformed iodinated homopolymer, poly(MAOTIB), synthetized by radical polymerization of the 2-methacryloyloxyethyl(2,3,5-triiodobenzoate) monomer (MAOTIB). The process developed allows an accurate control of the nanoparticle properties (mean size can range from 140 nm to 200 nm in function of the formulation parameters) along with unprecedented important X-ray attenuation properties (concentration of iodine around 59 mg I/mL) compatible with a follow-up *in vivo*. Routine characterizations such as FTIR, DSC, GPC, TGA, ^{1}H and ^{13}C NMR and finally SEM were accomplished to get main properties of the optimal contrast agent. Owing to excellent colloidal stability against physiological conditions evaluated in presence of fetal bovine serum, the selected PNPs suspension was administrated to mice. Monitoring and quantification by micro-CT show that iodinated PNPs are endowed strong XR attenuation capacity towards blood pool, and underwent a fast and passive accumulation in liver and spleen.

Keywords

Radiopaque polymeric nanoparticles; nanoprecipitation; contrast agent; micro-CT; X-ray imaging.

Abbreviations

CA	Contrast agent
$CDCl_3$	Deuterated chloroform
CT	Computed tomography
DCM	Dichloromethane
DLS	Dynamic light scattering
DSC	Differential scanning calorimetry
FBS	Fetal bovine serum
FTIR	Fourier transformed infrared spectroscopy
GPC	Gel permeation chromatography
HEMA	2-hydroxyethylmethacrylate
MAOTIB	2-Methacryloyloxyethyl(2,3,5-triiodobenzoate)
Micro-CT	Micro-computed tomography
NPs	Nanoparticles
PBS	Phosphate bovine serum
PDI	Polydispersity index
PEG	Poly(ethylene glycol)
PNPs	Polymeric nanoparticles
PY	Polymerization yield
ROI	Region of interest
SPR	Surfactant-to-polymer weight ratio (surfactant/(surfactant+polymer))
SEM	Scanning electron microscopy
TGA	Thermogravimetric analysis
THF	Tetrahydrofurane
TIB	2,3,5-Triiodobenzoic acid
TIB-Cl	2,3,5-Triiodobenzoyl chloride
XR	X-ray

1. Introduction

Over the past decades, many advances have been done in the early-stage pathology diagnostic field by non-invasive *in vivo* visualizations over a wide imaging scale, from cells to human whole-body. Nowadays, the medicine field possesses an arsenal of biomedical imaging tools preventing patient from undergoing unpleasant experience or surgery to get an accurate diagnosis. Whatever the imaging modalities used, X-ray computed tomography (XR CT), magnetic resonance imaging (MRI), positron emission tomography (PET) or single photon emission computed tomography (SPECT), etc., *in vivo* imaging aims at providing reconstructed 2D or 3D images where morphology, anatomy and physiologic functions of a region of interest (ROI) can be explored and checked up. Although they all contribute to identify pathologic tissues among healthy ones, each technique differs from each other regarding their principle, their resolution, sensibility, depth of tissues penetration, quantification, etc., which make them quite complementary.[1–4]

Historically, XR imaging is the oldest modality. The first computer-assisted XR imager prototype was set up in clinic in 1972, several years after the discovery of XR by Roentgen in 1895. Allan M. Cormark and Godfrey N. Hounsfield shared along Nobel Prize in Physiology or Medicine 1979 for this tremendous breakthrough for preclinical research and medicine.[5–10] Since ever, CT scanner has gained great interest and is routinely performed due to its compromise between low cost of operation, efficiency for establishing high resolution images, low energy consumption, and availability compared to other imagers. Based on X photons attenuation by electron-dense materials in body, XR-CT images can provide details about tissues and skeleton due to differences of opacification. Currently, XR-CT finds key role for imaging abdomen (gastrointestinal track, kidneys, liver, spleen), cardiorespiratory system, head, bones and tumor tissues.[1,6,8,10–12] To make progresses in early disease detection, studying at small scale with living laboratory animals remains so far the most useful pathway. For this purpose, XR micro-CT has been developed and dedicated to small animals scanning.[13,14]

It is well-known that soft tissues XR images suffer from a lack of enhanced contrast due to their similar XR absorption ability. To overcome this limitation, administration of radiopaque contrast agents (XR-CA) is applied. Current XR-CAs are made of low molecular weight water-soluble molecules. However, they have been shown not compatible with X-ray imaging application in small laboratory animals due to fast excretion by renal clearance and the small

blood volume of animal prevents from injecting high volume. This implies the use of concentrated dose of XR-CA to ensure contrast enhancement during image-guided procedure, potentially causing nephrotoxicity issue, high viscosity and osmolality. Literature already showed scope of CA alternatives for XR micro-CT involving nanoparticles (NPs) of inorganic elements[7] like noble metal (gold, silver, platinum), heavy metal (thorium, bismuth, tantalum, etc.), or lanthanide (gadolinium, ytterbium, etc.) and soft NPs made of lipids[4] (nano-emulsion, micelle, liposome, emulsion) or polymeric materials (nanosphere, nanocapsule, dendrimer) in which active compounds can be encapsulated or embedded.

Soft NPs were actually revealed as appealing kind of XR probes because: i) there is a wide range of biocompatible designs and chemical constituents safer than metallic NPs suitable for *in vivo* environment but also because ii) they provide protective shield surrounding the contrasting core and prevent iii) cargo from leaking and iv) from fast clearance.[4,6–12,15–19] Typically, NPs-based XR-CAs must fulfill additional requirements to constitute a real advanced type of XR-CA.[1,4,8,16,19–21] They should i) have a core exhibiting a high attenuation ability compared to the dose injected by means of loading molecules with a high content of contrasting element. This will though lead to reduce ii) osmolality and viscosity close to ones of physiological fluids rendering the intravenous injection more tolerable[7] They should have a iii) specific biodistribution (which will avoid as well to work with concentrated CA formulation) and iv) good pharmacokinetic profile (retention time long enough to image, possible excretion of CA without adverse effect from CA or from break-down products).[22–26] Basically, *in vivo* NPs fate is dictated by v) physicochemical properties, mostly surface and size. Those were pointed out as two key parameters because stealth surface functionality obtained by a decoration with PEG, active targeting properties obtained by a decoration with specific ligands, and small size (< 200 nm to avoid vessel embolism) would prevent NPs from undergoing opsonization mechanism by fooling immune system, and/or from fast excretion by renal clearance (< 50nm) and would ensure stability in physiological media until they reach and accumulate in the targeted tissues.[22–31]

Among all nanoscale assemblies abovementioned, polymeric nanoparticles (PNPs) are promising NPs-based CA due to the control over their architectures – including morphology, size, surface charge, functionalities and rigidity – and their compositions, imparting proper bioavailability, biostability and long persistence in systemic compartment and finally generating high-loaded iodine biomaterials.[2,32,33] There are several synthesis and formulation techniques allowing to prepare PNPs-based probes: from heterogeneous

polymerization process (in emulsion, suspension or dispersion) to yield *in situ* PNPs or from post-synthesis process (emulsion solvent -diffusion, -evaporation, salting out, solvent displacement, supercritical fluid) for bulk of preformed synthetic polymers and biopolymers.[34–38] Over the last couple of decades, researches have focused their attention on the preparation of iodinated biodegradable[39,40] and/or biocompatible[41–44] PNPs and macromolecules as XR probes.

Unfortunately, there is still a need in figuring out how to get a balance between high iodine content on polymer structure and suitable design to aim at the preparation of an injectable and efficient XR-CA. Radiopaque PNPs from the polymerization of iodinated derivatives of 2-hydroxyethylmethacrylate (HEMA) monomer, such as the 2-methacryloyloxyethyl(2,3,5-triiodobenzoate) monomer (MAOTIB) with an iodine content of 62 wt.%, seem an outstanding compromise to achieve this goal. Most of the studies on this MAOTIB monomer relied on heterogeneous polymerization and bulk process leading to micron-sized particles or copolymeric NPs with consequently low iodine loading on macromolecules backbone and slight *in vivo* contrast enhancement.[45–50] Therefore, Poly(MAOTIB) appeared as a good candidate for the synthesis of XR contrast agent, but actually not yet optimized and used in that sense.

In the present paper, we investigated a straightforward approach to produce biocompatible, radiopaque and controllable size distribution polymer-based nanospheres as XR micro-CT CA. To this end, we applied an innovating nanoprecipitation dropping technique to obtain PEGylated PNPs from a preformed iodinated homopolymer, poly(MAOTIB), synthetized by radical polymerization of the MAOTIB monomer. As mentioned in the literature, nanoprecipitation or solvent displacement method was developed by Fessi *et al.*[51] many authors studied this technique since it appeared as a low cost, simply and reproducible method.[35,52,53] Furthermore, nanoprecipitation has been reported as very efficient technique to formulate monodisperse and nano-scale colloids by playing on key parameters such as the polymer and surfactant weight ratio. In our case, it appears as the most suitable method to cope with trouble of balancing size distribution and iodine content. In the present study, we adapted the dropping technique which involved the dropwise pouring of an organic solution of our polymer in a non-solvent containing the surfactant. After diffusion of the solvents in each other, hydrophilic poly(MAOTIB) NPs were obtained thanks to a PEGylated stabilizer coating. PEGylated surfactant was used to provide control over the size, stealth and stabilizing properties for *in vivo* media.

In a nutshell, the strength of such PNPs formulation lies not only on its XR attenuation properties but also on the control over the design of PNPs to impart suitable physicochemical features for *in vivo* use. Formulation parameters like components amount, phase volume ratio, stirring, etc. have been reported as drastically impacting PNPs size distribution. Consequently, herein, the role of polymer loading as the inner core of the nanoconstruct and the surfactant-to-polymer weight ratio were both studied and elucidated to optimize nanoprecipitation process and identify the best compromise between high iodine content within the injectable PNPs suspensions, size distribution and colloidal stability. Several poly(MAOTIB)-based PNPs were thus produced with iodine concentration from 15.5 to 62 mg I/mL and with surfactant-to-polymer weight ratio varying from 30 to 80 wt.%. Discrimination among all suspensions relied on iodine content needed for good XR attenuation ability and on size distribution measurement by DLS. An optimal suspension was so subjected to further characterization such as SEM and *in vitro* study in physiological conditions to check iodine content, cells interactions and colloidal stability once exposed to biological media. These studies revealed that the formulation was composed of 163 nm spherical PNPs with 59 mg I/ml with excellent performance in simulated *in vivo* media. *In vivo* assays on mice after intravenous administration indicated that the passive accumulation drove PNPs into hepatic and splenic compartments in which very satisfying opacification allowed clear delineation of both soft tissues. Complete micro-CT follow-up was carried out to evaluate pharmacokinetics profile of the selected suspension.

2. Materials and methods

2.1. Materials

All chemicals were commercially available agents and were used as received. 2,3,5-Triiodobenzoic acid (TIB), 4-dimethylaminopyridine (DMAP), 2-hydroxylethyl methylmethacrylate (HEMA), benzoyl peroxide (Luperox® A75), triethylamine (NEt_3), thionyl chloride, cyclohexane, dichloromethane (DCM), ethyl acetate, methanol, tetrahydrofuran (THF) and toluene were purchased from Sigma-Aldrich (France). Non-ionic surfactant (Kolliphor ELP® Castor oil PEG-35) was donated by Laserson (Etampes, France). Kolliphor ELP® is a parenteral grade nonionic hydrophilic surfactant made by reacting ethylene oxide to castor seed oil at an ethylene oxide to oil molar ratio of 35.[54] Lumogen Red was purchased from ORGANICA® Feinchemie GmbH Wolfen. Fetal bovine saline (FBS), Dulbecco's modified Eagle medium (DMEM) Phosphate buffered saline (PBS) were from PAN Biotech (Aidenbach, Germany).

2.2. Syntheses and formulation

2.2.1. Synthesis of iodinated monomer MAOTIB by esterification.

Thionyl chloride (10.4 g, 0.087 mole) was added dropwise to a magnetically stirred solution of TIB (5 g, 0.01 mole) in DCM (250 mL) cooled by an ice bath. After completion of the addition, the reaction mixture was heated to reflux at 75°C. Reflux was maintained for 3h after obtaining clear solution. The excess of thionyle chloride was then removed under reduced pressure. HEMA (1.25 g, 0.0096 mole) and DMAP (0.023 g, 0.192 mmole) were sequentially added to a magnetically stirred solution of the as-preprared triiodobenzoyl chloride (TIB-Cl) in DCM (150 mL). NEt_3 (1.015 g, 0.01 mole) was added dropwise to the previous mixture cooled by ice bath and covered by a blanket of nitrogen. The esterification reaction was performed over 1h at room temperature and kept under a blanket of nitrogen. The organic phase was then washed with distilled water, 1N HCl solution, saturated $NaHCO_3$ solution and saturated NaCl solution and dried with anhydrous Na_2SO_4. DCM was removed under reduced pressure and the orange product was purified by gradient elution method on silica gel column using cyclohexane and ethyl acetate as eluent. Reactions produced a white powder product (mp 95°C) with 70% yield and iodine content 62.3 wt.%. The scheme of synthesis is reported in Figure 1.

^{1}H and ^{13}C NMR spectra were obtained with a Bruker Top Spin 3.0 operating at 400 MHz using deuterated chloroform ($CDCl_3$) as a solvent. Chemical shifts (δ) were expressed in ppm from tetramethylsilane as internal reference: ^{1}H NMR ($CDCl_3$, δ/ppm) 8.31 (d, 1H, H^{13}), 7.74 (d, 1H, H^{11}), 6.17 (s, 1H, olefinic), 5.62 (s, 1H, olefinic), 4.57 and 4.48 (m, 4H, H^5, H^6) and 1.97 (s, 3H, H^3). ^{13}C NMR ($CDCl_3$, δ/ppm): 167.04 (C3), 165.66 (C4), 148.95 (C11), 141.03 (C8) 137.23 (C13), 135.84 (C2), 126.45 (C1), 113.47 (C10), 106.64 (C9), 93.72 (C12), 64.02 (C6), 62.01 (C5) and 18.41 (C3).

2.2.2. Synthesis of poly(MAOTIB)

Poly(MAOTIB) was synthetized through a typical free radical polymerization process (Figure 1). Prior to polymerization, MAOTIB (4 g, 0.0065 mole) was dissolved in toluene (9.5 mL) in a round-bottom flask equipped with a condenser and bubbled with nitrogen gas to exclude air from the reaction mixture and prevent inhibition reaction, after which a blanket of nitrogen was maintained over the solution during the whole polymerization course. Radical polymerization was carried out by heating solution to 73°C for 15h in the presence of benzoyl peroxide initiator (0.04 g, 1 wt.% of monomer) under gentle magnetic stirring. After cooling

down to room temperature, the solution was placed in an ice bath and methanol was added to yield full recovery of poly(MAOTIB) from organic supernatant as a yellowish solid precipitate. Poly(MAOTIB) was extensively washed by centrifugation cycles with methanol until supernatant remained colorless. The final white polymer was dried by vacuum and kept overnight in oven (40°C). The polymerization yield (PY) was determined by the following expression:

$$PY(\%) = \left(wt_{poly(MAOTIB)}/wt_{MAOTIB}\right) \times 100$$

where $wt_{poly(MAOTIB)}$ and wt_{MAOTIB} are respectively the weight of poly(MAOTIB) obtained and the weight of MAOTIB at the initial stage of the polymerization. A PY of 90% of monomer was achieved.

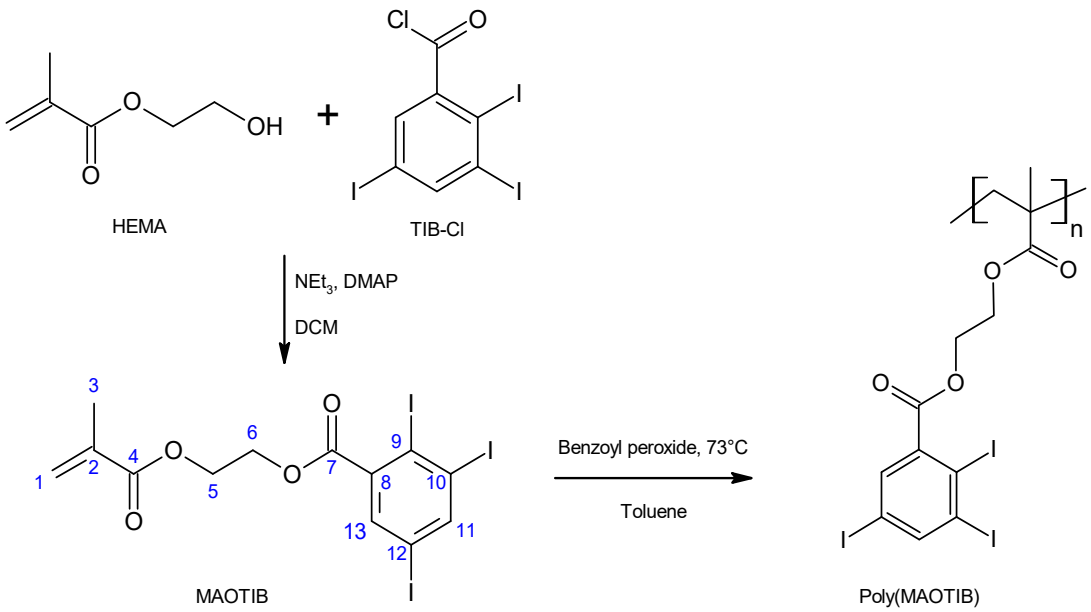

Figure 1: Synthesis of MAOTIB monomer and radical polymerization in poly(MAOTIB) homopolymer.

2.2.3. Formation of PEGylated-coated poly(MAOTIB) NPs

PNPs based on poly(MAOTIB) were formulated *via* a dropping nanoprecipitation process (Figure 2) in presence of hydrophilic nonionic surfactant to get water-dispersible radiopaque PNPs. Different amounts of polymer (25, 50 and 100 mg) were used to prepare three series of PNPs suspensions (PNPs-1, PNPs-2 and PNPs-3) with final iodine content of 15.5 mg I/mL, 31 mg I/mL and 62 mg I/mL respectively (ends-of-chain of polymer were neglected which meant that the iodine content of poly(MAOTIB) was assimilated to the iodine content of MAOTIB). PNPs-1, PNPs-2 and PNPs-3 were all composed of six samples for which the surfactant-to-polymer weight ratio, SPR = 100 × (surfactant/(surfactant + polymer)) was

varied from 30 to 80 wt.% (Table 1). Typical dropping technique applied here consisted in dissolving poly(MAOTIB) in THF (10 mL) as good solvent resulting in a yellow organic solution after 5 min homogenization in a sonication bath. This phase was added dropwise under magnetic stirring (500 rpm) to a dispersing phase based on ethanol (40 mL) as non-solvent of the polymer and PEGylated stabilizer agent. Stirring was kept over 3h, the bluish ethanolic suspension was then concentrated under vacuum. Excess of surfactant was removed from PNPs by extensive washing by centrifugation with milliQ water. PNPs were finally dispersed in PBS as an aqueous phase and subjected to 1h in a sonication bath to form well-dispersed PNPs radiopaque suspension. All samples were prepared in triplicate to evaluate reproducibility of process.

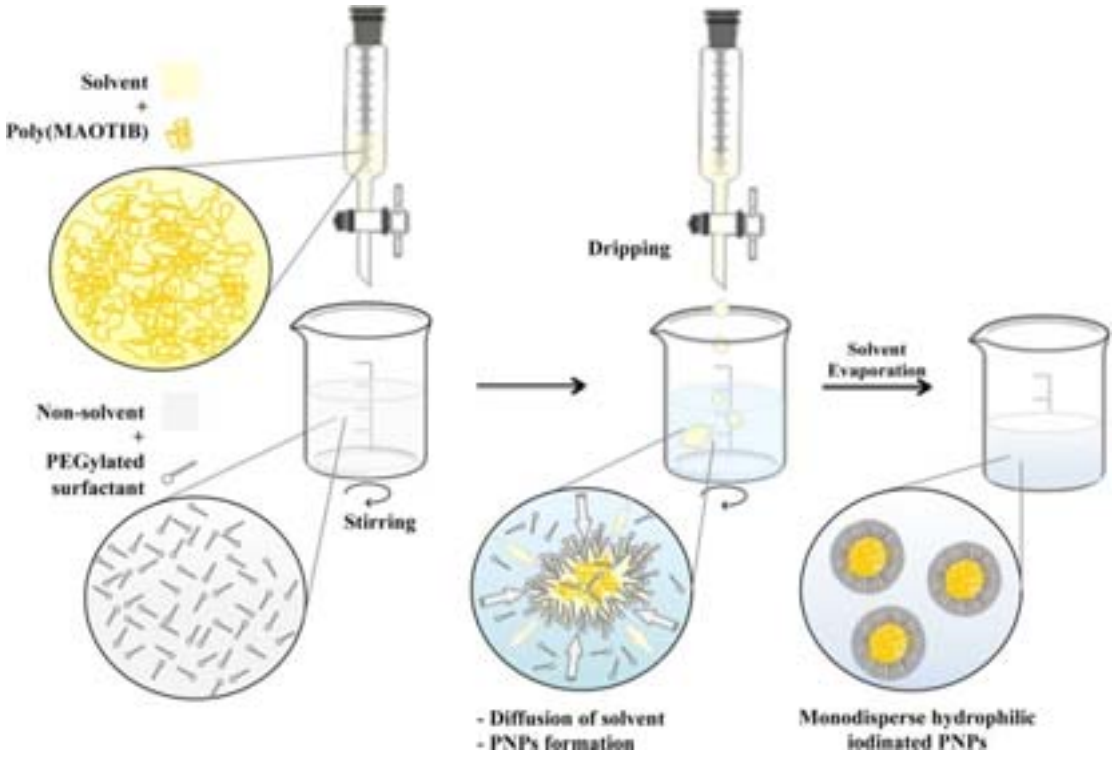

Figure 2: Nanoprecipitation process relying on the dropping technique.

Table 1 : Quantities of surfactant and polymer for the PNPs-1, PNPs-2 and PNPs-3 formulations.

			Surfactant (mg)					
Series	Iodine content (mg I/mL)	Polymer (mg)	SPR30%	SPR40%	SPR50%	SPR60%	SPR70%	SPR80%
PNPs-1	15.5	25	11	17	25	38	58	100
PNPs-2	31	50	21	33	50	75	117	200
PNPs-3	62	100	43	67	100	150	233	400

2.3. Characterizations

2.3.1. Differential scanning calorimetry (DSC)

DSC curves of poly(MAOTIB) and PNPs were recorded using TA DSC Q200 (TA Instruments) to acquire information about glass transition temperature (Tg) and physical state of pure polymer and its nanoparticulate form. The analysis was carried out after equilibrating samples at 20°C for 30 min and calibration of DSC temperature and enthalpy scale with indium standard. Samples were then sealed in aluminum pans and heat up to 170°C at rates of 10°C/min with a constant flow of nitrogen as inert atmosphere (flow rate of 15.8 mL/min, linear velocity 35 cm/sec and pressure 24.7 kPa).

2.3.2. Fourier transform infrared spectroscopy (FTIR)

Chemical structure was determined by FTIR analysis. FTIR spectra were recorded at room temperature with Nicolet™ 380 routine FT-IR spectrometer apparatus, Thermo Electron Corporation, on dried samples pressed between internal reflection element crystal and gripper plate. Scanning was done in the range between 4000 and 400 cm^{-1}. Resolution of 4 cm^{-1} at 32 scans was used.

2.3.3. Gel permeation chromatography (GPC)

Purified poly(MAOTIB) was characterized by conventional gel permeation chromatography (GPC) in THF at a flow rate of 1 mL/min (Waters). The number-average molecular weight was 2.761 10^5 g/mol (Mw/Mn = 1.968).

2.3.4. Thermogravimetric analysis (TGA)

TGA measurements were acquired on TGA Mettler TG50 (Mettler Toledo). The mass losses of samples were assayed under nitrogen atmosphere from 20 to 400°C with a heating rate of 10°C/min.

2.3.5. Dynamic light scattering (DLS)

Size distribution, polydispersity indices and zeta potential (ξ) were measured by DLS with a Malvern apparatus (NanoZS®, Malvern, Orsay, France). Mean particle size was assimilated to z-average hydrodynamic diameter and the width of size distribution to polydispersity index (PDI). DLS measurements were run using a helium/neon laser, 4 mW, operated at 633 nm, with the scatter angle fixed at 173° and temperature maintained at 25 °C on diluted sample. DLS data were analyzed using a cumulants-based method assuming spherical shape. Zeta potential of PNPs suspensions (diluted 1/10 000 in double distilled water) was calculated

from the electrophoretic mobility by the Helmholtz–Smoluchowski equation. All experiments were performed in triplicate.

2.3.6. Scanning electron microscopy (SEM)

Surface morphology of PNPs was investigated on dry sample using SEM Philips SIRION FEI apparatus working at 20 kV. Sample was spread on a glass slide, dried at room temperature and then metallized by a thin palladium layer under vacuum before viewing by SEM.

2.3.7. Biocompatibility experiments

2.3.7.1. Stability of PNPs in serum

To establish colloidal and biological stability of PNPs in a biological system, stability study was performed by incubation of PNPs (0.1 mL) with FBS (0.9 mL) at 37°C over 24h under gentle stirring. Concentration of PNPs in FBS was chosen to correspond to the one in blood after injection (see *In vivo experiment on small animal*

. Size distribution in serum was monitored in time (1h, 2h, 3h, 4h, 5h, 7h, 18 h and 24h) in order to evaluate potential degradation of PNPs that might influence their pharmacokinetics once administrated to mice.

2.3.7.2. Cellular uptake experiment

Cellular uptake and internalization localization were carried out using a Leica TCS SPE confocal microscope with KB cells line (HeLa cells derivatives). To visualize PNPs, Lumogen Red dye was incorporated to the process of formulation by solubilization (0.5 wt.%) in the THF organic solution before dropping. The cells were seeded overnight in cell culture glass chamber slides (304 cells per well) at 37°C in humidified atmosphere (5% CO_2) in DMEM supplemented with 10% FBS. Dye-loaded PNPs suspension was then added after dilution (1/200) with Opti-MEM medium. Cells incubation was performed over 1h at 37°C in the same controlled atmosphere. After this amount of time, extensive rinsing with Opti-MEM medium was then performed to remove excess of dye-loaded PNPs and staining agent. Cells membranes were stained with WGA 488 green dye (1 µg/mL) and the cells were finally observed with Leica TCS SPE confocal microscope equipped with oil immersion objective. Excitation wavelengths were 488 and 560 nm, fluorescence signals were collected in 498-540 and 570-700nm respectively for cell membrane (green channel) and dye loaded-PNPs (red channel).

2.3.8. XR micro-CT assays

2.3.8.1. In vitro experiment for iodine quantification

Iodine content was evaluated through *in vitro* quantification of radiopacity property by XR micro-CT scanner (1076 Skyscan, Kartuizersweg, Belgium). Experimental parameters were as follows: X-ray: 49 keV, 129 mA; resolution: 35 mm; pitch: 0.4°; aluminum filters: 0.5 and 632 ms. Calibration curve, correlating radiopacity to iodine concentration, was established using commercially available contrast agent (Hexabrix® 320) and allowed to determine iodine content of optimal PNPs suspension.

2.3.8.2. In vivo experiment on small animal

In vivo images were acquired with a micro-CT scanner (INVEON, Siemens, Munich, Germany). The experimental X-ray parameters were as follows: X-ray, 50 keV, 500 µA; resolution, 111.25 µm; pitch, 2°; aluminum filters, 0.5 and 900 ms Imaging experiment was performed on 3 Swiss mice. Before acquisition, mice were anesthetized with isoflurane. Then, optimal iodinated PNPs supensions were intravenously injected (using a catheter) in the tail vein, with an injection volume corresponding to 10% of the blood volume (*i.e.* 7.5 µL of PNPs suspension/g of mouse). Scans were performed before administration, immediately after injection, and after 30 min, 1h, 2h, 3h, 4h, 6h, 24h, 48h, 72h and 7 days. The micro-CT raw data were treated with OsiriX viewer to establish 2D maximum projection slices and 3D volume rendering images and then to quantify the signal by placing the region of interests in the heart, liver and spleen.

3. Results and discussion

After syntheses and purification, poly(MAOTIB) was formulated into PNPs through nanoprecipitation process. As mentioned in Table , three quantities of polymer and six SPR were used rendering three series of suspensions PNPs-1, PNPs-2 and PNPs-3 with their own theoretical iodine content (see ***Formation of PEGylated-coated poly(MAOTIB) NPs*** section), and thus radio-opacity ability, from 15.5, 31 to 62 mg of Iodine/mL with specific size distributions depending on the amount of surfactant involved.

Before starting to detail the results, two precursory assays should have been checked. The first one concerned PNPs sturdiness once exposed to physiological environment. It has to be mentioned that loss of consistency of the polymeric construct because of body temperature (37°C) may lead to changes in PNPs morphology, leakage of iodinated macromolecules and

thus low iodine concentration in accumulation tissue(s). In other words, it had to be ensured that PNPs would remain solid nanoparticulate assembly once administrated *in vivo*. DSC analysis was so carried out on Poly(MAOTIB) to determine the glassy temperature (Tg), indicating the temperature above which the polymer state turns into rubbery state. Macroscopic aspect of the radiopaque homopolymer led to believe that Tg was effectively higher than 25°C due to its solid powder state. DSC results proved that Tg was around 65°C of the pure polymer, and similar experiment done for PNPs gave 80°C, which confirm that they keep their glassy state well-above 37°C. Optimal XR contrast near PNPs location *in vivo* could have been looked forward. Further stability experiment concerning the *in vivo* fate of PNPs will be introduced in the next sections to complete this point.

Second assay aimed at evaluating the need of a stabilizer agent to form NPs from poly(MAOTIB) since the nanoprecipitation method does not always require such component to achieve formation of nano-sized polymeric colloids. Macroscopic observations of the process without PEGylated stabilizer showed that poly(MAOTIB) did not yield PNPs but only gave polymer precipitate Figure 3 (left vial). Only the involvement of surfactant led to homogeneous dispersion of hydrophilic poly(MAOTIB) colloids (Figure 3, right vial). We studied of the effect of the amount of Kolliphor ELP® surfactant (*i.e.* SPR value), as an essential parameter of the formulation. In addition, PEG-anchored surface works as a shield against protein plasma adsorption.

Figure 3: Aqueous dispersion of poly(MAOTIB) colloids obtained after nanoprecipitation without (Left) and with (Rigth) the PEGylated stabilizing agent in the non-solvent phase.

Our choice to play on surfactant content was also justified by the huge impact on the size distribution of PNPs suspensions (Figure 4). Typically, from SPR30% to SPR80%, the mean hydrodynamic size of all samples formulated decreased drastically regardless the amount of polymer involved. Considering our main goal to turn a radiopaque homopolymer into stealth and efficient NPs-based XR-CA, size remained one of most important parameter, for which the size distribution have to centered in values smaller than 200-300 nm to be compatible with

a parenteral administration, preventing embolism. Regarding now the influence of polymer quantity, it was also quite obvious that it would have significant consequences on size distribution: the more poly(MAOTIB) was concentrated in the dropping phase, the bigger PNPs were. The strategy so applied here was established on the principle to increase little by little the amount of radiopaque polymer in the process in order to find the optimal balance between iodine content in PNPs-suspension, monodispersity and suitable dimension to get injectable XR-CA by playing on SPR to offset impact of polymer concentration on size distribution. As shown in Figure 4, poly(MAOTIB) content in PNPs-1, PNPs-2 and PNPs-3 led to the formation of bigger PNPs, however SPR increase offered the expected offset since size distributions ranged from: 137 nm to 178 nm, 142 nm to 183 nm and 153 to 184 nm, respectively for PNPs-1, PNPs-2 and PNPs-3 and for SPR from 80 wt.% to 30 wt.%. It should be mentioned that even with the smallest amount of surfactant (SPR30%) and the most concentrated suspension in poly(MAOTIB) (PNPs-3), PNPs were not bigger than 200 nm which means that all prepared samples formed adequate candidates for *in vivo* use regardless the radio-opacity property. Finally, it has to be highlighted that raising SPR narrowed the size distribution with some limitations. The curves reach in general a stabilization plateau around SPR70%. Another limitation concerned the rheology of PNPs suspensions, using more surfactant increased a little bit the viscosity, although macroscopic observation made conclude that all samples remained fluid enough for intravenous injection.

In reason to our abovementioned comment about the satisfying hydrodynamic diameters of PNPs-1, PNPs-2 and PNPs-3, we decided to select PNPs-3 (blue curve on Figure 4) as the most promising suspensions range because of the iodine content, high enough to get significant XR attenuation and because size distributions complied with *in vivo* assays despite the important loading of polymer.

To pick best sample among suspensions from PNPs-3, another parameter was evaluated. Generally, size measurement goes along with determination of polydispersity of colloidal suspension. It is important to understand that monodispersity is a fundamental parameter to improve the stability, impacting on the behavior *in vivo* like circulation time in blood. All suspensions herein produced exhibited monodisperse PNPs populations; PDI evolution for the selected three series (see inset in Figure 4) depicted similar profile to its size distribution since above a certain amount of surfactant, PDI stopped decreasing and remained stable proving once more that the effect of surfactant was limited. In this way, using excess of stabilizer much higher than SPR50% was useless to get infinite control over size distribution. To find

out optimal suspension over PNPs-3, it was necessary to keep in mind that surfactant was certainly biocompatible but still to consider as foreign molecular entity for *in vivo* media. Consequently, to prepare the safest poly(MAOTIB) PNPs-based CA it was rather chosen to consider the suspension with SPR60% from PNPs-3 for injection because it formed the best compromise up to SPR50% owing to a very low PDI (0.09) and average hydrodynamic diameter of 163 nm. Besides, samples formulated with SPR70% and SPR80% did not exhibit much greater characteristics regarding higher amount of PEGylated surfactants.

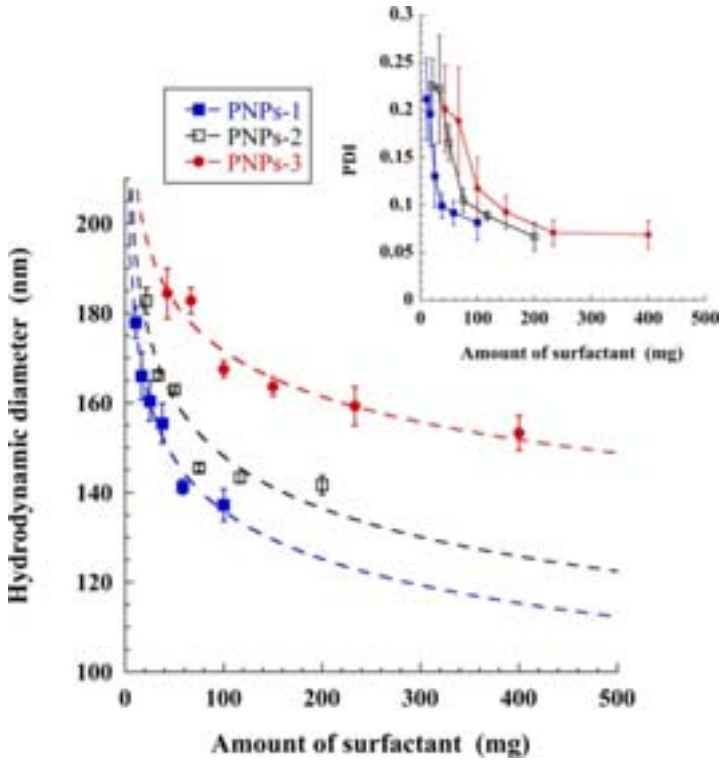

Figure 4: Effect of the surfactant amount on size distribution of PNPs suspensions, function of their poly(MAOTIB) content. Gray delimitation indicates limits of acceptable size. Top right inset shows evolution of PDI along with amount of surfactant of PNPs-3.

To accurately evaluate the iodine content of the selected PNPs-3/SPR60% suspension, calibration curve based on quantification of radiopacity of commercially available CA (Hexabrix® 320) was used to get correlation between radiopacity property and iodine concentration. *In vitro* experiment with XR micro-CT was carried out and provided the results shown in Figure 5. The iodine concentration in the as-prepared polymeric suspension was estimated at 59 mg I/mL which was quite close to the theoretical concentration previously assumed at 62 mg I/mL. The difference was so attributed to initiator fractions on the backbone of iodinated macromolecules. In any cases, these *in vitro* experiments let us expect

similar radiopaque property once suspension will be administrated to mice for *in vivo* XR micro-CT imaging assays.

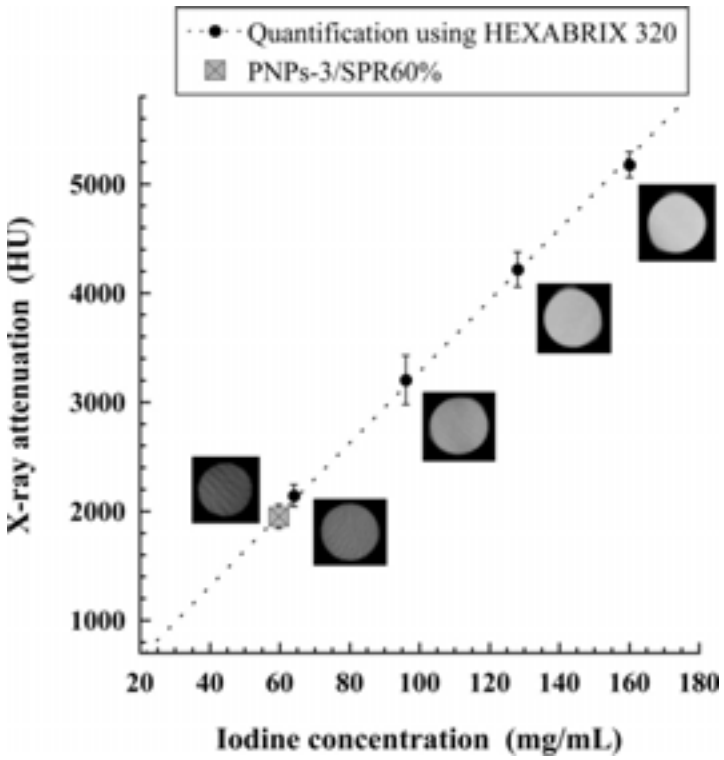

Figure 5: *In vitro* evaluation of XR attenuation property of the optimal suspension. Quantification curve was made with several dilutions of Hexabrix® 320, an injectable commercial CA at 320 mg I/mL. Values of radiopacity are indicated by filled square and circles respectively for PNPs-3/SPR60% and quantification curve. Insets report phantoms tubes of each dilutions and PNPs-3/SPR60%.

The following sections will thus focus on the optimized suspension (PNPs-3/SPR60%). Next part deal first of all with basic characterizations of the construct of the as-selected sample.

Poly(MAOTIB) and PNPs-3/SPR60% were both subjected to thermal treatment *via* TGA. Applying TGA remains a quite useful method to check poly(MAOTIB) purity and its resistance to heat. It was concluded that poly(MAOTIB) was pure without any traces of solvent and volatiles and showed excellent resistant to high temperature over 300°C without any decomposition (Figure 6). TGA experiment on PNPs proved that all organic material including surfactant and polymer were effectively consumed over a range of temperature from 300 to 350°C, then from 350°C to 400°C the thermogram showed a plateau assimilated to the non-degradation of residual material such as inorganic element like iodine.

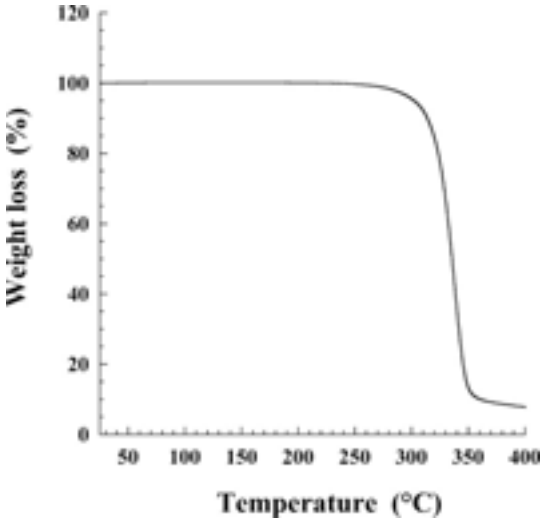

Figure 6: TGA of poly(MAOTIB) over 300°C.

Although TGA helped to prove radiopaque polymer and its formulated form were both made of organic compounds without traces of inorganic elements and devoid of remaining solvents, it did not discriminate how many macromolecules, including poly(MAOTIB) and Kolliphor ELP® macromolecules, were organized into our nanoconstruct. So far, it remains to clearly identify the way of Poly(MAOTIB) and stabilizer are combined both together into the selected PNPs dispersion to impart hydrophilic surface property, content of radiopaque homopolymer and colloidal stability.

In the next part, FTIR spectroscopy and resistance to centrifugation will be presented. These studies will be used as proof of concept to explain how macromolecules assembling built up our hydrophilic PNPs-based XR-CA.

Figure 7 shows typical FTIR spectra of poly(MAOTIB), nonionic hydrophilic Kolliphor ELP® surfactant and PNPs-3/SPR60% in dried state. The poly(MAOTIB) (Figure 7A) was free of monomer traces as verified by the lack of stretching band of MAOTIB C=C double bond usually observed at 1626 cm^{-1}. FTIR spectrum of poly(MAOTIB) shows symmetric and asymmetric stretching of C-H bond in the region of 2950 cm^{-1}. Absorption bands at transition frequencies of 1725 cm^{-1} and 1262 cm^{-1} are attributable to carbonyl C=O and ester C-O stretching bands respectively. Bending vibrations peaks of C-H bonds are observed in the region of 1420-1464 cm^{-1} whereas multiple stretching vibrations peaks of aromatic C=C double bond from TIB-Cl synthon appear in the region of 695-901 cm^{-1}. Figure 7B depicts FTIR spectrum of Kolliphor ELP® which indicates features corresponding to C-H bond stretching from aliphatic alkyl chains from 2856 cm^{-1} to 2922 cm^{-1}. Kolliphor ELP® is based

on PEGylated carbon medium-chains macromolecules which thus implies a higher absorption signal for C-H stretching peaks than for poly(MAOTIB) ones. Bending vibrations are also observed for C-H at 1467 cm^{-1}. As poly(MAOTIB), carbonyl C=O and C-O stretching vibrations peaks appear at 1730 $cm^{-1}$and 1246 cm^{-1} but a quite broad absorption band around 1100 cm^{-1} corresponding to C-O stretching vibrations arises too. FTIR spectrum of PNPs-3/SPR60% (Figure 7C) shows peaks attributable to both Kolliphor ELP® and poly(MOATIB) which proved combination of those macromolecules into the polymeric colloidal formulation. The assembling of PNPs based on poly(MAOTIB) and surfactant relied basically on a physisorption of surfactant macromolecules onto the radiopaque polymeric core of the PNPs. Such adsorption was highlighted by performing extensive dialysis against ethanol of PNPs-3/SPR60% and followed by FTIR. After several washing by dialysis it appears that surfactant was removed from PNPs since FTIR spectra of the dialyzed PNPs revealed being identical to poly(MAOTIB) one and did not exhibit any specific absorption bands from Kolliphor ELP®.

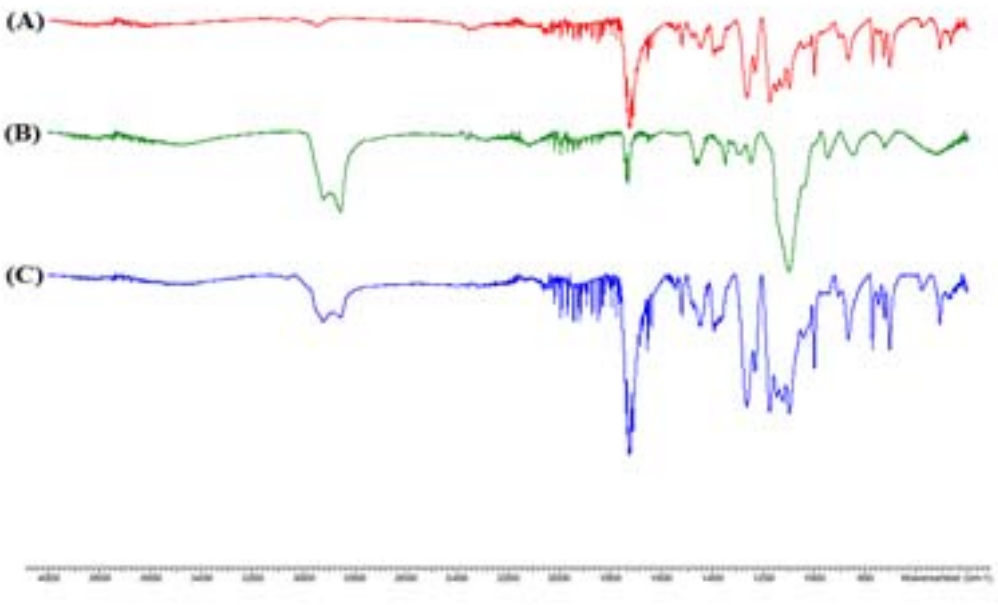

Figure 7: FTIR spectra of (A) poly(MAOTIB) homopolymer, (B) Kolliphor ELP® and (C) dried PNPs typically obtained with nanoprecipitation process.

Since it has been experimentally evidenced the poly(MAOTIB) core- Kolliphor ELP® structure, the next aspect investigated was the resistance of PNPs-3/SPR60% core-shell assembling.

To figure how stable and resistant is PNPs-3/SPR60% assembling, harsh treatment by extensive centrifugation cycle were carried out. It has been demonstrated that surfactant

macromolecules were bonded onto polymeric core by non-covalent bonding by means of adsorption. Even though adsorption is a weak link between surfactant and NPs, it still provides an efficient steric barrier preventing from aggregation. As shown in Figure 8, several cycles of centrifugation (6 cycles), commonly used here as an extraction method of PNPs from the excess of surfactant used (see ***Formation of PEGylated-coated poly(MAOTIB) NPs*** section), did not impact notably the PNPs size distribution. Average values of size distribution gradually increased from 163 nm (1 cycle), 170-178 nm (2, 3 and 4 cycles) and up to 200 nm (5 and 6 cycles). Although, those aggregates were not visible by visual examination and redispersion, the suspensions are gradually more polydisperse since PDI value finally reach 0.33-0.34 after 5 cycles of centrifugation. This means that surfactants strongly interacted with the PNPs boundaries since it took 5 harsh cycles of centrifugation to impact significantly the mean hydrodynamic diameter of PNPs.

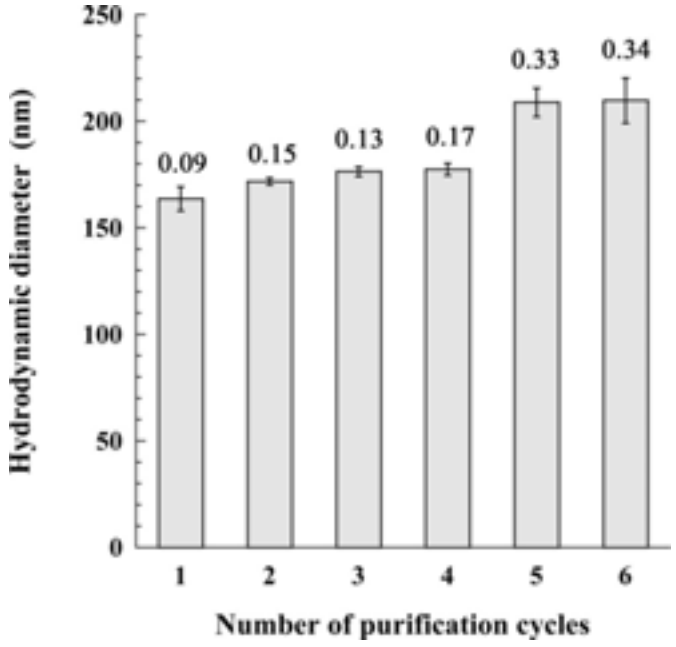

Figure 8: Evolution of the hydrodynamic diameter in function of the number of centrifugation cycle. PDI value is indicated by the figure for each purification cycle.

Scanning electron microscopy was performed to the PNP-3/SPR60% sample in order to obtain a proper observation of the as-prepared XR-CA. According to the morphology and structural investigation performed through SEM (Figure 9), the nanoprecipitation process applied in this study allowed to get spherical and monodisperse nanoparticles. SEM pictures illustrate higher magnifications of the PNPs-3/SPR60% sample and reveal a smooth surface of PNPs. We assumed that the agglomerated appearance of the sample is mainly due to the drying required to succeed in SEM imaging. Figure 9 proved indeed that PNPs-3/SPR60%

dispersion had a narrow size distribution when dispersed into PBS without the clustering issue visible on dry state on SEM pictures.

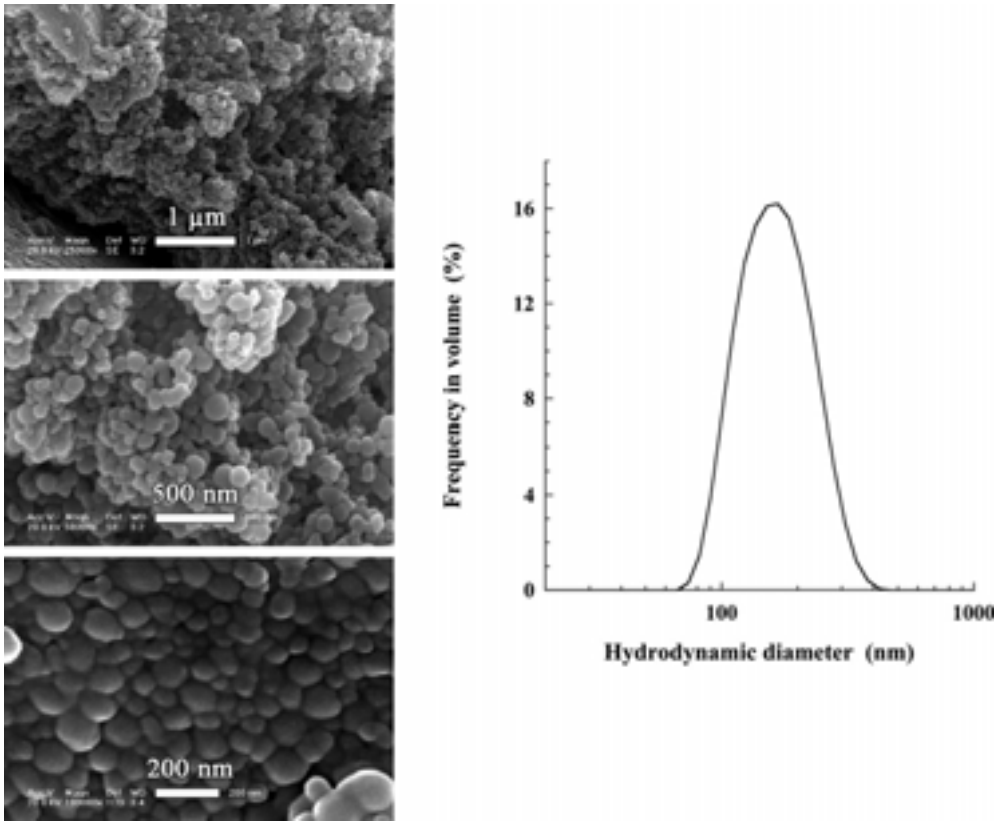

Figure 9: SEM and DLS characterizations of the optimized PNPs suspension for *in vitro* and *in vivo* assays.

Following part will focus on experiments aiming to evaluate *in vitro* and *in vivo* fate of PNPs-3/SPR60%, including studies of its biocompatibility and its fate in physiological environment such as on cells line and after administration to mice.

Considering that the PNPs-3/SPR60% were administrated to mice at 7.5 µL/g of mouse (10% of blood volume), the *in vitro* stability study of a diluted (1/10) aliquot of PNPs-3/SPR60% incubated in serum was performed to determine if PNPs were stable in blood pool and compatible with parenteral administration route. As reported in Figure 10, PNPs suspension retained their average size without significant variation over 24h of experiment. During the incubation period, we never notified any aggregates of our colloidal materials indicating high stability against biological media.

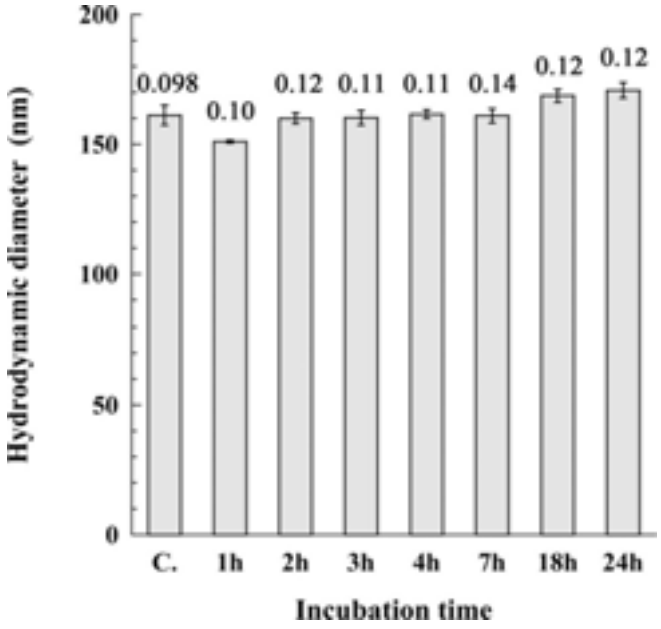

Figure 10: *In vitro* evaluation of PNPs stability in serum. PDI value is indicated by the figure for each incubation time.

Another aspect of the evaluation of the fate of our PNPs suspension in physiological environment was carried out through cellular uptake study on KB cells, derived from HeLa cells line with monolayer-like morphology, after cell membrane labeling with green fluorescent dye probe (Figure 11A). To this end, PNPs were loaded with red-emitting fluorophore following a protocol used for PLGA nanoparticles, [55] Lumogene Red. During nanoprecipitation process, no change of size distribution was notified despite this change of formulation composition. KB cells were incubated for 1h in the presence of the fluorescently labeled PNPs and visualized by laser scanning confocal microscopy after staining of the plasma membrane with help of WGA-488. Figure 11 discloses no leacking once the dye-doped PNPs were in presence of cells media, internalization of free-dye would have been visualized by intense red fluorescence within cell matrix. Tracing by fluorescence imaging was thus feasible. This experiment on KB cells showed that no internalization took place (Figure 11B), even more, PNPs were mainly stuck on the glass surface indicating that there was non-specific interaction between cells and PNPs (Figure 11C). Zeta potential measurement have revealed a surface charge of -30 mV, endorsing as well the satisfying colloidal stability noticed on the sample, which might promote sticking to glass material. In addition, MAOTIB has important iodine weigh content compared to molecular weight of the native non-iodinated monomer.

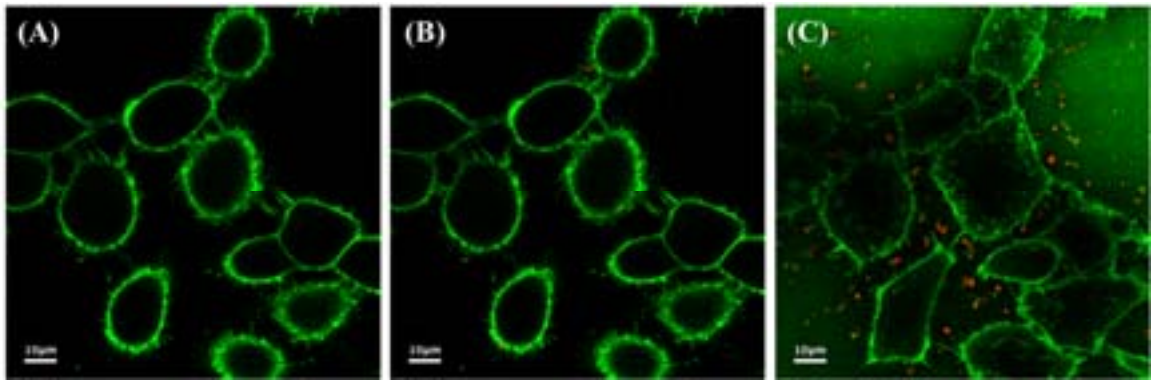

Figure 11: Confocal microscopy pictures of membrane-labeled KB cells with Lumogene Red dye-doped PNPs (A) Green channel for KB cells membrane observation, (B) green and red channels for visualization of potential engulfing of dye-doped PNPs and (C) green and red channels at glass surface.

In this last part let us consider now the application on small animal. Three Swiss mice were subjected to a single intravenous administration of a 10% dose of PNPs-3/SPR60% in the vein-tail. No side effects were observed on animals all along experiments duration, the weight of mice was followed over the 7 days exploration by XR micro-CT and remained stable over this period. *In vivo* acquisitions *via* XR micro-CT scanner are illustrated in Figure 12A at different representative times (before, after and 1h post-injection) from both coronal sections and transverse slices through the liver and the spleen. In an early stage once injected to the mice, polymeric suspensions were instantly spread in i) the vascular system of animals for a short retention period, for which contrast enhancement in bloodstream remain visible during approximately 30 min, during the vascular phase, before being co-distributed to ii) RES organs such the spleen and liver where a strong contrast enhancement was observed and persisting over experiments duration after a single administration. Owing to the clear delineation of the heart and its whole vascular structure (cardiac ventricles and arterial) emerging immediately after injection followed, only 1h post-injection, by the contrast enhancement arising from the liver and the spleen, it could have been assumed that blood clearance mechanism performed by these two organs. The 3D volume rendering of the liver and the spleen (1h post-injection) induced by accumulation of the dose of PNPs-3/SPR60% is presented in Figure 12B. Both organs appear very clearly on the reconstructed image, details of their surfaces are so visible. However, the spleen exhibited a slightly higher brightness, that means the best accumulation ability.

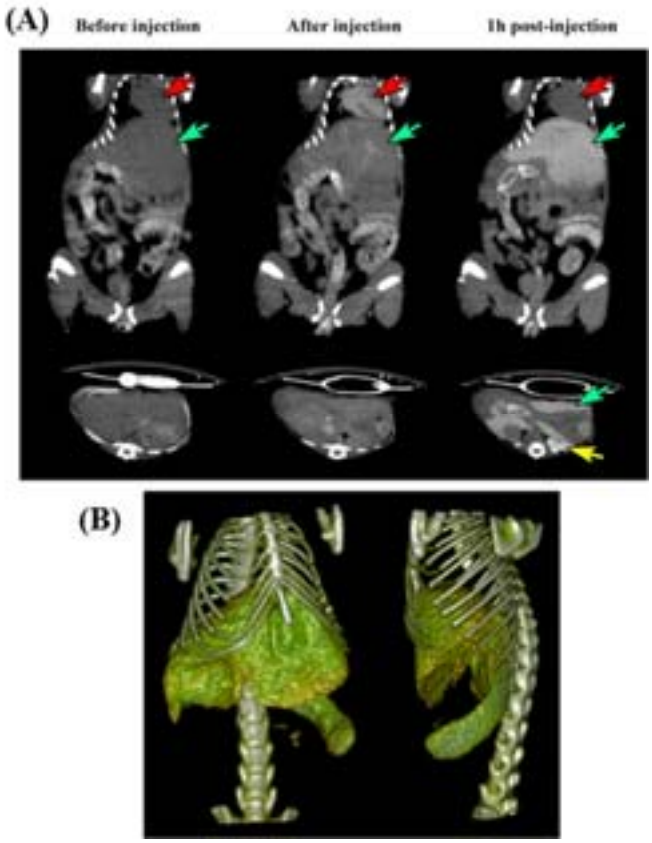

Figure 12: *In vivo* micro-CT scans (A) before, after and 1h after intravenous injection of the as-prepared CA. Pictures show coronal and axial sections of mice. Heart, liver and spleen are respectively indicated by red, green and yellow arrows. (B) Liver and spleen 3D volume rendering imaging.

From these data, the quantification of the XR attenuation was performed various time post-injection to precisely quantify the fate *in vivo*, kinetic and biodistribution. The representative timescale chosen to depict contrast enhancement after administration was from before injection to 100h post-injection to show the actual efficiency of our NPs CA since XR attenuation profiles by liver and spleen were assumed linear after PNPs-3/SPR60% clearance from bloodstream. Several ROI were located in the heart, the liver, the spleen and the kidneys and monitored to highlight and quantify brightness over the abovementioned timescale. Contrast enhancement of ROI was expressed with ΔHU_t^{ROI} corresponding to the subtraction of the normalized XR attenuation value at the acquisition time t to the one before injection. XR attenuations expressed with Hounsfield scale of ROI are reported in Figure 13. Right after administration (t = 0 h), blood pool XR attenuation was observed by measuring value in the heart which reached $\Delta HU_0^{heart} = (130 \pm 20)$ HU before collapsing and bottoming up near 0 beyond 2h post-injection. Elimination kinetics for blood pool was fitted by the following mono-compartmental exponential equation:

$$\Delta HU_t^{heart} = \Delta HU_0^{heart} \times \exp(-k_{heart} \times t)$$

where ΔHU_0^{heart} is the initial value of the contrast enhancement in the heart and so assimilated to blood pool and k_{heart} is the blood elimination constant rate, here k_{heart} = 2.2 h^{-1}. As mentioned before half-time of our poly(MAOTIB) NPs in blood was estimated, with the above equation, at around 20 min ($\Delta HU_{t_{1/2}}^{heart}$ = 80 HU), indicating that blood clearance mechanism occurs pretty quickly after their introduction in the bloodstream. Immediately after introduction of our NPs CA, liver and spleen regions showed mild contrast enhancement, typically due to organs irrigation by blood carrying radiopaque PNPs. However, meanwhile blood clearance gets forward, XR attenuation of liver and spleen tissues become more and more significant. According to the Figure 12A, PNPs elimination from bloodstream was assumed to be performed through hepatic and splenic routes due to the accurate distinction of those tissues among other soft tissues from the abdominal zone 1h after administration. Quantifications of XR attenuation of both organs showed a very fast rise of the contrast enhancement during the first 30 min post-injection, that made difficult the extrapolation mono-compartmental accumulation model. A few fluctuations over next hours of the XR micro-CT follow-up are disclosed on Figure 13 (filled circles and empty square curves respectively for the spleen and the liver pharmacokinetic profiles). The mean values of the stabilized contrast agent after 30 min to 100h post-injection ($\Delta HU_{average}^{spleen}$ and $\Delta HU_{average}^{liver}$), are $\Delta HU_{average}^{spleen}$ = 191 HU and $\Delta HU_{average}^{liver}$ = 141 HU, giving significantly higher values for spleen. Splenic contrast appeared more significant than hepatic one regarding quantification. According to these observations, it appears that we produced here an efficient and non-toxic nanoparticulate CA based on a radiopaque homopolymer with optimized formulation parameters as it has been shown in the first parts of this study. It has to be noted, that kidneys were also pointed as ROI in order to determine if CA was eliminated through renal clearance. Based on the evaluation of contrast enhancement for kidneys (empty circles curve on Figure 13), it seems that loss of PNPs-3/SPR60% through renal route remains negligible compared to RES route.

However, to make an accurate discrimination of the biodistribution between blood, spleen and liver compartments, the quantification of the amount of PNPs-3/SPR60% in each ROI is required since their volume and thus their ability to carry NPs differ, regardless the affinity of PNPs with tissues. Determination of real biodistribution of the CA was expressed as a percentage of the dose injected for each passively targeted organ or ROI where contrast

enhancement was observed. Normalization of XR attenuation signals for the different acquisition time (Figure 13) is done taking into account that liver and spleen of Swiss mice represents respectively (4.4±0.2)% and (0.5±0.1)% of its body weight. Based on this normalization, it appears that the dose was respectively shared at 61% in the liver and 9% in the spleen. The PNPs suspension was though strongly accumulated in the liver but spleen exhibited highest XR attenuation as abovementioned. According to these results, the difference of volume promote a better visualization of spleen compartment due to the possibility to concentrate more the accumulated dose of PNPs compared to the liver in which the CA was, for sure accumulated in huge amount, but much more diluted owing to its volume.

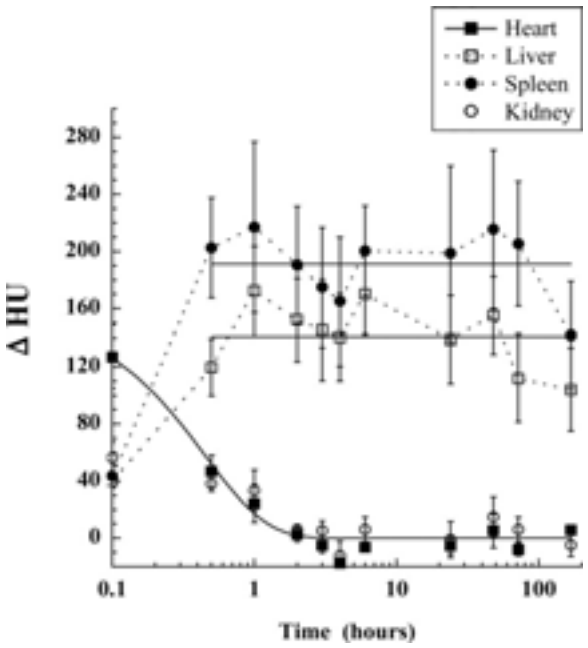

Figure 13: Follow-up of the quantification of XR attenuation after intravenous administration of PNPs-3/SPR60% over time (n = 4). ROI were placed in the heart (filled squares), the liver (open squares), the spleen (filled circles) and the kidneys (open circles). Curve was fitted with mono-compartmental exponential equation for the heart whereas liver and spleen curves profiles were assimilated to plateau.

4. Conclusion

This study presents the preparation of a biocompatible injectable CA for soft tissues XR micro-CT imaging. A novel method based on nanoprecipitation was applied to form hydrophilic and stealth nanoparticles from poly(MAOTIB) homopolymer produced by bulk radical polymerization of MAOTIB monomer (62 wt.% of the molecular weight is iodine). The effects of polymer and PEGylated surfactant weight ratio and the polymer content were

elucidated to find out the best compromise between iodine content and suitable size for *in vivo* application. The suitable iodinated PNPs suspension was so formulated with a narrow size distribution of 163.7 nm (PDI 0.09) and iodine concentration of 59 mg I/mL. Investigations of radiopaque property once exposed to *in vivo* environment were performed on mice (10% of the blood volume) and demonstrated that passive accumulation occurred in liver and spleen compartments after a short circulation time in bloodstream ($t_{1/2}$ = 20min), indicating that blood clearance takes place through hepatic and splenic routes. A loss of contrasting materials was however notified leading us to believe that our targeting strategy may still be improved and optimized. Besides, contrast enhancement displayed in liver and spleen remains very satisfying to consider the as-developed radiopaque PNPs formulation as an efficient and non-toxic CA for small animal and preclinical imaging.

5. Acknowledgement

Authors acknowledge the ICS Characterization Platform for the use of ATG and DSC and thank Mrs. M. Legros and C. Saettel for the analyses. *In vivo* imaging of this study was performed on the imaging facilities of CERMEP-Imagerie du vivant, Bron, F-69677, France, imaging facilities. The authors thank the technical staff of the platform.

6. References

[1] M.A. Hahn, A.K. Singh, P. Sharma, S.C. Brown, B.M. Moudgil, Nanoparticles as contrast agents for *in-vivo* bioimaging: Current status and future perspectives, Anal. Bioanal. Chem. 399 (2011) 3–27. doi:10.1007/s00216-010-4207-5.

[2] M. Elsabahy, G.S. Heo, S.-M. Lim, G. Sun, K.L. Wooley, Polymeric Nanostructures for Imaging and Therapy, Chem. Rev. 115 (2015) 10967–11011. doi:10.1021/acs.chemrev.5b00135.

[3] J. Key, J.F. Leary, Nanoparticles for multimodal *in vivo* imaging in nanomedicine, Int. J. Nanomedicine. 9 (2014) 711–726. doi:10.2147/IJN.S53717.

[4] X. Li, N. Anton, G. Zuber, T. Vandamme, Contrast agents for preclinical targeted X-ray imaging, Adv. Drug Deliv. Rev. 76 (2014) 116–133. doi:10.1016/j.addr.2014.07.013.

[5] G.N. Hounsfield, Computerized transverse axial scanning (tomography): Part I description of system, Br. J. Radiol. 46 (1973) 1016–1022. doi:10.1259/0007-1285-46-552-1016.

[6] D.P. Cormode, P.C. Naha, Z.A. Fayad, Nanoparticle contrast agents for computed tomography: A focus on micelles, Contrast Media Mol. Imaging. 9 (2014) 37–52. doi:10.1002/cmmi.1551.

[7] A. Jakhmola, N. Anton, T.F. Vandamme, Inorganic nanoparticles based contrast agents for X-ray computed tomography, Adv. Healthc. Mater. 1 (2012) 413–431. doi:10.1002/adhm.201200032.

[8] F. Hallouard, N. Anton, P. Choquet, A. Constantinesco, T. Vandamme, Iodinated blood pool contrast media for preclinical X-ray imaging applications - A review, Biomaterials. 31 (2010) 6249–6268. doi:10.1016/j.biomaterials.2010.04.066.

[9] N. Lee, S.H. Choi, T. Hyeon, Nano-sized CT contrast agents, Adv. Mater. 25 (2013) 2641–2660. doi:10.1002/adma.201300081.

[10] S.-B. Yu, A.D. Watson, Metal-Based X-ray Contrast Media, Chem. Rev. 99 (1999) 2353–2378. doi:10.1021/cr980441p.

[11] J.C. De La Vega, U.O. Häfeli, Utilization of nanoparticles as X-ray contrast agents for diagnostic imaging applications, Contrast Media Mol. Imaging. 10 (2014) 81–95. doi:10.1002/cmmi.1613.

[12] N. Anton, T.F. Vandamme, Nanotechnology for computed tomography: A real potential recently disclosed, Pharm. Res. 31 (2014) 20–34. doi:10.1007/s11095-013-1131-3.

[13] C.T. Badea, M. Drangova, D.W. Holdsworth, G.A. Johnson, *In vivo* small-animal imaging using micro-CT and digital subtraction angiography., Phys. Med. Biol. 53 (2008) R319–R350. doi:10.1088/0031-9155/53/19/R01.

[14] D.W. Holdsworth, M.M. Thornton, Micro-CT in small animal and specimen imaging, Trends Biotechnol. 20 (2002) S34–39. doi:10.1016/S0167-7799(02)02004-8.

[15] W. He, K. Ai, L. Lu, Nanoparticulate X-ray CT contrast agents, Sci. China Chem. 58 (2015) 753–760. doi:10.1007/s11426-015-5351-8.

[16] H. Lusic, M.W. Grinstaff, X-ray Computed Tomography Contrast Agents, Chem. Rev. 113 (2013) 1641–1666. doi:doi.org/10.1021/cr200358s.

[17] J.-M. Idée, B. Guiu, Use of Lipiodol as a drug-delivery system for transcatheter arterial chemoembolization of hepatocellular carcinoma: A review, Crit. Rev. Oncol. Hematol. 88 (2013) 530–549. doi:10.1016/j.critrevonc.2013.07.003.

[18] J.M. Widmark, Imaging-related medications: a class overview, Proc. (Baylor Univ. Med. Center). 20 (2007) 408–417.

[19] S. Parveen, R. Misra, S.K. Sahoo, Nanoparticles: a boon to drug delivery, therapeutics, diagnostics and imaging, Nanomedicine Nanotechnology, Biol. Med. 8 (2012) 147–166. doi:10.1016/j.nano.2011.05.016.

[20] V.P. Torchilin, Multifunctional nanocarriers, Adv. Drug Deliv. Rev. 64 (2012) 302–315. doi:10.1016/j.addr.2012.09.031.

[21] D.P. Cormode, T. Skajaa, Z.A. Fayad, W.J.M. Mulder, Nanotechnology in medical imaging: probe design and applications, Arter. Thromb Vasc Biol. 29 (2010) 992–1000. doi:10.1161/ATVBAHA.108.165506.

[22] L.K. Bogart, G. Pourroy, C.J. Murphy, V. Puntes, T. Pellegrino, D. Rosenblum, D. Peer, R. Lévy, Nanoparticles for imaging, sensing, and therapeutic intervention, ACS Nano. 8 (2014) 3107–3122. doi:10.1021/nn500962q.

[23] V.P. Torchilin, Targeted pharmaceutical nanocarriers for cancer therapy and imaging., AAPS J. 9 (2007) E128–E147. doi:10.1208/aapsj0902015.

[24] V.P. Torchilin, PEG-based micelles as carriers of contrast agents for different imaging modalities, Adv. Drug Deliv. Rev. 54 (2002) 235–252. doi:10.1016/S0169-409X(02)00019-4.

[25] G. Storm, S.O. Belliot, T. Daemen, D.D. Lasic, Surface modification of nanoparticles to oppose uptake by the mononuclear phagocyte system, Adv. Drug Deliv. Rev. 17 (1995) 31–48. doi:10.1016/0169-409X(95)00039-A.

[26] I. Brigger, C. Dubernet, P. Couvreur, Nanoparticles in cancer therapy and diagnosis, Adv. Drug Deliv. Rev. 54 (2002) 631–651. doi:10.1016/S0169-409X(02)00044-3.

[27] V.P. Torchilin, V.S. Trubetskoy, Which polymers can make nanoparticulate drug carriers long-circulating?, Adv. Drug Deliv. Rev. 16 (1995) 141–155. doi:10.1016/0169-409X(95)00022-Y.

[28] P. Aggarwal, J.B. Hall, C.B. McLeland, M.A. Dobrovolskaia, S.E. McNeil, Nanoparticle interaction with plasma proteins as it relates to particle biodistribution, biocompatibility and therapeutic efficacy, Adv. Drug Deliv. Rev. 61 (2009) 428–437. doi:10.1016/j.addr.2009.03.009.

[29] T. Ahmad, H. Bae, I. Rhee, Y. Chang, J. Lee, S. Hong, Particle size dependence of relaxivity for silica-coated iron oxide nanoparticles, Curr. Appl. Phys. 12 (2012) 969–974. doi:10.1016/j.cap.2011.12.020.

[30] H. Kobayashi, R. Watanabe, P.L. Choyke, Improving conventional enhanced permeability and retention (EPR) effects; What is the appropriate target?, Theranostics. 4 (2014) 81–89. doi:10.7150/thno.7193.

[31] K.H. Bae, H.J. Chung, T.G. Park, Nanomaterials for cancer therapy and imaging, Mol. Cells. 31 (2011) 295–302. doi:10.1007/s10059-011-0051-5.

[32] A. V Fuchs, A.C. Gemmell, K.J. Thurecht, Utilising polymers to understand diseases: advanced molecular imaging agents, Polym. Chem. 6 (2015) 868–880. doi:10.1039/c4py01311e.

[33] A. Kumari, S.K. Yadav, S.C. Yadav, Biodegradable polymeric nanoparticles based drug delivery systems, Colloids Surfaces B Biointerfaces. 75 (2010) 1–18. doi:10.1016/j.colsurfb.2009.09.001.

[34] A. Mahapatro, D.K. Singh, Biodegradable nanoparticles are excellent vehicle for site directed *in-vivo* delivery of drugs and vaccines., J. Nanobiotechnology. (2011) 9:55. doi:10.1186/1477-3155-9-55.

[35] C. Pinto Reis, R.J. Neufeld, A.J. Ribeiro, F. Veiga, Nanoencapsulation I. Methods for preparation of drug-loaded polymeric nanoparticles, Nanomedicine Nanotechnology, Biol. Med. 2 (2006) 8–21. doi:10.1016/j.nano.2005.12.003.

[36] K.S. Soppimath, T.M. Aminabhavi, A.R. Kulkarni, W.E. Rudzinski, Biodegradable polymeric nanoparticles as drug delivery devices, J. Control. Release. 70 (2001) 1–20. doi:10.1016/S0168-3659(00)00339-4.

[37] J.P. Rao, K.E. Geckeler, Polymer nanoparticles: Preparation techniques and size-control parameters, Prog. Polym. Sci. 36 (2011) 887–913. doi:10.1016/j.progpolymsci.2011.01.001.

[38] C. Vauthier, K. Bouchemal, Methods for the Preparation and Manufacture of Polymeric Nanoparticles, Pharm. Res. 26 (2009) 1025–1058. doi:10.1007/s11095-008-9800-3.

[39] E. Jin, Z.R. Lu, Biodegradable iodinated polydisulfides as contrast agents for CT angiography, Biomaterials. 35 (2014) 5822–5829. doi:10.1016/j.biomaterials.2014.03.054.

[40] D. Mawad, H. Mouaziz, A. Penciu, H. Méhier, B. Fenet, H. Fessi, Y. Chevalier, Elaboration of radiopaque iodinated nanoparticles for *in situ* control of local drug delivery., Biomaterials. 30 (2009) 5667–5674. doi:10.1016/j.biomaterials.2009.06.027.

[41] S. Shiralizadeh, H. Nasr-Isfahani, A. Keivanloo, M. Bakherad, Mono- and triiodophenyl isocyanate as radiopacifying agents for methacrylate-based copolymers; biocompatibility and non-toxicity, RSC Adv. 6 (2016) 110400–110408. doi:10.1039/C6RA17860J.

[42] A. Benzina, M.A.B. Kruft, F. Bar, F.H. Van der Veen, C.W. Bastiaansen, V. Heijnen, C. Reutelingsperger, L.H. Koole, Studies on a new radiopaque polymeric biomaterial, Biomaterials. 15 (1994) 1122–1128. doi:10.1016/0142-9612(94)90232-1.

[43] D. Mawad, A. Lauto, A. Penciu, H. Méhier, B. Fenet, H. Fessi, Y. Chevalier, Synthesis and characterization of novel radiopaque poly(allyl amine) nanoparticles, Nanotechnology. 21 (2010) 335603 (8pp). doi:10.1088/0957-4484/21/33/335603.

[44] Y.B.J. Aldenhoff, M.-A.B. Kruft, P.A. Pijpers, F.H. van Der Veen, S.K. Bulstra, R. Kuijer, L.H. Koole, Stability of radiopaque iodine-containing biomaterials, Biomaterials. 23 (2002) 881–886. doi:10.1016/S0142-9612(01)00197-1.

[45] C. Zaharia, T. Zecheru, M.F. Moreau, F. Pascaretti-Grizon, G. Mabilleau, B. Marculescu, R. Filmon, C. Cincu, G. Staikos, D. Chappard, Chemical structure of methylmethacrylate-2-[2′,3′,5′-triiodobenzoyl]oxoethyl methacrylate copolymer, radio-opacity, *in vitro* and *in vivo* biocompatibility, Acta Biomater. 4 (2008) 1762–1769. doi:10.1016/j.actbio.2008.06.009.

[46] K. Saralidze, Y.B.J. Aldenhoff, M.L.W. Knetsch, L.H. Koole, Injectable polymeric microspheres with X-ray visibility. Preparation, properties, and potential utility as new traceable bulking agents, Biomacromolecules. 4 (2003) 793–798. doi:10.1021/bm030002m.

[47] A. Galperin, D. Margel, S. Margel, Synthesis and characterization of uniform radiopaque polystyrene microspheres for X-ray imaging by a single-step swelling process, J. Biomed. Mater. Res. - Part A. 79 (2006) 544–551. doi:10.1002/jbm.a.30863.

[48] A. Galperin, D. Margel, J. Baniel, G. Dank, H. Biton, S. Margel, Radiopaque iodinated polymeric nanoparticles for X-ray imaging applications, Biomaterials. 28 (2007) 4461–4468. doi:10.1016/j.biomaterials.2007.06.032.

[49] A. Galperin, S. Margel, Synthesis and Characterization of New Radiopaque Microspheres by the Dispersion Polymerization of an Iodinated Acrylate Monomer for X-ray Imaging Applications, J. Polym. Sci. Part A Polym. Chem. 44 (2006) 3859–3868. doi:10.1002/pola.

[50] H. Aviv, S. Bartling, F. Kieslling, S. Margel, Radiopaque iodinated copolymeric nanoparticles for X-ray imaging applications, Biomaterials. 30 (2009) 5610–5616. doi:10.1016/j.biomaterials.2009.06.038.

[51] C. Fessi, Curt; Devissaguet, Jean-Philippe; Puisieux, Francis; Thies, Precipitation of film-forming material and biologically active substance from solvent-non-solvent mixture, Fessi, Curt; Devissaguet, Jean-Philippe; Puisieux, Francis; Thies, Curt, 'Precipitation of Film-Forming Material and Biologically Active Substance from Solvent-Non-Solvent Mixture', 1992.

[52] J. Hitanga, N. Sharma, H. Chopra, S. Kumar, Nanoprecipitation technique employed for the development of nanosuspension: a review, Worl J. Pharm. Res. 4 (2015) 2127–2136.

[53] E. Lepeltier, C. Bourgaux, P. Couvreur, Nanoprecipitation and the "Ouzo effect": Application to drug delivery devices, Adv. Drug Deliv. Rev. 71 (2014) 86–97. doi:10.1016/j.addr.2013.12.009.

[54] J. Szebeni, F.M. Muggia, C.R. Alving, Complement Activation by Cremophor EL as a Possible Contributor to Hypersensitivity to Paclitaxel : an *In Vitro* Study, J. Natl. Cancer Inst. 90 (1998) 300–306.

[55] K. Trofymchuk, A. Reisch, I. Shulov, Y. Mély, A.S. Klymchenko, Tuning the color and photostability of perylene diimides inside polymer nanoparticles: towards biodegradable substitutes of quantum dots., Nanoscale. 6 (2014) 12934–12942. doi:10.1039/c4nr03718a.

Chapter III: Study and use of magnetite nanoparticles for biomedical applications

Chapter III: Study and use of magnetite nanoparticles for biomedical applications

The chapter III.1 (**Chapter III.1 – Initiation to magnetite nanoparticles for *in vivo* uses**) is a bibliographical review presenting a state of the art of magnetite Fe_3O_4 iron oxide nanoparticles (IONPs) dedicated to biomedical applications. It outlines all aspects from the basic of nanoparticles (NPs) magnetism, the synthesis and characterization of magnetite to requirements for applications in nanomedicine. This review is mainly dedicated to beginners in superparamagnetic IONPs (SPIONs) for biomedical purposes.

Following this overview about magnetite SPIONs, we proposed a novel study on the use of magnetite-loaded radiopaque nano-emulsion (NE) as bimodal contrast agent (CA) for X-rays/magnetic resonance imaging (MRI) modalities in the chapter III.2 (**Chapter III.2 – Magnetite and iodine-containing nano-emulsion as contrast agent for X-ray/MR imaging**). This project was carried out in order to propose a dual modal CA in case of multimodality needs. As introduced before, conjecture of several imagers' information may furnish useful and complementary data about a target. In this study we chose to produce contrast agents exhibiting radiopaque and magnetic properties to promote contrast enhancement for X-ray imaging and MRI.

Oil-in-water NE is a lipid-based nanocarrier (NC) capable of being loaded with lipophilic ingredients in its oily inner core. We chose to use radiopaque oil from the modification of vitamin E (α-tocopherol) by grafting triiodo-benzoic aromatic compound as oily phase. Magnetite Fe_3O_4 SPIONs were also incorporated into this oily phase to generate contrast enhancement for T2- and T2*-weighted MRI. It should be mentioned that we selected this iron oxide phase owing to its magnetism (called superparamagnetism for NPs).They were synthetized by high temperature process, named thermal decomposition, with lipophilic ligands for *in situ* functionalization of their surface. Three times of reaction (2h, 4h and 6h) were performed to estimate its impact on magnetic properties of SPIONs (SPIONs 2h, SPIONs 4h and SPIONs 6h). This radiopaque and magnetic oil was subjected to spontaneous emulsification process which yields bimodal NEs with PEGylated surfactant for stealth properties. We chose to formulate NE for each batch of SPIONs (NE-SPIONs 2h, NE-SPIONs 4h and NE-SPIONs 6h) as follows: 0.28 wt.% of SPIONs, 23.72 wt.% of iodinated vitamin E, 16 wt.% of surfactant and 60 wt.% of aqueous phase. Once formulated into NE, magnetic properties were assessed and r2/r1 ratios were determined. Results demonstrated

that SPIONs 4h were the best candidate as CA for T2- and T2*-weighted MRI once formulated into NE because NE-SPIONs 4h exhibit highest value of ratio (r2/r1 = 16). It was assumed that such difference of magnetic property was due to differences of morphology and size distribution of SPIONs, TEM investigations elucidated these characteristics. SPIONs 4h were anisotrope whereas SPIONs 2h and 6h were spherical. In addition, their mean diameter was estimated between 5 and 10 nm whereas SPIONs 2h and 6h' ones were 5-7 nm and 7-10 nm. As to NEs, they were all similar in size distribution and around 60 nm (by DLS) with good monodispersity. *In vivo* bimodal imaging study was run on 5 Swiss mice. MRI showed a high accumulation of contrast agent in liver and kidneys (contrast in spleen is debatable owing to the heterogeneity aspect of this tissue by MRI). X-rays imaging allowed to visualize the liver and the spleen. Kidneys were not clearly detected indicating that NE assembly was damaged once it passed through kidneys filters: the iodinated part was excreted whereas SPIONs 4h remained in the tissues to provide MRI contrast. No adverse effects on animals were observed. This study was initially carried out to propose a novel bimodal contrast agent based on nanocarriers, and as the results confirmed, this novel probe was quite efficient for liver investigations. However, it provided also an insight of biodistribution and elimination route of NEs, thanks to such probe it seems that understanding pharmacokinetic profile of nanoparticles would be possible and easier thanks to bimodal imaging.

The schematic representation describes the proposed study:

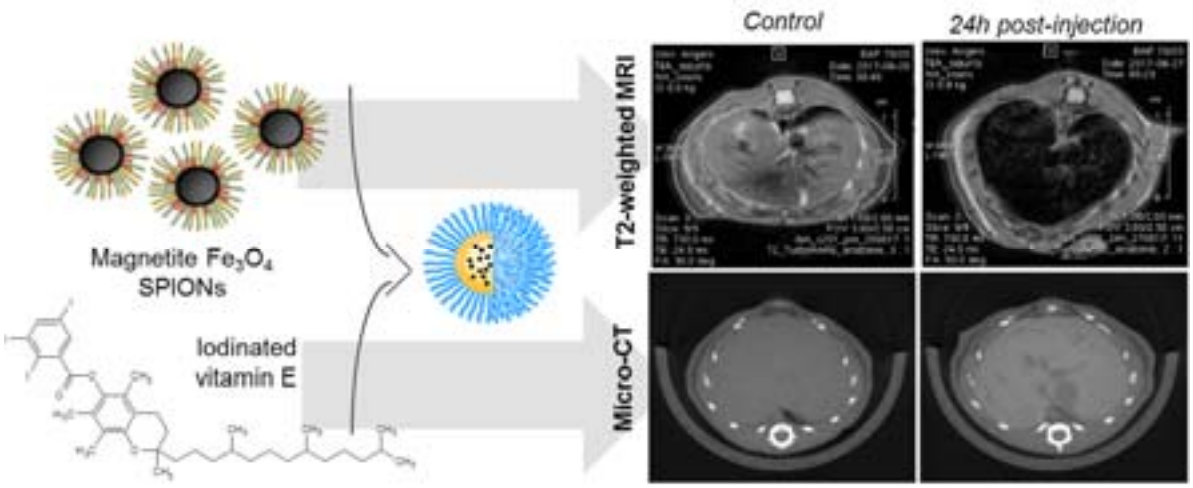

Chapter III.1 – Initiation to magnetite nanoparticles for *in vivo* uses

Justine Wallyn, Nicolas Anton, Thierry F. Vandamme

Université de Strasbourg, CNRS, CAMB UMR 7199, F-67000 Strasbourg, France

Abstract

The current nanotechnology era is marked by the emerging of various magnetic inorganic nanometer-sized colloidal particles. Those have been extensively applied and hold an immense potential in biomedical applications as, for examples, cancer therapy, drug nanocarriers (NCs), or in targeted delivery systems and diagnosis involving both two guided-nanoparticles (NPs) as nanoprobes and contrast agents. Considerable efforts have been devoted to design iron oxide NPs (IONPs) due to their superparamagnetic (SPM) behavior (SPM IONPs or SPIONs) and their large surface-to-volume area allowing to render them more biocompatible, stealth and easily bonded to natural biomolecules thanks to grafted ligands, selective-site moieties and/or organic and inorganic corona shells. Such nanomagnets with adjustable architecture have been the topic of significant progresses since modular designs enable SPIONs to carry out several functions simultaneously like a local drug delivery with a real-time monitoring and imaging of targeted area. Syntheses of SPIONs and adjustments of their physical and chemical properties have been achieved and paved novel routes for a safe use of those tailored magnetic ferrous nanomaterials. We will emphasis basic notion about NPs magnetism in order to have a better understanding of SPIONs assets for biomedical applications; we will mainly focus on magnetite iron oxide owing to its outstanding magnetic properties. Then, we will summarize general methods of preparation and typical characteristics of magnetite. Finally, major biomedical applications of magnetite will be introduced.

Keywords

Magnetite; nanoparticles; superparamagnetism; syntheses; characterizations; *in vivo* uses.

1. Introduction to magnetism: from particles to nanoparticles

Nowadays, it is well known that some particles and nanoparticles (NPs) exhibit magnetic properties. As a matter of fact, magnetism properties are not only related to the composition of nanomaterials but are also size-dependent. Thereby, particles and NPs possess their own

magnetism due to their size and will not similarly behave under a magnetic field. To explain why there are differences of behavior depends on the size of magnetic materials; microstructure of particles and NPs has to be briefly introduced.

In magnetic applications, particles with an average diameter up to 100 nm are generally called bulk material; whereas below this size, particles belong to the category of NPs. In the first case, bulks made of ferromagnetic, ferrimagnetic, or antiferromagnetic particles possess a microstructure composed of many magnetic domains called Weiss domains separated by walls named Bloch walls as shown in Figure 1A. Those domain walls aim to reduce magnetic stray energy. In every domain of the particle, a collective coupling of spins makes spins be collinear along one direction due to magnetic anisotropy energy.[1-3]

On the contrary, bulk is made of multi magnetic domains, typically inferior to 100 nm, where the magnetization is uniform in any of them but different from one domain to another one. At room temperature and under a zero magnetic field, all domains have their own spin alignment rendering the bulk material macroscopically non-magnetic or with a global magnetization near zero due to the balance of every Weiss domains' magnetism by their next neighbor domains (Figure 1A). However, an external magnetic field can induce wall movement - or in other words domains nucleation - in the case of a small magnetic field or, in the case of large magnetic field, make every spins from each single Weiss domain rotate away from their easy axis magnetization and be reoriented along an unique and same direction aiming to turn the bulk material into a magnet. This uniform and finite magnetization persists as long as the magnetic field is applied and stops right after its removal.[2-4] Temperature (T) has also an influence on magnetic particles behavior (Figure 1B). As previously mentioned, at room temperature and under a zero magnetic field, magnetic moments interact to align themselves in every magnetic domain. The influence of the interaction, called exchange interaction, can be offset by reaching Curie temperature (T_C) or Néel temperature (T_N), respectively for ferrimagnetic and ferromagnetic particles and for antiferromagnetic particles[5] causing spin disorder in every Weiss domain. At Curie and Néel temperatures, all single magnetic domains contain disoriented spins and cannot be then distinguished from each other. The bulk material seems at that characteristic temperature to be composed of one big single disordered domain which means a paramagnet (paramagnetism state) where the global magnetization is also balanced and near zero.[2]

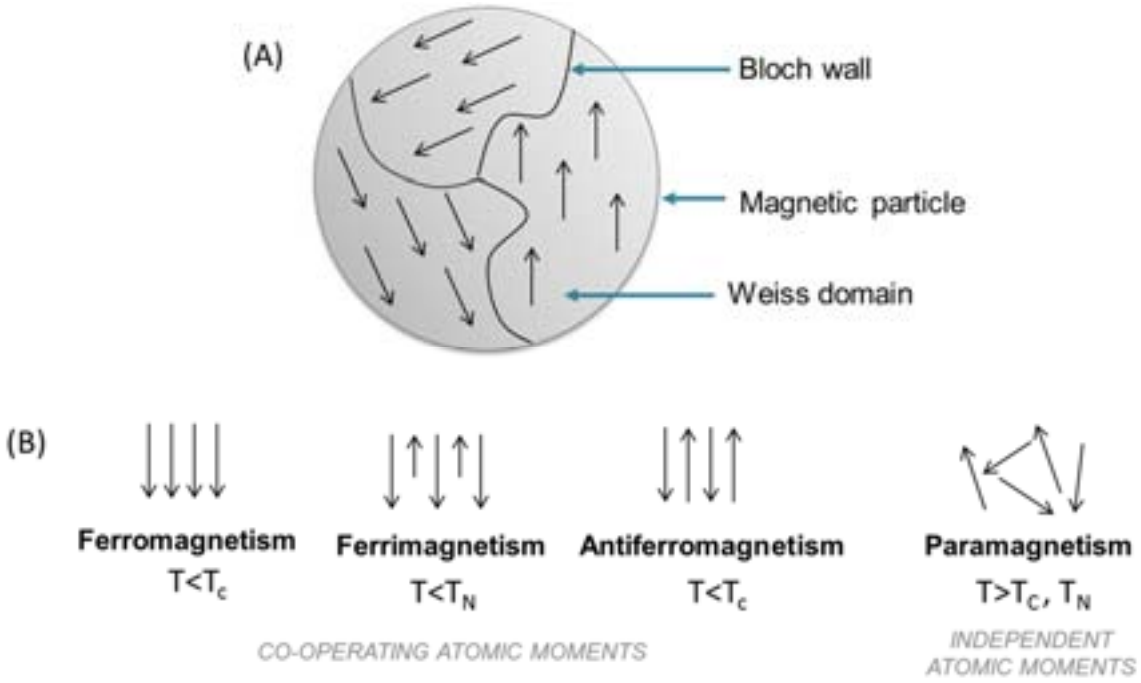

Figure 1: (A) Schematic representation of the internal structure of a ferromagnetic particle showing Weiss domains separated by Bloch walls. (B) Types of magnetism (Adapted from Ref. [5]).

Since magnetism is size-dependent, the particle size has to reach a low diameter, so called critical small diameter (D), to consider a particle as a single-domain particle *i.e.* a NP. The limit diameter is equal to:

$$D = \frac{18\sqrt{A.K_{eff}}}{\mu_0.M_s^2}$$

Where A is the exchange constant, K_{eff} is the effective anisotropy constant, M_s is the magnetic saturation and μ_0 is the vacuum permeability.[1,4]

NPs or single domain particles are generally smaller than 100 nm and saturated even in the absence of an external magnetic field in reason of their size comparable to a magnetic domain size. Above a specific temperature called the Blocking temperature, NPs exhibit a superparamagnetic (SPM) behavior like particles exhibiting paramagnetic behavior above Curie or Néel temperature. Such a change of the magnetic behavior is due to a spin reversal, on contrary to particles for which temperature causes spins disorder. A spin relaxation time (τ), corresponding to the time needed for spin reversal, is attributed to this phenomenon and is expressed by the Arrhenius formula from Néel-Brown theory[1,2,4,6]:

$$\tau = \tau_0.\exp.(\frac{K_{eff}.V}{k_B.T})$$

Where τ_0 is the expected time of spin reversal, K_{eff} is the anisotropy constant of the material, V is the NP volume, k_B is the Boltzmann constant and T is the temperature.

It should be pointed out that magnetic behavior of NPs has to be described, like for magnetic bulk, for well-defined conditions of experiment like temperature, magnetic field intensity and experimental time scale. If τ is shorter than experimental time scale (t), SPM property will be notified since magnetic moments will be reversed so many times that the magnetization of the NP will seem close to zero since all magnetization measured would cancel each other by summation. On the contrary, if τ is longer than the measure time, NPs' magnetism will be described in a blocked-state (and so characterized as ferromagnetic, ferrimagnetic or antiferromagnetic depends on the magnetic ordering "observed") since magnetic moments do not have enough time to rotate.

In many experiments, measurement time is constant but temperature is increased inducing a transition to SPM state. This temperature of transition, aforesaid under the name "blocking temperature", is thereby described as the temperature separating two magnetic regimes. To pass from blocked-state regime to SPM regime, the energy barrier ($K_{eff}.V$) has to be overcome or at least balanced by the thermal energy ($k_B.T$) ($k_B.T>K_{eff}.V$). Thus, the smaller the NP is, the easier thermal energy exceeds energy barrier at a low temperature. At this point, NP acts as a giant magnetic moment, generally called superparamagnet. That is why temperature can also induce state transition since above blocking temperature, the thermal energy is high enough to reverse spins, causes a decrease of magnetization and so that the transition from blocked-state to SPM regime. Such a change caused by thermal conditions is approximately similar to magnetic particle becoming a paramagnet, but in the precise case of a nanoscale magnet, a NP becomes a superparamagnet thanks to a collective movement of spins and not a fuzzy spins disorder like it commonly occurs in particles.[1,2,4,6]

The Figure 2 displays schematic magnetic regime transition from blocked-state to superparamagnetism along with variation of temperature or impact of measuring scale t.

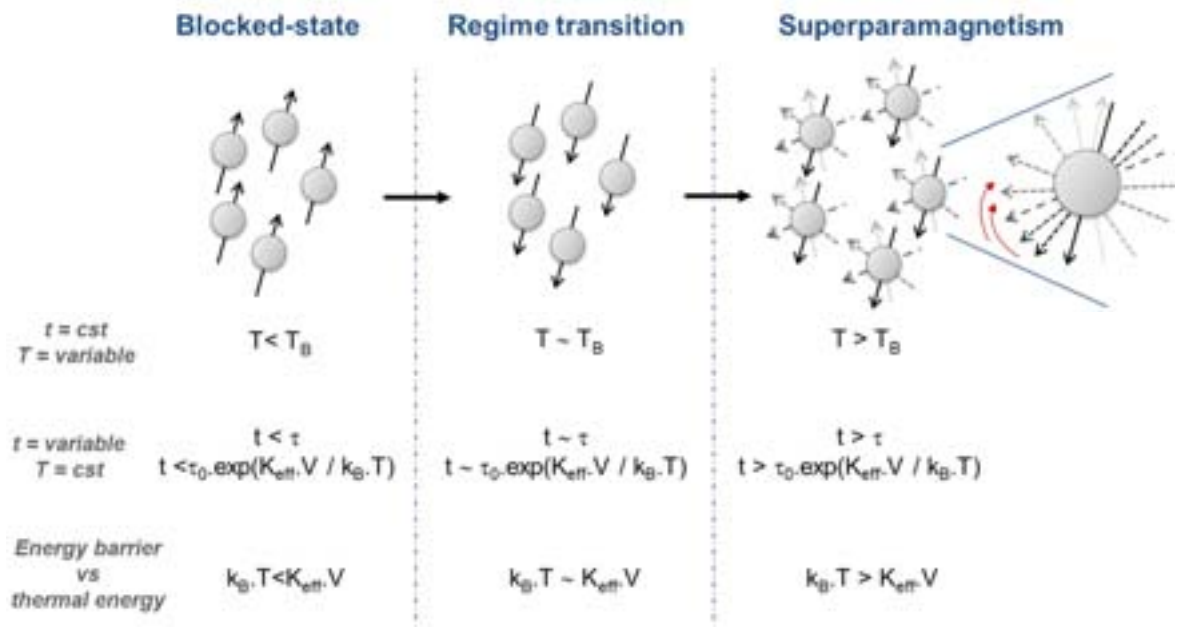

Figure 2: Magnetic state transition from blocked-state to superparamagnetism of a single-domain NP depending on time of measurement and temperature conditions under zero magnetic field.

Differences between bulks and NPs can be more extended to others magnetic notions like the coercivity. The latter magnetic term is basically defined as the intensity of the magnetic field required to reduce magnetization to zero. Generally spin reversal for NP transition from blocked-state to SPM regimes requires more energy than domains nucleation for magnetic transition of bulk material. Therefore getting NPs magnetism back to a stable magnetic regime, referring to the blocked-state, implies higher coercivity than particles need for its own transition back to a stable magnetic state.[2] To keep bringing to light some nanomagnetism notions, a rigorous approach will then present hysteresis loops. This second magnetic notion is currently qualified as the magnetization cycle or the magnetic response of magnetic materials under a magnetic field. Lots of information about magnetic properties of a material can be learned by studying its hysteresis cycle. It is mostly described by monitoring the variation of degree of magnetization (B) with the intensity of magnetic field (H), commonly referred as B-H loop. Such a curve is obtained thanks to the "memory" of the magnetic material. In other words, magnetic particles can retain a memory of an applied field once it is removed. The shape of loops is size-dependent. The presence of several Weiss domains in particles induces hysteresis because all magnetic domains do not return to their original magnetization because they all respond to a force, the magnetic field, depends on their own history with that force. For particles small enough to be single domain but not small enough to be NPs, there are broader hysteresis loops because more energy is required to make spin

reversal than walls move occurring in multi-domain particles under a magnetic field (Figure 3A). In case of NPs, there is an antihysteretic B-H curve as sigmoidal curve fashion (Figure 3B).[6]

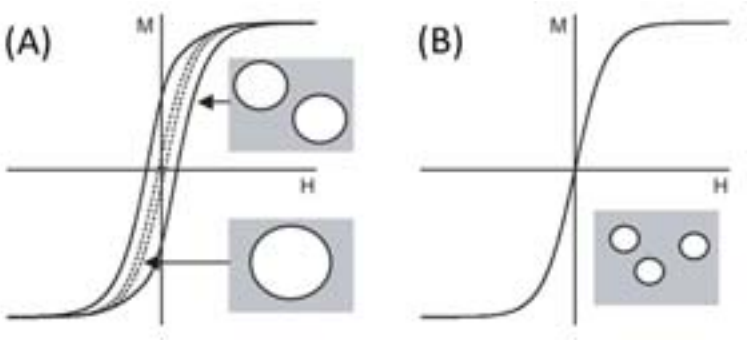

Figure 3: Magnetic responses of (A) ferromagnetic particles with a range of sizes from micron scale (multi-domain) to nanometric scale (single-domain particles) and (B) SPM NPs (single-domain) (Adapted from Ref. [6]).

Once more, the temperature can have significant impact on material magnetism and be observed on hysteresis loops. An example of typical NPs hysteresis loops is shown in Figure 4 representing two trials of hysteresis cycle of 4.3 nm and 6.0 nm magnetite SPIONs at 5K and 300K. Thanks to those curves, the dependence of hysteresis loops to the size of a magnetic material and the temperature can be clearly highlighted.

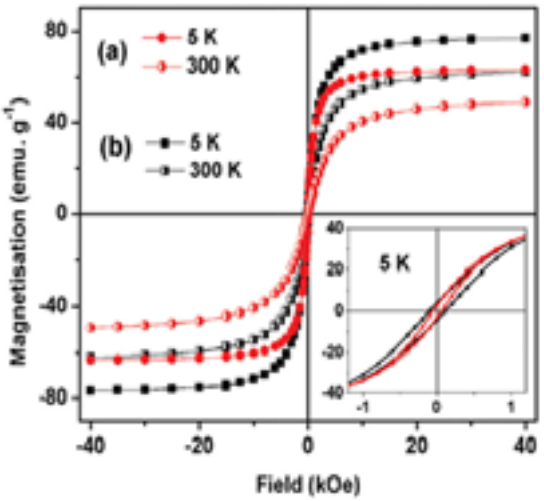

Figure 4: Example of hysteresis loops of (a) 4.3 nm and (b) 6.0 nm magnetite NPs at 5K and 300K. [7]

Main characteristics of hysteresis loops can be pointed out in Figure 5. In Figure 5, starting from a zero magnetic field (point "a") and then applying a high external magnetic force (H), magnetization of magnetic material reaches a maximum called the magnetic saturation (point

"b") and levels off. The material is magnetically saturated because all spins are aligned. When H is reduced to zero (from "b" to "c") and then increased in negative direction (from "c" to "d"), magnetization drops to zero at the point "d". At the point "c", the degree of magnetization B is higher than zero since the material has been disturbed by the magnetizing force and keeps a memory of it. This latter point materializes the magnetic retentivity of the material corresponding to the magnetic flux remaining within the material when H has been reduced to zero. The coercivity (point "d") corresponds to the force needed to remove the magnetic remanence, which means reducing B to zero or, like shown on the graph from "c" to "d". To reach the coercivity (point "d"), the reversed magnetizing force has to flip enough to reduce the degree of magnetization close to zero. If the magnetizing force H keeps decreasing in negative direction, material will be once more saturated but with an opposite magnetic saturation (point "e"). From "e" to "b", H is increased back in positive direction until the magnetization of the material moves up again to the positive magnetic saturation and makes the material complete its hysteresis cycle. However, the curve will take a different way and will not cross the point "a" or the origin of the graph to reach again "b" owing to a residual magnetization in the material (point "f"). This is referred again to a residual magnetism in the material. Consequently, to go from "f" to "b", B will firstly reach point "g", strictly opposed to the coercivity point, before filling its hysteresis loop in point "b".

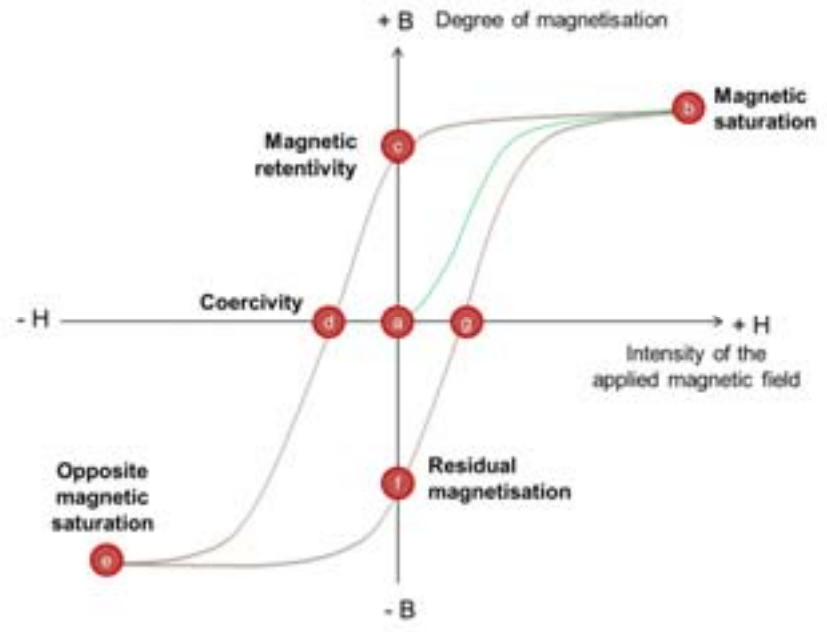

Figure 5: Typical hysteresis loop of a magnetic material.

Magnetic NPs currently attract scientists owing to their fascinating properties and magnetic tunability. First reported work using magnetic NPs was published during seventies and was about *in vitro* magnetic separation of enzymes by Robinson *et al.*[8]. Over next decades, applications have been extended to *in vivo*. As the hereinafter section of this work will show, it has already been reported that magnetic nanometer materials are quite useful for *in vivo* applications as nanocarriers (NCs) and nanoprobes.[9,10] NCs and nanoprobes, so-called nanoplatforms, are the design of liposomes, polymeric NPs, micelles, inorganic materials of 1–100 nm in diameter corresponding to delivery systems and/or targeted systems. In the case of magnetic nanomaterials, this growing interest is not only due to their magnetic properties but also in reason to their nanosize providing thus a high surface-to-volume ratio, and consequently an increase chemical reactivity, and a quantum confinement effects exerting size-dependent properties like magnetism.[11,12]

2. Nanoscale magnetic material for biomedical applications: current trends and requirements

Since few past decades, there is an important development of magnetic NPs in biomedical fields, like for diagnosis and therapy. The general term magnetic NPs takes account structures composed of different metallic elements (iron, cobalt, nickel, platinum…), or bimetallic and metal alloys NPs. Iron may be classified separately because of its use in biomedicine as iron NPs and as iron oxide or bimetallic SPIONs. SPIONs play nowadays an important role in nanomedicine fields like in magnetic resonance imaging (MRI) for non-invasive diagnostic purpose. Owing to the combination of magnetism properties with nanometer scale, magnetic NPs compose a very attractive material for biomedical and technological applications.[13] They play an important role in healthcare needs because of their ability to function at cells-scale level. Due to a small controllable size and shape, magnetic NPs are comparable to biological entities and are able to easily interact with those entities or to “get close” to them.[6] Indeed, the range of sizes of NPs can be near the sizes of virus (20–450 nm), proteins (5-50 nm) and cells (10-100 μm), depending on the methods of preparations and promote the uptake by cells.[6,14]

In this way, magnetic NPs have already been involved into various biomedical applications like dental applications[15], illnesses local treatment like neurological diseases[16] and cardiovascular diseases[13] for instance. As many reviews reported[2,6,12], magnetic nanomaterials are also applied for magnetic separation of cells labelled by

biological entities like proteins[17], in bio-imaging as a MRI contrast agent since being exposed to a magnetic field has not been contraindicated for living beings (except for patients bearing magnetizable medical devices)[18], for hyperthermia cancer therapy[19] and targeted drug or gene releases.[20] Regarding to targeting strategies, it should be mentioned that the interests of local treatments lie on the facts that targeting a specific site *via* NPs-based biomarkers[21], like a group of tumor cells, can reduce side effects and avoid the attack of regular cells by the treatment, even more the dosage can also be cut down since the cytotoxic treatment will not be uptake by healthy cells.[13,19] It must be mentioned that most of applications, and even those introduced, require iron-based NPs, like SPIONs. Investigations about magnetic iron-based NPs, mostly magnetite and maghemite, have been achieved since they have been assimilated to promising candidates for biological applications.[22] This kind of metallic NPs, especially SPIONs, will be deeply introduced in next parts of this study.

Although magnetic NPs seem quite useful for plenty of *in vivo* applications, the recognition by the immune system and an eventual unfavorable biodistribution constitute their main disadvantages. First of all, they are composed of elements different from those composing natural organic biomolecules provoking a spontaneous immune system response. Consequently a lack of furtive property leads to a fast excretion from the blood stream, a decrease of stability in physiological media and also a risk of toxicity on the patients because of metabolites. It should be pointed out that involving magnetic NPs into therapeutic treatments requires to know the half-life time in plasma and final biodistribution of NPs and their metabolites for an efficient and safer use.[18] Second of all, the nanometer size promotes their penetration through tissues or capillaries and sometimes causes extravasation issues after intravenous injection. Extravasation issues are quite frequent in cancerous tissues because tumor tissues possess a vascular system with an heterogeneous morphology. Current cancer treatments are based on NPs innovation offering real-time imaging and local drugs release (NCs and nanoprobes). Since while, magnetic NPs used as drug NCs have been qualified “theranostic” or “nanotheranostic” meaning therapeutic and diagnostic in reason to the possibility to encapsulate guest bioactive compounds, to protect them and to gradually release them to targeted sites by guided-NPs. So, in case of theranostic magnetic NPs for cancer treatment, extravasation issues in tumor tissue may occur even more easily than in regular tissues and may generate a decrease of the theranostic nanomaterial rate within the sick area.[2,23–25] To know the fate of magnetic materials *in vivo*, a well understanding of pharmacokinetic mechanisms related to NPs is required. Basically, the mechanism of

distribution-metabolization-excretion after the exposure corresponds to a renal clearance process (filtration) of the invading NPs from the blood compartment. In case of hydrosoluble and small NPs, the excretion will be the next step whereas lipophilic compounds and/or bigger NPs will be metabolized by others organs because of their ability to bypass renal filtration.[13] A sequestration in organs or tissues belonging to the reticuloendothelial system (RES) (like the liver, the spleen, the bone marrow or lymph nodes) where biotransformation mechanism occurs (opsonization, phagocytosis, endocytosis) is so far necessary to get hydrosoluble metabolites which will then be excreted like other water-soluble substances. The typical biodistribution few minutes after a NPs blood stream cleaning up is 90 % in the liver, 2 % in the spleen and 8 % in the bone marrow[18], but that remains highly dependent to the NP size.[25] Many other factors enable to affect the behavior in physiological media and the biodistribution of NPs have to be managed to prevent NPs from fast excretion and to be distributed to targeted zones. Those factors are mostly, as aforementioned, the size, the composition, the morphology and the surface chemistry (charge, moieties, shells…) but recent achievements allow to obtain magnetic NPs possessing a tunable surface which makes them be inconspicuous regarding to immune system and be associated to an effective and non-toxic biomedical magnetic NPs platform.[13]

To obtain nanomagnets for biological uses, researchers have focused their efforts on the functionalization of magnetic NPs surface to render them stealth and stable in physiological media. It has been reported that NPs can be functionalized on their surfaces by lots of chemical surface modifications involving some biocompatible molecules like polymers, hydrophilic molecules or silica layer for example.[6,25] Working on magnetic NPs surface charges has also been studied in order to facilitate the interaction or adherence of those nanoprobes onto cellular membranes, which are generally negatively charged.[14] In this way, NPs can be coated to form core-shell nanostructures, functionalized or embedded in a matrix for targeting applications and having stealth properties. Such strategies could mislead immune system, postpone metabolism stage, and so far enhance magnetic NPs retention within blood stream which constitutes an asset for all theranostic applications.

Therefore, the design of magnetic nanocrystals for biomedical applications needs to be well controlled in order to get specific properties dictating magnetic NPs' fate *in vivo*. Otherwise an injection of magnetic NPs for biomedical purposes will be useless if their blood circulation time is not extended enough to let NPs do what they are injected for. In addition, fundamental magnetic properties have to be clear and optimized to be controlled depending

on conditions of applications.[26] In other words, syntheses of nanoscale magnets coated by organic or inorganic shells, bearing ligands capable of bonding to specific receptors, having a specific narrow range of size and a high degree of biocompatibility have to be fully mastered.[18,25] Magnetic NPs should also exhibit high uptake efficiency in a case of targeting strategy, not to be subject to aggregation to prevent from vessel embolism or get structural damage after being exposed to *in vivo* environment.[27,28] Even if this review is mainly focused on magnetic NPs, it has to be precise that other NPs, like polymers, liposomes, ceramics, dendrimers and many others, have also to fulfil those specific requirements prior to envisage *in vivo* translation.[21]

3. Magnetic iron oxide nanoparticles

3.1. Three main iron oxide nanoparticles

As it has already been reported in this dissertation, metallic ferrous NPs belong to the kind of NPs the most widely applied in therapeutics, diagnosis and real-time imaging domains. Metallic ferrous NPs referred in literature are generally based on three main iron oxides. Basically those are hematite (α-Fe_2O_3), maghemite (γ-Fe_2O_3) and magnetite (Fe_3O_4 or $FeO.Fe_2O_3$); they are the most common in nature and mainly found in soil and rocks from volcanic eruptions and also from air pollution (emissions from traffic and industries).[5,29,30]

Categories related to their size allow to classify them from micrometer-sized (300 nm-3.5 µm) to standard (50-150 nm) and to ultra-small (<50 nm) iron oxide crystals. Such a classification is useful to identify general advantages and disadvantages that we would have to deal with if we are confronted to SPIONs. For example, for *in vivo* purpose, NPs biodistribution is size-dependent and NPs must have an optimal average diameter to avoid sequestration (occurring with micrometer-sized iron oxides) or an early renal clearance (occurring with ultra-small iron oxides) which correspond to the diameter of NPs belonging to the second class, standard iron oxide nanocrystals.[11,13,21,30] Those should be able to remain within blood stream over an extended period of time to promote local accumulation and avoid vessel embolizations. Owing to a specific biodistribution for each category of iron oxide nanocrystals, *in vivo* applications are size-dependent. For example, standard and ultra-small SPIONs have respectively been used as contrast agents for the diagnosis of liver diseases in reason to the easy uptake or passive targeting of liver cells (Kupffer cells) and for blood-pool and lymph-node imaging.[21,25]

Iron oxides vary significantly in color (Table 1) which can help for their identification. They also differ on their oxidation state or oxidation number and so their composition, their crystallographic structures and their magnetic properties. Hematite α-Fe_2O_3 is the oldest iron oxide known; it is kinetically and thermodynamically stable. Maghemite γ-Fe_2O_3 is on the contrary only kinetically stable, which means metastable, and turns slowly into a stable iron oxide form (hematite) leading to a drastic drop of magnetization. Hematite and maghemite vary from red, brown to grey depends on α or γ Fe_2O_3 ($Fe^{(3+)}{}_2O^{(2-)}{}_3$) polymorph. Magnetite Fe_3O_4 or FeO. Fe_2O_3 is the black iron oxide, commonly called Hercule stone, presenting the strongest magnetic behavior. It is composed of iron(II) and iron(III) and belongs to the category of mixed-oxide ($Fe^{(+2)}Fe^{(3+)}{}_2O^{(2-)}{}_4$ or $Fe^{(2+)}O^{(2-)}.Fe^{(3+)}{}_2O^{(2-)}{}_3$). Mixed-valent magnetite is so far considered in the literature as a charge frustrated iron oxide due to the distribution of both iron(II) and (III) in crystallographic sublattice sites.[5,29,31]

Table 1: Chemical formula and color of main iron oxides (Adapted from Ref. [29]).

Iron oxide	Chemical formula (Current name)	Color
Ferrous oxide (iron(II) oxides)	FeO (Wüstite)	Black
Mixed-oxide (iron(II, III) oxides)	Fe_3O_4 ou $FeO.Fe_2O_3$ (Magnetite)	Black
Ferric oxides (iron(III) oxides)	α-Fe_2O_3 (Hematite) β-Fe_2O_3 γ-Fe_2O_3 (Maghemite) ε-Fe_2O_3	Grey, brown, red

As shown in Table 1, magnetite is one of the black iron oxide, wüstite is also a jet black color iron oxide but it is a quite rare type of iron oxide. In this way, even though color may help to distinguish one iron oxide to another one, it is certainly better to compare magnetic properties. As presented in Table 2, magnetic property is clearly size-dependent since magnetite and maghemite exhibit both at room temperature superparamagnetism below 6 nm and 10 nm, respectively. Above those dimensions, they are in magnetic blocked-state which means that the magnetic ordering at room temperature is the one followed at the particle scale. In this way, magnetite (≥ 6 nm) and hematite are both ferromagnetic whereas maghemite (≥ 10 nm) is ferrimagnetic. Contrary to the other two iron oxide types, hematite does not show SPM ordering below a tens of nanometer at room temperature but it is able to change of magnetic ordering to antiferromagnetic below the so-called Morin temperature (~ 260 K). This change of magnetic ordering can be suppressed by a decrease of crystallinity and/or of size NP (≤ 10-20 nm). Regardless Morin transition, it is possible to recognize ferromagnetic hematite to ferromagnetic magnetite despite of their similar magnetic ordering since

magnetite exhibits the highest magnetic saturation (300 times higher than hematite saturation).[5]

Table 2: Magnetic properties of iron oxides particles and NPs (Adapted from Ref. [5]).

Iron oxide	**Hematite**	**Maghemite**		**Magnetite**	
Magnetic saturation	0,3 A.m²/kg	60-80 A.m²/kg		92-100 A.m²/kg	
Curie Transition	~ 1000 K	~ 820-980 K		~ 850 K	
Grain size	-	≥ 10 nm	≤ 10 nm	≥ 6 nm	≤ 6 nm
Magnetism ordering at room temperature	Ferromagnetic	Ferrimagnetic	SPM	Ferromagnetic	SPM

Applications of this group of metallic iron oxide-based nanocrystals can vary quite significantly and are extended ranging from nanomedicine, as many reviews reported by Laurent *et al.* [32] or Mahmoudi *et al.*[24], to catalysis disciplines as showed Schüle *et al.*[33] performing styrene synthesis over iron oxide catalysis or even to water-detoxification presented by Girginova *et al.*[34] using a ferrofluid of silica coated magnetite NPs for mercury removal from water. To the best of our knowledge, interest on iron oxide nanocrystals in biomedical fields started a few decades ago and keeps growing as a very interesting approach. Consequently, significant progresses have been made to figure out advantages and drawbacks of SPIONs for *in vivo* uses. However, even though they belong to the group of magnetic nanomaterials, they possess among other qualities making them apart from random magnetic nanostructures. Indeed, in addition of being nanoscale materials which confer the ability of getting close to biological entities and enhances interaction with them because of a high surface-to-volume ratio, SPIONs possess the asset of being non-toxic and easily controllable by an external magnetic field and so far highly suitable for *in vivo* magnetically-driven treatment.[6] For instance, tumors are treated by hyperthermia process based on the use of magnetic NPs driven by an external magnetic field and then accumulated in injured tissues. Magnetic stimulation would cause an increase in NPs temperature up to 42°C leading to the death of tumor cells by cells necrosis after several minutes of exposure to a radiofrequency magnetic field. Damage of regular tissues, generally occurring as a side effect in cancer treatment, located near injured cells would not happen by applying such therapy in reason to their natural resistance to heat.[2,6]

Main requirements, when magnetic NPs are employed in biomedical applications, are to use SPM nanostructures exhibiting the highest magnetic saturation and so far the less toxic

components. These two requirements constitute arguments that make scientists think SPIONs are more promising for *in vivo* applications than other magnetic materials. It should be remembered that superparamagnetism is size-dependent and can be enhanced by an increase of NP size (without reaching multi-domain nanostructure). Despite of a probable improvement in magnetism by using bigger SPM NPs, it appears to be contraindicated to employ too large magnetic nanostructures to ensure a well diffusion of SPIONs through a limited size access area in human body.[1,4,19] As a result, it seems quite clear that working on SPIONs is a dilemma because a balance between the biodistribution and the magnetic properties has to be found out for *in vivo* experiments. In this way, and like for all kinds of nanoscale magnets, researchers have been developing plenty of methods for SPIONs synthesis allowing to have an accurate control on the size of the produced NPs.

3.2. The need of surface functionalization and stabilization of iron oxide nanoparticles

However, even though dimensions of produced NPs constitute an important parameter to manage, it appears in the literature that iron oxide nanocrystals get a coating corona or ligands layers not only to be turned into more biocompatible and stealth nanoscale material but also to be capable of being selectively attached to specific biological entities, to be well-dispersed or solubilized and to be protected from conditions of the media where they are dispersed (oxidation and erosion by acids or bases[1]). Indeed, magnetite is easily oxidized to maghemite in ambient conditions and requires a corona protection to remain into the magnetite phase. It turns out that several core-shell or -ligands layer constructs have already widely been described in literature and are mainly based on organic and/or inorganic stabilizing agents. For instance, Liu *et al.*[35] have been achieved a study indicating that surface modification could lead to a better NPs stability, enhancement of their biodistribution and a long blood circulation time due to a proper balance between hydrophilic/lipophilic and stealth properties of outer layer capping the nanomaterial. It has been reported that polyethoxylated amphiphilic compounds are very often used because of their anti-fouling nature and their ability to bypass natural barriers. Gold or silica outer layers represent as well an interesting alternative to get pH-sensitive properties, to enhance hydrophilic properties or to provide easy tailorable surface to graft bioactive materials for targeting.[5,11,25,32]

Moreover, iron oxide nanocrystals have a high surface-to-volume ratio and thereby a strong tendency to aggregation leading to the formation of clusters which is quite contraindicated for all biomedical disciplines. Thus, NPs stability needs to be controlled.

Derjaguin, Landau, Verwey and Overbeek have long time ago proposed a theory (DLVO theory) about colloids stability and brought the idea that stability of particles dispersed in solution was relative to electrostatic repulsion and Van Der Waals attraction. However, taking account the nanosize and magnetic properties, four forces eventually render iron oxides NPs stable or unstable in suspension: as mentioned (i) electrostatic repulsion and (ii) Van Der Waals attraction; and (iii) magnetic dipolar force and (iv) steric repulsion.[24,32] Attractive Van Der Waals forces are mostly the cause of aggregation of NPs because clusters have a lower interfacial energy compared to NPs due to a smaller total area. As it has been implied, the surface charge is also involved into the colloidal stability of iron oxides. Even though positively charged NPs hold a good potential for interacting with negatively charged natural entities, it does not correspond to a selective sticking and it could occasionally render particles unstable in aqueous physiological environment owing to potential neutralization by electrolytes existing in blood. Neutral surface is therefore the most promising surface state to minimize nonspecific binding and to avoid a stability lack. Zeta potential value (or also Debye-Huckel length related to screening-charges layer surrounding water-dispersed colloids) is consequently an important parameter to check when NPs are designed for being stable in physiological environment and could predict their stability in similar conditions of pH and temperature. Steric repulsions can also play a significant role as a stability factor since the attachment of molecules/ligands onto surfaces can lead to NPs repulsions. *In situ* or post synthesis polymeric coating (chitosan, polyvinyl alcohol, alginate, dextran, polyethylene glycol[32,36]) provides so steric barrier in reason to the polymer conformation and its chain length, but others criterion can alter its stabilization effects (biodegradation, weak bonding, ability to cover NPs surface…). However, none quantitative values can predict how grafted polymers would dictate SPIONs stability. To bring few more details about post-synthesis treatment, other route than *in situ* functionalization may be applied to adjust specific surface feature. Ligand exchange method with biocompatible ligands has been reported as an approach to overcome iron oxide surface failure. Although, most of iron oxide syntheses achieved the preparation of hydrophilic materials, a need of more tunable surface may lead to an exchange capping layer.[11] In this way, to prevent SPIONs from a loss of physical and chemical stability, two types of modification strategies have widely been explored in order to preserve iron oxides from the impacts of the external and *in vivo* medias.[13,24,32,37]

However, it has to be mentioned that a coating strategy provides a core-shell structure and provokes consequently an enlargement of final magnetic nanostructure. Hopefully, this

change is generally about few nanometers which cannot be considered as a problem for being driven through limited size access area. What is more, a core-shell structure can confer novel and specific physical and chemical properties to SPIONs thanks to further functionalization which can be done on the corona layer. This approach would provide high effective NPs or nanobiomarkers[21] for selected biological entities. For example, thanks to an approach of surface functionalization, accumulation of SPIONs within a target tissues, like cancer cells, is currently a prominent topic for hyperthermia cancer therapy.[19,37] Such specific and local accumulation in injured cells mostly occurs because a targeting strategy, so called active targeting, has been applied. Injured tissues generally constituted of abnormal vascular structures are subject to extravasation as previously pointed out but also to a phenomenon of high permeation and retention, referring to the enhance permeability and retention effect (EPR). This effect renders abnormal tissues be able to uptake and accumulate more easily nanoscale entities like NPs and provides thereby a passive targeting. Passive targeting cannot prevent from accumulation within regular cells which may leads to cytotoxic side effect on them. On the contrary, active targeting can avoid a non-selective accumulation and so the damage of some regular tissues.[13]

3.3. Effect of iron oxide design on magnetism

Nevertheless, applying surface modifications strategy can impact the magnetic behavior, which implies a small enhancement or a decrease depends on the outer layer composition.[1,25] When surface modifications refer to the coordination of organic ligands, it has been shown that their adsorption onto magnetic NPs can influence magnetic saturation. As Daou *et al.*[38] have proposed in their work about magnetite NPs, the nature of a coupling agent of grafted ligands would not have the same impact on the SPIONs spins. Even more, physorption or chimisorption would also differently impact spin orientation. For example, the chimisorption of phosphonate coupling agent do not affect spins at all whereas the physisorption of carboxylate ligands enable modify the colinearity of spins along the boundaries of the single magnetic domain. This latter phenomenon is known as the spin canting effect and can make a core-shell material be assimilated to a $(\text{core-shell})_a\text{-shell}_b$. Indeed, the existence of a coating corona or adsorbed-ligands (shell_b) causes a non collinear arrangement of spins along the core's boundaries (shell_a), due to interactions between spins from shell_a and shell_b, compared to collinear arrangement within the deep core (core_a). Consequently, the initial core is not anymore magnetically uniform regarding to its boundaries and its deep structure, that is why it can be associated to an inner core-shell

structure ((core-shell)$_a$).[39] Moreover, the crystal morphology of magnetite nanocrystal could also affect its magnetic behavior and provokes an increase in coercivity from spherical and cubic shapes to an octahedral shape indicating an enhancement of magnetism following this series of morphologies. Like the size, magnetic crystal morphology can be controlled with synthesis conditions.[5,40]

Synthetic conditions may influence magnetic properties because of structure may be different from one method to another one and also because of the potential presence of dead magnetic layer like (shell$_a$). Regarding to the size of the iron oxide particles, which is directly related to the synthetic pathway, magnetic saturation may differ from NPs to bulk materials. For magnetite iron oxide, a decrease of 2 or 3 fold can be observed for the magnetic saturation from bulk to NPs. Such difference results in surface curvature of NPs. The smaller the particle is, the more the crystal orientation will be disordered.[22] The effect of disorder in the crystal orientation can be also observed between magnetite and maghemite. Indeed, maghemite is a less symmetric crystal than magnetite which leads to a decrease of magnetism (as shown in Table 2).

3.4. What about the consequence after in vivo injection of iron oxide nanoparticles?

For real-time biomedical imaging, referring to MRI, the involvement of SPIONs needs some requirements. Indeed, the NP size impacts a lot on the contrast, and that impacts the quantity which needs to be injected to patients and the ability of human body to excrete the substance.[25] It should be mentioned that nanoparticulate contrast agents are basically composed of three main parts: i) a signal enhancement core, ii) a biocompatible and iii) furtive shell and grafted functional chains onto the core-shell nanostructure for targeting purpose. Most of iron oxides NPs are excreted by the liver, due to a selective uptake by Kupffer cells composing the tissue of this organ. The spleen, the kidneys and the bone marrow are also involved into the metabolism procedure of NPs, as mentioned above with RES. Owing to a fast uptake, a fast excretion from human body rapidly occurs which lets short period for SPIONs to carry out what they are injected for. For instance, such a rapid metabolic response can consequently induce a lack of accuracy in diagnosis in a case of real-time imaging. Such an excretion process, commonly referred to opsonization process leading to recognition and clearance mechanism performed by RES, is actually compromising for any kind of NPs but as mentioned above several factors (size, morphology, surface state…) can be controlled to overcome that fast excretion issue.[13]

When iron oxide crystalline forms are used for *in vivo* applications, human body is able to metabolize them into iron ions and uses the iron released for biological process like for red blood cell.[11,30] However, NPs should not be subject to unexpected iron release leading to an increase of iron quantity that would be added to the quantity already existing in the blood stream and causing an overload of iron.[28] Such an unbalanced iron homeostasis could provoke cellular response. Although employing SPIONs seems so far to be quite safe due to all significant progresses made to adjust them or to make them fit for *in vivo* applications, an exposure to a high dose can induce potential cytotoxicity, impair the functions of some major entities involved into human biological system, like DNA and mitochondria, and causes mild and short duration side effects (nausea, urticarial, diarrhea). Considerable efforts have been devoted to design SPIONs possessing physico-chemical characteristics and to produce very low toxic nanostructures. But, it seems still important to carry out a follow-up of human body response in order to prevent the toxicity related to break-down products and the potential interactions between metabolites and tissues where SPIONs are accumulated.[30] In other words, a complete stability study in physiological conditions of iron oxides NPs should be performed for any new designs. Also, this concerns consequently functionalized core-shell structures because the involvement of biocompatible polymers, organic or inorganic shells like silica which require a toxicity study in reason to current debates about those compounds and their effects on health.[11]

Consequently, it is challenging to produce desired SPIONs exhibiting optimal morphological dimensions, good magnetism behavior, high stability and dispersibility to form a biocompatible colloidal suspension in a physiological environment. Those characteristics are certainly parameters which have to be fully controlled and some others might have to be deeply investigated, like the toxicity. However, magnetism remains also an important parameter. Indeed, to remind that SPIONs magnetism can easily be altered it should briefly be reminded how it can be affected: It is quite dependent to (i) the composition and consequently (ii) the crystallographic structure (magnetite, maghemite and hematite), (iii) the particle size (single domain or multi-domains) and (iv) the surface state (coating or ligands).

Among all iron oxide nanomaterials, maghemite and magnetite are very popular and promising nanocrystals in biomedical disciplines.[37] Besides, the Table 2 inventorying magnetic saturation indicates that magnetite is the most magnetic type of iron oxide. It appears that it corresponds also to the iron oxide the most sensitive to oxidation[5] and inevitably needs a protective capping layer. Yet, magnetite seems increasingly attractive due

to its large magnetism and the huge development of functionalization after an adapted chemistry of surface.

4. Preparation of magnetite

4.1. Formation of iron oxide nanoparticles

As it has been widely aforementioned, the design is a key parameter for *in vivo* applications and to govern the *in vivo* fate of SPIONs. Biomedical disciplines require indeed high quality magnetic NPs; *i.e* narrow size distribution, stability in physiological environment (weak aggregation tendency, no premature degradation and release of material, stealth surface properties), biocompatible components, specific accumulation by vectorization or simple passive targeting, etc. and that regardless magnetic properties. Most of these features can be adjusted during NPs formation thanks to appropriate conditions of synthesis. Typically, SPIONs like magnetite are produced *via* a two-steps mechanism by homogeneous precipitation, *i.e.*, single liquid phase process. This two-steps mechanism was proposed by LaMer et *al.*[41] and was completed by other authors like Ng et *al.*[42]. However, yielding monodisperse NPs is actually related to several parameters, main conditions to control are the concentration of precursor involved into the reaction, the amount and the nature of ligands, and the temperature. Gathering optimum conditions lead to the formation of SPIONs as described in Figure 7. Basically, it begins with the supersaturation of the solution in solute, this phenomenon can be done by a high increase in solute concentration thanks to their solubilization in the reaction media and/or an increase in temperature. This leads to a fast second step of nucleation corresponding to a burst nucleation and providing tiny crystalline nuclei. Nucleation is an endothermic process due to the splitting bonding of reactants, desorption of solvent shell from compounds and so counteracting surface tension consuming energy. Afterward, an exothermic step follows and is assimilated to nuclei growth (third step) where those grains grow by diffusion of solute from the solution towards the grain surface. Such step is actually energetically favorable since it reduces the surface-to-volume ratio of particles. Growth step can be kept under control since surfaces of iron oxide grains are generally covered by surfactant, organic ligands or other electrostatic or steric stabilizers preventing polydispersity issue from happening. To sum-up, monodisperse NPs can then be obtained by a high initial supersaturation level forcing the system to incorporate solute to growing nuclei. Besides, clusters, aggregates or bigger NPs might be formed in case of

uncontrolled reaction conditions, in some case Ostwald ripening may occur and can then be assimilated to another step of nucleation (fourth step).[4,12,24,32,36,43]

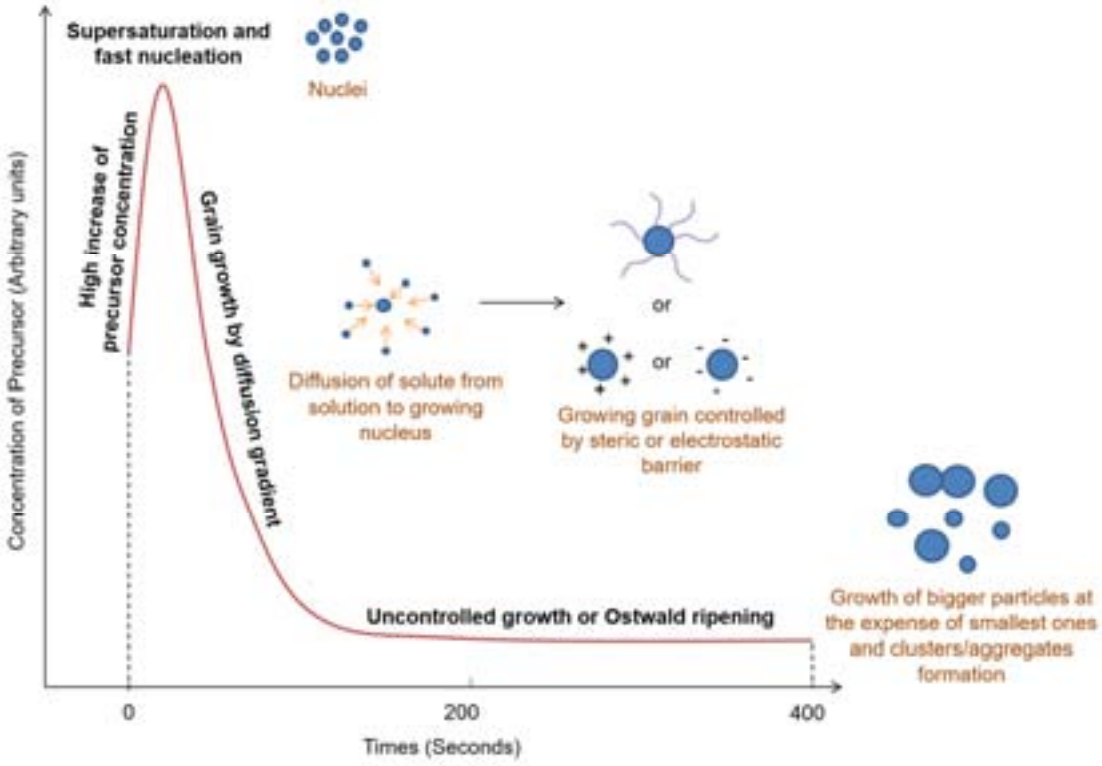

Figure 6: Illustration of the steps of formation of NPs initiated by an increase in precursor concentration (Adapted from Ref. [4,12]).

As mentioned, the temperature is also a key factor to control the formation of monodisperse SPIONs because it can help to differentiate nucleation to growth steps. Zhao *et al.*[44], suggest a thermal decomposition of an organometallic complex of iron in methoxy polyethylene glycol (MPEG), assumed that nucleation is a process occurring around 200°C whereas growth happens at higher temperature around 240°C. They also reported that the formation of nuclei would be initiated by reaction of ferric ion and hydroxyl group from MPEG leading to partially oxidized MPEG-coated iron oxide magnetite nuclei.

This mechanism of formation has been introduced for a single phase procedure, however, it has been reported that SPIONs can be prepared by two phases procedure, like aerosols methods or laser pyrolysis involving gas and liquid phases. Nevertheless, the as-produced iron oxide nanocrystals are mostly based on maghemite and hematite iron oxides which correspond to less magnetic iron oxide types. In addition, such procedures induce a decrease of magnetic saturation compared to an homogeneous precipitation technique. Moreover, scale-up remains challenging and conditions to optimize the reaction yield and the purity are

not fully managed yet.[5,43] Consequently, we will now focus on pathway to synthetize the most magnetic iron oxide, the magnetite Fe_3O_4. In order to figure out which technique yield suitable design of SPIONs depends on the desired applications, an overview of synthetic methods will be present hereinafter.

4.2. Synthesis of magnetite SPIONs

The challenge of producing SPIONs for biomedical uses is to find a method allowing to get high amount of very low toxic and monodisperse NPs by, if possible an ecofriendly and scale-up route. In addition, some specifications related to the design may be necessary to fulfill depends on the biomedical applications.

A long time ago, syntheses of magnetite SPIONs by using a microorganism route with bacteria (magnetostatic bacteria) or fungi were discovered[24,37] In 2005, Bharde *et al.* used *Actinobacter spp.* bacteria[45] and *Fusarium oxysporum* and *Verticillium sp.* fungus[46] for that purpose. Nowadays, it is more common to work with chemical methods *via* iron precursor reduction (metal salt or organometallic complex) due to the need of well-designed NPs for large-scale synthesis.[24,37] Researchers have been focused their efforts on two main pathways to produce tailorable and monodisperse magnetite SPIONs. Among all techniques developed, we can mention the coprecipitation, the high temperature decomposition, the constrained environment procedures, the polyol method, the hydrothermal method, the sonochemical procedure, and the electrochemical methods; coprecipitation and the high temperature decomposition, commonly called thermal decomposition or pyrolysis, have widely been applied to synthesize magnetite during the last decade. Many reviews[1,5,22,24,32,36,37,43] have actually reported particularities of each chemical techniques and have indicated that coprecipitation and thermal decomposition correspond to the scale-up pathways in reason to the reproducibility and the production of monodisperse nano-sized magnetite particles. Before going deeply in details for those two kinds of synthesis, a brief overview regarding to the other ways remains still interesting to do in order to sum-up some advantages and disadvantages of these methods.

Constrained environment procedure: To begin with constrained environment reactions, it has to be distinguished three main systems which are microemulsions, dendrimers and liposomes constructs. For procedures involving dendrimers or liposomes, the organic structures of dendrimers and liposomes are used as template hosts and provide generally magnetodendrimers and magnetoliposomes owing to the encapsulation of SPIONs within

their cores.[36,43] Microemulsion method has been more detailed in literature. Microemulsion structure involved into iron oxide synthesis is mostly a reverse emulsion corresponding to a water-in-oil (W/O) suspension. Such colloidal suspension is based on a stable dispersion of two immiscible liquids in a shape of microdroplets (1-50 nm) of an aqueous phase, containing reactants, surrounded by an interfacial film of surfactant molecules assemblies and dispersed in an oily phase. The confinement of reactants within droplets is the key of monodispersity since it prevents NPs produced *in situ* from aggregation and allows as well to have an accurate control over the size range by adjusting conditions like the temperature of formulation, the surfactant concentration and the flexibility of the interface. Microemulsion's microcavities are basically used as nanoreactors since two identical W/O microemulsions, containing respectively one reactant, can be mixed in order to make droplets coalesce to finally provide SPIONs within micelles. Final product can then be extracted from droplets core by breaking down the emulsion for instance with hydrotrope molecules (ethanol, acetone…) and precipitate from the continuous oily phase. Magnetite NPs can be then obtained through this process, but the yield remains quite low and high amount of solvent is required.[1,5,22,43] NPs are also poorly crystallized but smaller than 50 nm. In addition, surfactant molecules can be still present as impurities from the reaction onto NPs surface which might be contraindicated for *in vivo* use.[1,24] Recently, Lee *and al.*[47] proposed a compromise to overcome the lack of crystallinity and monodispersity of magnetite NPs prepared within nanoreactors based on reverse micelles. Gathering stable nanoreactor formulation under high temperature condition with small amount of solvent, they so settled an ecofriendly scale-up process providing highly crystallized and monodisperse 10 nm magnetite NPs. Their synthesis of SPM NPs was considered as an improvement of the constrained environment technique since it involved small amount of solvent, high temperature causing enhancement of crystallinity and corresponds to a one-step procedure in reason to production of monodisperse NPs without post-synthesis size-selection.

Polyol method: Polyol method seems also a convenient method to prepare magnetite NPs due to the possibility to obtain NPs with a narrow size distribution. In this kind of procedure, polyol plays many roles like the solvent of inorganic components, the reducing agent of iron precursor, the stabilizer during the nuclei growth step preventing the form aggregation and the protective capping as hydrophilic ligand adsorbed onto magnetite NPs surface. Basically, microparticles and NPs are easily dispersed in an aqueous polar media and possess a high crystallinity because of the high temperature, near the boiling point of the polyol, applied

during the process. This technique is a one-step procedure since suspension of iron precursor in polyol leads by an increase of temperature to a solubilization of the precursor and its reduction providing iron oxide nuclei.[32,43] After the growth step, SPIONs precipitate from the solution. Metallic alloys are mostly produced by the polyol method[48–50] rather than from oxide alloys but literature still reported magnetite NPs preparation. For instance, Wan *et al.*[51] reported the preparation of water-soluble magnetite SPIONs for MRI. This work was focused on the finding of a compromise between the ease of coprecipitation process and the high quality of magnetite NPs provided by thermal decomposition. The non-aggregated and polyol functionalized magnetite NPs were synthetized by reacting iron precursor, iron(III) acetylacetonate, in triethylene glycol near the boiling point of the polyol. True diameter was found by TEM close to 10 nm but the hydrated polyol chains provided by DLS a hydrodynamic size near 16.5 nm. The magnetic saturation was 80 $emu.g^{-1}$ suggesting that NPs magnetically behaved mostly like a bulk material by using a high temperature process. It seemed quite clear now that working a under high temperature may help to get high crystalline nanomaterials leading to high magnetic magnetite nanomaterials. Combining nanoscale dimension and high magnetism, the magnetite NPs were suggested to proton relaxation time measure revealing as a potential as contrast agent for MRI (r_2 = 82.86 $mM^{-1}.s^{-1}$).

Hydrothermal technique: Hydrothermal process is referred as the oldest method used for preparing uniform nanostructures like magnetite NPs and composites. It is based on the ability of water to hydrolyze and dehydrate metal salts under harsh conditions of pressure and temperature. Those two parameters are keys to control nucleation and growth of iron oxides nuclei. Owing to the absence of organic solvent, hydrothermal procedure is eco-friendly but the main disadvantage is the impossibility to functionalize *in situ* NPs surface. However, it appears to be a good method to obtain highly crystalline NPs with well-defined morphology and size. Finally, if the process is fully managed, magnetic property will be optimized, indeed, magnetic saturation of NPs would be quite close to that from bulk materials which is a very rare property.[1,5,24,52] Daou *et al.*[53] worked on magnetite synthesis and showed that post-synthesis hydrothermal treatment allowed to recover magnetite with an unoxidized surface. They proved in this work that slight deviation of stoichiometry on magnetite grains surface, corresponding actually to maghemite layer, lead to a decrease of crystallinity and so a decrease of magnetic properties. Thanks to hydrothermal treatment almost whole nanocrystals were constituted of pure magnetite and exhibited a higher magnetic saturation than before

treatment. It seems that hydrothermal method might be more interesting to perform as post-synthesis treatment if NPs display high degree of oxidation.

Sonochemical procedure: It involves a high energy ultrasonication to create acoustic cavitations into a liquid media causing the formation and the growth of bubbles containing the reactant in gas state. This leads to a local increase of pressure close to 1800 atm and hot spot at around 5000 K making chemicals in gas state react and the bubbles collapse. The sonochemistry applied to SPIONs allows to get materials with unusual properties like a low magnetic saturation for magnetite and different shapes. As mentioned, sonochemical method induces a very high increase of pressure and temperature rendering this process difficult to be managed and inappropriate for scale-up production.[24,37,43] Vijayakumar *et al.*[54] reported a sonochemical procedure to prepare 10 nm Fe_3O_4 SPIONs with a very poor magnetism, like amorphous particles do, despite crystalline structure. So far, sonochemical synthesis provides generally amorphous materials, or non-crystalline phase, because of quick transition from harsh conditions to standard ones.

Electrochemical method: This is certainly the less applied method to prepare SPIONs for biomedical applications. Few details are available in the literature but it has been identified as a method providing magnetite and maghemite SPIONs. Electrochemical pathway involves an anode and a cathode, the first electrode, a sacrificial electrode, gets oxidized into a water-soluble metallic species which is then reduced onto the cathode in metal in presence of stabilizers. Even though it is not a widely applied technique, it allows to obtain NPs with a good control over the size by a direct control over the current density.[24,43] Cabrera *et al.*[55] achieved by iron electrooxidation the synthesis of 20-30 nm spherical ferromagnetic Fe_3O_4 NPs and suggested that synthesis was dependent to the distances between electrodes which must be short enough to make sure that species will be able to reach both electrodes, the pH to optimize reactions involved, and the potential to avoid production of gases (H_2 and O_2) on electrodes surface preventing complete reaction from occurring. In addition, authors exposed the impact of current density on polydispersity. As aforementioned, redox media led here to maghemite layer capping magnetite NPs, indicating oxidation issue during the process.

Coprecipitation and thermal decomposition possess many advantages. Nevertheless, different disadvantages can be pointed out in the literature. They have at least a common point of being considered as scale-up techniques. Many arguments have been debated about those

two procedures regarding the size distribution, the conditions of preparation (solvent, temperature) and the surface property of the SPIONs. For example, it is assumed that coprecipitation would provide nanomaterials with a quite large size distribution leading to a non-ideal magnetic behavior compared to the uniform size NPs obtained from thermal decomposition. Indeed, within a batch of nanomaterials produced by coprecipitation, several monodisperse populations of particles would coexist and would be magnetically unequivalent regarding the blocking temperature. So, instead of exhibiting an unique temperature of transition, like does an entire batch produced with a very narrow range of size, polydisperse batch would have a range of blocking temperature since each population with a given size of NPs would have its own blocking temperature. However, post-reaction size selection can be performed to reduce the range of size.[1,37] The positive side for coprecipitation relative to thermal decomposition is that coprecipitation is a simple, ecofriendly and solvent-free process giving water-soluble and so biocompatible SPIONs.[5,36] For imaging applications like MRI, it is imperative to use stable colloidal suspensions and non-toxic NPs in physiological conditions[11], so far this seems achievable by coprecipitation. The dilemma here is about the quality of the colloids from coprecipitation reaction as it has just been pointed out. High quality SPIONs are mostly produced by thermal decomposition. High quality NPs refer to high crystalline NPs based on a single monodisperse population with a well-defined magnetic property. However, a thermal decomposition procedure involves organic solvents and lipophilic stabilizers whose use might be detrimental for the biocompatibility. In addition, SPIONs from high-temperature decomposition are consequently mainly hydrophobic and so insoluble in aqueous or polar solvent.[1,5,11,36,37,43]

Coprecipitation: Coprecipitation corresponds to precipitation of substances normally soluble and which can be carried out by two pathways to obtain magnetite NPs in alkaline aqueous media: (i) the partial oxidation of Fe^{2+} salts or (ii) the aging of a stoichiometric mixture of Fe^{3+} and Fe^{2+} salts [43]. Though, all procedures assimilated to the conditions of (i) turn into (ii) since Fe^{2+} gets slightly oxidized, generates Fe^{3+} and form a mixture of both iron salts. The general reaction principle is basically the following one[56]:

$$Fe^{2+}2Fe^{3+} + 8HO^{-} \rightarrow 2Fe(HO)_3 + Fe(HO)_2 \rightarrow Fe_3O_4 + 4H_2O$$

Several parameters have to be carefully mastered to keep a control over the range of size, the colloidal stability and the oxidation surface of the produced nanocrystals of magnetite. Those have been widely studied since the increasing interest of researchers in the simple

procedure of coprecipitation. First, the reaction might be done in an oxygen-free environment to prevent the formation of magnetite NPs from oxidation and second it should involve hydrophilic ligands *in situ* (dextran, polysaccharide, polyvinyl alcohol, starch, hydrophilic polymer…) to stabilize and avoid any unexpected aggregation by a quick adsorption right onto the just formed nuclei.[1,36,43] Surface composition and charge are *ipso facto* related to the type of ligand adsorbed onto NPs but those are as much important on the control over the growth step of nuclei. Third, regarding charges, it should be mentioned that coprecipitation is basically performed in water suggesting the presence of electrolytes. The pH, the ionic force and the counterion of the metallic salts (and consequently the nature of the metallic precursor) are so involved to stabilize NPs. Indeed, all of these parameters play a role in the surface state of the NPs in an aqueous suspension since controlling them can lead to the formation an electrostatic double layer (Stern layer) less compressed and so generate an efficient electrostatic barrier preventing from coagulation.[5] Consequently it has been identified as important to work in the case of (ii) with a Fe^{2+}/Fe^{3+} ratio of 0.5 at a pH around 8-14 for performing a reaction in favorable thermodynamic conditions to obtain magnetite.[36] Finally, the temperatures of reaction are also important for the size. Like in polyol procedure and thermal procedure, it seems better to work close to the boiling point of an aqueous solvent or a polar solvent.[1]

Typical example highlighting the importance of reaction condition to control the design of SPIONs is the study performed by Aslam and co-workers.[57] They worked on the synthesis of uniform water-dispersible magnetite nanoparticles surrounded by amine ligands from a single precursor $FeCl_2$. They indeed showed the influences of molar ratio between dodecylamine and iron precursor and reaction time on the size distribution and the magnetic properties like magnetic saturation and transverse relaxivity (r2). Their results suggested that working in a high amount of amine (from 1:1 to 7:1) would provide smaller magnetite nanocrystals (from 40 to 8.5 nm) with a narrow size distribution by reacting over a long time of reaction (from 3 to 12 h) and with good property as T2-weighted MRI contrast agent (r2 from 80 to 232 $mM^{-1}.s^{-1}$). Another case showed also that coprecipitation can easily be a green process and yield biocompatible SPIONs. Lu *et al.*[58] reported a simple procedure involving $FeCl_3$ and α-D-glucose for its reducing property providing hydrophilic magnetite SPIONs functionalized by the oxidized form of glucose, the gluconic acid. By applying a simple green chemistry synthesis at 80°C, they generated 12.5 nm uniform and spherical magnetite nanocrystals exhibiting a magnetic saturation close to 60 $emu.g^{-1}$. The same team introduced a

parallel work using the as-introduced magnetite nanoparticles as seed template for selenium corona growth to extend its applications from drug carrier[58] to further functions in biology and medicine fields.[59]

To go further into the understanding of impacts of reaction parameters over SPIONs design and their resulting properties, we can mentioned Lyon *et al.*[60] using coprecipitation inspired from Kang *et al.*[61] and a gold coating by an iterative procedure to yield magnetite core with maghemite layer and gold corona shell. Here, oxidized surface has been pointed out as an asset to easily coat grain surface with gold due to a better reduction of Au^{3+} to $Au^{(0)}$ onto the maghemite surface. It was reported that magnetism would have not been affected by gold deposition; however magnetic saturation remained quite low for a magnetite core ($45 emu.g^{-1}$). Although non applications were cited for future uses of the assembly, this construct could hold potential for X-ray/MR bimodal imaging since it appeared like well-designed water-soluble and nanoscale material for this end. Gold coating is certainly the most applied gold capping whatever the synthetic method used to make magnetite nanograins, despite on that some authors then worked on the attachment of gold clusters on 10 nm SPM biocompatible magnetite to overcome potential alteration of magnetic behavior due to the thickness of gold coating. So, Caruntu *et al.*[62] synthesized magnetite by coprecipitation and in order to attach 2-3 nm gold clusters onto the as-prepared SPIONs. In this case, the Fe_3O_4-Au nanocomposites exhibited a magnetic saturation near bulk material, indicating the absence of impact of clusters attachment on contrary to gold coating in the previous study. Sun *et al.*[63] introduced also the impact of biocompatible ligands on magnetite nanoparticles behavior. Surfactants, sodium oleate and polyethylene glycol, were respectively implied as surface grafted ligands. Experiments allowed to conclude that the sodium oleate was the best candidate to optimize the magnetic saturation of the coprecipitated magnetite, the biocompatibility and dispersion in aqueous media. To go deeper about feasibility of tuning the magnetite from coprecipitation, Wang *et al.*[64] achieved the first fabrication of multifunctional assembly based on the combination of layer-by-layer self-assembly method and dendrimer chemistry on magnetite iron oxides nanoparticles from coprecipitation to constitute a platform for MR imaging and cancer cell targeting. Positively charged magnetite NPs were subjected to the addition of negatively charged polyelectrolyte and then to dendrimer formation by layer-by-layer technique. The outer layer of the dendrimer was prefunctionalized with moieties, based on folic acid, specific to receptors over-expressed onto cancer cells for targeting ends and to avoid any unexpected sticking to random *in vivo*

biomolecules. The magnetic core showed good potential for T2-weighted contrast for MRI. Wang *et al.*[64] introduced a novel route for cancer cells imaging by applying a biocompatible targeting strategy with dendrimer surface design encapsulating SPIONs with enhanced contrasting properties.

As it can be noticed, coprecipitation is widely applied owing to its simplicity and capacity to yield SPIONs with satisfying properties for *in vivo* uses by involving biocompatible and water-soluble components. In addition, this brief overview of examples can also be used as a proof of concept concerning the importance of the surface chemistry of magnetite not only for the desired application but also to tune magnetic properties.

Thermal decomposition: The three iron oxide nanoparticles can be produced by this high temperature process under different temperature of reaction: the higher the temperature is, the more oxidized the iron oxide will be. Basically, the thermal decomposition lays on the decomposition of an iron organometallic precursor by high temperature *via* the use of high boiling point organic solvent (phenyl ether, diphenyl ether) in presence of surfactant (fatty acids, fatty amine) introduced in a specific ratio compared to the iron complex. Many organometallic complexes are used, the most common ones are divided up in three families: (i) iron carboxylate (iron acetylacetonate $Fe(acac)_3$, iron oleate $Fe(oleate)_3$), (ii) iron carbonyl (iron pentacarbonyl $Fe(CO)_5$) and (iii) iron cupferronate ($Fe(Cup)_3$).[1,4,5,36,37,43] Deep investigations about those three families have been done over the two last decades and have led to identify (ii) and (iii) as iron precursor families mostly applied for preparations of γ-Fe_2O_3 maghemite nanoparticles. Regarding to the most referenced works, it appears clearly that $Fe(CO)_5$ and $Fe(Cup)_3$ were both involved into γ-Fe_2O_3 syntheses by thermal decomposition like it was achieved fifteen years ago by Hyeon *et al.*[65] and Rockenberger *et al.*[66]. Counter to (ii) and (iii), iron complex (i) has mainly been referred in papers for magnetite nanocrystals synthesis. Regarding major works related to magnetite synthesis by thermal decomposition, $Fe(acac)_3$ was used by Sun *et al.*[67,68] who have established a work which has inspired dozens authors have then been inspired. In order to pursue this goal, Sun *et al.*[67,68] reported a thermal decomposition procedure providing hydrophobic magnetite SPIONs from 4 nm to 20 nm (by seed-mediated growth for sizes up to 8 nm) followed by ligand exchange post synthesis procedure with tetramethylammonium 11-aminoundecanoate to turn those lipophilic magnetite nanoparticles into hydrophilic nanomaterials.[67] Nucleation and growth steps were performed by applying two temperatures yielding to

monodisperse magnetite; oleylamine and oleic acid were used as ligands. In thermal decomposition, surfactants work as stabilizers molecules by acting as steric barrier between particles and inhibit uncontrolled nuclei growth during the process, which is why this method provides dispersed nanoparticles with very well-defined morphology without aggregation issue.[1,36]

Numerous researchers got interest on Sun *et al.*'s thermal decomposition.[67,68] Many of them inspired their work from their protocols. For examples, Wang *et al.*[69] produced a core-shell assembly called Fe_3O_4@Au based on hydrophobic NPs coated with gold layer by in-situ reduction of Au^{3+} into Au^0. Gallo *et al.*[70] achieved recently a work about water-soluble gold-coated magnetite functionalized with neoglycoconjugates and linker for specific biological entities recognition. Magnetic property was unchanged after the attachment of ligands, thus ligands-grafted core-shell was expected to be efficient for MR imaging (r_2 = 155-157 $mM^{-1}.s^{-1}$). Similarly, Garcia *et al.*[71] made 6 nm magnetite-gold core-shell nanomaterials based on antibody-magnetic glyconanoparticles for immunolabeling of cells. MRI contrast was proved and showed the potential of the magnetite core of being T2-weighted contrasting for cells imaging (r_2 = 156.7 $mM^{-1}.s^{-1}$). The gold shell was included into this novel structure due to the gold-thiol chemistry offering a range of possibility for further functionalization by reacting the thiol-end of chain with antibodies. By applying the same synthetic method, Pandey *et al.*[72] have reported recently the use of magnetite nanoparticles as biosensors for *Escherichia coli* bacteria.

The use of magnetite produced by thermal decomposition described by Sun *et al.*[67,68] has also been investigated in the field of multimodal imaging. Preparation of a multimodal probe usable in MR, X-rays and optical imaging were reported by Dong *et al.*[73] for cancer diagnosis. Magnetite was chosen to enhance MRI contrast, rhodamine compound was used as a dye for fluorescent imaging and a gold corona layer was involved in a double role as (i) X-ray contrast agent and (ii) a shell easily modified to get anti-fooling property by grafting thiolated polyethylene glycol polymer by thiol-gold chemistry. Biocompatible nanospheres with 101 nm hydrodynamic diameter were formed with a well-defined shape and a good colloidal stability in physiological media. Focusing on the magnetite core, MR imaging of mice showed significant darkening of hepatic lesions over half an hour indicating promising ability for contrasting in T_2-weighted imaging (r_2 = 242 $mM^{-1}.s^{-1}$). Carrìl *et al.*[74] proposed another version of multifunctional nanocomposites for multimodal imaging based on magnetite glyconanoparticles as a 4 nm SPM core produced with Gallo *et al.*[70] and Garcìa

et al.[71] procedures for T2-weighted MRI (r_2 = 160 $mM^{-1}.s^{-1}$) with a gold coating for X-ray contrast. Ultrasound contrast was also investigated for this assembly.

Different types of stabilizers other than oleylamine and oleic acid have also been attached; new design of magnetite has in this way been introduced. For instance, Li and co-workers[75] proposed a thermal decomposition to provide hydrosoluble magnetite nanoparticles by reacting $Fe(acac)_3$ and 2-pyrrolidone used as solvent, reducing agent, stabilizer and coordination agent *via* carbonyl-iron interaction. It should be notified that this method constitutes an enhancement because water-soluble iron oxide nanoparticles were made in a one-step procedure avoiding as a result the need of applying a ligand exchange procedure. SPIONs (5 nm) were so prepared by a one-step reaction whereas bigger SPIONs (11 nm) were produced by seed-mediated growth. They respectively showed low magnetic saturation of 31 $emu.g^{-1}$ and 65 $emu.g^{-1}$ supporting the impact of an increase of size and a change of surface state on magnetism. Indeed, the difference of ligands covering the nanoparticles surface generated a higher spin-canting effect due to the high polarity of 2-pyrrolidone and consequently a decrease of magnetic saturation.

As to the role of temperature, working like in polyol process with high boiling point solvent is needed to obtain highly crystallized nanoparticles. Larger nanoparticles are also generally produced by working at high temperatures.[1,36] Such characteristics, and also the impact of the ratio between surfactants and organometallic complex, were widely notified and even more in cases of $Fe(oleate)_3$ uses. $Fe(oleate)_3$ or iron carboxylate salts are mainly involved in procedures including the formation of stable $Fe(oleate)_3$ starting material and its *in situ* thermal decomposition in presence of solvent with a boiling point up to 300°C (octadecene, trioctylamine..). Yu *et al.*[76] explored that pathway to get magnetite SPIONs with a high quality as spherical magnetic colloids. By applying different ranges of molar ratios of oleic acid and iron precursor to generate $Fe(oleate)_3$, times of reaction and reaction temperatures, they investigated impacts on nanoparticles size distributions which got broader and broader by increasing the two last parameters due to Ostwald ripening. An excess of oleic acid had caused an inhibition of magnetite nuclei formation indicating the importance of the ratio between reactants and stabilizers. Park *et al.*[77] attempted a two-steps procedure consisting in first place to the synthesis of $Fe(oleate)_3$ salt and in second place to the large scale production of monodisperse magnetite SPIONs without size-selection requirement. Authors highlighted the need of distinction between nucleation and growth kinetics by introducing an hypothetic mechanism of formation pointing out the role of the $Fe(oleate)_3$ and the

temperature. As the impact of temperature factor, they worked with various solvents to form high crystalline nanoparticles with higher size (9 to 22 nm) due to the higher boiling point (274 to 365°C). Although those authors have not proposed applications for the future, Lee *et al.* [78] have recently been worked on thermal decomposition of $Fe(oleate)_3$ from Park *et al.* [88] for multimodal imaging including MRI of tumor allowing to discriminate vascular region of a rat tumor. To conclude, the ratio between the surfactants and the organometallic complex has so to be managed as much as the time and the temperature of reaction. Other parameters like the stirring, or even the ratio between the different types of stabilizers involved [79], must be taken into account to keep a control over the size, the crystallinity and the shape to end to an enhancement of magnetic properties.

A lot of techniques are described in the literature to yield SPIONs exhibiting suitable features for *in vivo* uses. The Figure 7 summarizes the different methods to obtain SPIONs, and consequently magnetite, how to turn them into biocompatible nano-assembling and stringent requirements to considered SPIONs as ideal NPs for nanomedicine.

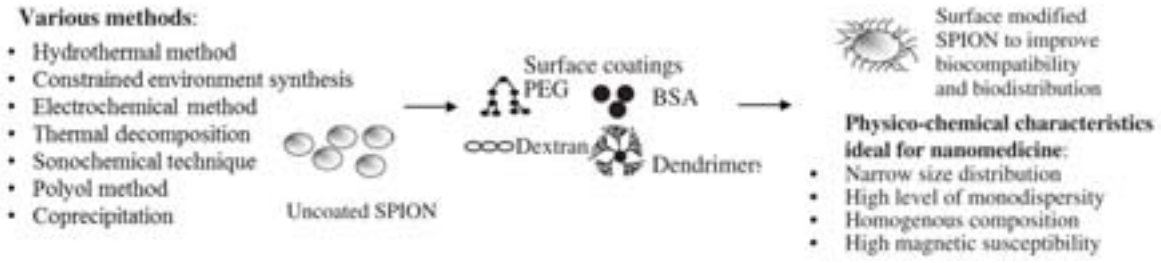

Figure 7: Methods and *in situ* and/or post-synthesis treatment to form biocompatible SPIONs for nanomedicine purposes (Adapted from Ref. [30]).

Although it is important to have an overview of methods to produce SPIONs with suitable properties, it is also interesting to be aware of techniques to determine in an efficient way how to characterize SPIONs to identify, quantify and define their composition, their design (shape, size, surface features), their physico-chemical and magnetic properties. To this end, we can briefly establish a listing of the most applied methods Characterization techniques commonly presented in the literature can be divided in several groups depending on the information that they provide: there are i) methods of identification like spectroscopic techniques by means of infrared spectroscopy (FTIR)[40,43,80–83], X-ray photoelectron spectroscopy (XPS)[84,85], Mössbauer spectroscopy[3,31,86–89] but also X-ray diffraction[5,67,82] and ii) methods of quantification like relaxometry titration[90], thermogravimetric analysis (TGA)[57,67,91,92], inductively coupled plasma (ICP)[93] and rarely High resolution magic

angle spinning (HR-MAS)[94] (XPS can also be included in such kind of characterization due to its principle). Finally, there are techniques providing iii) physico-chemical information like dynamic light scattering (DLS) and electronic microscope pictures by transmission electron microscopy (TEM) (morphology, size)[24,36,95] and iv) magnetic properties (hysteresis loops, magnetic saturation, and coercivity) by superconducting quantum interference device (SQUID) (and also Mössbauer spectroscopy)[96,97] and relaxometry[98]. A complete review could be dedicated to the description of all of these techniques in order to provide a complete guide for SPIONs characterizations from basic technique (infrared spectroscopy, X-rays diffraction, DLS, etc.) to most specific methods (relaxometry, SQUID, HR-MAS).

5. Conclusion

IONPs, and more precisely magnetite-based SPIONs, have gained huge interest in the past decades in nanomedicine. This is why we chose here to summarize essential information to begin study of IONPs. Not only these magnetic NPs can possess all assets of NPs dedicated to biomedical uses but they also exhibited additional properties owing to their inherent magnetism, so-called superparamagnetism. It has been overviewed in this work, main notions about magnetism of NPs and stringent requirements to fulfill to apply SPIONs into nanomedicine. A focus was done on IONPs in order to show why magnetite turned out to be the most used IONPs. The impacts of IONPs design (surface properties, size, shape) were all mentioned to bring to light that careful attention must be paid to prepare IONPs with desired magnetic and physico-chemical properties. Although magnetite and other SPIONs were described as efficient NPs for applications involving magnetism, it seems that some debates remain concerning the *in vivo* fate of SPIONs once administrated to living being. Consequently, preclinical research needs to keep going in such direction in order to provide a better understanding of the *in vivo* impact of SPIONs on health and to provide significant data to go further for human applications. We also emphasized in the present report major routes of synthesis of magnetite with several examples to show the potential of each method and also to highlight the wide range of studies already available and how such kind of magnetic nanotechnology can be tuned by playing with chemistry and conditions of preparation.

6. References

[1] A.H. Lu, E.L. Salabas, F. Schüth, Magnetic nanoparticles: Synthesis, protection, functionalization, and application, Angew. Chemie - Int. Ed. 46 (2007) 1222–1244.

[2] G.C. Papaefthymiou, Nanoparticle magnetism, Nano Today. 4 (2009) 438–447. doi:10.1016/j.nantod.2009.08.006.

[3] S. Kamali-M., T. Ericsson, R. Wäppling, Characterization of iron oxide nanoparticles by Mössbauer spectroscopy, Thin Solid Films. 515 (2006) 721–723. doi:10.1016/j.tsf.2005.12.180.

[4] N.A. Frey, S. Peng, K. Cheng, S. Sun, Magnetic nanoparticles: synthesis, functionalization, and applications in bioimaging and magnetic energy storage., Chem. Soc. Rev. 38 (2009) 2532–2542. doi:10.1039/b815548h.

[5] A.S. Teja, P.-Y. Koh, Synthesis, properties, and applications of magnetic iron oxide nanoparticles, Prog. Cryst. Growth Charact. Mater. 55 (2009) 22–45. doi:10.1016/j.pcrysgrow.2008.08.003.

[6] Q.A. Pankhurst, J. Connolly, S.K. Jones, J. Dobson, Applications of magnetic nanoparticles in biomedicine, J. Phys. D. Appl. Phys. 36 (2003) R167–R181. doi:10.1088/0022-3727/36/13/201.

[7] K. Abdulwahab, M.A. Malik, P. O'Brien, K. Govender, C. Muryn, G. a. Timco, F. Tuna, R.E.P. Winpenny, Synthesis of Monodispersed Magnetite Nanoparticles from Iron Pivalate Clusters, Dalt. Trans. 42 (2012) 196–206. doi:10.1039/c2dt32478d.

[8] P.J. Robinson, P. Dunnill, M.D. Lilly, The properties of magnetic supports in relation to immobilized enzyme reactors, Biotechnol. Bioeng. XV (1973) 603–606. doi:10.1002/bit.260150318.

[9] V.P. Torchilin, Multifunctional nanocarriers, Adv. Drug Deliv. Rev. 64 (2012) 302–315. doi:10.1016/j.addr.2012.09.031.

[10]P.A. Jarzyna, A. Gianella, T. Skajaa, G. Knudsen, L.H. Deddens, D.P. Cormode, Z. a. Fayad, W.J.M. Mulder, Multifunctional imaging nanoprobes, Wiley Interdiscip. Rev. Nanomedicine Nanobiotechnology. 2 (2010) 138–150. doi:10.1002/wnan.72.

[11]H. Bin Na, I.C. Song, T. Hyeon, Inorganic nanoparticles for MRI contrast agents, Adv. Mater. 21 (2009) 2133–2148. doi:10.1002/adma.200802366.

[12]H. Goesmann, C. Feldmann, Nanoparticulate functional materials, Angew. Chemie - Int. Ed. 49 (2010) 1362–1395. doi:10.1002/anie.200903053.

[13]C. Sun, J.S.H. Lee, M. Zhang, Magnetic nanoparticles in MR imaging and drug delivery, Adv. Drug Deliv. Rev. 60 (2008) 1252–1265. doi:10.1016/j.addr.2008.03.018.

[14]N. Pimpha, S. Chaleawlert-Umpon, P. Sunintaboon, Core/shell polymethyl methacrylate/polyethyleneimine particles incorporating large amounts of iron oxide nanoparticles prepared by emulsifier-free emulsion polymerization, Polymer (Guildf). 53 (2012) 2015–2022. doi:10.1016/j.polymer.2012.03.019.

[15]M. Niinomi, Recent metallic materials for biomedical applications, Metall. Mater. Trans. A. 33 (2002) 477–486. doi:10.1007/s11661-002-0109-2.

[16]Y.Z. Wadghiri, J. Li, J. Wang, D.M. Hoang, Y. Sun, H. Xu, W. Tsui, Y. Li, A. Boutajangout, A. Wang, M. de Leon, T. Wisniewski, Detection of Amyloid Plaques Targeted by Bifunctional USPIO in Alzheimer's Disease Transgenic Mice Using Magnetic Resonance Microimaging, PLoS One. 8 (2013) 1–10. doi:10.1371/journal.pone.0057097.

[17]R.S. Molday, D. MacKenzie, Immunospecific ferromagnetic iron-dextran reagents for the labeling and magnetic separation of cells., J. Immunol. Methods. 52 (1982) 353–367. doi:10.1016/0022-1759(82)90007-2.

[18]S. Mornet, S. Vasseur, F. Grasset, E. Duguet, Magnetic nanoparticle design for medical diagnosis and therapy, J. Mater. Chem. 14 (2004) 2161–2175.

[19]M. Bañobre-López, A. Teijeiro, J. Rivas, Magnetic nanoparticle-based hyperthermia for cancer treatment, Reports Pract. Oncol. Radiother. 18 (2013) 397–400. doi:10.1016/j.rpor.2013.09.011.

[20]B. Sahoo, K.S.P. Devi, S. Dutta, T.K. Maiti, P. Pramanik, D. Dhara, Biocompatible mesoporous silica-coated superparamagnetic manganese ferrite nanoparticles for targeted drug delivery and MR imaging applications, J. Colloid Interface Sci. 431 (2014) 31–41. doi:10.1016/j.jcis.2014.06.003.

[21]M.A. Hahn, A.K. Singh, P. Sharma, S.C. Brown, B.M. Moudgil, Nanoparticles as contrast agents for in-vivo bioimaging: Current status and future perspectives, Anal. Bioanal. Chem. 399 (2011) 3–27. doi:10.1007/s00216-010-4207-5.

[22]A.K. Gupta, M. Gupta, Synthesis and surface engineering of iron oxide nanoparticles for biomedical applications, Biomaterials. 26 (2005) 3995–4021. doi:10.1016/j.biomaterials.2004.10.012.

[23]S.K. Mouli, P. Tyler, J.L. McDevitt, A.C. Eifler, Y. Guo, J. Nicolai, R.J. Lewandowski, W. Li, D. Procissi, R.K. Ryu, Y.A. Wang, R. Salem, A.C. Larson, R. a. Omary, Image-guided local delivery strategies enhance therapeutic nanoparticle uptake in solid tumors, ACS Nano. 7 (2013) 7724–7733. doi:10.1021/nn4023119.

[24]M. Mahmoudi, S. Sant, B. Wang, S. Laurent, T. Sen, Superparamagnetic iron oxide nanoparticles (SPIONs): Development, surface modification and applications in chemotherapy, Adv. Drug Deliv. Rev. (2011). doi:10.1016/j.addr.2010.05.006.

[25]D.P. Cormode, T. Skajaa, Z.A. Fayad, W.J.M. Mulder, Nanotechnology in medical imaging: probe design and applications, Arter. Thromb Vasc Biol. 29 (2010) 992–1000. doi:10.1161/ATVBAHA.108.165506.

[26]A.G. Kolhatkar, A.C. Jamison, D. Litvinov, R.C. Willson, T.R. Lee, Tuning the magnetic properties of nanoparticles, Int. J. Mol. Sci. 14 (2013) 15977–16009. doi:10.3390/ijms140815977.

[27]R. Bardhan, W. Chen, M. Bartels, C. Perez-Torres, M.F. Botero, R.W. McAninch, A. Contreras, R. Schiff, R.G. Pautler, N.J. Halas, A. Joshi, Tracking of multimodal therapeutic nanocomplexes targeting breast cancer *in vivo*, Nano Lett. 10 (2010) 4920–4928. doi:10.1021/nl102889y.

[28]W. Zheng, F. Gao, H. Gu, Magnetic polymer nanospheres with high and uniform magnetite content, J. Magn. Magn. Mater. 288 (2005) 403–410. doi:10.1016/j.jmmm.2004.09.125.

[29]I.J. Bruce, J. Taylor, M. Todd, M.J. Davies, E. Borioni, C. Sangregorio, T. Sen, Synthesis, characterisation and application of silica-magnetite nanocomposites, J. Magn. Magn. Mater. 284 (2004) 145–160. doi:10.1016/j.jmmm.2004.06.032.

[30]N. Singh, G.J.S. Jenkins, R. Asadi, S.H. Doak, Potential toxicity of superparamagnetic iron oxide nanoparticles (SPION), Nano Rev. (2010) 1:5358. doi:10.3402/nano.v1i0.5358.

[31]I. Leonov, A.N. Yaresko, On the Verwey charge ordering in magnetite, J. Phys. Condens. Matter. 19 (2007) 021001(3pp). doi:10.1088/0953-8984/19/2/021001.

[32]S. Laurent, D. Forge, M. Port, A. Roch, C. Robic, L. Vander Elst, R.N. Muller, Magnetic iron oxide nanoparticles: Synthesis, stabilization, vectorization, physicochemical characterizations and biological applications, Chem. Rev. 108 (2008) 2064–2110. doi:10.1021/cr068445e.

[33]A. Schüle, U. Nieken, O. Shekhah, W. Ranke, R. Schlögl, G. Kolios, Styrene synthesis over iron oxide catalysts: from single crystal model system to real catalysts., Phys. Chem. Chem. Phys. 9 (2007) 3619–3634. doi:10.1039/b700483d.

[34]P.I. Girginova, A.L. Daniel-da-Silva, C.B. Lopes, P. Figueira, M. Otero, V.S. Amaral, E. Pereira, T. Trindade, Silica coated magnetite particles for magnetic removal of Hg^{2+} from water, J. Colloid Interface Sci. 345 (2010) 234–240. doi:10.1016/j.jcis.2010.01.087.

[35]S. Liu, Y. Han, R. Qiao, J. Zeng, Q. Jia, Y. Wang, M. Gao, Investigations on the Interactions between Plasma Proteins and Magnetic Iron Oxide Nanoparticles with Different Surface Modifications, J. Phys. Chem. C. 114 (2010) 21270–21276. doi:10.1021/jp1086653.

[36]J. Lodhia, G. Mandarano, N.J. Ferris, P. Eu, S.F. Cowell, Development and use of iron oxide nanoparticles (Part 1): Synthesis of iron oxide nanoparticles for MRI, Biomed. Imaging Interv. J. 6 (2010) e12. doi:10.2349/biij.6.2.e12.

[37]W. Wu, Q. He, C. Jiang, Magnetic iron oxide nanoparticles: Synthesis and Surface Functionalization Strategies, Nanoscale Res. Lett. 3 (2008) 397–415. doi:10.1007/s11671-008-9174-9.

[38]T.J. Daou, J.M. Grenèche, G. Pourroy, S. Buathong, A. Derory, C. Ulhaq-Bouillet, B. Donnio, D. Guillon, S. Begin-Colin, Coupling agent effect on magnetic properties of functionalized magnetite-based nanoparticles, Chem. Mater. 20 (2008) 5869–5875. doi:10.1021/cm801405n.

[39]D.H. Han, J.P. Wang, H.L. Luo, Crystallite size effect on saturation magnetization of fine ferrimagnetic particles, J. Magn. Magn. Mater. 136 (1994) 176–182. doi:10.1016/0304-8853(94)90462-6.

[40]N.R. Jana, Y. Chen, X. Peng, Size- and Shape-Controlled Magnetic (Cr, Mn, Fe, Co, Ni) Oxide Nanocrystals *via* a Simple and General Approach Oxide Nanocrystals *via* a Simple and General Approach, Chem. Mater. 16 (2004) 3931–3935. doi:10.1021/cm049221k.

[41]V. LaMer, R. Dinegar, Theory, production and mechanism of formation of monodispersed hydrosols, J. Am. Chem. Soc. 72 (1950) 4847–4854. doi:10.1021/ja01167a001.

[42]J.D. Ng, B. Lorber, J. Witz, A. Théobald-Dietrich, D. Kern, R. Giegé, The crystallization of biological macromolecules from precipitates: evidence for Ostwald ripening, J. Cryst. Growth. 168 (1996) 50–62. doi:10.1016/0022-0248(96)00362-4.

[43]P. Tartaj, M. del Puerto Morales, S. Veintemillas-Verdaguer, T. Gonzalez-Carreno, C.J. Serna, The preparation of magnetic nanoparticles for applications in biomedicine, J. Phys. D. Appl. Phys. 36 (2003) R182–R197.

[44]F. Zhao, B. Zhang, L. Feng, Preparation and magnetic properties of magnetite nanoparticles, Mater. Lett. 68 (2012) 112–114. doi:10.1016/j.matlet.2011.09.116.

[45]A. Bharde, A. Wani, Y. Shouche, P. a. Joy, B.L. V Prasad, M. Sastry, Bacterial aerobic synthesis of nanocrystalline magnetite, J. Am. Chem. Soc. 127 (2005) 9326–9327. doi:10.1021/ja0508469.

[46]A. Bharde, D. Rautaray, V. Bansal, A. Ahmad, I. Sarkar, S.M. Yusuf, M. Sanyal, M. Sastry, Extracellular biosynthesis of magnetite using fungi, Small. 2 (2006) 135–141. doi:10.1002/smll.200500180.

[47]Y. Lee, J. Lee, C.J. Bae, J.-G. Park, H.-J. Noh, J.-H. Park, T. Hyeon, Large-Scale Synthesis of Uniform and Crystalline Magnetite Nanoparticles Using Reverse Micelles as Nanoreactors under Reflux Conditions, Adv. Funct. Mater. 15 (2005) 503–509. doi:10.1002/adfm.200400187.

[48]G. Viau, F. Fiévet-Vincent, F. Fiévet, Monodisperse iron-based particles: precipitation in liquid polyols, J. Mater. Chem. 6 (1996) 1047-1053. doi:10.1039/jm9960601047.

[49]P. Toneguzzo, G. Viau, O. Acher, CoNi and FeCoNi fine particles prepared by the polyol process: Physico-chemical characterization and dynamic magnetic properties, J. Mater. Sc. 35 (2000) 3767–3784.

[50]F. Fievet, J. Lagier, B. Blin, B. Beaudoin, M. Figlarz, Homogeneous and heterogeneous nucleations in the polyol process for the preparation of micron and submicron size metal particles, Solid State Ionics. 32/33 (1989) 198–205. doi:10.1016/0167-2738(89)90222-1.

[51]J. Wan, W. Cai, X. Meng, E. Liu, Monodisperse water-soluble magnetite nanoparticles prepared by polyol process for high-performance magnetic resonance imaging., Chem. Commun. 4 (2007) 5004–5006. doi:10.1039/b712795b.

[52]H. Wang, Y. Hu, Y. Jiang, L. Qiu, H. Wu, B. Guo, Y. Shen, Y. Wang, L. Zhu, A. Xie, Facile synthesis and excellent recyclable photocatalytic activity of pine cone-like Fe_3O_4@Cu_2O/Cu porous nanocomposites., Dalton Trans. 42 (2013) 4915–4921. doi:10.1039/c2dt32290k.

[53]T.J. Daou, G. Pourroy, S. Bégin-Colin, J.M. Grenèche, C. Ulhaq-Bouillet, P. Legaré, P. Bernhardt, C. Leuvrey, G. Rogez, Hydrothermal synthesis of monodisperse magnetite nanoparticles, Chem. Mater. 18 (2006) 4399–4404. doi:10.1021/cm060805r.

[54]R. Vijayakumar, Y. Koltypin, I. Felner, A. Gedanken, Sonochemical synthesis and characterization of pure nanometer-sized Fe_3O_4 particles, Mater. Sci. Eng. A. 286 (2000) 101–105. doi:10.1016/S0921-5093(00)00647-X.

[55]L. Cabrera, S. Gutierrez, N. Menendez, M.P. Morales, P. Herrasti, Magnetite nanoparticles: Electrochemical synthesis and characterization, Electrochim. Acta. 53 (2008) 3436–3441. doi:10.1016/j.electacta.2007.12.006.

[56]T. Indira, P.K. Lakshmi, Magnetic Nanoparticles: A Review, Int. J. Pharm. Sci. Nanotechnol. 3 (2010) 1035–1042. http://ijpsnonline.com/Issues/1035_full.pdf.

[57]M. Aslam, E.A. Schultz, T. Sun, T. Meade, V.P. Dravid, Synthesis of amine-stabilized aqueous colloidal iron oxide nanoparticles, Cryst. Growth Des. 7 (2007) 471–475. doi:10.1021/cg060656p.

[58]W. Lu, Y. Shen, A. Xie, W. Zhang, Green synthesis and characterization of superparamagnetic Fe_3O_4 nanoparticles, J. Magn. Magn. Mater. 322 (2010) 1828–1833. doi:10.1016/j.jmmm.2009.12.035.

[59]W. Lu, Y. Shen, A. Xie, X. Zhang, W. Chang, Novel Bifunctional One-Dimensional Fe_3O_4/Se Nanocomposites *via* Facile Green Synthesis, J. Phys. Chem. 114 (2010) 4846–4851.

[60]J.L. Lyon, D.A. Fleming, M.B. Stone, P. Schiffer, M.E. Williams, Synthesis of Fe oxide Core/Au shell nanoparticles by iterative hydroxylamine seeding, Nano Lett. 4 (2004) 719–723. doi:10.1021/nl035253f.

[61]Y.S. Kang, S. Risbud, J.F. Rabolt, P. Stroeve, Synthesis and Characterization of Nanometer-Size Fe_3O_4 and γ-Fe_2O_3 Particles, Chem. Mater. 8 (1996) 2209–2211. doi:10.1021/cm960157j.

[62]D. Caruntu, B.L. Cushing, G. Caruntu, C.J. O'Connor, Attachment of gold nanograins onto colloidal magnetite nanocrystals, Chem. Mater. 17 (2005) 3398–3402. doi:10.1021/cm050280n.

[63]J. Sun, S. Zhou, P. Hou, Y. Yang, J. Weng, X. Li, M. Li, Synthesis and characterization of biocompatible Fe_3O_4 nanoparticles, J. Biomed. Mater. Res. - Part A. 80 (2007) 333–341. doi:10.1002/jbm.a.30909.

[64]S.H. Wang, X. Shi, M. Van Antwerp, Z. Cao, S.D. Swanson, X. Bi, J.R.B. Jr., Dendrimer-Functionalized Iron Oxide Nanoparticles for Specific Targeting and Imaging of Cancer Cells, Adv. Funct. Mater. 17 (2007) 3043–3050. doi:10.1002/adfm.200601139.

[65]T. Hyeon, S.S. Lee, J. Park, Y. Chung, H.B. Na, Synthesis of highly crystalline and monodisperse maghemite nanocrystallites without a size-selection process, J. Am. Chem. Soc. 123 (2001) 12798–12801. doi:10.1021/ja016812s.

[66]J. Rockenberger, E.C. Scher, A.P. Alivisatos, A New Non-Hydrolytic Single-Precursor Approach to Surfacant-Capped Nanocrystals of Transition Metal Oxides - supporting information, J. Am. Chem. Soc. 121 (1999) 11595–11596.

[67]S. Sun, H. Zeng, D.B. Robinson, S. Raoux, P.M. Rice, S.X. Wang, G. Li, Monodisperse MFe_2O_4 (M = Fe, Co, Mn) Nanoparticles, J. Am. Chem. Soc. 126 (2004) 273–279.

[68]S. Sun, H. Zeng, Size-controlled synthesis of magnetite nanoparticles, J. Am. Chem. Soc. 124 (2002) 8204–8205. doi:10.1021/ja026501x.

[69]L. Wang, J. Luo, Q. Fan, M. Suzuki, I.S. Suzuki, M.H. Engelhard, Y. Lin, N. Kim, J.Q. Wang, C.-J. Zhong, Monodispersed core-shell Fe_3O_4@ Au nanoparticles, J. Phys. Chem. B. 109 (2005) 21593–21601.

[70]J. Gallo, I. García, D. Padro, B. Arnáiz, S. Penadés, Water-soluble magnetic glyconanoparticles based on metal-doped ferrites coated with gold: Synthesis and characterization, J. Mater. Chem. 20 (2010) 10010–10020. doi:10.1039/c0jm01756f.

[71]I. García, J. Gallo, N. Genicio, D. Padro, S. Penadés, Magnetic glyconanoparticles as a versatile platform for selective immunolabeling and imaging of cells, Bioconjug. Chem. 22 (2011) 264–273. doi:10.1021/bc1003923.

[72]C.M. Pandey, A. Sharma, G. Sumana, I. Tiwari, B.D. Malhotra, Cationic poly(lactic-co-glycolic acid) iron oxide microspheres for nucleic acid detection., Nanoscale. 5 (2013) 3800–3807. doi:10.1039/c3nr34355c.

[73]W. Dong, Y. Li, D. Niu, Z. Ma, X. Liu, J. Gu, W. Zhao, Y. Zheng, J. Shi, A simple route to prepare monodisperse Au NP-decorated, dye-doped, superparamagnetic nanocomposites for optical, MR, and CT trimodal imaging, Small. 9 (2013) 2500–2508. doi:10.1002/smll.201202649.

[74]M. Carril, I. Fernández, J. Rodríguez, I. García, S. Penadés, Gold-coated iron oxide glyconanoparticles for MRI, CT, and US multimodal imaging, Part. Part. Syst. Charact. 31 (2014) 81–87. doi:10.1002/ppsc.201300239.

[75]Z. Li, H. Chen, H. Bao, M. Gao, One-Pot Reaction to Synthesize Water-Soluble Magnetite Nanocrystals, Chem. Mater. 16 (2004) 1391–1393. doi:10.1021/cm035346y.

[76]W.W. Yu, J.C. Falkner, C.T. Yavuz, V.L. Colvin, Synthesis of monodisperse iron oxide nanocrystals by thermal decomposition of iron carboxylate salts., Chem. Commun. (2004) 2306–2307. doi:10.1039/b409601k.

[77]J. Park, K. An, Y. Hwang, J.-G. Park, H.-J. Noh, J.-Y. Kim, J.-H. Park, N.-M. Hwang, T. Hyeon, Ultra-large-scale syntheses of monodisperse nanocrystals., Nat. Mater. 3 (2004) 891–895. doi:10.1038/nmat1251.

[78]N. Lee, H.R. Cho, M.H. Oh, S.H. Lee, K. Kim, B.H. Kim, K. Shin, T. Ahn, J.W. Choi, Y. Kim, S.H. Choi, T. Hyeon, Multifunctional Fe_3O_4/TaO_x Core/Shell Nanoparticles for Simultaneous Magnetic Resonance Imaging and X-Ray Computer Tomography, J Am Chem Soc. 134 (2012) 10309–10312. doi:10.1021/ja3016582.

[79]J.J. Ibarra-Sánchez, R. Fuentes-Ramírez, A.G. Roca, M. Del Puerto Morales, L.I. Cabrera-Lara, Key parameters for scaling up the synthesis of magnetite nanoparticles in organic media: Stirring rate and growth kinetic, Ind. Eng. Chem. Res. 52 (2013) 17841–17847. doi:10.1021/ie403250p.

[80]M.P. Morales, C. Pecharroman, T. Gonzalez Carreno, C.J. Serna, Structural Characteristics of Uniform γ-Fe_2O_3 particles with Different Axial (Length/width) Ratios, J. Solid State Chem. 108 (1993) 158–163.

[81]M.P. Morales, M. Andres-Vergés, S. Veintemillas-Verdaguer, M.I. Montero, C.J. Serna, Structural effects on the magnetic properties of Fe_2O_3 nanoparticles, J. Magn. Magn. Mater. 203 (1999) 146–148.

[82]N. Guigue-Millot, Y. Champion, M.J. Hÿtch, F. Bernard, S. Bégin-Colin, P. Perriat, Chemical heterogeneities in nanometric titanomagnetites prepared by soft chemistry and studied ex situ: Evidence for Fe-segregation and oxidation kinetics, J. Phys. Chem. B. 105 (2001) 7125–7132. doi:10.1021/jp010661y.

[83]P. Perriat, B. Domenichini, B. Gillot, A model for oxidation in finely divided ferrites taking into account the stresses generated during reaction, J. Phys. Chem. Solids. 57 (1996) 1641–1652. doi:10.1016/0022-3697(96)00055-8.

[84]E. Paparazzo, On the quantitative XPS analysis of Fe_2O_3 and $Fe_{1-x}O$ oxides, J. Electron Spectros. Relat. Phenomena. 154 (2006) 38–40. doi:10.1016/j.elspec.2006.09.004.

[85]T. Yamashita, P. Hayes, Analysis of XPS spectra of Fe^{2+} and Fe^{3+} ions in oxide materials, Appl. Surf. Sci. 254 (2008) 2441–2449. doi:10.1016/j.apsusc.2007.09.063.

[86]U. Herr, J. Jing, R. Birringer, U. Gonser, H. Gleiter, Investigation of nanocrystalline iron materials by Mössbauer spectroscopy, Appl. Phys. Lett. 50 (1987) 472–474. doi:10.1063/1.98177.

[87]R. Zboril, M. Mashlan, D. Petridis, Iron(III) oxides from thermal processes-synthesis, structural and magnetic properties, Mössbauer spectroscopy characterization, and applications, Chem. Mater. 14 (2002) 969–982. doi:10.1021/cm0111074.

[88]W. Kündig, R.S. Hargrove, Electron hopping in magnetite, Solid State Commun. 7 (1969) 223–227. doi:10.1016/0038-1098(69)90729-7.

[89]F. Walz, The Verwey transition - a topical review, J. Phys. Condens. Matter. 14 (2002) R285–R340. doi:10.1088/0953-8984/14/12/203.

[90]S. Boutry, D. Forge, C. Burtea, I. Mahieu, O. Murariu, S. Laurent, L. Vander Elst, R.N. Muller, How to quantify iron in an aqueous or biological matrix: a technical note, Contrast Media Mol. Imaging. 4 (2009) 299–304. doi:10.1002/cmmi.291.

[91]A.W. Coats, J.P. Redfern, Thermogravimetric Analysis, Anayst. 88 (1954) 906-924. doi:10.1038/1731011b0.

[92]J. Mohapatra, A. Mitra, D. Bahadur, M. Aslam, Surface Controlled Synthesis of MFe_2O_4 (M = Mn, Fe, Co, Ni and Zn) Nanoparticles and Their Magnetic Characteristics, CrystEngComm. (2012) 524–532. doi:10.1039/c2ce25957e.

[93]E.R. Dadashzadeh, M. Hobson, L.H. Bryant Jr, D.D. Dean, J.A. Frank, Rapid Spectrophotometric Technique for Quantifying Iron in Cells Labeled with Superparamagnetic Iron Oxide Nanoparticles: Potential Translation to the Clinic, Contrast Media Mol. Imaging, 8 (2013) 50–56. doi:10.1002/cmmi.1493.Rapid.

[94]C. Henoumont, S. Laurent, R.N. Muller, L. Vander Elst, HR-MAS NMR Spectroscopy: An Innovative Tool for the Characterization of Iron Oxide Nanoparticles Tracers for Molecular Imaging, Anal. Chem. 87 (2015) 1701–1710. doi:10.1021/ac5035105.

[95]J. Lim, S.P. Yeap, H.X. Che, S.C. Low, Characterization of magnetic nanoparticle by dynamic light scattering., Nanoscale Res. Lett. (2013) 8:381. doi:10.1186/1556-276X-8-381.

[96]S. Gangopadhyay, G.C. Hadjipanayis, B. Dale, C.M. Sorensen, K.J. Klabunde, V. Papaefthymiou, A. Kostikas, Magnetic properties of ultrafine iron particles, Phys. Rev. B. 45 (1992) 9778–9787. doi:10.1103/PhysRevB.45.9778.

[97]N.L. Adolphi, D.L. Huber, J.E. Jaetao, H.C. Bryant, D.M. Lovato, D.L. Fegan, E.L Venturini, T.C. Monson, T.E. Tessier, H.J. Hathaway, C. Bergemann, R.S. Larson, E.R. Flynn, Characterization of Magnetite Nanoparticles for SQUID- relaxometry and Magnetic Needle Biopsy, J. Magn. Mater 321 (2009) 1–20. doi:10.1016/j.jmmm.2009.02.067.

[98]C. Henoumont, S. Laurent, L. Vander Elst, How to perform accurate and reliable measurements of longitudinal and transverse relaxation times of MRI contrast media in aqueous solutions, Contrast Media Mol. Imaging. 4 (2009) 312–321. doi:10.1002/cmmi.294.

Chapter III.2 – Magnetite and iodine-containing nano-emulsion as contrast agent for X-Ray/MR imaging

Justine Wallyn[a,b], Nicolas Anton[a,b,*], Damien Mertz[c], Sylvie Begin-Colin[c], Florence Franconi[d], Laurent Lemaire[e,f] , Thierry Vandamme[a,b]

[a] Faculty of Pharmacy, 74 route du Rhin, 67401 Illkirch, University of Strasbourg, France

[b] CNRS UMR 7199, Laboratoire de Conception et Application de Molécules Bioactives, équipe de Pharmacie Biogalénique, Illkirch, France

[c] CNRS UMR 7504, Institut de Physique et Chimie des Matériaux de Strasbourg (IPCMS), University of Strasbourg, Strasbourg, France

[d] Plateforme d'Ingénierie et d'Analyse Moléculaire, LUNAM University, Angers, France

[e] Ingénierie de la Vectorisation Particulaire, LUNAM University, Angers, France

[f] INSERM U646, Angers, France

[*] Corresponding author: nanton@unistra.fr (N. Anton)

Abstract

Non-invasive diagnostic by imaging combined with contrast enhancer pharmaceutics is now on the most used technique an insight visualization of human body. X-rays imaging and Magnetic resonance imaging (MRI) are high technology instruments able to produce high resolution 2D or 3D images. More and more, imaging instruments are used in conjuncture to get complementary data from one technique to another one. To yield clear delineation of a desired *in vivo* target, contrast agents (CAs) are necessary. For X-ray imaging, these substances must be radiopaque and bearing heavy element, such as iodine whereas MRI required magnetic element-containing CAs. Nowadays, it seems clear that a need of bimodal CAs is present to facilitate the access to one imaging technique to another one. Nanoparticles (NPs) were pointed out as suitable biocompatible nanocarriers (NCs) to this end owing to a versatile design, promoting long-time retention and high payload capacity. In this study, we investigated a novel and efficient lipids-based nanoparticulate system as dual modal injectable contrast agent for X-ray imaging and MRI. To this end, we formulated superparamagnetic iron oxide nanoparticles (SPIONs) and iodine-containing PEGylated nano-emulsions (NEs). The strength of these new CAs lie not only in their dual modal contrasting properties and biocompatibility, but also in the simplicity of the nanoparticulate assembling: iodinated oily core was synthesis by triiodo-benzene group grafting on vitamin E (41.7% of iodine) by esterification and SPIONs were produced by high temperature process during 2h, 4h and 6h

(SPIONs 2h, SPIONs 4h and SPIONs 6h) to generate magnetite Fe_3O_4 NPs with different morphology and magnetic property. Discrimination of NEs encapsulating iodinated oil and SPIONs 2h, 4h or 6h was done based on relaxivity parameters (r2,r1) and r2/r1, which means their ability as being efficient CA for MRI. The selected NE was subjected to *in vivo* imaging and administrated to Swiss mice (9% dose). Excellent contrast enhancement was visible by MRI for liver and kidneys whereas X-rays imaging allowed to image liver and spleen. Not only this study provided efficient bimodal CAs but it also provided an understanding of biodistribution and bioaccumulation of such kind of probe and show how complementary MRI and X-ray imaging are.

Keywords

Dual modal nano-emulsion; *in vivo*; magnetic resonance imaging; microcomputed tomography; iron oxide; iodinated oil

Abbreviations

CA	Contrast agent
CT	Computed tomography
DLS	Dynamic light scattering
FBS	Fetal bovine serum
FTIR	Fourier transformed infrared spectroscopy
Micro-CT	Micro-computed tomography
MRI	Magnetic resonance imaging
NE	Nano-emulsion
NP	Nanoparticle
PBS	Phosphate bovine serum
PDI	Polydispersity index
PEG	Poly(ethylene glycol)
ROI	Region of interest
SOR	Surfactant-to-oil weight ratio (surfactant/(surfactant+oil))
SPION	Superparamagnetic iron oxide nanoparticle
TEM	Transmission electron microscopy
TIB	2,3,5-Triiodobenzoic acid
TIB-Cl	2,3,5-Triiodobenzoyl chloride
XRD	X-ray diffraction

1. Introduction

Many advances have been done in non-invasive *in vivo* visualization field not only on the imagers but also on pharmaceutics involved for contrast enhancement. Typical imaging modalities are X-ray computed tomography (X-ray CT), magnetic resonance imaging (MRI), positron emission tomography (PET) or single photon emission computed tomography (SPECT), etc. In any cases, those scanners aim at exploring and checking up the morphology, the anatomy and physiological functions of a region of interest (ROI) *via* reconstructed 2D or 3D images without invasive gesture to patient. Fundamental and technical differences distinguish one imaging technique from the other one such as their physical principle on which they are based on, their resolution, sensitivity, depth of tissues penetration, quantification, etc., which make them quite complementary.[1–4]

X-ray CT scanner is the oldest modality and was developed by G.N. Hounsfield and A.M. Cormark few decades after X-ray discovery by Roentgen (1895). Ever since, the first computer-assisted X-ray scanner set up in clinic (1972), X-ray CT became one of the most used non-invasive tool for insight observation of human body.[5–10] Using the ability of electron-dense materials in body to absorb X-ray beam, X-ray CT images provide details about tissues such as abdomen region (gastrointestinal track, kidneys, liver, spleen), cardiorespiratory system, head, tumors and skeleton due to differences of opacification.[6,11–14] Early diagnostic of soft tissues pathology remains so far quite challenging due to a lack of clear delineation because of subtle changes in their X-ray attenuations. Contrast enhancer pharmaceutics, or contrast agent (CA), based on small hydrosoluble iodinated compounds are generally used. Because of their physicochemical nature promoting high viscosity and osmolality, fast renal clearance once exposed to *in vivo* media and the technique limitation of current X-ray CT, large doses of CA are often administrated causing serious adverse effects on patient health and poor image quality.[7,10,14–16]

In parallel to the development of X-ray CT at clinical stage, MRI development began and tremendous progresses were quickly made in a decade from the first small laboratory animal imaging, the first *in vivo* abdominal investigation[17–19], the first clinical MRI prototype and whole human body imaging[20,21] to real time imaging[22]. Initially inspired by nuclear magnetic resonance[23], MRI aims at providing images by evaluating relaxation times (longitudinal T1 and transverse T2) of water molecules exposed to magnetic field and radiofrequency pulse. Due to their location in the different tissues, each compartment would

have water molecules with their own relaxation speed.[24] Typical contrast agents for MRI are based on gadolinium chelates for T1-weighted MRI and superparamagnetic iron oxide nanoparticles (SPIONs) for T2-weigthed MRI (it should be noted that MRI can also be T2*-weighted MRI which correspond to the measure of T2*, more sensitive to macroscopic magnetization and consequently more accurate than T2-weighted MRI).[25–27]

At clinical stage, X-ray CT and MRI are the most used imaging techniques for disease diagnostic. However, as all advanced techniques, they both suffer from inherent drawbacks. For instance, X-ray CT is cost-effective and short processing time but has very low sensitivity. MRI is much more sensitive and provides detailed images but even if its accuracy is superior to X-ray CT it has a lower resolution and remains expensive to use. Consequently, MRI can complete X-ray CT information to aim to accurate diagnostic. Many others modalities may be combined to obtain detailed images with quantitative data on physiologic functions and health issues. In order to limit the discomfort to patient, a single multimodal CA should be the best alternative in case of multimodal imaging needs. To perform the multiple incorporation of several imaging components into a single formulation, nanoparticles (NPs) and nanocarriers (NCs) seem the perfect match as shown many researches (if no interaction between imaging components occurs).[1,28–33]

Nowadays, early-stage pathology diagnosis through preclinical imaging is moving forward into nanomedicine by the use of innovating and multifunctional nanoprobes as CA. The versatility of NPs makes them really attractive to form a new class of CA with advanced properties such as theranostic property.[2,34] Although, MRI CAs already involved NPs based of inorganic material as abovementioned, literature also showed scope of NPs-based CA for X-ray CT. Typically, studies on NPs dedicated to X-ray imaging used inorganic elements[6,9] like heavy metal (thorium, bismuth, tantalum, etc.), noble metal (gold, silver, platinum) or lanthanide (gadolinium, ytterbium, etc.) and soft NPs[8,10,11,35] made of lipids (nano-emulsion, micelle, liposome, emulsion) or polymeric materials (nanosphere, nanocapsule, dendrimer) in which active compounds can be encapsulated or embedded.

Soft NPs were actually revealed as appealing multivalency nanovehicle platform to carry imaging components to ROI because those can fulfill many requirements: First, i) the cargo can be concentrated in contrasting element, meaning that the encapsulation ratio of contrasting materials is high which allows to ii) reduce the dose to administrate and to iii) cut down side effects and toxicity issues of current CAs. Second, iv) contrast enhancement can be

local by means of specific accumulation of NPs in a ROI. Such targeting can be accomplished thanks to v) a neutral, stealth and hydrophilic surface preventing from premature excretion by involving an hindrance shell based on PEGylated macromolecules ("chameleon effect" fooling opsonins and providing colloidal stability[13,36,37]) in case of passive targeting and with ligands decorating the NPs surface to bond with desired biological entities in case of active targeting. Consequently, *in vivo* fate of NPs including vi) their pharmacokinetic profile and biodistribution, vii) their colloidal stability in physiological environment and viii) their retention time[38] can be controlled due to their tunable design. However, although surface functionalization[39] aims to improve properties from v) to viii), the dimension of the nanoprobes must be considerate as well. Indeed, ix) the size should not be less than 10 nm to avoid renal filtration and more than 200 nm to postpone opsonization process. Finally, a very large scope of materials is now provided in literature so x) all components involved into the NPs construct and all metabolites can be non-toxic and biocompatible to be neutral once exposed to *in vivo* conditions and tissues.[1,4,10,11,13,35,40–44]

Multimodality imaging NPs are so nowadays in line of sights in research not only for all advantages aforementioned but also because such an excellent alternative to clinical CAs remains debates due to their nanoparticulate constitution and all debates concerning the effects of NPs on human health.[45] Studying on small animal is typically the pathway to conduct experiment for further clinical translation for humans. Working with NPs on mice will actually have a double goal: i) mice have small blood pool volume rendering administration delicate to handle but the high payload in contrasting materials of NPs would provide enough contrast for a small volume to administrate[13,46] and ii) the multimodality will provide enough details of mice anatomic and physiologic functions and consequently details of NPs effects on mice health and answer to current debates on NPs and health.

Herein, we describe a novel and simple strategy of formulation of bimodal NPs CA relying on the spontaneous nano-emulsification of iodinated oil (triiodobenzene-grafted vitamin E) and SPIONs based on lipophilic magnetite Fe_3O_4, respectively for X-ray CT and T2-weighted MRI contrast enhancement. Recent studies proved that iodinated oil trapped within nano-emulsion core exhibited strong contrast enhancement for X-ray CT during *in vivo* assays.[47,48] Same observations have been done about Fe_3O_4 encapsulation in nano-droplets for T2-weighted MRI contrast.[49,50] This work covers all the aspects of the development of a new nanoparticulate contrast agent for soft tissues imaging by X-ray CT/MRI, from syntheses to formulation of the bimodal nano-emulsion, physicochemical characterization and

in vivo applications. A particular attention was paid to the SPIONs and the impact of their design on their relaxivity property. A selection of the optimum formulation was done based on properties, such as the contrasting material content, the biocompatibility and the physico-chemical characteristics, needed for *in vivo* imaging.

2. Materials and Methods

2.1. Materials

The synthesis was carried out using commercially available agents. Absolute ethanol, cyclohexane, dichloromethane (DCM), diphenyl ether, ethyl acetate and hexane were used as received. 2,3,5-Triiodobenzoic acid (TIB), 4-dimethylaminopyridine, 1,2-dodecanediol, α-tocopherol, iron(III) acetylacetonate ($Fe(acac)_3$), oleylamine, oleic acid, triethylamine and thionyl chloride were purchased from Sigma-Aldrich (France). Non-ionic surfactant (Kolliphor ELP® Castor oil PEG-35) was donated by Laserson (Etampes, France). Kolliphor ELP® is a parenteral grade nonionic hydrophilic surfactant made by reacting ethylene oxide to castor seed oil at an ethylene oxide to oil molar ratio of 35[51]. Phosphate buffered saline (PBS) Dulbecco's modified Eagle medium (DMEM) was from PAN Biotech (Aidenbach, Germany).

2.2. Syntheses and formulations

2.2.1. Synthesis of magnetite iron oxide nanoparticles by thermal decomposition

A modified procedure of thermal decomposition from both works Sun *et al.*[52] and Wang *et al.*[53] was applied here to form lipophilic Fe_3O_4 SPIONs (Figure 1): $Fe(acac)_3$ (2 mmole or 0.71g), 1,2-dodecandiol (10mmole or 2.02g), oleic acid (6 mmole or 2ml), oleylamine (6 mmole or 2ml) and diphenyl ether (20 ml) were mixed and magnetically stirred in a 100ml round bottom flask. The mixture was heated to reflux (200°C) in an oil bath. The black-brown oily mixture was then cooled to room temperature by removing the heating source and purified by dialysis against ethanol (~ 5 cycles). A black material precipitated within the dialysis membrane and was displaced in a round bottom flask. Ethanol was then removed from the product under reduced pressure. The final black product was finally dispersed in hexane (10 ml) to form stock solution of black ferrofluid containing SPIONs. The aforementioned reflux process was carried out over 2h, 4h and 6h to produce 3 batches of SPIONs (SPIONs 2h, SPIONs 4h and SPIONs 6h) with different morphological and magnetic

properties. Final suspensions in hexane of SPIONs were consequently and respectively based on SPIONs 2h, SPIONs 4h and SPIONs 6h.

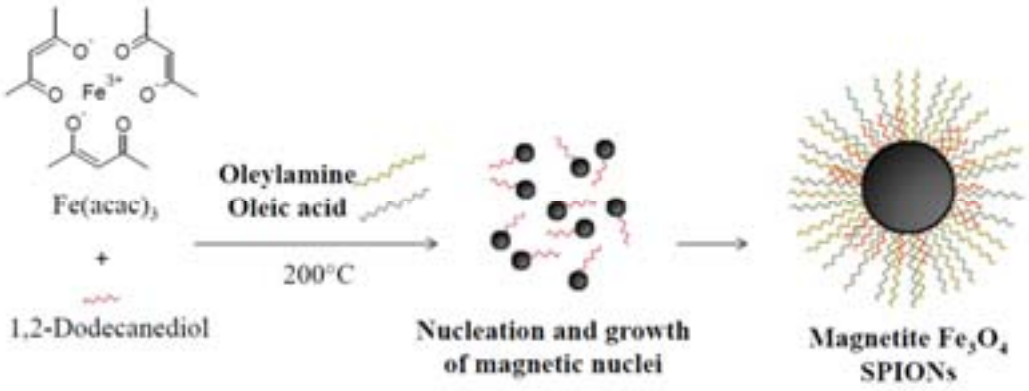

Figure 1: Schematic representation of SPIONs synthesis by thermal decomposition.

2.2.2. Synthesis of iodinated vitamin E or α-tocopherol by esterification

Thionyl chloride (103 mmole, 20 mL) was added dropwise to a magnetically stirred solution of 2,3,5-triiodobenzoic acid (20.0 mmole, 10.0 g) in 400 mL of DCM cooled by an ice bath. After completion of the addition and solubilization, the reaction mixture was heated to reflux at 75°C for 3h. The excess of thionyle chloride was removed under reduced pressure. The as-preprared triiodobenzoyl chloride (TIB-Cl) (11.6 mmole, 6.00 g) and 4-dimethylaminopyridine (2.10 mmole, 0.26 g) were sequentially added to a magnetically stirred solution of α-tocopherol (11.6 mmole, 5.00 g) in DCM (400 ml). Triethylamine (23.2 mmole, 3.23 ml) was added dropwise to the previous mixture cooled by ice bath and covered by a blanket of nitrogen. The esterification reaction was performed over 24h at room temperature and kept under a blanket of nitrogen. The organic phase was then washed with 1N HCl solution, saturated $NaHCO_3$ solution and saturated NaCl solution and dried with anhydrous Na_2SO_4. Dichloromethane was removed under reduced pressure and the product was purified by gradient elution method on silica gel column using cyclohexane and ethyl acetate as eluent. Reactions produced a yellow oily product with a 76% yield and iodine content 41.7%. The scheme of syntheses is reported in Figure 2.

^{1}H NMR spectra was obtained with a Bruker Top Spin 3.0 operating at 400 MHz using deuterated chloroform ($CDCl_3$) as a solvent. Chemical shifts (δ) were expressed in ppm from tetramethylsilane as internal reference: 1H NMR ($CDCl_3$, δ/ppm) 8.34 (s, 1H, H^6), 8.05 (s,1H, H^4), 2.63 (t, 2H, H^{14}), 2.15 (s, 6h, H^{31}, H^{32}), 2.10 (s, 3H, H^{30}), 1.83 (m, 2H, H^{15}), 1.59 (m, 3H,

H^{20}, H^{24}, H^{28}), 1.28 (s, 3h, H^{33}), 1.27 (m, 18H, all CH_2), 0.89 (d, 9H, $3CH_3$) and 0.88 (d, 3H, $1CH_3$).

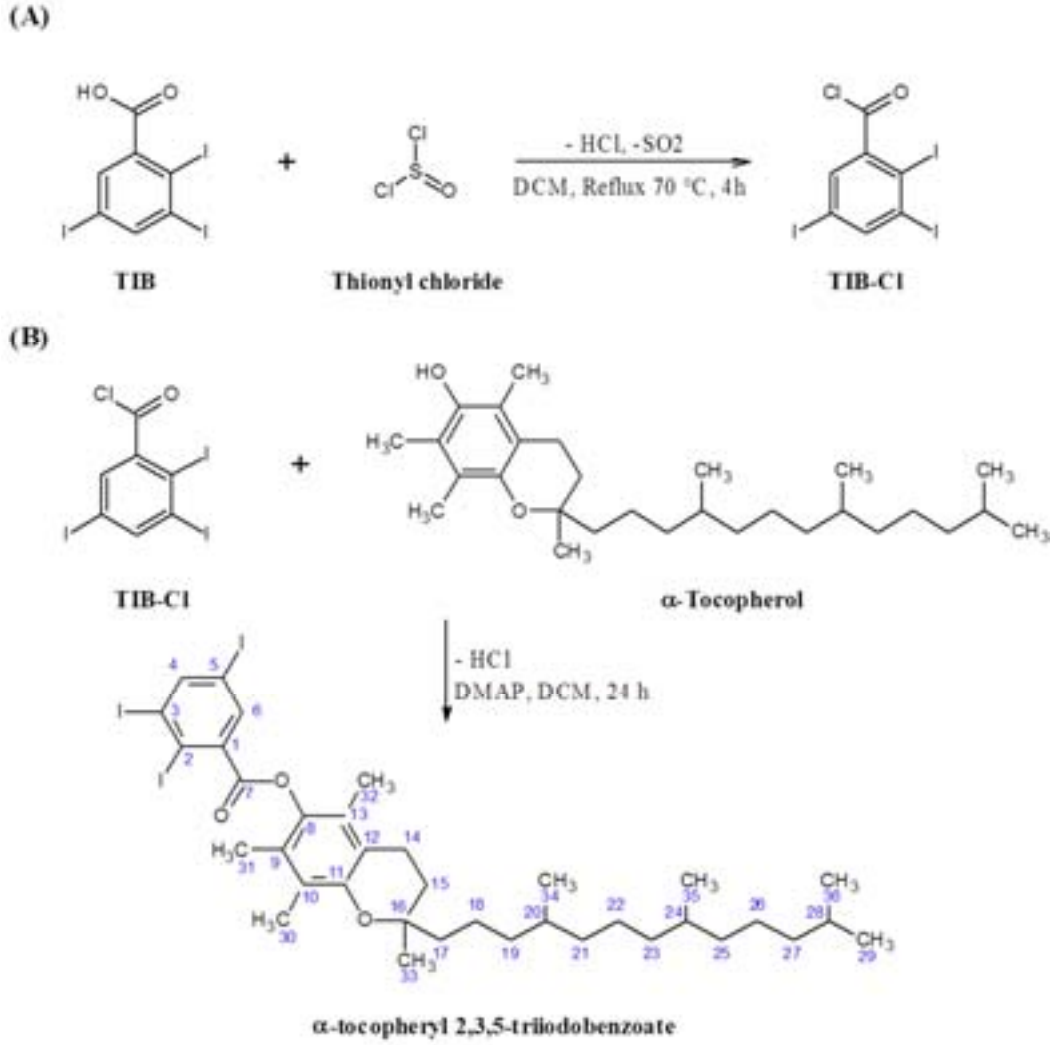

Figure 2: Syntheses of (A) TIB-Cl synthon and (B) iodinated oil, α-tocopheryl 2,3,5-triiodobenzoate.

2.2.3. Formulation of NEs

NEs were formulated by spontaneous nano-emulsification process as previously reported.[45,46,52–54] Formulation parameters were elected to provide NE with optimum nano-droplets size, size distribution and iodine content. They were defined by weight ratio such surfactant-oil weight ratio (SOR) 40 wt.% and surfactant-oil-water weight ratio (SOWR) 40 wt.%. More precisely, NEs were composed of 0.28 wt.% SPIONs (ligands attached onto Fe_3O_4 SPIONs core were neglected for calculations), 23.72 wt.% iodinated oil (9.89 wt.% of iodine), 16 wt.% surfactant and 60 wt.% PBS.

$$SOR = 100 \times \frac{w_{surfactant}}{w_{surfactant} + w_{iodinated\ oil} + w_{SPIONs}}$$

$$SOWR = 100 \times \frac{w_{surfactant} + w_{oil} + w_{SPIONs}}{w_{surfactant} + w_{iodinated\ oil} + w_{SPIONs} + w_{PBS}}$$

Briefly, the oil phase (0.2372 g) was mixed to an aliquot of SPIONs in hexane (0.0028 g of SPIONs 2h, 4h or 6h) by vigorous vortex. Kolliphor ELP® (0.16 g) was then added to the resulting oily and magnetic mixture (0.24 g). Hexane was then allowed to evaporate by heating. Homogenization was carried out by Thermomixer® (70°C, 2000 rpm, 10 min). PBS (0.6 g) was finally quickly poured to the hot mixture. Emulsification was performed by vortex to lead to NE-SPIONs 2h, NE-SPIONs 4h and NE-SPIONs 4h respectively along with SPIONs 2h, 4h and 6h encapsulated within iodinated oily cores. NEs were sterilized by filtration through 0.22 µm polyethersulfone (PES) membrane.

2.3. Characterizations

2.3.1. Fourier transform infrared spectroscopy (FTIR)

Chemical structure was determined by FTIR analysis. FTIR spectra were recorded at room temperature with Nicolet™ 380 routine FT-IR spectrometer apparatus, Thermo Electron Corporation, on dried samples pressed between internal reflection element crystal and gripper plate. Scanning was done in the range between 4000-400 cm^{-1}. Resolution of 4 cm^{-1} at 32 scans was used.

2.3.2. X-ray diffraction (XRD)

Determination of crystalline phase of SPIONs was performed by XRD study. XRD patterns of powdered SPIONs were recorded and taken from SmartLab® Rigaku instrument equipped with Cu-Kα (λ = 1.5406 Å) tube as radiation source of X-ray beam. Samples were scanned over 2σ range from 20° to 70° with a step size of 0.02° at room temperature (25°C). Generator voltage and tube current were respectively 40 kV and 40 mA.

2.3.3. Transmission electron microscopy (TEM)

X-ray attenuation properties of iodinated oily core of NEs and the inorganic nature of SPIONs also result in good contrast by TEM without using negative staining agent. TEM pictures of SPIONs were taken using a JEOL 2100F electron microscope operating at 200 kV. TEM was performed on a drop of SPIONs suspension (3.5 mg/mL in hexane) deposited on carbon coated mesh (carbon type-A, 300 mesh, copper, Ted Pella Inc. Redding, PA) and air-

dried for 5 min. NEs were subjected to TEM using Philips Morgagni 268D operating at 70 kV (lower voltage was applied in order to avoid any oil vaporization due to electron beam in TEM chamber). They were diluted with MilliQ water (1/2000), deposited on grid and rested for 15 min at 60°C before observation by electron microscope.

2.3.4. Dynamic light scattering (DLS)

Size distribution, polydispersity indices and zeta potential (ξ) were measured by DLS with a Malvern apparatus (NanoZS®, Malvern, Orsay, France). Mean particle size was assimilated to z-average hydrodynamic diameter and the width of size distribution to polydispersity index (PDI). DLS measurements were run by the use of helium/neon laser, 4 mW, operated at 633 nm, with the scatter angle fixed at 173° and temperature maintained at 25 °C on diluted sample. DLS data were analyzed using a cumulant-based method assuming spherical shape. All experiments were performed in triplicate.

2.3.5. Iron titration by relaxometry measurement

To ensure the amount of SPIONs encapsulated within the nano-droplets' oily core, determination of the weight ratio between ligands-based capping layer and the magnetic core was carried out by iron titration[57] using Minispec MQ60 NMR Relaxometer. To this end, a complete dissolution of iron oxides NPs is required by digestion *via* acidic and oxidative solutions. The general procedure is the followed one: an aliquot of SPIONs (3.2 mg) from their stock organic solution was placed in glass vial before being dried. After complete removal of solvent, distilled water (100 µL), nitric acid 69% (900 µL) and hydrogen peroxide (30%) (300 µL) were added. The vial was then sealed and subjected to heating at 80°C leading to a limpid yellow ferric solution. Mineralization is basically carried out to solubilize SPIONS and to oxidize ferrous ion Fe^{2+} into ferric ions Fe^{3+}. After digestion completion, solution was diluted to reach 2% as nitric acid concentration in order to get along with measurement method set in Minispec Bruker instrument. The relaxation rate R1 or 1/T1 value of mineralized magnetite NPs was recorded at 37°C and 1.41T. Iron concentration was then estimated from calibration curve (Figure 3) built by measuring the R1 relaxation rate of various Fe^{3+} standard solutions in 2% nitric acid.

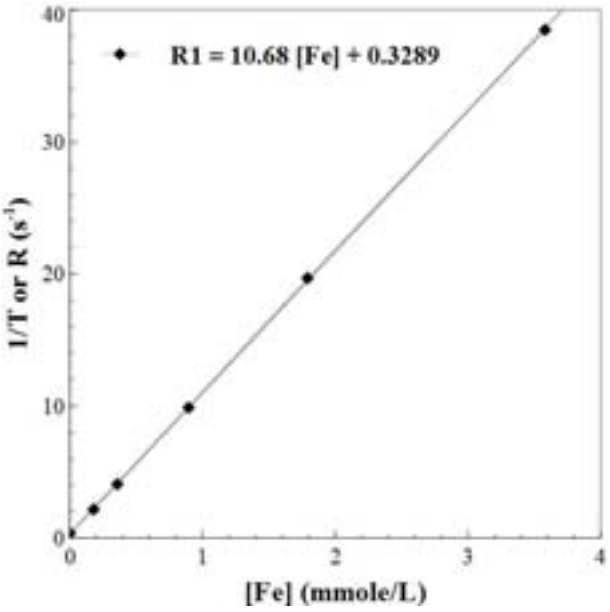

Figure 3: Standard curve of R1 *vs* iron concentration (1.41 T in 2% HNO_3 at 37°C) (R^2 = 0.999).

2.3.6. Relaxivity measurement

All NEs were subjected to relaxometry measurement to evaluate their potential as T2-weighted MRI contrast agent. For each NE, concentration series were done by dilution over a range of iron concentration from 0.8 to 3.5 mmole Fe/L with MilliQ water. Relaxometry properties were then investigated on aliquots (200 µL) of each diluted samples by measuring T1 and T2 relaxation times using Minispec MQ60 NMR Relaxometer operating at 37°C and 1.41 T. Plots of iron concentration *vs* T1 and T2 provided respectively longitudinal and transversal relaxivities r1 and r2 parameters of NEs. The sample exhibiting highest transverse relaxometry parameters and r2/r1 ratio was selected for *in vivo* dual modal X-ray CT/MR imaging. Relaxivities measurement by MRI (7 T) was performed on the selected bimodal NE to evaluate *in vitro* r2, r1 and r2/r1 at similar magnetic field than during imaging procedure. Same dilution range of the optimal NE was used for relaxivities measurement by MRI.

2.3.7. Stability of NEs in serum

Evaluation of colloidal stability of nanodroplets once exposed to biological environment was carried out by incubation of NE (0.1 mL) in FBS (0.9 mL) at 37°C. Concentration of NE in FBS was chosen to correspond to the one in blood after injection. Size distribution was monitored over 24h (1h, 2h, 3h, 6h, 18 h and 24h) in order to determine potential degradation of NEs and/or protein adsorption onto NEs that might influence NEs pharmacokinetics once administered to mice.

2.4. In vivo experiment

2.4.1. MRI

Abdominal exploration by MRI was performed with a 7T Biospec 70/20 Avance III scanner (Bruker Wissembourg, France) equipped with an horizontal bore magnet, a G12S gradient system (675mT/m) and a resonant circuit 35 mm. Data were collected using ParaVision 6.0.1 software (Bruker Wissembourg, France). Swiss mice (34 g) were placed in mice bed and monitored by following respiration rate (30-40 resp/min) with chest probe (gating parameters were adjusted to coincide with respiratory motion) and body temperature regulated at 38°C with heating pad. Acquisition by MR scanner was performed prior to and after administration of a 9% of blood volume administration (250 µL of selected NE) through the vein tail once mice were anesthetized with 5% isoflurane. Anesthesia was maintained with 0.5-1% isoflurane (0.5 L O_2/min) during MR protocol. Anatomical exploration was performed to confirm position of animal for abdominal investigation. RARE sequence was applied with following parameters to this end: TE = 24 ms, TR = 730 ms, nex = 8, RF = 8, 30*30 mm field of view, 256*256 matrix, 9 axial slices thickness of 1 mm. T2-weighted MR images were acquired using MSME sequence with the following parameters: 25 TE (TE = 4.5 ms), TR = 2000 ms, alpha 50, 30*25 mm field of view, 256*128 matrix, 9 axial slices thickness of 1 mm. T2*-weighted MR images were recorded with MGE sequence with following operating conditions: 10 TE (TE = 1.7 ms), IE = 1.35 ms, TR 800 ms, alpha 50, 30*25 mm field of view, 64*64 matrix, 9 axial slices thickness of 1 mm. Signal quantification for T2- and T2*-weighted MRI was performed by placing region of interest (ROI) in abdominal muscle, liver, spleen and kidneys and measuring T2 and T2*. Scans were performed before administration, immediately after injection, and after 1h, 5h, and 24h.

2.4.2. X-ray micro-CT

In vivo X-ray micro-CT analyses of the abdominal region of injected mice were performed using SkyScan 1076 X-ray computed micrograph (Bruker, Aartselaar, Belgium) dedicated to preclinical research equipped with an X-ray tube working at 49 kV/200 µA. The rotation step was fixed at 0.5° and exposure, which was done with a 0.5 mm aluminum filter, at 70 ms. Specimen were imaged at 37.92 microns per pixel resolution. Acquisitions were performed on Swiss mice 24h post-injection of the selected NE, mice were anesthetized with xylazine/ketamine injection. For each specimen, 900 axial 2D sections were obtained for the

abdominal region to image liver, spleen and kidney after 2D reconstruction using SkyScan NRecon software. The micro-CT images were treated with OsiriX viewer to quantify the signal by placing the region of interests in the liver, the spleen and the kidneys. At the end of the imaging protocols, the animals were sacrificed and tissues of interest were collected for potential *ex vivo* quantification.

3. Results and Discussions

Lipids-based NEs become more and more used as pharmaceutics owing to their potential to improve active pharmaceutical ingredient bioavailability and efficiency once administrated to living organism. Simple method of NE formulation relying on low-energy nano-emulsification technique allows to prepare monodisperse, stable and non-toxic colloidal suspension, perfectly suitable to intravenous injection. In our study, we choose biocompatible and PEGylated surfactant in order provide strong oil/water interface, stable entrapment of the contrasting materials and anti-fooling immune system property for long-time retention within the blood pool. As to the bimodal contrasting materials trapped within the NEs' inner core, they required few steps of preparations before being formulated with the surfactant into NEs. Indeed, using a two imaging components core to form oi-in-water NE led us to synthesis the oily phase, made of iodinated vitamin E offering radiopaque property to our formulations, as a dispersion phase for Fe_3O_4 SPIONs for the MRI contrast, also prepared here as shown in the experimental section. Typical dual modal nanovehicles were so formulated with iodinated vitamin E or α-tocopherol and Fe_3O_4 SPIONs. Optimal NEs were produced taking in account compromise between size distribution, polydispersity and contrasting materials content for both SPIONs and radiopaque oil to make sure that NEs will i) not be subjected to premature opsonization and renal filtration and ii) be capable of being accumulate in ROI with enough contrasting cargo to iii) ensure significant contrast for both imaging modalities after being injected to mice.

Iodinated vitamin E or α-tocopherol has already been shown as excellent liver contrast enhancer product once formulated with SOR 40% and has not been reported as toxic on small laboratory animal.[48] Simple esterification process allowed to graft triiodobenzene carboxylic acid on vitamin E and yield iodinated oil with 41.7 wt.% of iodine.

Elaboration of SPIONs can rely on very original and numerous pathways (coprecipitation, thermal decomposition, microemulsion, sonochemical method, hydrothermal technique…)

but according to our expectations to involve SPIONs as an efficient T2- and T2*-weighted MRI CA, SPIONs needed to possess specific physicochemical and magnetic properties.[58–60] This is why we selected thermal decomposition as method of synthesis in order to form monodisperse and highly magnetic nanocrystals of magnetite Fe_3O_4 with aliphatic C_{18} carbon chains as lipophilic ligands for stable dispersion within a lipidic media. As a proof of concept, we went over a dispersion study of SPIONs in a range of solvents from polar protic and aprotic solvents to apolar and aprotic solvent. Basically, this fast and concise assessment was to confirm qualitatively that the outer shell of SPIONs was hydrophobic and lipophilic to promote stable SPIONs encapsulation into the lipids-based core of NEs. Not only SPIONs should have been easily dispersed in oil but they should not have had affinity for aqueous media in order to prevent them from leaking from the inside to the outside of nano-droplets. Figure 4 shown trials of dispersion of SPIONs 2h, SPIONs 4h and SPIONs 6h from most hydrophilic and lipophobic solvents to most hydrophobic and lipophilic ones by means of adding milliQ water (H_2O), methanol (MeOH), ethanol (EtOH), dimethyl sulfoxide (DMSO), acetone, pyridine, tetrahydrofurane (THF), DCM, cyclohexane and hexane to aliquot of dried SPIONs. For all batch of SPIONs (2h, 4h or 6h), SPIONs behaved in same fashion once in contact with the abovementioned selection of organic and aqueous media. As predicted, SPIONs were all well-dispersed in solvent closer to lipophilic media regarding their proticity and polarity (from THF to hexane). Consequently, it was expected, and proved in Figure 4, that mixture of SPIONs with polar solvents (from H_2O to pyridine) would not have led to homogeneous magnetic colloidal suspension. In such environment, SPIONs remained mostly stick on vial wall, a little part of the amount of SPIONs were able to mix with EtOH, acetone and a bit more in pyridine but without leading to a complete and nice dispersion of whole aliquots.

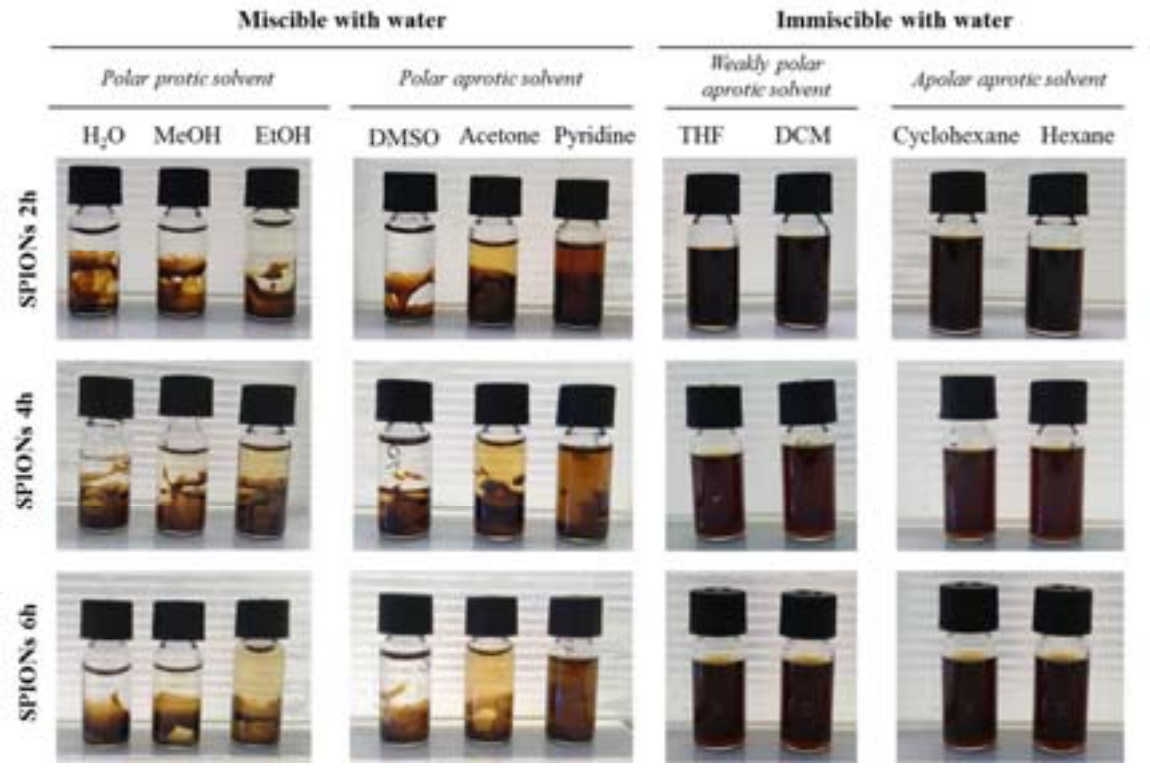

Figure 4: Dispersion of SPIONs in MillQ water (H_2O), methanol (MeOH), ethanol (EtOH), acetone, pyridine, tetrahydrofurane (THF), DCM, cyclohexane and hexane. Solvents were categorized according to their water-solubility along with their polarity and proticity from (left) the most polar and protic solvent to (right) the most apolar and aprotic solvent.

To go further in details of the characterization of SPIONs, the physico-chemical properties were investigated. As introduced, we attempted here to find out optimum magnetite SPIONs to formulate suitable dual modal contrasting NEs. It is well-referred about magnetic NPs that the size and morphology are both key-parameters impacting drastically magnetism and, in our case of nano-scale magnetic particles, the superparamagnetism. This is why we tried here to explore as much as possible the reaction medium to get most efficient SPIONs in regard to their contrast enhancement ability. To this end, we selected three different times of reaction, 2h, 4h and 6h, to evaluate impact of size and morphology on the NEs magnetism.

Morphology and size distribution estimation of Fe_3O_4 SPIONs were investigated by TEM. As depicted by Figure 6, shape and size of SPIONs were subjected to the influence of time of reaction owing to a subtle change of their morphology. After 2h of thermal decomposition process, SPIONs 2h exhibited spherical and a narrow size distribution estimated at 5 to 7 nm. Increasing reaction time to 4h as illustrated by Figure 5 proved that SPIONs 4h were still subjected to reactant content since SPIONs 4h appeared much more anisotrope in shape and slightly larger (7-10 nm). Finally, after 6h at 200°C, SPIONs 6h did not increase in size but

looked smoother on their boundaries and consequently more spherical and uniform. As a result, keeping heating SPIONs did not yield to particles bigger and bigger because size remained similar after 4h and 6h but impacted the general form of the SPIONs demonstrating the possibility to rearrange the SPIONs structure along with the heating range. Typically and as Sun *et al.*[52] shown in their works on seed-mediated growth process on SPIONs, SPIONs can be assimilated to seeds which can be fed during the thermal process and grow as long as reactants are present in enough quantity to make nucleation process continue. Here, it appeared clearly that SPIONs 4h are like an intermediary step in the SPIONs growth since SPIONs 2h and 6h possess both spherical shape, proving that at that time of reaction SPIONs 4h were like seed feeding by the reactant media with Fe_3O_4 nuclei. It seems as well, that up to 6h of reaction no significant change would be visible owing to the absence of change of size distribution after 4h and 6h.

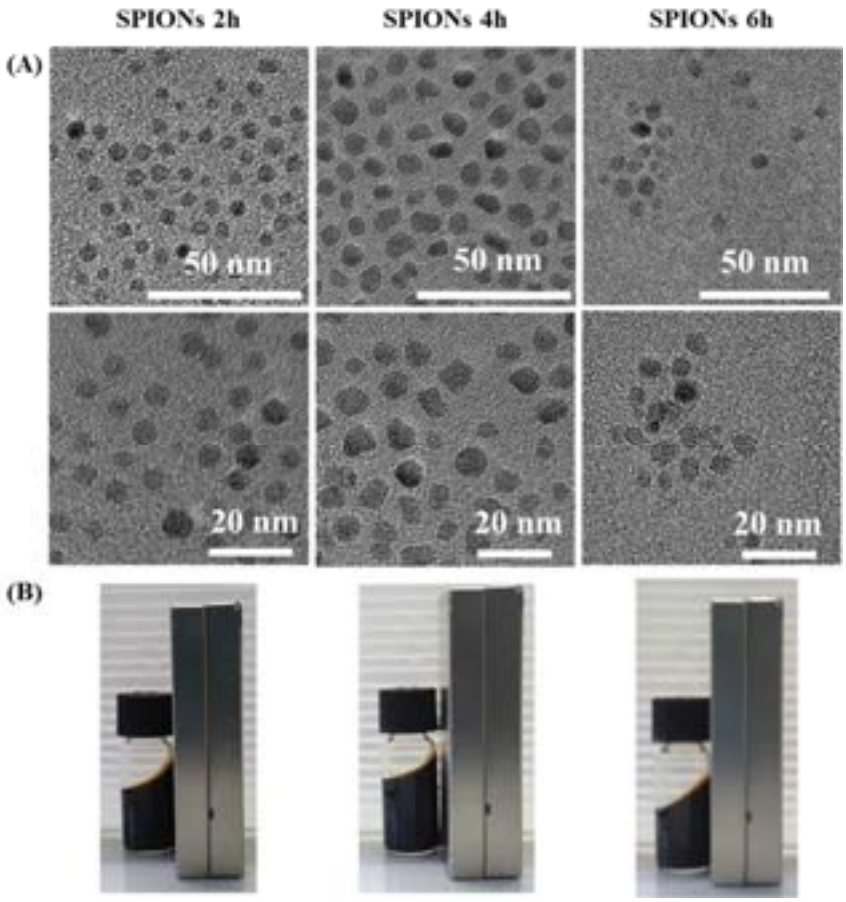

Figure 5: (A) TEM pictures of SPIONs 2h, SPIONs 4h and SPIONs 6h (from left to right) at different magnification. (B) Visual aspect near magnet of ferrofluids formed by dispersion of SPIONs 2h, SPIONs 4h and SPIONs 6h in hexane.

On the hand, storage in hexane was an excellent choice to protect SPIONs from air oxidation and aggregation by keeping them in colloidal ferrofluid dispersion. On the other hand, it also proved that SPIONs were lipophilic due to their good affinity with such apolar solvent (Figure 4).

To confirm observation in Figure 4 *via* an analytical technique, FTIR investigation was so performed to shown presence of lipophilic and aliphatic ligands onto the SPIONs surface. FTIR was also an efficient technique to determine SPIONs phase. It is not rare that Fe_3O_4 SPIONs with small dimension possess a high surface-to-volume ratio and are so very sensitive to oxidation on their surface because of the large surface available for oxidation by oxygen from the air. Phenomenon of oxidation of magnetite, which is basically a mixed iron oxide since it contains both ferric Fe^{3+} and ferrous Fe^{2+} ions, provide maghemite (γ-Fe_2O_3) iron oxide, the oxidative form of Fe_3O_4 based on Fe^{3+} ions only. Typical FTIR spectra (Figure 6) of SPIONs 2h, 4h and 6h were all identical. Basically they all reveal bands relative to iron oxide at 590 cm^{-1} and 440 cm^{-1} for the vibration and stretching of Fe-O bonds suggesting the formation of Fe_3O_4 phase. However, a shoulder at 720 cm^{-1} indicates the presence of an oxidative phase of iron oxide which is attributed to an outer layer of maghemite onto the main core of SPIONs. As to the detection of aliphatic C_{18} carbon chain ligands on SPIONs, a double broad band at 2920 cm^{-1} and 2851 cm^{-1} was observed and assimilated to $–CH_2$ bonds stretching, a small peak around 2990 cm^{-1} was considered a $–CH_3$ stretching bond (owing to the length of the carbon chains of ligands, it seems normal that $–CH_2$ bands are much more intense than $–CH_3$ one). Oleylamine and oleic acid ligands possess C_{18} carbon chains as just revealed on FTIR spectrum of SPIONs but have also a double bond on C_9 position visible on FTIR as several small peaks from 1670 cm^{-1} to 1640 cm^{-1}. Double broad band and single one from 3000 cm^{-1} to 2800 cm^{-1} were both observed on pure ligands FTIR spectra also presented on Figure 6. The absence of peak with high intensity corresponding to C=O stretching from oleic acid at 1708 cm^{-1} on SPIONs spectra was mainly attributed to the absorption of the oleic acid onto SPIONs surface through electrostatic bond between the carboxylic acid function of oleic acid and the magnetic core of SPIONs. It could also have been assumed that the aforementioned peak was misled with double bond peaks from1670 cm^{-1} to 1640 cm^{-1} due to potential shifting of peaks because of coordination.

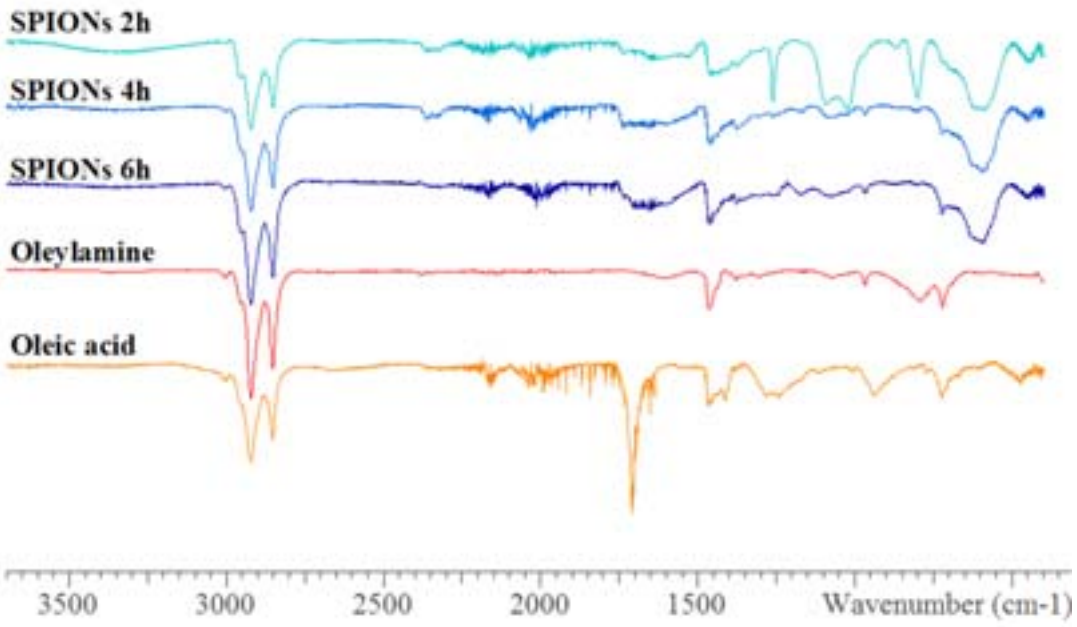

Figure 6: FTIR spectra of SPIONs 2h, SPIONs 4h, SPIONs 6h and lipophilic ligands (oleylamine and oleic acid).

To complete information extracted from FTIR investigation, XRD analyses were carried out to find diffraction peaks specific to iron oxide crystals on XRD patterns. Position and relative intensity of all diffraction peaks from the diffraction patterns of SPIONs 2h, 4h and 6h (Figure 7), recorded and attributed to lattice planes (220), (311), (400), (422), (511) and (440), match well with the structure of Fe_3O_4. Additional peaks might be visible on patterns at smaller angle and attributed to γ-Fe_2O_3 lattice planes but no quantitative information was surely recorded.

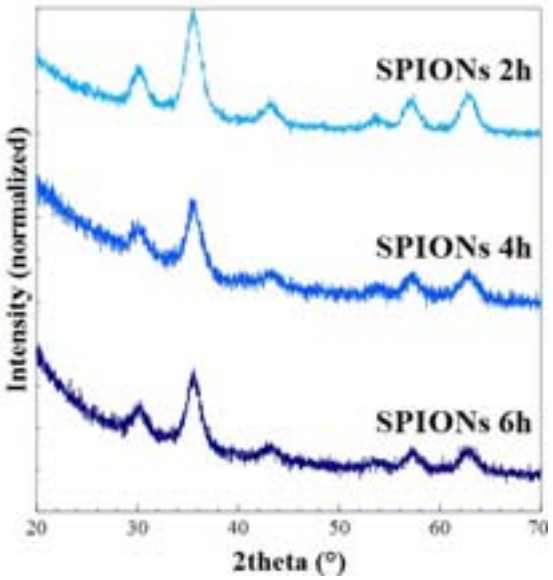

Figure 7: Diffraction patterns of SPIONs 2h, SPIONs 4h and SPIONs 6h (λ(Cu-Kα) = 1.5406 Å).

Distances between two adjacent planes (d_{hkl}) in lattice were calculated with Bragg's law ($2\times d_{hkl}\times \sin\theta = n\times\lambda$), all lattice spaces are displayed in Table 1 and corroborated that nanocrystals have spinel structure and were consequently based on magnetite iron oxide.[52]

Table 1 : Calculated lattice spacing from Bragg law along with indexes obtained from XRD measurement in Figure 8 (n = 1, $\lambda_{(Cu\text{-}K\alpha)}$ = 1.5406 Å).

	hkl	**220**	**311**	**400**	**422**	**511**	**440**
SPIONs 2h	d_{hkl} (Å)	2.99	2.53	2.10	1.71	1.60	1.48
SPIONs 4h	d_{hkl} (Å)	2.97	2.56	2.09	1.71	1.60	1.48
SPIONs 6h	d_{hkl} (Å)	2.95	2.52	2.11	1.72	1.61	1.49

Owing to the need to have lipophilic SPIONs for efficient encapsulation within an NE oily core, lipophilic ligands were involved during the synthesis of SPIONs and were adsorbed onto SPIONs surface as it has also been proved by FTIR investigation and by the excellent dispersion of SPIONs in several organic solvents. Because of the high sensitivity of MRI to the CA concentration within a ROI, the accurate concentration of SPIONs and more precisely the iron content must be determined.

The as-prepared SPIONs all include an organic part in their structure. As depicted before by Figure 4 and 6, SPIONs possess an organic outer layer providing them lipophilic surface property and steric barrier against aggregation. The next part on the study aims at quantifying the weight content of iron and ligands. SPIONs were so digested in a mixture of nitric acidic and hydrogen peroxide at 80°C to dissolve Fe_3O_4 core into a mixture of ferrous and ferric ions upon oxidation of Fe^{2+} ferrous ions into Fe^{3+} ferric ions. The as-digested solution was subjected to relaxometry measurement at 2% nitric acid. Weight ratio between iron and ligands was so elucidated for each batch of SPIONs as summarized in Table 2. Briefly, all SPIONs 2h, 4h and 6h have their own magnetite and ligands content ranging from 57 wt.% Fe_3O_4 to 46 wt.% Fe_3O_4 and from 54 wt.% ligands to 43 wt.% ligands, which indicated that SPIONs were based on around half magnetic core and half lipophilic shell. The first point to highlight here is that not only the time of reaction impacted the morphology and the size distribution of SPIONs like shown by TEM investigation (Figure 5) but also the accumulation of ligands onto the SPIONs surface. Considering now values for each batch of SPIONs, SPIONs 2h, 4h and 6h contain respectively 54.44 wt.% Fe_3O_4 (39.50 wt.% Fe), 56.86 wt.% Fe_3O_4 (41.26 wt.% Fe) and 46.26 wt.% Fe_3O_4 (33.58 wt.% Fe). As a result, it appears that the highest magnetite content is in SPIONs 4h. Compared to the batch with the lowest magnetite

content, the SPIONs 6h, a difference of 18 % can be estimated. SPIONs 2h got a difference of 15% of magnetite content with SPIONs 6h and a difference of 4% of magnetite content with SPIONs 4h. Once more, SPIONs 4h stand out from the crowd due to a weight composition much more based on inorganic and magnetic materials than organic ones. Consequently, owing to the iron content in magnetite of 73.56 wt.% Fe, the iron contents for SPIONs 2h, 4h and 6h were respectively 39.50 wt.% Fe, 41.26 wt.% Fe and 33.58 wt.% Fe.

Table 2: Quantification of the magnetite Fe3O4, iron and ligands contents in SPIONs 2h, SPIONs 4h and SPIONs 6h *via* iron titration by relaxometry measurement.

	SPIONs 2h	**SPIONs 4h**	**SPIONs 6h**
Fe_3O_4	54.44 wt.%	56.86 wt.%	46.28 wt.%
Iron	39.50 wt.%	41.26 wt.%	33.58 wt.%
Ligands	45.56 wt.%	43.14 wt.%	53.72 wt.%

Such difference of inorganic and organic material weight ratio may have been explained by the change of morphology (size and shape) for each batch of SPIONs. In fact, since these three batches of SPIONs had their own size and shapes, the surface-to-volume ratios were for sure altered along with the time of reaction leading to different surface available for ligands adsorption.

The next part of this work will be now focused on the formulation of magnetic and radiopaque NE. All NEs were formulated with same parameters in order to possess similar composition and weight ratio in radiopaque oil, nonionic PEGylated surfactant, SPIONs, and dispersion phase, here a biocompatible phosphate buffer (pH 7.4). Nanoparticulate bimodal contrast agents were so prepared with followed conditions: 0.28 wt.% SPIONs, 23.72 wt. % iodinated vitamin E, 16 wt.% PEGylated surfactant and 60 wt.% PBS. Parameters were fixed in such way to get good stability and good compromise between the size distribution and the polydispersity. All NEs were subjected to physico-chemical characterizations to determine the size distribution by DLS and their general aspect by TEM investigations. Basically, NEs showed very good size profile and monodispersity (Figure 8A). Mean size ranged 60.65 nm (PDI0.145), 57.87 nm (PDI 0.148) and 62.16 m (0.154) respectively for NE-SPIONs 2h, NE-SPIONs 4h and NE-SPIONs 6h. NEs were so very similar regarding their size distribution and were all compatible for injection following the requirements mentioned about the use of NPs for *in vivo* purpose (see Introduction section). As to TEM micrographs (Figure 8B), pictures disclose important information about the nano-droplets structure and morphology.

The iodinated core of nano-droplets led to negative contrast because of the attenuation of the electron beam by heavy element grafted on the modified vitamin E. However, images showed homogenous droplet with spherical shape and well-dispersed, no flocculated or coalesced droplets were observed. Size distributions were a bit larger than those acquired by DLS, indeed, TEM investigation involve to dry specimen which may have promotes droplet spreading on grid, but generally dried NEs remained based on nano-droplets. Altough nano-droplets were clearly visualized by TEM, their inner cores were not observed. Consequently, SPIONs were not detected on TEM pictures, however since SIONs were lipophilic, they must have been expected within the nano-droplet core. To investigate and confirm the SPIONs were loaded inside nano-droplets, iodinated vitamin E was substitute by a non-radiopaque oil, Labrafac™ Lipophile WL 1349, and SPIONs were formulate into a NE using same conditions of preparation. Figure 8C shows TEM pictures of such non-radiopaque NE, images clearly disclosed homogenous nano-droplet and presence of SPIONs within droplet core. SPIONs seems perfectly dispersed in the oily core and do not aggregate after formulation into NE. None free SPIONs were found, except those from nano-droplets spread and altered by the preparation of the specimen for TEM investigation. Briefly, such microscopic investigation can be used as a proof a concept to confirm that SPIONs were indeed included within the inner part of the droplets.

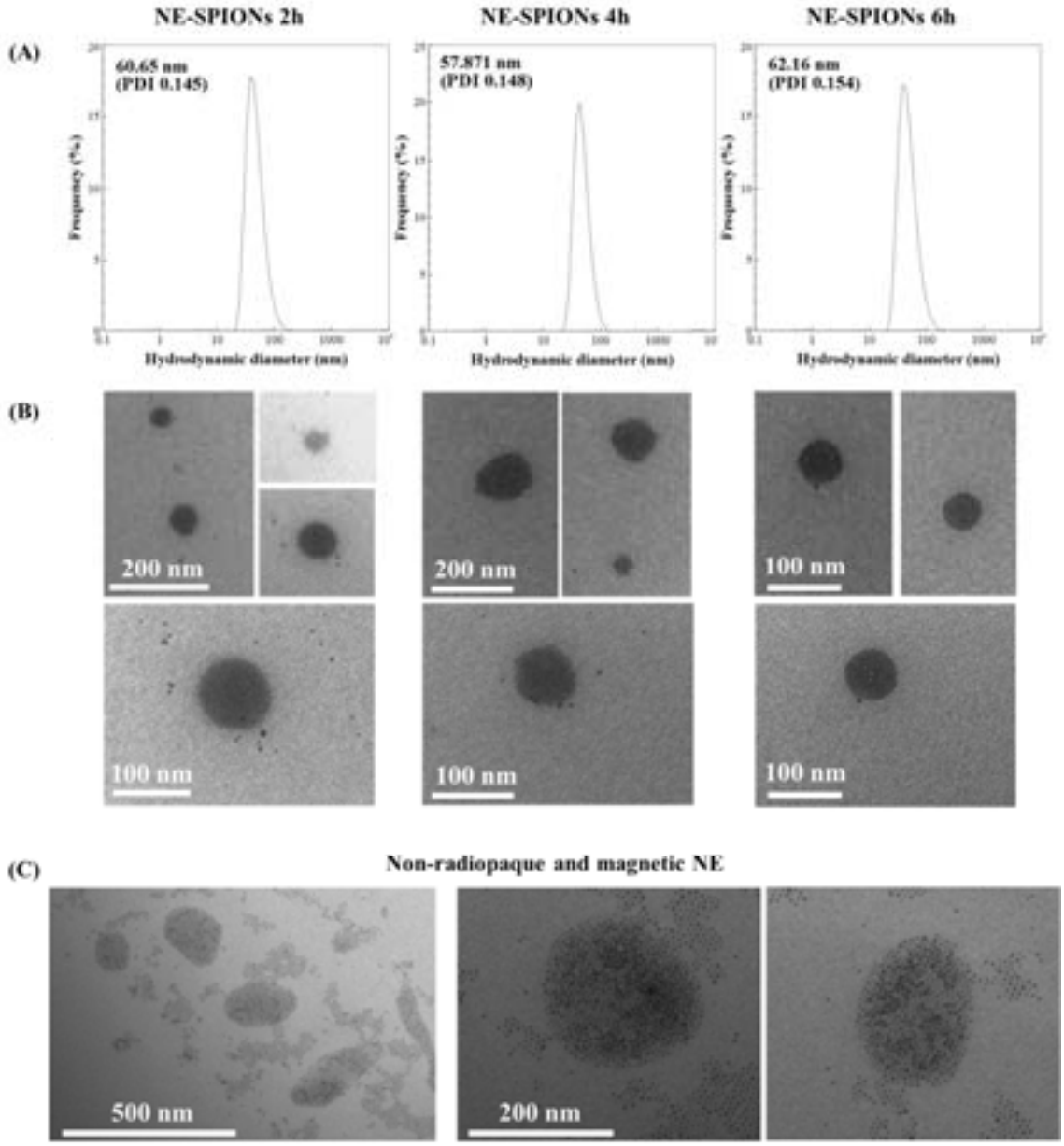

Figure 8 : (A, B) Physico-chemical characterization by DLS and TEM investigations of radiopaque and magnetic NE. (A) Size distribution and (B) TEM micrographs at different magnification of the NE-SPIONs 2h, NE-SPIONs 4h and NE-SPIONs 6h. Use of radiopaque modified vitamin E provokes darkening of NEs inner cores by TEM. (C) Example of TEM micrographs of NE encapsulating SPIONs in non-radiopaque oil (Labrafac™ Lipophile WL 1329) at two different magnifications (NE was formulated with same formulation parameters). Pictures clearly show efficient encapsulation of SPIONs within an oily core of nano-droplet due to the absence of contrasting material.

The next part will aim to introduce to the evaluation of magnetic properties and the potential of NEs-SPIONs to be efficient CAs for T2- and T2*- weighted MRI by determining longitudinal and transverse relaxivity parameters, respectively r1 and r2, and their ratio r2/r1. A range of dilution of NEs-SPIONs was performed from 0.8 to 3.5 mmole Fe/L with MilliQ

water. The Figure 9 gathers results of relaxometry measurement of NE-SPIONs 2h (Figure 9A), NE-SPIONs 4h (Figure 9B) and NE-SPIONs 6h (Figure 9C):

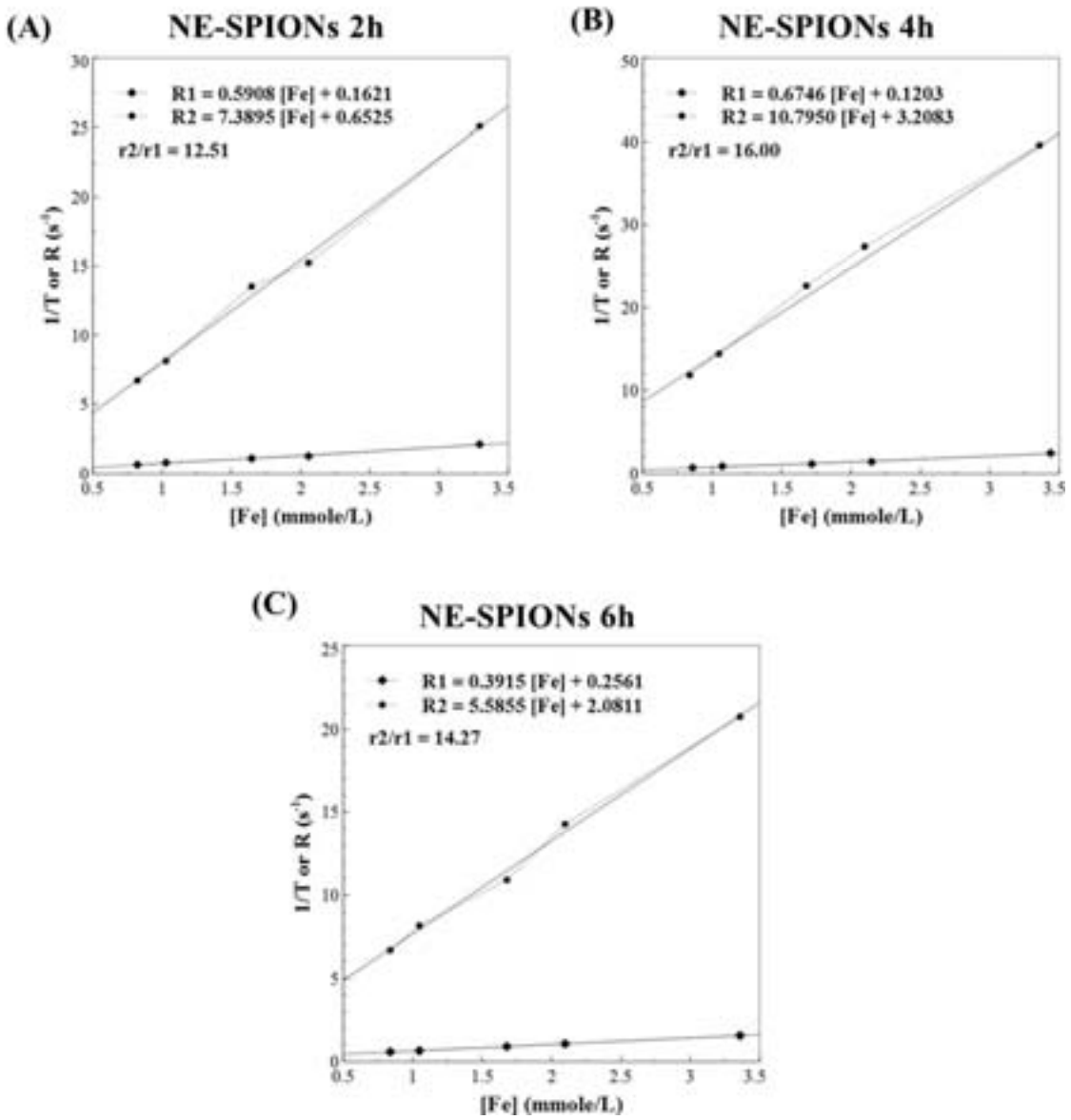

Figure 9: R1 and R2 relaxation rates of (A) NE-SPIONs2h, (B) NE-SPIONs 4h and (C) NE-SPIONs 6h at different iron concentrations, measured at 37 °C and 1.41 T by low field strength relaxometer. Longitudinal and transversal relaxivities parameters, r1 and r2 respectively, were obtained by calculating the slope of each plot.

Several points can be extracted from such graphs: r1, r2 and their ratios. Relaxivity parameters, r1 and r2, correspond to the slope of 1/T1 (R1) or 1/T2 (R2) *vs* [Fe]. Since this study lies on the preparation of T2- and T2*-weighted MRI CAs, it is important to remember that transverse relaxation of a selected ROI will be impacted by introduction of this type of CA. Although, T2 and r2 seem consequently more relevant to estimate, r1 remains quite

important too because of it has to be small enough to lead a high r2/r1 ratio. Typical CA for T2- and T2*-weighted MRI have a r2/r1 higher than 10 because r2 is high but mainly because r1 is very low. In this work, it appears that all r2/r1 were above 10, values were: r2/r1 = 12.51 (NE-SPIONs 2h), r2/r1 = 16.00 (NE-SPIONs 4h) and r2/r1 = 14.27 (NE-SPIONs 6h). Once more, SPIONs 4h promote highest value for the as-evaluated parameter even when they are encapsulated into NEs; whereas, NE-SPIONs 2h indicated lower ratio than NE-SPIONs 6h. Similar trends were observed for r1 and r2: NE-SPIONs 4h has r1 = 0.6746 $mM^{-1}.s^{-1}$ whereas NE-SPIONs 2h and NE-SPIONs 6h have respectively r1 = 0.5908 $mM^{-1}.s^{-1}$ and r1 = 0.3915 $mM^{-1}.s^{-1}$. Although NE-SPIONs 4h has the highest r1, it also exhibits the highest r2 (r2 = 10.7950 $mM^{-1}.s^{-1}$) to lead to the highest r2/r1 ratio. Transverse relaxivity parameters r2 were respectively for NE-SPIONs 2h and NE-SPIONs 6h: r2 = 7.3895 and r2 = 5.5855 $mM^{-1}.s^{-1}$. It has to be highlighted that NE-SPIONs 2h seem more suitable than NE-SPIONs 6h as T2- and T2*-weighted MRI CA since its r2 is superior to the NE-SPIONs 6h one, however its r1 is superior too causing a lower r2/r1 compared to NE-SPIONs 6h. This indicates how r1 and r2 are both important parameters to determine to perform an efficient discrimination of samples based on their relaxivities. In any case, r2/r1, r2 and r1 remain all quite close after comparison of these three bimodal NEs. However, NE-SPIONs 4h exhibited properties a little bit superior to the two other NEs.

To conclude our set of experiments and to have a complete overview of NEs-SPIONs characteristics, we run *in vitro* test to study colloidal stability in physiological environment in FBS at 37°C over a 24h period of incubation. This typical *in vitro* experiment aims at assaying behavior of NEs once exposed to simulated *in vivo* conditions, *i.e.* once in presence of *in vivo* entities in the blood pool at body temperature after administration to mice. Stability was assayed by checking size distribution over the period of 24h at body temperature; all results are displayed in Figure 10. No aggregates or flocculates were visible by macroscopic observation; this study revealed that NEs were perfectly stable once exposed to plasma proteins from FBS after DLS measurement. Change in size distribution for NE-SPIONs 2h, NE-SPIONs 4h and NE-SPIONs 6h was so subtle that it can be considered as non-significant. Plasma proteins were consequently not adsorbed onto nanodroplets assuming that extended circulation time within the bloodstream could be expecting when *in vivo* tests will be performed. Generally, all NEs did not show any lack of stability of any kind.

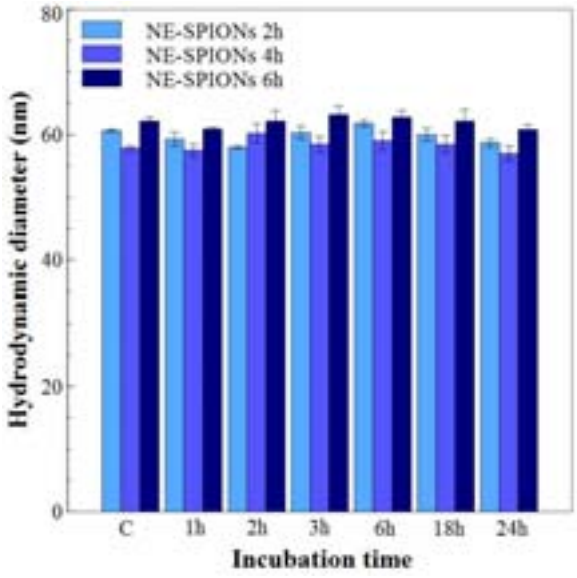

Figure 10: *In vitro* evaluation of NE-SPIONs stability in FBS incubated at 37°C for 24h. "C" is the control sample without serum.

Owing to similar characteristics regarding size distribution, stability and composition, conclusion of our set of tests to discriminate NEs was mainly based on magnetic property and potential of NEs to be efficient MRI CAs. Besides, radiopaque property was not a discriminating parameter since all NEs were formulated with same iodinated vitamin E amount, inducing same ability to attenuate X-rays. As demonstrated before, NE-SPIONs 4h and encapsulated SPIONs 4h were always a little bit different and better than other candidates. Besides, since magnetic ability of NEs were due to SPIONs payload, ability of NEs to be efficient MRI probes for *in vivo* tests relies only on their SPIONs as suggesting before. Actually, it can be assumed that the anisotropic shape of SPIONs 4h was at the origin of improved magnetic property for T2- and T2*-weighted MRI. It has been reported that shape would influence crystalline structure at nanocrystals' boundaries and higher radii. Consequently SPIONs with anisotropic shape would behave as larger NPs regarding magnetic properties *i.e.* SPIONs with enhanced magnetic property.[61] Consequently, we selected NE-SPIONs 4h as optimum candidate for *in vivo* assay as nanoparticulate bimodal CA for MRI and X-ray imaging.

First of all, we performed same *in vitro* measurement of r1, r2 and r2/r1 on NE-SPIONs 4h with a large magnetic field in order to estimate how magnetic properties can be modified along with the magnetic field. The Figure 11 shows graph obtained from this experiment. Same range of diluted samples from NE-SPIONs 4h were used and introduced into MRI instrument at 7T. Typically, r1 decreases from 0.6748 $mM^{-1}.s^{-1}$ to 0.1198 $mM^{-1}.s^{-1}$ when

magnetic field is respectively 1,41T and 7T indicating a significant decrease of r1 when magnetic field is large. As to r2, significant change was noticed: r2 (1.41T) was as determined before 10.7950 $mM^{-1}.s^{-1}$ whereas r2 (7T) is 17.61 $mM^{-1}.s^{-1}$ that to say higher than at low magnetic field. As a result, r2/r1 rose drastically to 146.99 at 7T compared to 16.00 at 1.41T. Such ratio increases almost 10 fold when magnetic change from 1.41T to 7T. It can be assumed that previous evaluation of magnetic properties of our selected NE would be much more important than expected with experiment with 1.41T magnetic field.

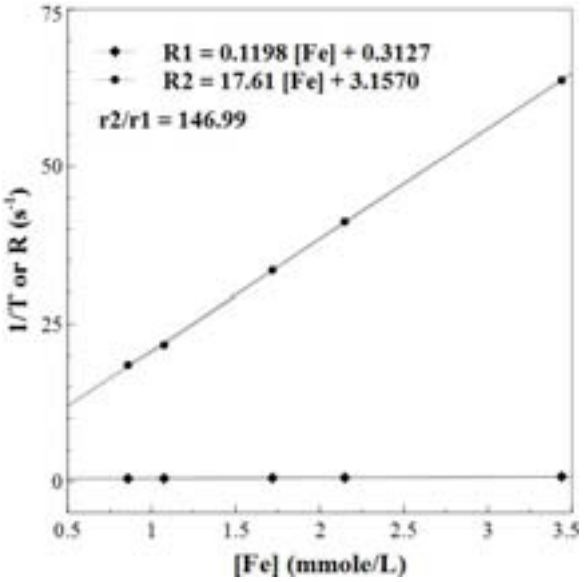

Figure 11: R1 and R2 relaxation rates of NE-SPIONs 4h at different Fe concentrations, measured at 37 °C and 7T by high field strength MRI analysis.

In vivo experiments were assays on 6 Swiss mice (5 injected and 1 control). Bimodal imaging was used to image healthy mice and to investigate *in vivo* biodistribution and accumulation of radiopaque and magnetic nano-droplets from NE-SPIONs 4h after a 9% dose intravenous injection in the vein tail. MRI acquisitions were performed before administration of the CA and 5h and 24h post-injection. X-ray micro-CT images were done at 24h post-injection due to incompatible anesthesia pharmaceutics between modalities; a control specimen (non-injected) was used as a reference for X-ray imaging.

Once administrated by intravenous way, no clinical signs of toxicity and health disorders were observed on mice, same observations were done through all experiment duration. Repetitive anesthesia and imaging protocols did not impact animals' health. Administrations of CA by injection to each specimen did not cause any reaction on animals, indicating the

compatibility (pH, viscosity, osmolality) of the CA formulation with physico-chemical properties of the blood pool, and were easily handled despite the delicacy of the gesture.

In vivo contrast enhancement was measured by MRI at different representative time in order to perform a follow-up of the bioaccumulation of the CA over a significant period. ROI were picked for signal quantification following visual localization of hypointense region. Figure 12 illustrated *in vivo* MRI experiment and signal quantification in ROI.

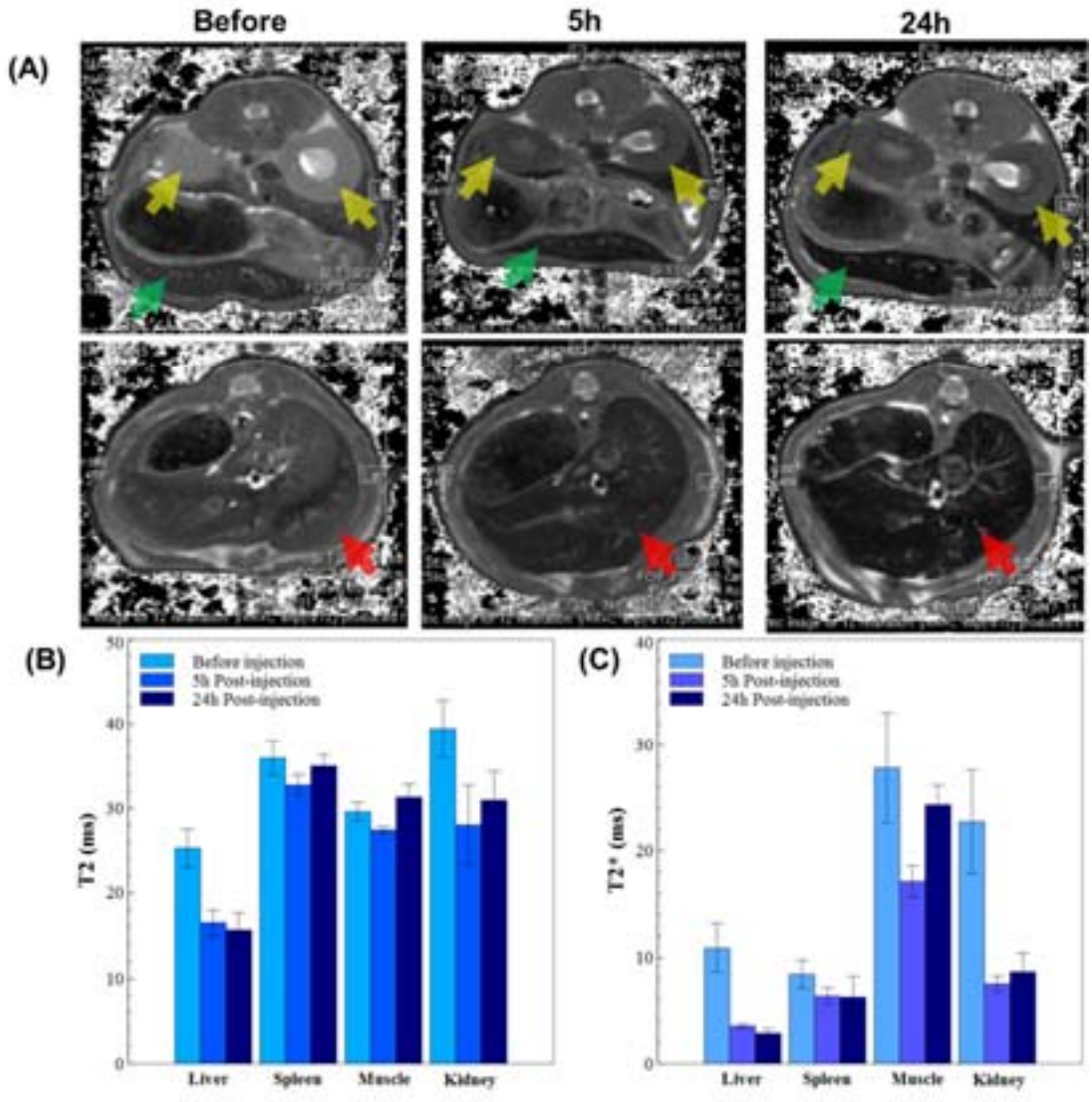

Figure 12: (A) *In vivo* T2-weighted MRI reconstructed 2D images before administration of a 9% dose of CA (NE-SPIONs 4h) and 5h and 24h post-injection. Each picture shows axial sections through the abdominal region of mice. Kidneys, spleen and liver are respectively indicated by yellow, green and red arrows. (B,C) Quantification of contrast enhancement *via* the measurement of relaxation times (B) T2 and (C) T2* signal at each representative time after administration of NE-SPIONs 4h for liver, spleen, muscle and kidney, chosen as ROI for MRI signal quantification.

After administration of the CA, product spread in vasculature of animals. Muscle was chosen as ROI to detect and quantify contrast enhancement caused by circulation of CA within the blood pool. As displays on Figure 12A, 5h post-injection, significant contrast enhancement was induced in liver, spleen and kidneys (cortex region) and measured by both T2- and T2*-weighted MRI. Signal from spleen remained debatable because of its heterogeneity owing to its composition (white pulp and red pulp), it is as a result difficult to extract relevant data for such tissue. Indeed, even before administration, the spleen appears already dark on images, consequently accumulation of CA would be subtle to notify. However, accumulation in liver and potentially in spleen indicated that blood clearance mechanism was performed through hepatic route (and maybe by splenic route too). Visualization of slight darkening in kidneys also demonstrated that a fraction of the administrated dose was cleaned out from vasculature by renal clearance; it can be assumed that the rest of the dose was distributed to liver and spleen. Similar observations on reconstructed images were done after 24h, confirming first conclusion regarding clearance mechanism and accumulation of the NE-SPIONs 4h. Although contrast enhancement from spleen was not surely significant, quantification was still carried out for all ROI including the spleen. The Figure 12 discloses both (B) T2 and (C) T2* measurements for selected ROI. For MRI, contrast enhancement can be detect by decrease of relaxation time, in the case of this study decrease of T2 and T2* was measured to provide quantitative data of the effect of our formulation once used as CA. Considering each ROI, biodistribution and pharmacokinetic evolution can be determined. T2 and T2* for muscle indicated presence of contrasting materials since decreases of T2 and T2*, respectively from 29.60 ms to 27.44 ms and from 27.84 to 17.10 ms, are visible at 5h post-injection. Both relaxation times almost leveled off their initial values after 24h post-injection meaning that CA was eliminated from blood pool and distributed to organs in charge of excretion mechanism. It could be noted that T2* is much more sensitive than T2 since decreases of signal between two representative time is much more important and significant than for T2. As to the spleen, T2 and T2* variations over the 24h experiment were as expected not drastically different. X-ray imaging will consequently be really useful to evaluate accumulation of bimodal probe in splenic compartment. On the contrary, liver exhibited really low value of T2 and T2* compared to data collected before administration. As visualized, contrast enhancement remained quite similar after 5h and 24h post-injection for the hepatic compartment. Initially measured at 25.28 ms and 10.91 ms for T2 and T2* respectively, relaxation times both decreases drastically as histogram in Figure 12(B,C) shows at 5h post-injection and reached 16.49 ms

(T2) and 3.55 ms (T2*). At 24h post-injection, T2 (15.61 ms) and T2* (2.85 ms) were aforementioned also very short and close to previous values. It seems that liver received the highest fraction of the injected dose, certainly due to its bigger volume compared to spleen and kidneys. Finally, kidneys also accumulated contrasting agent since, as for the liver, pronounced differences in T2 and T2* were observable on histograms. Briefly, similar profile to liver can be observed since a high decrease, especially for T2* due to its higher sensitivity, at 5h (from 38.44 ms to 28.04 ms for T2 and from 22.74 ms to 7.54 for T2*) and similar value at 24h post-injection (30.96 ms for T2 and 8.66 ms for T2*) were measured. T2 and T2* values confirmed visual observations on 2D images. However it remained to elucidate the case of the splenic compartment because it is really common that when blood clearance is performed by hepatic route that splenic route is also involved due to their affiliation to the RES system.

To evaluate now radiopaque ability of NE-SPIONs 4h, same mice were subjected to X-ray micro-CT imaging at 24h post-injection (Figure 13). Iodinated vitamin E-based NE has already been study *in vivo* and showed excellent property for liver imaging[48], it was so interesting to perform same experiment to assay property of a bimodal version of this NE.

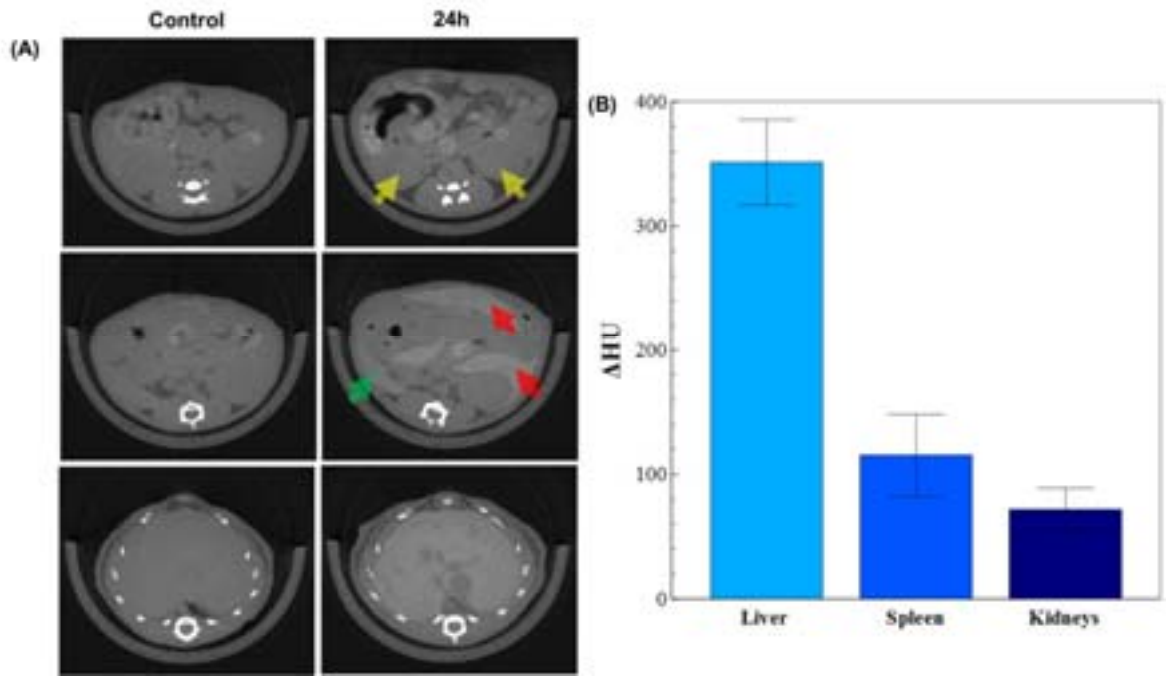

Figure 13: (A) *In vivo* X-rays micro-CT 2D images of non-injected and injected mice (24h post-injection) Each picture shows axial sections through the abdominal region of mice. Kidneys, spleen and liver are respectively indicated by yellow, green and red arrows. (B) X-ray attenuation of liver, spleen and kidneys at 24h post-injection. ΔHU values were provided with Hounsfield unit using control animal as reference.

As for MRI, same ROI were chosen that is to say liver, spleen and kidneys. Muscle was not checked because this kind of soft cannot be visualized by X-rays scanner without radiopaque material accumulated in it. However, it has been concluded by MRI that all contrasting material was cleaned from blood pool, and consequently form muscle, between 5h and 24h post-injection. Muscle was not anymore relevant to observe by imaging. On the contrary, hepatic and splenic compartments and kidneys were selected to estimate their radiopaque property since NE-SPIONs 4h fractions of the injected dose were distributed in these tissues. Typically, liver was the most contrasted tissue with a ΔHU = 351.14±34.22 HU which is a significant value taking in account that soft tissues have a ΔHU between -100 to +100 HU. In addition, clear delineation of soft tissue among others can only be done by a difference of their respective ΔHU of 50-100 HU. Regarding the spleen, it appears that X-ray attenuation occurred for such compartment indicating the presence of CA as assumed with MRI experiment. Contrast enhancement is so far less important than for liver but ΔHU was calculated at 115.41±32.89 HU which is quite enough to delineate spleen among others tissues from the abdominal region. The blood pool is so subjected to CA elimination through splenic and hepatic routes. The last but not the east, kidneys were not visible on images, ΔHU was besides measured and estimated at 71.70±17.29 HU indicating an absence of significant contrast enhancement. Such different conclusion between MRI and micro-CT for kidneys is one the most interesting data extracted from comparison of imaging results from each modality. Indeed, it seems that no radiopaque materials were detected within kidneys since no hyperintense signal was visible and no drastic X-ray attenuation was measurable. The only conclusion that we can conduct from such observations is that our NE-SPIONs 4h were not only accumulated in kidneys upon excretion by urinary way but they were also altered and deteriorated by renal filter causing the elimination of the iodinated vitamin E and the accumulation of SPIONs 4h within kidneys tissues. SPIONs 4h might have been stuck within renal filter due to their surface properties and small dimension within the cortex leading signal by MRI. Even though the fraction of dose eliminated by renal clearance has not been determined, MRI is more sensitive than X-rays scanner which means that thanks to the bimodality of our CA, the deeper understanding of the pharmacokinetics of NE-based CA could be achieved. Indeed without the use of MRI, the efficient dose involved into the contrast enhancement of each compartment would not be accurately determined. Finally, to go further in such work, it could be interesting to perform in parallel MRI and X-ray micro-CT imaging at representative time in order to have a real-time bimodal monitoring for a

complete follow-up of the biodistribution, the bioaccumulation and the pharmacokinetics of the administrated CA.

4. Conclusion

In the present study we developed a bimodal lipids-based nanoparticulate probe for X-rays imaging MRI. The formulation consists in oil-in-water NE, formulated by spontaneous emulsification process, with PEGylated hairy shell and an oily core composed of iodinated vitamin E (41.7% of iodine) and SPIONs which were synthetized for 2h, 4h or 6h (SPIONs 2h, SPIONs 4h and SPIONs 6h) to generate magnetite NPs with different morphology and magnetic property. Discrimination of bimodal NEs was done based on relaxivity parameters (r2,r1) and r2/r1, which means their ability as being efficient CAs for MRI. The selected NE was subjected to *in vivo* imaging and administrated to Swiss mice. Passive targeting strategy was applied here in order to lead to gradual and spontaneous biodistribution and bioaccumulation of the as-prepared dual modal CA. Strong and persistent hypointense signals by T2- and T2*-weighted MRI were detected in liver and also in kidneys indicating that a fraction of injected dose was eliminated by renal filtration; Major accumulation in liver proved that blood clearance was performed by hepatic route. It was consequently assumed that spleen would have accumulated CA since splenic and hepatic compartments are both generally involved in excretion mechanism by RES. X-ray imaging allowed to prove such hypothesis and showed clear delineation by hyperintense signals of liver and spleen; kidneys were not visible among others soft tissues from the abdominal region meaning that no radiopaque materials were accumulated. Thereby, fraction of NE filtrated through kidneys might have been destabilized and components separately subjected to *in vivo* respond: the SPIONs remained in kidneys tissues, causing MRI signal whereas the others components such as the radiopaque oil seemed to be eliminated by urinary way leading to the absence of contrast by X-rays investigation. Consequently, we formulated an efficient dual modal preclinical CA for soft tissue imaging opening a route for a better understanding of pharmacokinetic of NEs-based CAs. The step beyond will be to perform cellular uptake study to study interaction of the NE with hepatic and splenic cells. Furthermore, iron and iodine titration in liver, spleen and kidneys are in progress in order to determine the dose in each compartment and to go further into the determination of the pharmacokinetic profile of our radiopaque and magnetic CA.

5. References

[1] M.A. Hahn, A.K. Singh, P. Sharma, S.C. Brown, B.M. Moudgil, Nanoparticles as contrast agents for *in-vivo* bioimaging: Current status and future perspectives, Anal. Bioanal. Chem. 399 (2011) 3–27. doi:10.1007/s00216-010-4207-5.

[2] J. Key, J.F. Leary, Nanoparticles for multimodal *in vivo* imaging in nanomedicine, Int. J. Nanomedicine. 9 (2014) 711–726. doi:10.2147/IJN.S53717.

[3] V.P. Torchilin, Targeted pharmaceutical ncer therapy and imaging, AAPS J. 9 (2007) E128–E147. doi:10.1208/aapsj0902015.

[4] D.P. Cormode, T. Skajaa, Z.A. Fayad, W.J.M. Mulder, Nanotechnology in medical imaging: probe design and applications, Arter. Thromb Vasc Biol. 29 (2010) 992–1000. doi:10.1161/ATVBAHA.108.165506.

[5] G.N. Hounsfield, Computerized transverse axial scanning (tomography): Part I description of system, Br. J. Radiol. 46 (1973) 1016–1022. doi:10.1259/0007-1285-46-552-1016.

[6] S.-B. Yu, A.D. Watson, Metal-Based X-ray Contrast Media, Chem. Rev. 99 (1999) 2353–2378. doi:10.1021/cr980441p.

[7] N. Lee, S.H. Choi, T. Hyeon, Nano-sized CT contrast agents, Adv. Mater. 25 (2013) 2641–2660. doi:10.1002/adma.201300081.

[8] F. Hallouard, S. Briançon, N. Anton, X. Li, T. Vandamme, H. Fessi, Iodinated nano-emulsions as contrast agents for preclinical X-ray imaging: Impact of the free surfactants on the pharmacokinetics, Eur. J. Pharm. Biopharm. 83 (2013) 54–62. doi:10.1016/j.ejpb.2012.09.003.

[9] A. Jakhmola, N. Anton, T.F. Vandamme, Inorganic nanoparticles based contrast agents for X-ray computed tomography, Adv. Healthc. Mater. 1 (2012) 413–431. doi:10.1002/adhm.201200032.

[10]H. Lusic, M.W. Grinstaff, X-ray Computed Tomography Contrast Agents, Chem. Rev. 113 (2013) 1641–1666. doi:doi.org/10.1021/cr200358s.

[11]N. Anton, T.F. Vandamme, Nanotechnology for computed tomography: A real potential recently disclosed, Pharm. Res. 31 (2014) 20–34. doi:10.1007/s11095-013-1131-3.

[12]D.P. Cormode, P.C. Naha, Z.A. Fayad, Nanoparticle contrast agents for computed tomography: A focus on micelles, Contrast Media Mol. Imaging. 9 (2014) 37–52. doi:10.1002/cmmi.1551.

[13]F. Hallouard, N. Anton, P. Choquet, A. Constantinesco, T. Vandamme, Iodinated blood pool contrast media for preclinical X-ray imaging applications - A review, Biomaterials. 31 (2010) 6249–6268. doi:10.1016/j.biomaterials.2010.04.066.

[14]J.C. De La Vega, U.O. Häfeli, Utilization of nanoparticles as X-ray contrast agents for diagnostic imaging applications, Contrast Media Mol. Imaging. 10 (2014) 81–95. doi:10.1002/cmmi.1613.

[15]J.-M. Idée, B. Guiu, Use of Lipiodol as a drug-delivery system for transcatheter arterial chemoembolization of hepatocellular carcinoma: A review, Crit. Rev. Oncol. Hematol. 88 (2013) 530–549. doi:10.1016/j.critrevonc.2013.07.003.

[16]J.M. Widmark, Imaging-related medications: a class overview, Proc. (Baylor Univ. Med. Center). 20 (2007) 408–417.

[17]P.C. Lauterbur, Image Formation by Induced Local Interactions: Examples Employing Nuclear Magnetic Resonance, Nature. 242 (1973) 190–191. doi:10.1038/242190a0.

[18]A.N. Garroway, P.K. Grannell, P. Mansfield, Image formation in NMR by a selective irradiative process, J. Phys. C Solid State Phys. 7 (1974) L457–L462. doi:10.1088/0022-3719/7/24/006.

[19]P. Mansfield, A.A. Maudsley, Medical imaging by NMR, J. Magn. Reson. 27 (1977) 101–119. doi:10.1259/0007-1285-50-591-188.

[20]W.A. Edelstein, J.M.S. Hutchison, G. Johnson, T. Redpath, Spin warp NMR imaging and applications to human whole-body imaging, Phys. Med. Biol. 25 (1980) 751–756. doi:10.1088/0031-9155/25/4/017.

[21]J.M.S. Hutchinson, W.A. Edelstein, G. Johnson, A whole-body NMR imaging machine, J. Phys. E. 13 (1980) 947–955. doi:10.1088/0022-3735/13/9/013.

[22]I.L. Pykett, R.R. Rzedzian, Instant images of the body by magnetic resonance, Magn. Reson. Med. 5 (1987) 563–571. doi:10.1002/mrm.1910050607.

[23]R. Damadian, Tumor Detection by Nuclear Magnetic Resonance, Science. 171 (1971) 1151–1153. doi:10.1126/science.171.3976.1151.

[24]V.P.B. Grover, J.M. Tognarelli, M.M.E. Crossey, I.J. Cox, S.D. Taylor-Robinson, M.J.W. McPhail, Magnetic Resonance Imaging: Principles and Techniques: Lessons for Clinicians, J. Clin. Exp. Hepatol. 5 (2015) 246–255. doi:10.1016/j.jceh.2015.08.001.

[25]H. Bin Na, I.C. Song, T. Hyeon, Inorganic nanoparticles for MRI contrast agents, Adv. Mater. 21 (2009) 2133–2148. doi:10.1002/adma.200802366.

[26]Y.J. Wang, Superparamagnetic iron oxide based MRI contrast agents : Current status of clinical application, Quant. Imaging Med. Surg. 1 (2011) 35–40. doi:10.3978/j.issn.2223-4292.2011.08.03.

[27]Q.A. Pankhurst, J. Connolly, S.K. Jones, J. Dobson, Applications of magnetic nanoparticles in biomedicine, J. Phys. D. Appl. Phys. 36 (2003) R167–R181. doi:10.1088/0022-3727/36/13/201.

[28]M.F. Kircher, J.K. Willmann, Molecular Body Imaging : MR Imaging, CT, and US. Part II. Applications, Radiology. 264 (2012) 349–368.

[29]S. Xue, Y. Wang, M. Wang, L. Zhang, X. Du, H. Gu, C. Zhang, Iodinated oil-loaded, fluorescent mesoporous silica-coated iron oxide nanoparticles for magnetic resonance imaging/computed tomography/fluorescence trimodal imaging, Int. J. Nanomedicine. 9 (2014) 2527–2538. doi:10.2147/IJN.S59754.

[30]D. Niu, X. Liu, Y. Li, Z. Ma, W. Dong, S. Chang, W. Zhao, J. Gu, S. Zhang, J. Shi, Fabrication of uniform, biocompatible and multifunctional PCL-b-PAA copolymer-based hybrid micelles for magnetic resonance imaging, J. Mater. Chem. 21 (2011) 13825-13831. doi:10.1039/c1jm10929d.

[31]N. Lee, H.R. Cho, M.H. Oh, S.H. Lee, K. Kim, B.H. Kim, K. Shin, T. Ahn, J.W. Choi, Y. Kim, S.H. Choi, T. Hyeon, Multifunctional Fe_3O_4/TaO_x Core/Shell Nanoparticles for Simultaneous Magnetic Resonance Imaging and X-Ray Computer Tomography, J. Am. Chem. Soc. 134 (2012) 10309–10312. doi:10.1021/ja3016582.

[32]W. Dong, Y. Li, D. Niu, Z. Ma, X. Liu, J. Gu, W. Zhao, Y. Zheng, J. Shi, A simple route to prepare monodisperse Au NP-decorated, dye-doped, superparamagnetic nanocomposites for optical, MR, and CT trimodal imaging, Small. 9 (2013) 2500–2508. doi:10.1002/smll.201202649.

[33]M.H. Oh, N. Lee, H. Kim, S.P. Park, Y. Piao, J. Lee, S.W. Jun, W.K. Moon, S.H. Choi, T. Hyeon, Large-scale synthesis of bioinert tantalum oxide nanoparticles for X-ray computed tomography imaging and bimodal image-guided sentinel lymph node mapping., J. Am. Chem. Soc. 133 (2011) 5508–5515. doi:10.1021/ja200120k.

[34]P.A. Jarzyna, A. Gianella, T. Skajaa, G. Knudsen, L.H. Deddens, D.P. Cormode, Z. a. Fayad, W.J.M. Mulder, Multifunctional imaging nanoprobes, Wiley Interdiscip. Rev. Nanomedicine Nanobiotechnology. 2 (2010) 138–150. doi:10.1002/wnan.72.

[35] X. Li, N. Anton, G. Zuber, T. Vandamme, Contrast agents for preclinical targeted X-ray imaging, Adv. Drug Deliv. Rev. 76 (2014) 116–133. doi:10.1016/j.addr.2014.07.013.

[36]P. Aggarwal, J.B. Hall, C.B. McLeland, M.A. Dobrovolskaia, S.E. McNeil, Nanoparticle interaction with plasma proteins as it relates to particle biodistribution, biocompatibility and therapeutic efficacy, Adv. Drug Deliv. Rev. 61 (2009) 428–437. doi:10.1016/j.addr.2009.03.009.

[37]G. Storm, S.O. Belliot, T. Daemen, D.D. Lasic, Surface modification of nanoparticles to oppose uptake by the mononuclear phagocyte system, Adv. Drug Deliv. Rev. 17 (1995) 31–48. doi:10.1016/0169-409X(95)00039-A.

[38]V.P. Torchilin, V.S. Trubetskoy, Which polymers can make nanoparticulate drug carriers long-circulating?, Adv. Drug Deliv. Rev. 16 (1995) 141–155. doi:10.1016/0169-409X(95)00022-Y.

[39]F. Caruso, Nanoengineering of particle surfaces, Adv. Mater. 13 (2001) 11–22. doi:10.1002/1521-4095(200101)13:1<11::AID-ADMA11>3.0.CO;2-N.

[40]K.H. Bae, H.J. Chung, T.G. Park, Nanomaterials for cancer therapy and imaging, Mol. Cells. 31 (2011) 295–302. doi:10.1007/s10059-011-0051-5.

[41]S. Mornet, S. Vasseur, F. Grasset, E. Duguet, Magnetic nanoparticle design for medical diagnosis and therapy, J. Mater. Chem. 14 (2004) 2161–2175.

[42]S. Parveen, R. Misra, S.K. Sahoo, Nanoparticles: a boon to drug delivery, therapeutics, diagnostics and imaging, Nanomedicine Nanotechnology, Biol. Med. 8 (2012) 147–166. doi:10.1016/j.nano.2011.05.016.

[43]V.P. Torchilin, PEG-based micelles as carriers of contrast agents for different imaging modalities, Adv. Drug Deliv. Rev. 54 (2002) 235–252. doi:10.1016/S0169-409X(02)00019-4.

[44]V.P. Torchilin, Multifunctional nanocarriers, Adv. Drug Deliv. Rev. 64 (2012) 302–315. doi:10.1016/j.addr.2012.09.031.

[45]N. Singh, G.J.S. Jenkins, R. Asadi, S.H. Doak, Potential toxicity of superparamagnetic iron oxide nanoparticles (SPION), Nano Rev. (2010) 1-5358. doi:10.3402/nano.v1i0.5358.

[46]C.T. Badea, M. Drangova, D.W. Holdsworth, G.A. Johnson, *In vivo* small-animal imaging using micro-CT and digital subtraction angiography., Phys. Med. Biol. 53 (2008) R319–R350. doi:10.1088/0031-9155/53/19/R01.

[47]M.F. Attia, N. Anton, M. Chiper, R. Akasov, H. Anton, N. Messaddeq, S. Fournel, A.S. Klymchenko, Y. Mély, T.F. Vandamme, Biodistribution of X-ray iodinated contrast agent in nano-emulsions is controlled by the chemical nature of the oily core., ACS Nano. 8 (2014) 10537–10550. doi:10.1021/nn503973z.

[48]X. Li, N. Anton, G. Zuber, M. Zhao, N. Messaddeq, F. Hallouard, H. Fessi, T.F. Vandamme, Iodinated α-tocopherol nano-emulsions as non-toxic contrast agents for preclinical X-ray imaging, Biomaterials. 34 (2013) 481–491. doi:10.1016/j.biomaterials.2012.09.026.

[49]P.A. Jarzyna, T. Skajaa, A. Gianella, D.P. Cormode, D.D. Samber, S.D. Dickson, W. Chen, A.W. Griffioen, Z.A. Fayad, W.J.M. Mulder, Iron oxide core oil-in-water emulsions as a multifunctional nanoparticle platform for tumor targeting and imaging, Biomaterials. 30 (2009) 6947–6954. doi:10.1016/j.biomaterials.2009.09.004.

[50]Y. Fan, R. Guo, X. Shi, S. Allen, Z. Cao, J. Baker, S. Wang, Modified Nanoemulsions with Iron Oxide for Magnetic Resonance Imaging, Nanomaterials. 6 (2016) 223. doi:10.3390/nano6120223.

[51]J. Szebeni, F.M. Muggia, C.R. Alving, Complement Activation by Cremophor EL as a Possible Contributor to Hypersensitivity to Paclitaxel : an *In Vitro* Study, J. Natl. Cancer Inst. 90 (1998) 300–306.

[52]S. Sun, H. Zeng, D.B. Robinson, S. Raoux, P.M. Rice, S.X. Wang, G. Li, Monodisperse MFe_2O_4 (M = Fe, Co, Mn) Nanoparticles, J. Am. Chem. Soc. 126 (2004) 273-279.

[53]L. Wang, J. Luo, Q. Fan, M. Suzuki, I.S. Suzuki, M.H. Engelhard, Y. Lin, N. Kim, J.Q. Wang, C.-J. Zhong, Monodispersed core-shell Fe_3O_4@Au nanoparticles, J. Phys. Chem. B. (2005) 21593–21601.

[54]N. Anton, J.-P. Benoit, P. Saulnier, Design and production of nanoparticles formulated from nano-emulsion templates-A review, J. Control. Release. 128 (2008) 185–199. doi:10.1016/j.jconrel.2008.02.007.

[55]T.F. Vandamme, N. Anton, Low-energy nanoemulsification to design veterinary controlled drug delivery devices, Int. J. Nanomedicine. 5 (2010) 867–873. doi:10.2147/IJN.S13273.

[56]N. Anton, T.F. Vandamme, Nano-emulsions and Micro-emulsions: Clarifications of the critical differences, Pharm. Res. 28 (2011) 978–985. doi:10.1007/s11095-010-0309-1.

[57] S. Boutry, D. Forge, C. Burtea, I. Mahieu, O. Murariu, S. Laurent, L. Vander Elst, R.N. Muller, How to quantify iron in an aqueous or biological matrix: a technical note, Contrast Media Mol. Imaging. 4 (2009) 299–304. doi:10.1002/cmmi.291.

[58] P. Tartaj, M. del Puerto Morales, S. Veintemillas-Verdaguer, T. Gonzalez-Carreno, C.J. Serna, The preparation of magnetic nanoparticles for applications in biomedicine, J. Phys. D. Appl. Phys. 36 (2003) R182–R197.

[59]J. Lodhia, G. Mandarano, N.J. Ferris, P. Eu, S.F. Cowell, Development and use of iron oxide nanoparticles (Part 1): Synthesis of iron oxide nanoparticles for MRI, Biomed. Imaging Interv. J. (2010) 6:e12. doi:10.2349/biij.6.2.e12.

[60] W. Wu, Q. He, C. Jiang, Magnetic iron oxide nanoparticles: Synthesis and Surface Functionalization Strategies, Nanoscale Res. Lett. 3 (2008) 397–415. doi:10.1007/s11671-008-9174-9.

[61] Z. Zhou, X. Zhu, D. Wu, Q. Chen, D. Huang, C. Sun, J. Xin, K. Ni, J. Gao, Anisotropic shaped iron oxide nanostructures: Controlled synthesis and proton relaxation shortening effects, Chem. Mater. 27 (2015) 3505–3515. doi:10.1021/acs.chemmater.5b00944.

Conclusion and perspectives

Conclusion and perspectives

This PhD topic aimed at development of novel and efficient nanoparticulate blood-pool contrast agents for X-rays imaging and magnetic resonance imaging (MRI) for preclinical non-invasive diagnostic purpose.

We were seeking to formulate nanoparticles and nanocarriers capable of i) being non-toxic and biocompatible with ii) a design suitable for *in vivo* administration and iii) a high loading capacity to cargo contrasting materials by passive targeting to local area such as soft tissue. Two main studies were achieved in this regard: a first study was conducted to formulate iodinated polymer-based stealth nanoparticles as X-ray imaging contrast enhancers whereas the second work was aiming to prepare bimodal contrast agents based on a stealth nano-emulsions containing iodinated oil and magnetic iron oxide nanoparticles, respectively for X-rays imaging and MRI contrast enhancement.

A preliminary bibliographical study allowed to notice that several limitations were still present at clinical stage concerning the commercially available contrast agents. It has consequently been highlight the lack of long-time retention and renal toxicity issues of contrast agents for X-ray imaging, so called radiopaque contrast agents. Literature also revealed the need of multimodal probes to yield more accurate diagnostic by conjuncture of two or three imaging modalities. Basically, we dedicated this PhD work to the investigations of efficient preclinical contrast agents overcoming current issues. Nanoparticles and nanocarriers were described as promising platform to design new generation of contrast agent; this is why we proposed in the present work the development of two nanoparticulate systems as contrast agents respectively dedicated to X-rays imaging and X-rays/MRI bimodal imaging.

The first study describes a straightforward approach to produce biocompatible, radiopaque and stable polymer-based nanoparticle contrast agent. To this end, we applied a nanoprecipitation dropping technique to obtain hydrophilic and stealth nanoparticles from a preformed homopolymer, the poly(MAOTIB) produced by bulk radical polymerization of MAOTIB monomer (62 wt.% of the molecular weight is iodine). The effects of polymer and PEGylated surfactant weight ratio and the polymer content were elucidated to find out the best compromise between iodine content and suitable size for *in vivo* application. The best iodinated polymeric suspension was so formulated with a narrow size distribution of 163.7

nm (PDI 0.09) and iodine concentration of 59 mg I/mL. Investigations of radiopaque property once exposed to *in vivo* environment were performed on mice (10% of the blood volume). Monitoring and quantification by micro-CT show that iodinated polymeric nanoparticles are endowed strong XR attenuation capacity towards blood pool, and underwent a fast and passive accumulation in liver and spleen. Such passive accumulation, indicating that blood clearance takes place through hepatic and splenic routes, occurred after short time of circulation in bloodstream ($t_{1/2}$ = 20min). Dose of contrast agent in both soft tissues were estimated at 61% for the liver and 9% for the spleen whereas the contrast enhancements were measured at 141 HU for the liver and 191 HU for the spleen. Spleen was consequently much more visible on reconstructed images despite the lower content of contrasting substances. However, owing to its smaller volume compared to the hepatic compartment, the splenic compartment was able to concentration much more the dose accumulated compared to the liver leading to a better contrast enhancement. These observations lead us to believe that our contrast agent may have been capable of interacting with biological entities from the reticuloendothelial system; cellular study on macrophages and hepatic cells would be interesting to perform to validate this hypothesis. Another potential outlook for this first study could be to improve and optimize the targeting and to carry out surface chemistry to apply an active targeting strategy. Indeed, the as-developed radiopaque formulation showed very satisfying contrasting properties and no signs of adverse effect on mice health.

As to the second study, we formulated magnetite iron oxide nanoparticles and iodine-containing nano-emulsions as stealth bimodal lipids-based nanoparticulate probe for X-rays imaging and MRI. The strength of these new contrast agents lie on their dual modal contrasting properties, their biocompatibility and the simplicity of the nanoparticulate assembling. The formulation consists in oil-in-water nano-emulsion, formulated by spontaneous emulsification process, with PEGylated hairy shell and an oily core composed of iodinated vitamin E (41.7 wt.% of iodine) from the triiodo-benzene group grafting by esterification and magnetite iron oxide nanoparticles (SPIONs) produced by high temperature processes performed over 2h, 4h and 6h to yield different morphology and magnetic property. Discrimination of bimodal nano-emulsions was done based on relaxivity parameters (r2,r1) and r2/r1, which means their ability as being efficient contrast agents for MRI. The selected nano-emulsion was subjected to *in vivo* imaging and administrated to Swiss mice. Passive targeting strategy was applied here in order to lead to gradual and spontaneous biodistribution and bioaccumulation of the as-prepared dual modal contrast agents. Excellent contrast

enhancement was visible by strong and persistent hypointense signals by T2- and T2*-weighted MRI for liver and kidneys whereas X-rays imaging allowed to image liver and spleen. Not only this study provided efficient bimodal contrast agents, as indicated aforementioned results, but it also provided an understanding of biodistribution and bioaccumulation of such kind of probe and show how complementary MRI and X-ray imaging are. Clear delineation of liver and spleen, generally both together involved into excretion mechanism, proved that soft tissues from the abdominal region were easily imaged but the contrast by MRI from kidneys demonstrated that a fraction of nano-emulsion filtrated through kidneys might have been destabilized: the SPIONs remained in kidneys tissues, causing MRI signal whereas the others components such as the radiopaque oil seemed to be eliminated by urinary way leading to the absence of contrast by X-rays investigation. Consequently, we formulated an efficient dual modal preclinical contrast agent for soft tissue imaging opening a route for a better understanding of pharmacokinetic of nano-emulsion-based contrast agents. The step beyond will be to perform cellular uptake study to study interaction of the nano-emulsion with hepatic and splenic cells. Furthermore, iron and iodine titration in liver, spleen and kidneys are in progress in order to determine the dose in each compartment and to go further into the determination of the pharmacokinetic profile of our radiopaque and magnetic contrast agent.

This PhD work aimed to investigate new nanoparticulate systems, most of our formulations were usually about unimodal imaging nanocarriers and based on nano-emulsions. In the case of this research work we tried to extent our field of expertise to multimodality and polymeric nanocarriers. Additional studies like we were used to perform with nano-emulsion will be possible like active targeting strategy, co-loading of contrasting material and therapeutics agents for theranostic field, once complementary data regarding cells studies will be collected on the two as-developed studies.

Appendices:

Additional research works and scientific contributions

Appendix 1: Targeting agents conjugated to nano-carriers to increase drug efficiency

Mohamed F. Attia[1,2,3], Nicolas Anton[1,2], Justine Wallyn[1,2], Ziad Omran[4,*], Thierry F. Vandamme[1,2,*]

[1] Laboratoire de Conception et Application de Molécules Bioactives (CAMB) - UMR 7199 CNRS, Equipe de Pharmacie Biogalénique, Strasbourg, France.
[2] Université de Strasbourg (Unistra), Faculté de Pharmacie, Strasbourg, France.
[3] National Research Center, P.O. 12622, Cairo, Egyp.
[4] Department of Pharmaceutical Chemistry, Faculty of Pharmacy, Umm AlQura University, Kingdom of Saudi Arabia
*Corresponding authors**:** Ziad OMRAN **(**zhomran@uqu.edu.sa) and Thierry F. VANDAMME (vandamme@unistra.fr)

Abstract

Introduction. This review gives an overview of the drug delivery to tumor microenvironment and tumor cells, using targeted nano-carriers.

Area covered. This review discusses the physicochemical properties of the drugs, of the nano-carriers and of the tumor microenvironment, in order to illustrate the different strategies undertaken to deliver the active ingredient specifically to the lesion. The choice between passive targeting and active targeting is discussed, as well as their consequences on the type of nano-carrier, properties like size, surface charge, functionalization with ligands, and type of ligands.

Expert Opinion. This review aims to draw an overview of the concept of the drug targeting to tumors with the objective of explaining why the passive or active targeting strategy is chosen, and how they are worked out.

Keywords

Nano-carriers, nanoparticles; drug delivery system; ligand; receptor; active targeting; passive targeting; EPR effect; tumor.

Appendix 2: Inorganic nanoparticles for X-ray computed tomography imaging

Mohamed F. Attia[a,b], Justine Wallyn[a], Nicolas Anton[a], Thierry F. Vandamme[a]

[a] University of Strasbourg, CNRS UMR 7199, Laboratoire de Conception et Application de Molécules Bioactives, University of Strasbourg, 74 route du Rhin, 67401 Illkirch Cedex.
[b] National Research Center, P.O. 12622, Cairo, Egypt.

Abstract

This review provides a state-of-the-art overview of an important application for inorganic nanoparticles in biomedical imaging. We focused mainly on gold nanoparticles (AuNPs) as imaging agent for X-ray CT imaging, but included a short comparison to magnetic and fluorescent modalities. X-ray imaging, which forms the basis for computer tomography, presents many advantages over other imaging modalities, in terms of structural and functional imaging, as well as the potential to target specific tissues. The general principles of the imaging techniques are reviewed, and the impact of the formulation processes of nanoparticles, their structures, chemical nature, and surface functionalization, as well as *in vitro* and *in vivo* behaviors are reviewed and discussed. This review summarizes all the latest technologies for targeting nanoparticles designed to improve imaging techniques and advance therapeutic efficacy.

Keywords

X-ray CT; MRI; gold nanoparticles; Surface functionalization; Targeted nanoparticles; contrast agents; biomedical imaging; active/passive targeting.

Appendix 3: Microfluidic-assisted production of SPIONs-encapsulated PMMA nanoparticles

Shukai Ding[1,2], Mohamed F. Attia[2], Justine Wallyn[2], Christophe A. Serra[1,3]*, Nicolas Anton[2*], Mohamad Kassem[4], Marc Schmutz[1], Nadia Messaddeq[5], Wei Yu[1], Thierry F. Vandamme[2]

[1] Institut Charles Sadron (ICS) – UPR 22 CNRS, Strasbourg, France.
[2] Laboratoire de Conception et Application de Molécules Bioactives (CAMB) – UMR 7199 CNRS, Faculté de Pharmacie, Université de Strasbourg (Unistra), Strasbourg, France.
[3] École Européenne de Chimie, Polymères et Matériaux (ECPM), Université de Strasbourg (Unistra), Strasbourg, France.
[4] EA7293, Vascular and Tissular Stress in Transplantation, Federation of Translational Mdicine of Strasbourg, Faculté de Pharmacie, Université de Strasbourg (Unistra), Strasbourg, France.
[5] IGBMC (Institut de Génétique et de Biogie Moléculaire et Cellulaire), Inserm U964, CNRS UMR 7104, Université de Strasbourg, 1 rue Laurent Fries, Illirch, France
*Corresponding authors: C.A. Serra, Email: ca.serra@unistra.fr, N. Anton, Email: nanton@unistra.fr.

Abstract

In this paper, super paramagnetic iron oxide nanoparticles (SPIONs, around 6 nm) encapsulated in poly(methyl methacrylate) nanoparticles (PMMA NPs) with controlled sizes ranging from 100 nm to 200 nm have been successfully produced. The hybrid polymeric nanoparticles were prepared following two different methods: (1) nanoprecipitation and (2) nanoemulsification-evaporation. These two methods were implemented in two different microprocesses based on the use of an impact jet micromixer and an elongational-flow microemulsifier respectively. SPIONs-loaded PMMA NPs synthesized by the two methods presented completely different physicochemical properties. The polymeric nanoparticles prepared with the micromixer-assisted nanoprecipitation method showed a heterogeneous dispersion of SPIONs inside the polymer matrix, an encapsulation efficiency close to 100 wt.% and an irregular shape. In contrast, the polymeric nanoparticles prepared with the microfluidic-assisted nanoemulsification-evaporation method showed a homogeneous dispersion, almost complete encapsulation and spherical shape. The properties of the polymeric nanoparticles have been characterized by DLS, TGA and TEM. *In vitro* cytotoxicity assays were also performed on the hybrid and pure PMMA nanoparticles.

Keywords

Microfluidics; nanoprecipitation; nanoemulsification; contrast agent; nanoparticles.

Appendix 4: List of communications

· Justine Wallyn, Nicolas Anton, Christophe Serra, Michel Bouquey, Mayeul Collot, Jean-Luc Weickert, Nadia Messaddeq, Thierry F. Vandamme. ***Formulation of radiopaque polymeric nanoparticles as contrast agent for diagnosis via biomedical X-ray imaging*** (Oral Communication), Journée des doctorants en chimie 2016 (Collège doctoral européen, **Strasbourg**), November 2nd 2016.

· Justine Wallyn, Nicolas Anton, Christophe Serra, Michel Bouquey, Mayeul Collot, Jean-Luc Weickert, Nadia Messaddeq, Thierry F. Vandamme. ***Preparation of an injectable iodinated polymeric nanoparticulate contrast agent by nanoprecipitation for in vivo preclinical XR imaging*** (Oral Communication), Journée du Campus d'Illkirch (JCI) 2017 (Ecole Supérieure Biotechnologie de Strasbourg, **Illkirch**), March 27th-28th 2017, **awards from Fédération de la Recherche pour la Chimie (FRC) for the best oral contribution**.

· Justine Wallyn, Nicolas Anton, Christophe Serra, Michel Bouquey, Mayeul Collot, Jean-Luc Weickert, Nadia Messaddeq, Thierry F. Vandamme. ***Polymer-based nanoscale contrast agent encapsulating iodine for X-ray imaging*** (Oral Communication), 25th International Conference on Bioencapsulation (**La Chapelle sur Erdre**), June 3rd-6th 2017, **awards of the best student contribution by Bioencapsulation Research Group**.

· Justine Wallyn, Nicolas Anton, Christophe Serra, Michel Bouquey, Mayeul Collot, Jean-Luc Weickert, Nadia Messaddeq, Thierry F. Vandamme. ***Nanoparticulate contrast agent by nanoprecipitation of iodinated homopolymer for in vivo preclinical XR imaging*** (Poster), 44th Annual Meeting & Exposition of the Controlled Release Society (**Boston**, Massachusetts, United State), June 16th-19th 2017.

Appendix 5: Scientific publications

· Mohamed Attia, Nicolas Anton, Justine Wallyn, Ziad Omran, Thierry Vandamme. ***Targeting agents conjugated to carriers to increase drug sensitivity***. (Submitted to Expert Opinion on Drug Delivery)

· Mohamed Attia, Justine Wallyn, Nicolas Anton, Thierry Vandamme. ***Inorganic nanoparticles for X-ray computed tomography imaging***. (Submitted to Critical Reviews)

· Shukaï Ding, Mohamed Attia, Justine Wallyn, Nicolas Anton, Christophe Serra, Thierry Vandamme. ***Preparation of SPIONs-encapsulated poly(methyl methacrylate) nanoparticles by microfluidics as contras agents for MR imaging***. (Submitted to Langmuir)

· Justine Wallyn, Nicolas Anton, Christophe Serra, Michel Bouquey, Mayeul Collot, Jean-Luc Weickert, Nadia Messaddeq, Thierry F. Vandamme. ***Application of poly(MAOTIB) homopolymer as injectable iodinated nanoparticulate contrast agent from nanoprecipitation technique for in vivo preclinical XR imaging***. (Submitted to Acta Biomaterialia)

· Justine Wallyn, Nicolas Anton, Damien Mertz, Sylvie Begin-Colin, Florence Franconi, Laurent Lemaire, Thierry Vandamme. ***Radiopaque iodinated oil and magnetic iron oxide nanoparticles-loaded nano-emulsion as contrasting agent for dual modal X-ray/MR imaging***. (In progress)

· Justine Wallyn, Nicolas Anton, Thierry Vandamme. ***Magnetite iron oxide nanoparticles: from nanomagnetism notions, synthesis and characteristics for biomedical applications***. (In progress)

Justine Wallyn

Nanoparticules furtives pour l'imagerie préclinique à rayons-X et multimodale rayons-X/IRM

Abstract: Biomedical imaging is nowadays an essential tool to establish a diagnosis by means of observation of tissues and biological fluids. Combination of imaging instrument with contrast enhancers is a key to obtain clear delineation of a desired tissue by accumulation of a contrast agent into this specific target. The two main imagers are the X-ray scanner and the magnetic resonance imaging (MRI).These imagers are frequently used in conjuncture. Typically, small hydrosoluble iodinated molecules are used as contrasting material for radiography whereas MRI involves magnetic materials like iron oxide nanoparticles. In this work, we proposed two novel contrast agents, the first one was aiming to form an alternative to iodinated contrast agents suffering from fast excretion and causing renal toxicity whereas the second one was aiming at providing bimodal contrasting ability to facilitate access to bimodal imaging procedure in clinics. In the first case, iodinated polymeric nanoparticles, serving for preclinical X-ray imaging were formulated by nanoprecipitation technique. Parameters of formulation were elucidated to provide nanoparticles with size distribution suitable for *in vivo* administration and high iodine content for contrast enhancement. *In vivo* study revealed the efficacy of our nanoparticles to clearly visualize liver and spleen and limiting current issues associated with marketed radiopaque contrast agents. The second work achieved was aiming at formulating bimodal lipids-based nanocarriers capable of yielding contrast enhancement for X-ray imaging and MRI by combining iodinated oil and iron oxide nanoparticles within a nano-emulsion core. This would provide bimodal nanoparticulate platform to carry out fast and efficient dual modal imaging procedures. In this context we succeeded to generate efficient dual modal contrast agent yielding clear visualization of liver and kidney by MRI and liver and spleen by X-ray imaging. Pharmacokinetic profile was so determined thanks to bimodal imaging. Using MRI allowed to show that kidneys eliminated a fraction of the dose whereas X-ray imaging confirmed that both tissues, liver and spleen, were passively targeted. These two studies proposed solutions limiting current issues of radiopaque contrast agents and novel formulations to facilitate bimodal imaging for soft tissues imaging.

Keywords: *Nanoparticles, contrast agent, X-ray imaging, Magnetic resonance imaging.*

Résumé *:* L'imagerie biomédicale est aujourd'hui un outil essentiel pour établir un diagnostic grâce à l'observation des tissus et des fluides biologiques. L'usage d'instruments à imagerie combinée avec des produits de contraste est la clé pour réussir à distinguer précisément un tissu ciblé *via* l'accumulation de produit de contraste dans le tissu. Les deux principaux appareils à imagerie utilisés sont le scanner à rayons X et l'imagerie à résonance magnétique (IRM). Ils sont fréquemment employés en complément de l'un et l'autre. Typiquement, de petites molécules iodées hydrophiles sont utilisées comme produit de contraste pour la radiographie à rayons X tandis que l'IRM implique des matériaux magnétiques tels que des nanoparticules d'oxyde de fer. Dans le cadre de ce projet doctoral, nous avons donc proposé deux nouveaux produits de contraste dont le premier visait à constituer une alternative aux produits iodés dont la rapide élimination et la toxicité rénale forment deux problèmes récurrents et un second produit, cette fois-ci bimodale, afin de faciliter les procédures d'imagerie bimodale. Pour le premier point, des nanoparticules de polymères iodés pour l'imagerie à rayons X ont été formulées et ce, par une technique de nanoprécipitation. Les paramètres de formulation ont été élucidés de telle sorte que les nanoparticules possédaient une distribution de taille adaptée pour l'administration par voie intraveineuse et une teneur en iode suffisante en iode pour contraster sous rayons X. Une étude *in vivo* a révélé le potentiel du produit de contraste à visualiser distinctement le foie et la rate et ce, tout en ne présentant pas les principaux problèmes des produits iodés commerciaux. La seconde étude a eu pour but de formuler des nano-véhicules lipidiques capables de générer un contraste pour l'imagerie à rayons X et l'IRM de par l'incorporation d'huile iodée et de nanoparticules d'oxyde de fer dans le cœur de nano-émulsions. Ceci avait pour objectif de fournir une plateforme nanoparticulaire bimodale pour réaliser efficacement et rapidement des procédures d'imagerie multimodale. Nous avons réussi à produire un efficace agent de contraste bimodal permettant d'observer distinctement le foie et les reins par IRM et le foie et la rate par imagerie à rayons X. La pharmacocinétique de la substance administrée a ainsi pu être mise en avant grâce à la bimodalité de l'agent. Employer l'IRM a permis de montrer qu'une fraction de la dose injectée était éliminée par voie rénale tandis que l'imagerie à rayons X a confirmé que les deux tissus, foie et rate, étaient passivement ciblés par l'agent de contraste. Ces deux études ont donc fournies de potentielles solutions pour répondre aux besoins en produits pour l'imagerie à rayons X et en formulations facilitant l'imagerie bimodale des tissus mous.

Mots-clés : *Nanoparticules, produit de contraste, imagerie à rayons X, imagerie à résonance magnétique.*